Biofilms on electrodes and crosslinking of bovine pericardium tissue : application to biopower device development and anti-calcification of bioprosthetic valves

Submitted by:

Ali Ekhtiari M.Sc. (Hons)

Thesis is submitted for the Ph.D Degree by Research of

The National University of Ireland Galway

Research was conducted in: School of Chemistry & Ryan Institute,

The National University of Ireland Galway

Month and Year of Submission: November 2017

Supervisor of the Research: Professor Dónal Leech

Head of School: Professor Paul V Murphy

Declaration

The contents of this thesis is a result of my own work and was carried out in the School of Chemistry & Ryan Institute, National University of Ireland Galway / Boston Scientific Galway, Ireland and Department of Analytical Chemistry-Biochemistry and Structural Biology in Lund University, Lund, Sweden. The content of this dissertation are original and have not been submitted in whole or in part for consideration for any other degree or any other university.

Ali Ekhtiari

November 2017

Acknowledgements

I would like to thank all who helped and assisted me throughout postgraduate studies. First of all, I would like to express my special appreciation and thanks to my supervisor Prof. Dónal Leech for giving me the opportunity to carry out this project. Thank you for your understanding and availability whenever I have needed it.

Besides my primary supervisor, I would like to express my sincere thanks and gratitude to my co-supervisors in the Bioenergy consortium Prof. Lo Gorton and Dr Magnus Falk.

I would like to thank the post-doctoral researcher Dr Peter Ó Conghaile.

A special thanks to my friends in BERL group both past and present, and to all my fellow chemistry postgraduates.

To my many friends and family, you should know that your support and encouragement was worth more than I can express on paper.

To my sister, Elaheh, thank you for your love, encouragement, and support during the course of my studies.

To my parents, Manijeh and Javad, thank you for granting me a life of opportunity and for your unconditional support and encouragement to pursue my interests.

And finally, to Erika, for her love, support, patience and motivation when it was needed most.

Table of contents

Abstract

Advances in the electrical communications between enzymes and electrodes made it possible to the fabrication of new miniaturized implantable power devices. This thesis is devoted to study and improvement of enzyme electrodes by integration of enzymes and redox mediators capable of transferring electrons between enzymes and electrodes with a view to developing a semi- or fully implantable, miniature, membrane-less enzymatic fuel cell (EFC) exploiting enzymatic oxidation of glucose coupled to the enzymatic reduction of dissolved dioxygen. Miniaturisation is possible if appropriate enzymes are selected as catalysts, instead of non-selective precious metal catalysts, by removal of ion-exchange membrane from assembled fuel cells. The immobilisation chemistry of enzymes and redox complexes capable of shuttling electrons between enzymes and electrode surface can have an impact on the magnitude and stability of current response, with implications for application as biosensor and EFC development. Enzyme electrode prepared using co-immobilisation of redox mediators, multiwalled carbon nanotube and polymer support using a chemical crosslinker provide 3-dimensional biofilms for an electrocatalytic response for substrate, such as sugar, important in biosensor and biofuel cell applications. The objective of this thesis was to investigate the interactions of redox complexes, enzyme and nanostructure on electrode surface for application to developing a semi-or fully implantable, membrane-less EFC anode for energy generation. Furthermore, the optimisation of the electrochemical response of enzyme electrode was evaluated using a design of experiment approaches, in seeking to improve the current density under physiological conditions. Moreover as a part of the research programme, an industrial secondement project was undertaken in Boston Scientific Galway (BSG). The project involved development of a bio-reactor that can be used to simulate calcification of bovine pericardium *in vitro* and its application to study cross-linkers to attempt to inhibit calcification. The application of cross-linking chemicals to inhibit the calcification rates is a link to enzyme electrode modification for biosensor and biofuel cell application. A second, academic, secondement was conducted in Lund University under the supervision of Prof. Lo Gorton focused on a comparison of cross-linking reaction conditions for preparation of films of redox polymers, enzymes and supports on electrodes for application as biofuel cell anodes.

Chapter 2 focuses on the synthesis, characterisation and purification of a range of osmium polypyridyl complexes and redox polymers. Subsequently the products were characterised and purified using the relevant techniques. The purified osmium polypyridyl complexes and redox polymers are then utilised as redox mediators in chapters 3, 4 and 5 of this thesis. Chapter 3 reports on a comparison of glucose oxidation by enzyme electrodes based on coupling of GOx and an amine-functionalised osmium complex to carboxymethyl dextran (CMD) and a range of conductive and non-conductive nanoparticles as alternate supports to probe whether the properties of different supports with similar sizes can improve current density and/or stability for these electrodes. Multi-walled carbon nanotubes (MWCNT), gold and silica nanoparticle decorated enzymatic graphite anodes were developed and evaluated. The anodes decorated with MWCNT and Au nanoparticles produced current densities more than 100% higher than plain graphite anodes while those of silica-decorated anodes with similar morphologies produced 3.5 % higher than the control. The addition of MWCNT to enzymatic electrodes increases the stability and current density, indicating that MWCNT provide higher surface area and enhanced electrical conductivity for the immobilisation of film components. In addition, we report on comparison of enzyme electrodes based on coupling of GOx or FADGDH and an amine-functionalised osmium complex to carboxymethyl dextran (CMD) and acid treated MWCNT. Enzymatic electrodes provide 6.4 mA cm^{-2} at 0.2 V vs Ag/AgCl, for GOx-based electrodes, compared to 4.2 mA cm^{-2} for FADGDH-based electrodes operating at 100 mM glucose concentration in 50 mM phosphate buffer saline at 37 °C. Although a higher decrease in current density is observed for GOx-based electrodes when operated in the presence of oxygen, in comparison to the FADGDH-based electrodes. These enzymatic electrodes, thus, show promise for application as anodes in enzymatic fuel cells for *in vivo* or ex *vivo* power generation. Chapter 4 reports an investigation of design of experiment methodology in order to improve the performance of a biocathode electrode. These cathode enzyme electrodes were prepared using graphite electrodes modified with *Myrothecium verrucaria* bilirubin oxidase (*Mv*BOd) as enzyme, [Os(4,4′-dichloro-2,2′-bipyridine)$_2$ (polyvinylimidazole)$_{10}$Cl]$^{+/2+}$ (Os(dcbpy)$_2$PVI) ($E^{o'}$=0.35 V vs. Ag/AgCl) as redox polymer, crosslinked with poly (ethylene glycol) diglycidyl ether (PEGDGE) and a volume of the 46 mg mL^{-1} aqueous dispersion of acid-treated multi- walled carbon nanotubes (MWCNT) for electrocatalytic reduction of oxygen to water. Response

surface methodology was used for optimisation of the amount of the enzyme electrode components to produce the highest current density under pseudo-physiological conditions of saline buffer at 37°C was performed. A statistical analysis showed that the proposed model had a good fit with the experimental results. From the validated model, the addition of multiwalled carbon nanotube and osmium polymer components was identified as major contributing factors to the improved performance. Based on the optimised amount of components, enzyme electrodes display current densities of 0.32 ± 0.03 mA cm^{-2} and 0.8 ± 0.05 mA cm^{-2} at 0.1 V vs. Ag/AgCl in pseudo-physiological and oxygen saturation conditions, respectively, largely consistent with the predicted values. The results demonstrate that use of a design of experiment approach can be applied effectively and efficiently to improve the performance of enzyme electrodes as cathodes for biofuel cell device development. Chapter 5 reports on an investigation of the catalytic current out put of enzyme electrodes based on 3 different enzymes utilising 2 different mediators namely $Os(dmobpy)_2$ PVI or [Os(4,4'-dimethoxy-2,2'-bipyridine)$_2$ (poly(vinylimidazole))$_{10}$Cl]$^+$ osmium redox polymer and $Os(dmobpy)_2$4AMP or [Os (4,4´-dimethoxy-2,2´-bipyridine)$_2$(4-aminomethyl pyridine)Cl].PF_6 osmium redox complex using flow injection analysis (FIA). The application of redox mediators and immobilisation methodology of enzyme electrodes can have an impact on the magnitude and stability of the amperometric current response, with implications for the application as biosensors and as fuel cell electrodes. CMD bearing carboxylic functional groups, as chemical supports was applied for immobilisation of amine-containing osmium redox complexes and poly(ethylene glycol) diglycidyl ether (PEGDGE) as crosslinker for immobilisation of the redox polymer. The pH optima of immobilisation of all the three enzyme electrode preparations, namely, *Trametes villosa* CDH (*Tv*CDH) , D-fructose dehydrogenase from alphaprotobacteria (FDH) and *Aspergillus niger* glucose oxidase (GOx) were identified and used to compare the maximum current out put of the mediators in a range of buffers (4.5-7.5). The pH optima of immobilisation for both FDH and *Tv*CDH with both mediators were found to be in the acidic range while a slight change in pH optima of cross-linked *Tv* CDH was observed, which is due to its surface and residual charge interaction with EDC/NHS during cross-linking. The pH stability assays in the pH range of 4.5–7.5 showed that FDH and *Tv*CDH have almost identical acidic pH stabilities while high acidic condition is detrimental to GOx. The study showed that at the pH optima of immobilisation, enzyme coimmobilisation

with Os(dmobpy)$_2$PVI osmium polymer generated higher current outputs as compared to immobilisation with Os(dmobpy)$_2$4AMP. Finally chapter 6 involves development of a bio-reactor that can be used to simulate calcification of bovine pericardium *in vitro* and its application to study cross-linkers to attempt to inhibit this calcification. The use of cross linkers is a link to this thesis that is enzyme electrode modification for biosensor and biofuel cell application. Despite the fact that mechanical valves offer lifelong durability they also commit patients to anticoagulation treatment for the rest of their life. On the other hand, bio prosthetic valves with glutaraldehyde (Glut) treatment have superior hemodynamic performance but early onset calcification being the primary cause of biomaterial breakdown limits their use to the elderly. Considering that bioprosthetic valves are not reliant upon anticoagulation, there has been much focus on measures to overcome their issues with durability, therefore new treatments have been developed and tested. The main objective of this model is allowing the differentiation of calcification rates where the samples were subjected to different tissue treatments. Tissue valve calcification is initiated primarily within residual cells that have been devitalised, usually by Glut pretreatment. The mechanism involves reaction of calcium-containing extracellular fluid with membrane associated phosphorus to yield calcium phosphate mineral deposits. Calcification of bioprosthetic valves is quite complex and has a variety of determinants, including host factors, tissue treatment conditions, and mechanical effects. The most promising preventive strategies have included binding of calcification inhibitors to Glut-treated tissue, removal or modification of calcifiable components, modification of Glut treatment, and use of tissue cross linking agents other than Glut. The treated tissue samples were submerged in to the calcification solution and the nature of crystal phases grown on treated bovine pericardium *in vitro* was investigated for evaluation of progressive calcification. Light microscopy, scanning electron microscopy (SEM), X-ray energy dispersive spectroscopy (SEM/EDX) were used as tools for the qualitative and quantitative assessment of the calcification process. Chemical analysis of samples calcified *in vitro* showed that the content of the salts was mainly calcium and phosphate. We investigated a novel polyepoxide crosslinker that was hypothesised to confer both material stabilisation and calcification resistance when used to prepare bioprosthetic heart valves. An hyperbranched, water soluble Poly ethylene glycol (PEG) epoxy polymer (PEP) with epoxy functional groups was synthesised using PEG acrylates and epoxy monomers. High water

solubility is vital for better collagen crosslinking as it allows the polymer branches to spread and create more contact points with the tissue and initiate crosslinking, while the tissue's natural structure is preserved. The epoxy functional groups can be used as an alternative to Glut due to their ability to react with amine groups and/or carboxilic acid groups of the collagen chains and form irreversivle bonds, thus stabilising the tissue. PEP was used to crosslink bovine pericardium and control materials were crosslinked with Glut. In addition PEG diglycidyl ether (PEGDGE), a commercial epoxide crosslinker was used for comparison. For the *in vitro* calcification assessment, tissue treated with PEG epoxy had lower shrinkage temperature compared to Glut treatment. However, PEP crosslinking conferred significantly greater calcification resistance than Glut pretreatment, and significantly improved biochemical compliance.

List of abbreviations

Γ_{Os}	Osmium surface coverage
4-AMP	4-aminomethyl pyridine
Ag/AgCl	Ag/AgCl (3 M KCl) reference electrode
ANOVA	Analysis of variance
AuNP	Gold nanoparticle
BBD	Box-Behnken Design
bpy	2,2′-bipyridine
CDH	Cellobiose dehydrogenase
CMD	Carboxymethyl dextran
CNT	Carbon nanotube
CV	Cyclic voltammetry
D	Diffusion co-efficient
dcbpy	4,4′-dichloro-2,2′-bipyridine
DET	Direct electron transfer
dmbpy	4,4′-dimethyl-2,2′-bipyridine
dmobpy	4,4′-dimethoxy-2,2′-bipyridine
DoE	Design of experiment
DPV	Differential pulse voltammetry
EFC	Enzymatic fuel cell
EDC	N-(3-dimethylaminopropyl)-N′-ethylcarbodiimide
FADGDH	Flavin adenine dinucleotide-dependent glucose dehydrogenase

Glut	Glutaraldehyde
GOx	Glucose oxidase
MCO	Multicopper oxidase
MET	Mediated electron transport
MWCNT	Multiwalled carbon nanotube
MFC	Microbial fuel cell
MtL	*Myceliophthora thermophila* laccase
MvBOd	*Myrothecium verrucaria* bilirubin oxidase
NAD	Nicotinamide adenine dinucleotide
NHS	N-hydroxysuccinimide
$Os(dcbpy)_2PVI$	$[Os(4,4'\text{-dichloro-}2,2'\text{-bipyridine})_2\ (polyvinylimidazole)_{10}Cl]^+$
$Os(dmobpy)_2$4AMP	$[Os(4,4'\text{-dimethoxy-}2,2'\text{-bipyridine})_2\ (4\ aminomethylpyridine)Cl].PF_6$
$Os(dmobpy)_2PVI$	$[Os(4,4'\text{-dimethoxy-}2,2'\text{-bipyridine})_2\ (polyvinylimidazole)_{10}Cl]^+$
$Os(bpy)_2$4AMP	$[Os(2,2'\text{-bipyridine})_2(4\text{-aminomethyl pyridine})Cl]\ .PF_6$
PBS	Phosphate buffered saline
PEGDGE	Poly(ethylene glycol) diglycidyl ether
PEM	Proton exchange membrane
PEP	Poly(ethylene glycol) epoxy polymer
PQQ	Pyrrolo-quinoline quinone
PVI	poly-vinylimidazole
RSM	Response surface methodology
SWCNT	Single walled carbon nanotube

Chapter 1

Introduction

1.1 Introduction

Harvesting energy from renewable resources has become an important focus during the last couple of decades. One focus is on examining glucose as a potential fuel source, present at relatively high concentrations (5.5 mM) at normal blood sugar levels, with the long-term aim of developing self-powered implantable or semi-implantable biomedical devices [1]. Development and deployment of prototype biodevices with wireless capability and an ability to self-power is of scientific and practical importance for application as self-sustained medical and/or portable devices in the field of medical diagnostics and bioelectronics [2]. One energy conversion option that has been studied is enzymatic biofuel cells. EFC have the ability to convert energy derived from biofuels to electrical energy by means of the catalytic activity of oxidoreductase enzymes [3]. Use of enzymes as catalysts to oxidise glucose at an anode and to reduce O_2 at a cathode, that when combined act as a glucose | O_2 EFC, shows promise as technology for conversion of *in vivo* available chemical energy to electrical power [1, 4, 5]. The idea of being able to use cell-free enzyme systems to provide sufficient power to sustain pacemakers or a permanently implantable artificial heart was explored in the mid-1960s [6, 7]. It was not until the late 1990s, with advancements in enzyme immobilisation and stabilisation, that research effort toward the implementation of enzymatically driven power sources greatly increased [8, 9]. Although the first EFC was reported almost a half century ago [10], applications of the technology were largely neglected due to the technology limitations and the fast development of metallic electrocatalysts for fuel cells [11]. Currently, implantable and semi-implantable devices, such as insulin pumps, neurostimulators and pacemakers are powered by batteries with metallic electrocatalysts. These highly reactive lithium or alkaline

electrolyte batteries, provide electricity from internal chemical reactions. The metallic electrocatalyst-based battery technology used in medical devices, for example in pacemaker's batteries last an average 6 to 7 years depending on how active the pacemaker is. It's critically important for these power devices to be hermetically sealed in order to be protected from the very hostile environment of the human body- a warm, wet, and salty place. If medical devices were capable of being opened so that the battery could be replaced, hermetic sealing would be impossible. Instead, the battery must be permanently sealed within the device, making it necessary to change the battery with the device every time. Furthermore the lithium and alkaline electrolyte based battery technology contains components that are corrosive and highly toxic to humans. Therefore in order to avoid unwanted chemical side reactions, they require protective membranes and casings to ensure isolation from the surrounding environment and from each other limiting the degree of miniaturisation possible [12-17]. An alternative approach is the development of medical implantable devices that take advantage of other energy sources such as the heart motion or fuel cells that rely on ambient fuel and oxidant from the *in-vivo* environment. Immobilisation of substrate specific enzymes at electrode surfaces opens up the possibility of device miniaturisation, by eliminating the requirement of a separating ion-exchange interface between anolyte and catholyte: a membrane-less EFC [18]. Furthermore it facilitates continuous power generation throughout the host's lifespan by electrolysing ambient body fuels and oxidant such as glucose and oxygen and converting them into benign by-products, a conversion process through which electrical energy can be generated from chemical energy [19-21]. Although there is promise in EFC systems, there are still challenges that need to be addressed for the successful application of enzymatic fuel cells, such as obtaining improved stability and increased power density.

1.2 Fuel cells

Fuel cells are electrochemical devices that convert chemical energy in fuels directly into electrical energy, promising power generation with high efficiency. In addition, because combustion is avoided, fuel cells produce power with minimal pollutant. Fuel cells are different from batteries in that they require a continuous source of fuel and oxidant to sustain the

chemical reaction. In a typical fuel cell, fuel is fed continuously to the anode (negative electrode) and an oxidant (often oxygen from air) is fed continuously to the cathode (positive electrode). In principle, the fuel cell produces power for as long as fuel is supplied [22] whereas a battery will cease to produce electrical energy when the chemical reactants are consumed (i.e., discharged). The first fuel cell was invented in 1838 by German physicist Christian Friedrich Schönbein [23]. The Welsh judge and physical scientist Sir William Robert Grove demonstrated the first use of a fuel cell in 1839 using platinum electrodes and sulphuric acid electrolyte, with hydrogen and oxygen as reactants [24], and the first commercial use of fuel cells came more than a century later in NASA space programs to generate power for satellites and space capsules. The power output (P_{CELL}) of a fuel cell is a function of the cell voltage (V_{CELL}) and the rate of transfer of electrons through external circuit (I_{CELL}) as shown in equation1. The cell voltage is the potential difference between the anode (E_a) and the cathode (E_c) compartments taking into consideration irreversible energy losses in the voltage (termed an overvoltage, η) as a result of slow kinetics of heterogeneous electron transfer, ohmic resistance and mass transport limitation (equation 2) [22, 25]. The flow of charge through an external circuit from the anode to cathode (I_{CELL}) depends on the electrode size and rate of the reaction occurring in the fuel cell.

$$P_{cell} = V_{cell} \times I_{cell} \qquad \textit{Equation [1]}$$

$$V_{cell} = (E_c - E_a) - \eta \qquad \textit{Equation [2]}$$

Figure 1 demonstrates an example of a fuel cell, the hydrogen-oxygen proton exchange membrane fuel cell (PEMFC). The anodic and cathodic half reactions taking place within the PEMFC are as shown in equation 3 and 4.

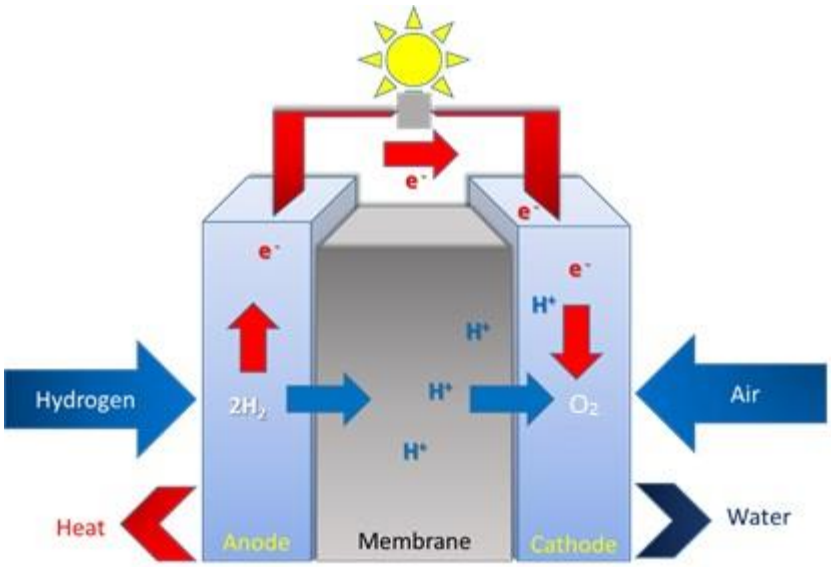

Figure 1: Simplified schematic of a hydrogen-oxygen proton exchange membrane fuel cell (PEMFC).

Anode: $2H_2 \rightarrow 4e^- + 4H^+ \ (E^0 = 0\ V)$ *Equation [3]*

Cathode: $O_2 + 4e^- + 4H^+ \rightarrow 2H_2O \ (E^0 = 1.23\ V)$ *Equation [4]*

At the anode hydrogen gas is oxidised via a metal catalyst that converts hydrogen gas into protons and electrons. The electrons flow up from the anode, through a wire, and onto the cathode. While flowing through the wire, an electrical current is generated that can be used to perform work. The protons flow via the proton exchange membrane that maintains the catholyte/anolyte separation towards the cathode. This process is driven by the electro-chemical gradient resulting from the high concentration of H^+ ions near the anode. At the cathode oxygen is catalytically combined, using a metal catalyst, with the protons and electrons and is reduced to form pure water. The standard potential difference (ΔE^0) between the anode and cathode of the hydrogen-oxygen fuel cell is 1.23 V as shown (equation 4) [26]. The metal catalyst (typically platinum) is highly effective however it is both expensive and non-specific towards fuel or oxidant. This non-specificity of the catalyst necessitates the use of membranes and protective casings to prevent migration and reaction of the fuel and oxidant at opposing electrodes [5, 25]. Recent fuel cell research focuses on the search for catalysts that are not as

prone as platinum to de-activation through surface poisoning, on minimising catalyst loading to reduce costs, and on electrolyte properties to prevent fuel-oxidant crossover between half-cells [28].

1.3 Biocatalytic fuel cells

Biofuel cells (BFCs) are low-temperature fuel cells that harness biological catalytic reactions, in place of metal catalysts in traditional low-temperature fuel cells, to produce electricity from electrolysis of fuel and oxidant. Early work with BFCs, which began in the early 20th century, was purely of the microbial variety [4]. Research on using enzymes directly for oxidation in biofuel cells began in the early 1960s, with the first enzymatic fuel cell being produced in 1964 [10]. This research began on development of an implantable power source into human body without external refueling, specifically for an artificial heart, taking advantage of the extreme selectivity of the enzymes to completely remove the barrier between anode and cathode, which is an absolute requirement in fuel cells not of the enzymatic type [30] as well as NASA's interest in finding ways to recycle human waste into usable energy on board spacecraft. These two applications remain the primary goals for the development of the two categories of biofuel cells, namely microbial and enzymatic [31]. A BFC configuration is based on the same principles as conventional fuel cells consisting of a fuel oxidising anode and an oxygen reducing cathode [32, 5]. However unlike the traditional fuel cell with precious metal catalysts, BFCs utilise living cells (bacteria, algae) or catalysts extracted from cells (enzymes, enzyme cascades and, more recently, mitochondria) as biological catalysts and due to versatility of nature, BFCs are not limited to use of hydrogen or methanol as a fuel, and can oxidise/reduce a wide range of substrates under moderate conditions of pH and temperature. Moreover biocatalysts are confined to the electrode surface, thus eliminating the need for a separating membrane and aiding miniaturisation of the device. Microbial fuel cells involve the use of entire microorganisms to convert a fuel and oxidant to electrical power, whereas enzymatic fuel cells involve the use of enzymes isolated from organisms for their conversion process. The concept of microbial fuel cells will only be briefly presented as the work carried out within this thesis focuses on research aimed at improving power output of enzymatic fuel cells.

1.3.1 Microbial fuel cells

Microbial fuel cells (MFC) are BFCs that generate power from organic substrates (frequently derived from waste) as a fuel using whole living organisms, such as algae or bacteria, as a catalyst and convert energy released in metabolic reactions into electrical energy. A typical MFC consists of two electrodes separated by a semi-permeable membrane submerged in an electrolyte solution. Figure 2 depicts a typical MFC set-up in a research laboratory.

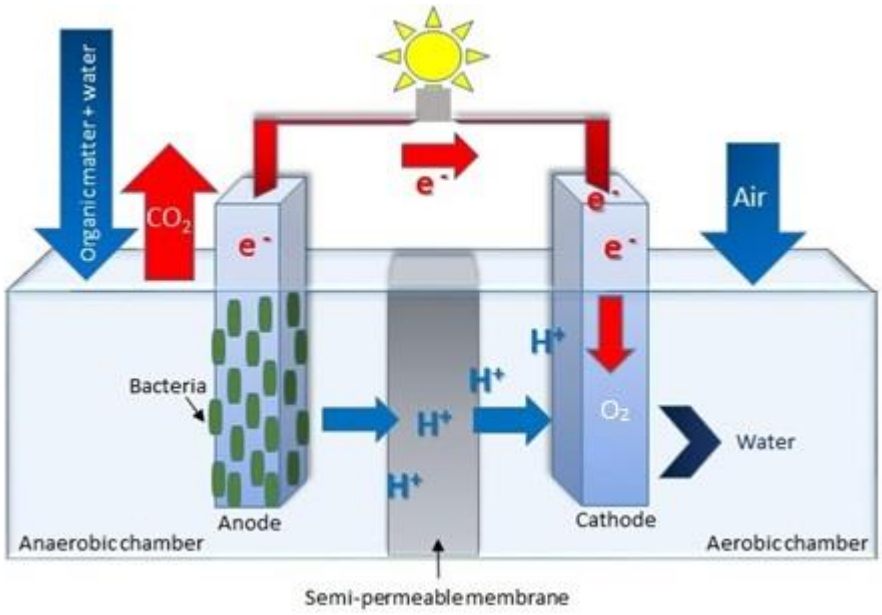

Figure 2: Simplified schematic of a microbial fuel cell.

The electrodes are connected by a wire and the anode compartment (negative electrode) has bacteria growing on it. These mixed or pure cultures of microbial organisms catalyse the decomposition of the organic matter into electrons and protons. The electrons are transferred to the cathode compartment through an external circuit while cations migrate to the cathode compartment through the membrane. The electrons and protons are consumed in the cathode compartment, combining with oxygen to form water [5, 33-37]. A metal is usually used to catalyse oxygen reduction, although it has recently been shown that microorganisms can be used for this purpose as well. Using microbes to generate electricity implies that the processes in an MFC are self-sustaining; the bacteria replicate and continue to produce power indefinitely as long as there is a food source to nourish the bacteria. Moreover, MFCs are very efficient, do

not rely on fossil fuels for energy, and can run effectively on sources like food waste and sewage.

1.3.2 Enzymatic fuel cell

An Enzymatic biofuel cell is a specific type of fuel cell that uses enzymes as a catalyst for fuel oxidation at the anode and oxidant reduction at the cathode. Enzymatic biofuel cells, while currently confined to research facilities, are promising source of energy in terms of their relatively inexpensive components and fuels, as well as a potential power source for implantable devices. Figure 3 presents the basic operating principle of a glucose-fueled EFC.

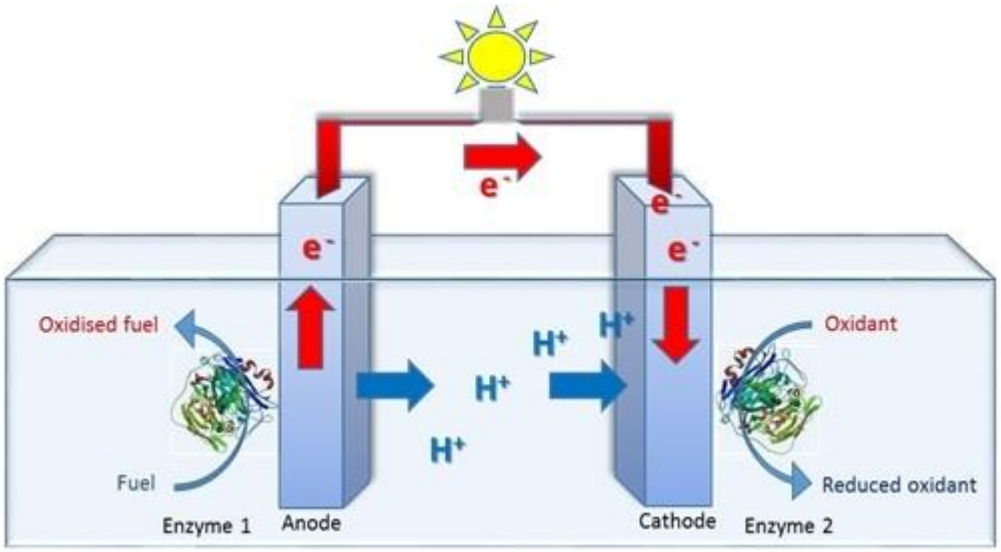

Figure 3. Simplified schematic of an enzymatic fuel cell.

In the early 1990s the interest in the development of biocatalytic fuel cells was renewed, with the advancements in electrochemistry and enzyme electrode production [38 - 41]. The first EFC based on glucose as a fuel and oxygen as oxidant was reported by Yahiro *et al*. in 1964 [10]. Enzymatic fuel cells have received increased attention following many improvements such as the discovery and development of new redox enzymes, electrode materials, nanostructures and enabling technologies to immobilise enzymes at electrodes [10, 42 - 44]. For example appropriate choice of enzyme allows current generation to occur under relatively mild conditions (neutral pH, ambient temperature) compared to conventional fuel cells. In addition,

the immobilisation of enzymes on catalytically inert electrode surfaces both increases local concentration of catalyst and permits removal of separating membrane between anode and cathode as no cross-reactions should occur. Due to such properties, enzymatic fuel cells have the capacity to be miniaturised, and consequently, micrometer dimension membrane-less EFCs have been developed [13, 45 - 47]. The power output of an EFC is the product of the cell voltage and the current. The maximum cell voltages for EFCs are usually determined by the difference between the formal redox potentials ($E°'$) of the redox enzyme cofactors, in the active site, utilised for the anode and cathode, depicted in the scheme in Figure 4. For example, in an EFC displaying 100% coulombic efficiency with no over voltages or ohmic losses, the thermodynamic reversible cell voltage for the complete oxidation of glucose to carbon dioxide and water (Equation 5) can be estimated as 1.24 V at 298 K. As recent EFC development has been predominately driven by potential application *in vivo*, most research has focused on using glucose as a fuel due to its availability in blood (~5 mM) and other tissues. For an EFC in order to operate continuously *in vivo*, it is vital that the cell operate under the physiological conditions (i.e. 5 mM glucose, pH 7.4, 37 °C). Consequently the most commonly described enzymatic fuel cell prototype consists of a glucose oxidising anode and an O_2 reducing cathode [48-50], although other systems utilising fuels such as methanol, fructose, alcohol (to name a few) and hydrogen peroxide as oxidant have been reported previously [51-53]. Whilst some effort has been focused on assembling multiple enzymes at the anode of an EFC to provide for extraction of up to 24 electrons from glucose [54–59], most EFC research has focused to date on use of a single enzyme at the anode to oxidise glucose to gluconolactone, as in Equation 6 with only 2 electrons per mole of glucose and a maximum reversible cell voltage of 1.18 V.

$$C_6H_{12}O_6 + 6O_2 \rightarrow 6CO_2 + 6H_2O \qquad Equation\ [5]$$

$$C_6H_{12}O_6 + {}^1/_2\, O_2 \rightarrow C_6H_{10}O_6 + H_2O \qquad Equation\ [6]$$

The electrochemical reactions of a glucose/O_2 EFC consist of two separate reactions: an oxidation half-reaction occurring at the anode and a reduction half-reaction occurring at the cathode. At the anode, β-d-glucose is catalytically converted into β-d-gluconolactone producing

protons, which travel through the electrolyte to the cathode, and electrons that travel through the circuit to the cathode. A reduction half reaction occurs at the cathode where oxygen is catalytically reduced by an enzyme and combines with protons to form water (Figure 4).

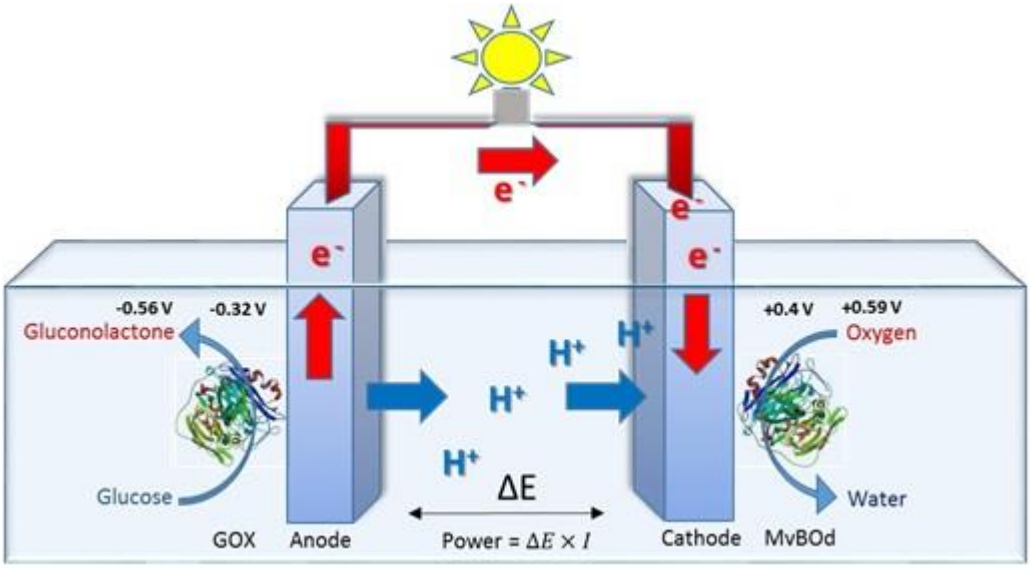

Figure 4: Operating principle of a fully enzymatic glucose/oxygen biofuel cell, with potential quoted vs. Ag/AgCl at pH 7.4.

For over 4 decades lithium ion batteries have been used for the implantable devices, one of their widest application *in vivo* is in the heart pacemaker in which the lithium battery is located below the skin between the shoulder and the neck and is connected to electrodes in the heart muscle with a power density of 1 Wcm^{-3} with the typical lifetime of ten years [60, 61] however their lifespan is usually much shorter than the desired period of implantation and depletion of the battery has resulted in the replacement of 20% of the 200,000 pacemaker implants each year in the United States alone [62, 63]. Substitution of the current Lithium ion batteries with EFCs faces some challenges such as low power/current outputs, short operational lifetime and the instability of the biocatalyst and incomplete oxidation of fuels [64-66]. For EFCs application as a power source for implantable devices, an operational lifetime of greater than five years is required whereas the lifetime of EFCs up to now is measured in days. An alternative approach is to use the EFC as a semi implantable power source located remotely from the operational implantable devices. For example the enzyme electrodes can be printed onto a subcutaneous cannula or patch that connects to an implanted electrical device, enabling for power generation

from glucose oxidation and oxygen reduction in body fluids, that could regularly be replaced [67, 68].

1.3.3 Enzymatic catalysts

Enzymes are macromolecular biological catalysts that have many attractive features over the traditional metal catalyst used in a fuel cell. Similar to all catalysts, enzymes accelerate the rate at which a reaction occurs by lowering its activation energy. Substrate is a molecule upon which enzymes may act to convert into different molecules called products. Enzymes are capable of conversion of substrate to product many millions of times faster and almost all metabolic processes in the cell need enzymes in order to occur at rates fast enough to sustain life [69]. Like all proteins, enzymes are linear chains of amino acids that fold to produce a three-dimensional structure. The catalytic site of the enzyme that is involved in catalysis consists of only a small portion of enzyme structure (around 2–4 amino acids) [70]. This catalytic site is located next to one or more binding sites where residues orient the substrates. The catalytic site and binding site together comprise the enzyme's active site where substrate conversion to product occurs [71]. The protection of enzyme's active site by the unique three dimensional structure of their protein structure allows them to be substrate-specific, catalysing conversion of only selected chemical reactions to product thereby making them attractive for use in biosensors and biofuel cells [72]. Selection of enzyme(s) as redox catalysts provides opportunity for oxidation of a wider variety of fuels compared to inorganic catalysts. Another significant advantage of enzymes over metal based catalysts is their ability to work efficiently under moderate operating temperature and mild conditions, such as physiological pH [73]. In addition enzymes are renewable and relatively inexpensive to produce which has led to extensive research on them as biocatalysts for fuel cells applications.

1.4 Enzyme anodes

Based on the availability of redox enzyme there is a wide range of fuels that can be targeted for oxidation by enzyme anodes such as glucose, methanol, ethanol, etc. [74]. However, as the focus of the studies contained within this thesis is on EFCs for operation *in vivo* conditions, the most suitable fuel in this context is glucose due to its relatively high concentration in human blood (~5 mM) [75, 76]. As a result the focus will be on introduction to enzymes that catalyse the oxidation of glucose namely glucose oxidase and glucose dehydrogenase.

1.4.1 Glucose oxidase

The glucose oxidase enzyme (GOx) is a dimeric oxido-reductase that is produced by certain species of fungi and insects which displays antibacterial activity when oxygen and glucose are present [77]. Glucose oxidase (GOx) was first discovered by Muller (1928) in *Aspergillus niger* extracts. GOx catalyses the oxidation of β-D-glucose to D-gluconolactone, coupled to oxygen reduction to hydrogen peroxide. It consists of two equal subunits with a molecular mass of 80 kDa each, encoded by the same gene. The GOx enzyme displays a high thermo-stability and enthalpy of denaturation. In solution its stability depends on the pH, being more stable at around pH 5 [77, 78]. In order for GOx to function as a biocatalyst, it requires a co-factor, Flavin adenine dinucleotide (FAD) which is deeply buried (~1.5 nm) within the enzyme. Figure 5 shows a representation of the crystal structure of one of the GOx subunits [79], and Figure 6 demonstrates $FADH_2$ structure and the relevant portion of the FAD active site in oxidised and reduced forms.

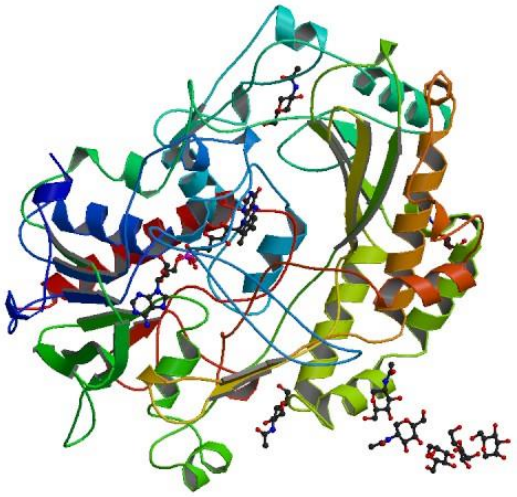

Figure 5: Crystal structure of the *Aspergillus niger* glucose oxidase (PDB ID: 3QVP [247]).

The FAD functions as initial electron acceptor and is reduced to $FADH_2$, which is then subsequently oxidised back to FAD by the final electron acceptor, oxygen, the natural acceptor, as in the equations 7 and 8, or an artificial acceptor (redox mediator) which replaces oxygen in the electron transfer mechanism.

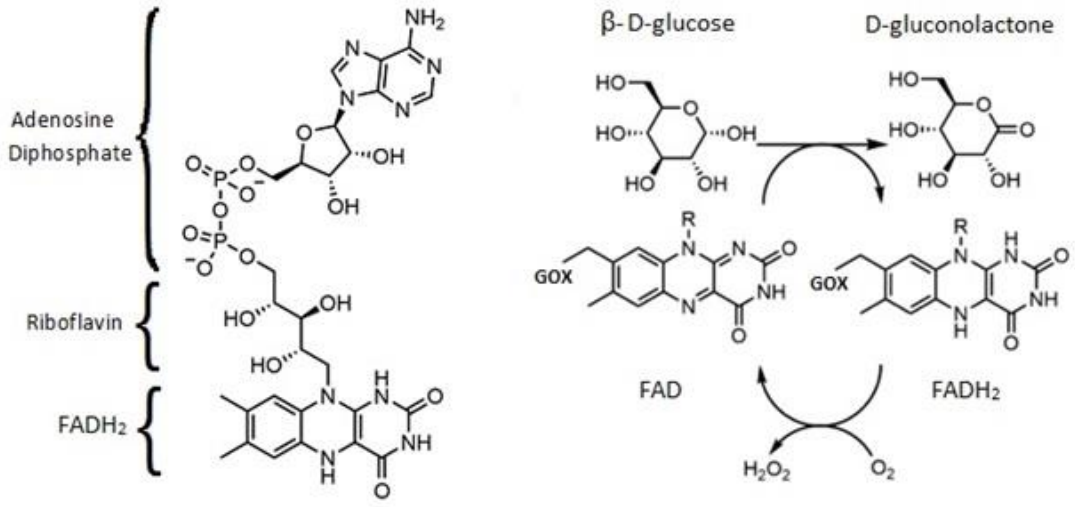

Figure 6: $FADH_2$ structure (left), the reduction reaction of FAD to $FADH_2$ at the active site of GOx upon oxidation of glucose and oxidised back to FAD by the final electron acceptor (right).

$$GOx(FAD) + 2e^- + 2H^+ \Leftrightarrow GOx(FADH_2) \qquad Equation\ [7]$$

$$GOx(FADH_2) + O_2 \rightarrow GOx(FAD) + H_2O_2 \qquad Equation\ [8]$$

The application of mediators to replace oxygen as the natural co-substrate facilitates the shuttling of the electrons from the enzyme active site to an electrode surface which in turn allows the current generation at lower overpotentials, in comparison to systems based on reduction of oxygen or oxidation of peroxide. However the presence of mediators leads to competition between oxygen and the mediator as the final electron acceptor. This can cause problems during development of *in vivo* enzyme anodes based on GOx, as oxygen present in the fuel cell electrolyte, competes with the mediator. In addition, the catalytic oxidation of glucose to gluconolactone by GOx produces hydrogen peroxide when oxygen is the electron acceptor: hydrogen peroxide is a highly toxic product and can be detrimental to the activity of bioactive materials [80-83]. Nonetheless, due to its stability, substrate specificity, high electron turnover rate and commercial availability, GOx is extensively used in biosensors and biofuel cells for *in vivo* or *ex vivo* power generation [16, 84].

Although the FAD co-factor is deeply buried within the enzyme there have been many studies purporting direct electron transfer (DET) from GOx active site to the electrode surfaces [85, 86]. In the case of GOx, the active centre of the enzyme is reportedly directly connected to the electrode surface, However, DET as a mechanism for a catalytic current generation in GOx is disputed [87]. Recent reports show that regardless of electrode matrix, DET between the active site of GOx and nanostructured electrodes is difficult to attain [88]. Despite the apparent simplicity of DET, catalytic current generated is hindered due to the large distance of the FAD active site of the enzyme to the surface of the electrode. In addition the correct orientation of enzyme at the electrode surface, that is difficult to control, further hampers catalytic current capture, as does blockage of access of substrate to the active site in the presence of the electrode. Moreover, the current density achieved by DET is considerably lower when compared to mediated electron transfer (MET), as a maximum monolayer coverage of enzyme at electrode surface is attainable. The use of MET overcomes DET challenges such as orientation and

distance to active site limitations. Mediators are artificial co-substrates that can participate in the redox reaction with the enzyme and effect transfer of electrons [18]. Co-immobilisation of enzymes and mediator on electrode surface provides a three dimensional mediating matrix around the enzymes, effectively "wiring" it the electrode surface. To conclude, the use of enzymes that are insensitive to oxygen such as dehydrogenases may prove advantageous for application to glucose/oxygen EFCs over the GOx-based anodes due to oxygen competition with mediator or production of hydrogen peroxide when oxygen is the electron acceptor.

1.4.2 Glucose dehydrogenase

Glucose dehydrogenase (GDH) belongs to the family of oxidoreductase capable of oxidising glucose by transferring one or more electrons and protons to their respective acceptor such as nicotinamide adenine dinucleotide (NAD) [89], a pyrrolo-quinoline quinone (PQQ) co-factor [90] or a flavin such as FAD [91] as illustrated in Figure 7.

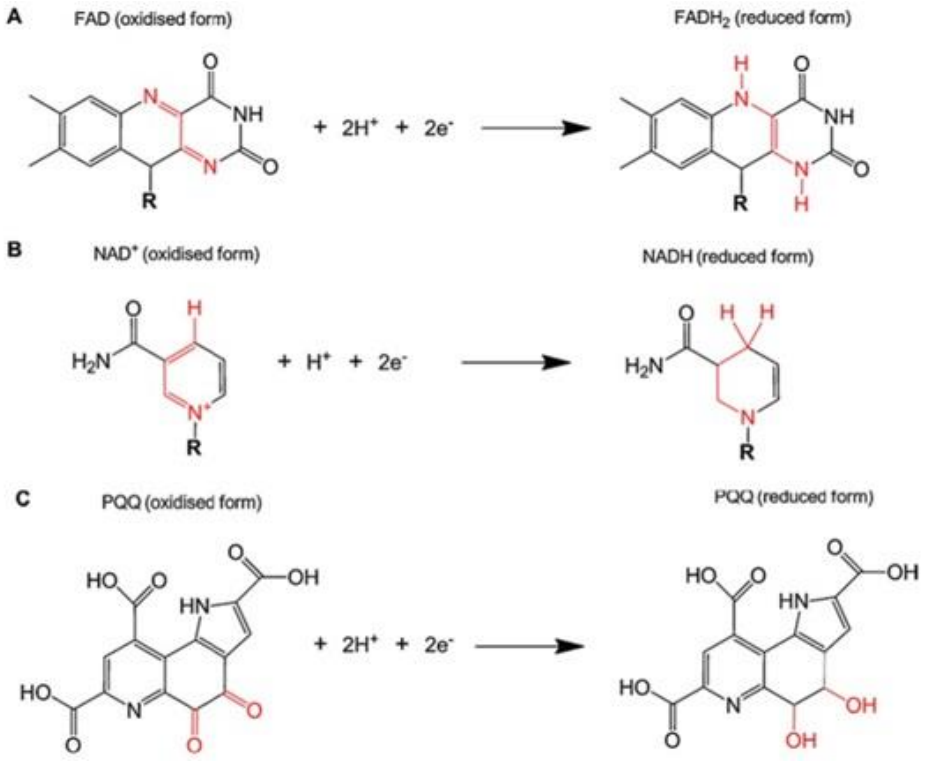

Figure 7: Structure and reaction of the FAD/$FADH_2$ **(A)**, NAD^+/NADH **(B)** and PQQ **(C)** co-factors.

The use of GDH is gaining increased attention as a catalyst for glucose oxidation in biosensing and biofuel cell applications. Unlike GOx, GDH is capable of oxidising glucose without competition from oxygen as electron acceptor, and without producing hydrogen peroxide.

The NAD^+/NADH co-factor is a dinucleotide, because it consists of two nucleotides joined through their phosphate groups. One nucleotide contains an adenine base and the other nicotinamide. Nicotinamide adenine dinucleotide exists in two forms, an oxidised and reduced form abbreviated as NAD^+ and NADH respectively. This cofactor is not directly bound to the enzyme, although its presence is necessary in the bioelectrocatalytic function of the enzyme. The thermodynamic redox potential of NAD^+/NADH is ~ – 0.56 vs Ag/AgCl at neutral pH. However, the NADH co-factor itself is not a useful redox mediator for redox signaling because of the high overpotential and lack of electrochemical reversibility for the NADH/NAD^+ redox process [92] and the interfering adsorption of the cofactor at electrode surfaces. The PQQ co-factor was discovered as the third redox cofactor after nicotinamide and flavin in bacteria, the enzymes containing PQQ are called quinoproteins. The utilisation of electrodes modified with PQQ-dependent GDH as glucose sensors and enzyme anodes has been investigated as a consequence of insensitivity to the presence of oxygen [39]. The PQQ has a high catalytic efficiency and a thermodynamic redox potential of approximately −0.16 V vs Ag/AgCl at pH 7.2 [93] and unlike NAD^+ - dependent GDH, the co-factor is bound to the enzyme [39, 94]. However the use of PQQ-dependent GDH in EFCs may be limited, at present, because of its relative instability when compared to GOx [39]. FAD co-factor in glucose dehydrogenases unlike GOx is insensitive to the presence of oxygen and is typically bound within the enzyme. The structural analysis reveals that the residues predicted to be associated with oxygen sensitivity in GOx are not observed in FADGDH which may account for its oxygen insensitivity [95]. As a result of its oxygen independency, high turnover rate and commercial availability, FAD-dependent GDH is gaining increased attention as a catalyst for glucose oxidation in biosensing and biofuel cell applications [96, 97].

1.5 Enzyme cathodes

In traditional fuel cells, metal catalyst such as platinum are employed to catalyse the oxygen reduction reaction (ORR) at the cathode. Although platinum is a highly efficient catalyst, it is non-specific and prone to poisoning, thereby necessitating the use of a membrane to prevent the migration of fuel to the cathode [90]. Alternatively, naturally occurring enzymes, known as multi-copper oxidases (MCOs), have shown promise as efficient ORR catalysts for the 4 electron reduction of oxygen to water when immobilised at electrode surfaces [98-100]. The utilisation of enzymatic biocatalysts offer substrate selectivity, compared to Pt, in favor of the oxidant over the fuel, eliminate the requirement for compartmentalisation of the anode and cathode, thus allowing miniaturisation. Presently the focus of investigation is on the utilisation of multi-blue-copper oxidases (MBCO), such as bilirubin oxidases and laccases due to their ability to reduce oxygen to water under mild conditions and at relatively high reduction potentials [90, 101-103]. Laccases are copper-containing oxidase enzymes that are isolated from various sources such as plants, fungi, and microorganisms. It was initially studied by Gabriel Bertrand in 1894 in Chinese lacquer tree sap [104], where it serves in the formation of lacquer (hence the name "laccase"). Laccases can be polymeric, and the enzymatically active form can be a dimer or trimer, usually containing four copper atoms per monomer distributed in three redox sites, capable of oxidising a broad range of substrates [105]. Since laccase belongs to the oxidase enzyme family, it requires oxygen as a second substrate for the enzymatic action. The copper active centers are classified into three types depending on their spectroscopic characteristics. Substrate oxidation takes place at a type 1 (T1) single “blue”copper site, where the catalytically produced electrons are then transferred intramolecularly to the oxygen reduction site, ~1.5 nm away. The four-electron reduction of oxygen takes place at the enzyme’s oxygen reduction site consisting of a trinuclear cluster of a type 2 (T2) copper site and a type 3 binuclear (T3) copper sites [106]. Figure 8 shows a representation of the crystal structure of laccase from *Steccherinum ochraceum* [107].

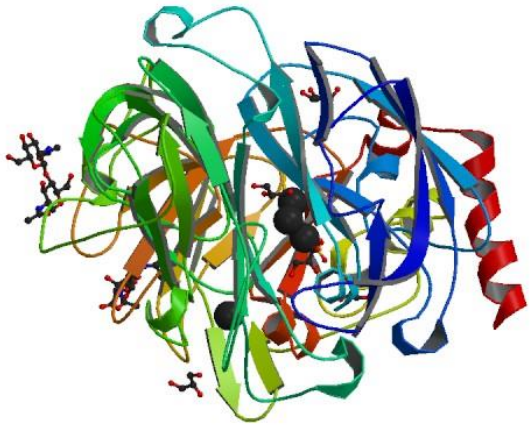

Figure 8: Crystal structure of laccase from *Steccherinum ochraceum.* (PDB ID: 3T6V [248]).

Laccases have been found in prokaryotic and eukaryotic sources of which the T1 copper site standard potential determines the potential at which substrate oxidation is driven [108,109]. Laccases isolated from plants have a low T1 potential of ~ +0.23 V vs Ag/AgCl, whereas T1 potential of fungal laccases range from mid ~ +0.27 V to +0.51 vs Ag/AgCl) or high range (~ +0.58 V vs Ag/AgCl) [110]. High range potential laccases are, however, inhibited by hydroxyl ions and produce maximal activity between pH 4 to pH 5. This inhibition limits their use as cathodes in an EFC operating in physiological conditions [48]. However, application of a laccase sourced from the *Streptomyces coelicolor* bacterium and a laccase sourced from the *Myceliophthora thermophila* fungus has been reported for EFCs operating in physiological conditions [111, 112]. As the focus of this thesis is on the development of EFCs that can operate under physiological conditions as *in vivo*, bilirubin oxidase is selected that operates efficiently under physiological pH conditions. Bilirubin oxidase (BOd) was first discovered and characterised in 1981 by Murao amd Tanaka [113] that catalyses the oxidation of bilirubin to biliverdin, coupled with the reduction of O_2 to water in a four electron reduction process [114]. BOd is a MBCO and belongs to the family of oxidoreductases and similar to Laccases, the enzyme has an active site that consists of a T1 substrate oxidising copper site and a tri-nuclear T2/T3 oxygen-reducing copper site [115]. The T1 copper site standard potential determines the potential at which substrate oxidation is driven that is in a mid-range of ~ + 0.47 V vs. Ag/AgCl

[116, 117]. A *Myrothecium verrucaria* bilirubin oxidase (*Mv*BOd) is the first reported BOd-based oxygen-reducing cathode. The *Mv*BOd, is a monomeric glycoprotein with a molecular mass of 68 kDa and a broad pH activity region of 7 to 11 [118, 119]. Figure 9 shows a representation of the crystal structure of of *Myrothecium verrucaria* bilirubin oxidase [120].

Figure 9: Crystal structure of *Myrothecium verrucaria* bilirubin oxidase. (PDB ID: 2XLL [249]).

The application of *Mv*BOd adsorbed onto carbon felt electrodes with 2,2'-azino-bis (3-ethylbenzothiazoline-6-sulphonic acid) (ABTS) in solution phase using the mediated electron transfer approach for reduction of oxygen in phosphate buffer pH 7.0 was first reported by the Ikeda group [119]. Moreover P. A. Jenkins *et al.* coimmobilised a *Mv*BOd and an osmium redox polymer, prepared by substitution of a Cl ligand of Os(2,2′-bipyridine)$_2$Cl$_2$ with poly(vinylimidazole), ($E^{o'}$=0.22 V vs. Ag/AgCl), and polyoxyethylene bis(glycidyl ether) (PEGE) crosslinker onto the active electrode surface achieving current densities of 6.4×10^{-5} A cm^{-2} in phosphate buffer pH 7.4, 0.15 M NaCl [144]. Steady-state current density of 0.85 mA cm^{-2} for oxygen reduction at potentials of ~ +0.2 V vs Ag/AgCl in oxygen saturated phosphate buffer at pH 7.0 with rotation at 1400 rpm is reported by Tsujimura *et al.* [116] using a direct electron transfer approach. In addition, Mano *et al.* co-immobilised BOd and a different osmium redox polymer, prepared by substitution of a Cl ligand of Os(4,4′-dichloro- 2,2′-bipyridine)$_2$Cl$_2$ with imidazole units of a co-polymer of poly(vinylimidazole) and polyacrylamide, on carbon cloth fibers to yield oxygen reduction current densities of 0.7 mA cm^{-2} and 6.25 mA cm^{-2} respectivlely in non-stirred and 4000 rpm conditions at a potential of +0.3 V vs Ag/AgCl in phosphate buffered saline at 37 °C [123,124].

1.6 Electron transfer mechanisms

Electron transfer (ET) is an elementary process which is governing majority of the electrochemical reactions, biological conversions, photosynthesis and respiration [125, 126] Compared to many chemical reactions, ET undergo without breaking or forming new bonds and happens rather fast. Instead, it is based on readjustments of bond distances and angles in the reaction partners, and rearrangements of the likely configurations of the reaction environment such as solvent molecules around reactants [127]. ET can be described as transfer of electron from donor to acceptor as shown in equation 9.

$$D + A \rightarrow D^{+} + A^{-} \qquad Equation\ [9]$$

All ET reactions can be classified into "inner-sphere" and "outer-sphere" reactions. "outer-sphere" is an electron transfer that takes place between two different chemical reactants with the electrons hopping through the space between donor and acceptor. The "inner-sphere" reactions appear for donor and acceptor which are covalently bound during the reaction [128]. Efficient electrical contact between biomaterials and electrode surface is of significant importance for bioelectronics application. There are many contributing factors for efficient ET such as the distance between the active centre of the redox enzyme and the electrode support. As a result the type of ET can be classified as: 1) direct electron transfer (DET) or 2) mediated electron transfer (MET) as depicted in Figure 10.

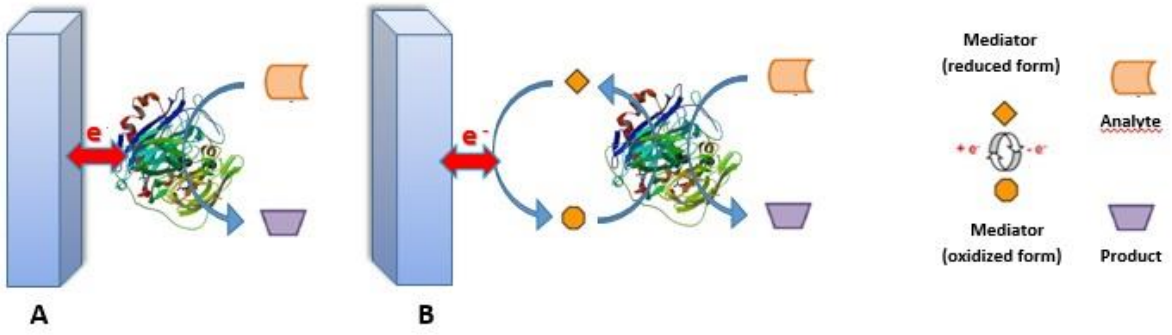

Figure 10: Schematic depicting (A) direct electron transfer and (B) mediated electron transfer oxidation of the substrate between an enzyme active site and an electrode.

For convenience of understanding different ET mechanisms Hill and co-workers roughly divided redox enzymes into three classes: 1) “extrinsic” enzymes with their active centre located in close distance from the surface of protein shell (e.g., cellobiose dehydrogenase) and therefore able to directly communicate with the electrode surface, 2) “extrinsic” enzymes with redox centre located away from the the protein shell (e.g., peroxidases, laccase) but accessible for the other redox site through the internal electron transfer mechanism (IET) and thus indirectly capable of transferring the electrons towards the electrode surface, and 3) “intrinsic” enzymes (diameter 80–150 Å) with their active centre deeply buried within the protein molecule (e.g., glucose oxidase) and thus unable to directly communicate with the electrodes [129,130].

1.6.1 Direct electron transfer

Electronic communication between electrode surfaces and biocatalysts can be achieved by DET. DET is an interesting phenomenon which can be described as an ability of the active centre in redox enzyme to directly communicate with the electrode surface. DET has attracted increasing interest in sense of fundamental understanding of redox processes and practical application for improved performance of biosensors and biofuel cells. Historically, DET was independently discovered in 1977 by two research groups. Eddowes and Hill [131] and Yeh and Kuwana [132] demonstrated reversible electrochemistry for cytochrome *c* – a small first class “extrinsic” protein on gold and tin-doped indium oxide electrodes, respectively. So far only a few redox enzymes containing metallocentres were reported to be capable of DET and showed catalytic response in the presence of the substrate [133]. Various factors are to be considered when using this approach, such as the thickness of the protein shell surrounding the redox centers of the enzyme and the requirement of correct enzyme orientation at electrodes for efficient electron transfer kinetics [87, 134]. For efficient DET, a majority of the publications focuses on modification of the electrode surface by carbon nanotubes, gold or silica nanoparticles or self-assembled monolayers (SAM) meant to increase the surface area and connection with the active centre of the enzyme [135-137]. In other reports, efficient DET is accomplished by decreasing the distance between the active centre of the enzyme and electrode surface by complete or partial removal of the glycan shell surrounding the protein peptide chain of glycosylated redox enzymes [138-140]. Compared to MET, current densities achieved by

DET are often quite low and therefore it is necessary in most cases to introduce an electron transfer mediator to shuttle electrons between the electrode and the redox active sites in the enzyme.

1.6.2 Mediated electron transfer

For most "intrinsic" enzymes establishing DET between the active center and the electrode support is a difficult task to attain. The main reason is due to the deeply buried active center of the enzyme and the space separation between the donor and the acceptor. Limitations associated with extracting efficient DET for electrically insulated enzymes can be overcome by utilising mediators – small molecules capable of diffusing in and out of enzyme's redox center and shuttling electrons to/from the electrode surface. In order to function properly a mediator should be able to operate under a number of constrains including: 1) reversible electrochemistry, 2) stability in both oxidised and reduced form, 3) fast reaction with the enzyme, 4) thermodynamically favourable $E^{o\prime}$ close to the $E^{o\prime}$ of redox enzyme, 5) nonreactivity towards oxygen, and 6) nontoxicity for *in vivo* applications [141]. With the growing demand of measuring glucose levels in diabetic patients, development of various mediation approaches started in early 70s. A very first device for measuring glucose in blood was developed by Clarks in 1962 with the introduction of the first generation of biosensors. The device measured glucose concentration in blood in connection to concentration of oxygen [142] or hydrogen peroxide produced in enzymatic reaction [143]. However the device suffered from a number of disadvantages such as high applied potential required for reduction of H_2O_2 at which many other compound present in biological liquid can be oxidised, variation of ambient oxygen concentration, and destructive effect of H_2O_2 on enzyme molecule. To eliminate all the above problems, Cass *et al.* introduced the second generation of biosensors developed by replacing oxygen with soluble mediator such as ferrocene [144]. Practical application of soluble mediator for *in vivo* measurements however was still restricted by potential toxicity associated with the leakage of the mediators into the surrounding environment. That led to a further development in the field of MET with the major breakthrough made by Heller and co-workers who proposed to incorporate soluble mediators into the protein molecules by covalent binding or coordination

[145-147]. The concept was further improved by introduction of redox hydrogels (or redox polymers and complexes) which have been extensively used in the present work.

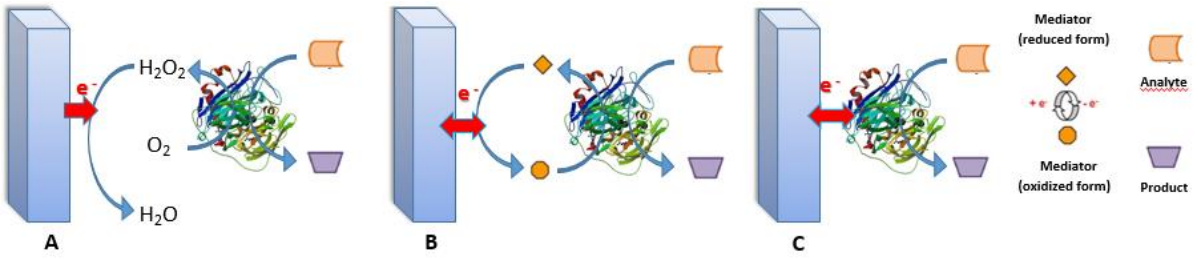

Figure 11. Three generations of amperometric biosensors. A) 1st generation, B) 2nd generation, C) 3rd generation.

In enzyme electrode technology mediators are preferably chemically stable in both oxidised and reduced states, which is important to permit continuous participation in the electrocatalytic cycle.Mediator redox potential plays a significant role in the operational cell voltage of an EFC, hence tailoring the design of such mediators is critical. Ideally for thermodynamically favourable conditions, the mediator potential should be slightly positive in the case of anode and negative in the case of cathode compared to the redox potential of the enzyme active site [148]. For an efficient MET, the redox potential of mediators are reported to require an approximately 50 mV potential thermodynamically downhill from the redox potential of enzyme [150, 151]. The osmium based polypyridyl redox complexes display redox potentials spanning a wider range in comparison to that observed for ferrocene derivatives. The osmium-based redox complexes are relatively stable in both reduced Os(II) and oxidised Os(III) states for redox cycling and the rapid self-exchange rate constants compared to other metal based mediators [152, 153]. In addition, the redox potentials of the Os(II/III) transition in osmium based polypyridyl complexes can be tuned through selection of, and chemical modification of the ligands attached to the osmium metal center [154], making them suitable as mediators for utilisation in both anodes and cathodes, for biofuel cell applications [18].

1.7 Osmium redox mediators

1.7.1 Polyvinyl-imidazole based osmium redox polymers

In 1990 Forster and Vos developed the polyvinyl-imidazole (PVI)-bound osmium bipyridine series of redox polymers [21] as illustrated in Figure 12. Redox polymers consist of redox center, which is formed by the metal ion of 8th group (osmium or ruthenium) complexes with a ligand (2, 2'-bipyridine), and covalently bound to a water-soluble polymer backbone (poly (vinylpyridine), poly (vinylimidazole) or poly-4-aminostyrene). The ET in redox hydrogels is believed to occur by outer-sphere self-exchange mechanism where the electrons are moved between the rapidly reduced and rapidly oxidised redox centers tethered to a cross-linked polymer backbone [155]. The diffusion of the electrons through the polymer matrix is a rate limiting step in overall ET reaction and can be increased by introducing long flexible spacers between the polymer backbone redox centers, as demonstrated by Mao *et al.* [156].

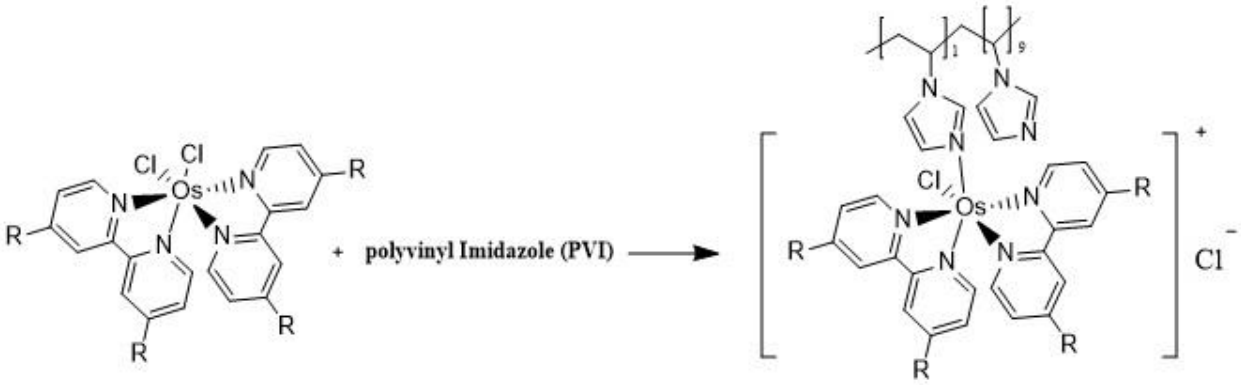

Figure 12: Gerenal structure of Os-bound polyvinylimidazole redox polymers formed by the coordination of osmium "starting complex" cis-[Os(N-N)$_2$Cl$_2$] to polyvinylimidazole (PVI) in a ratio that is usually 1:9.

Redox polymers possess a number of properties which make them exceptionally attractive for use in MET. A polymer-bound mediator provides for greater structural stability of the enzyme electrode, In addition, the adsorption of a redox polymer-bound mediator on an enzyme electrode allows control over the electroactive nature of an electrode and can prevent oxidation and/or reduction of other species at the electrode. Another advantage for application of redox polymers as mediators is their exceptional versatility in terms of $E^{o\prime}$ which can be tuned by the

ligand exchange and/or introduction of functional groups on the bipyridyl ligands [20, 21] The Os-bound polyvinylimidazole complexes exhibit different $E^{o\prime}$ defined by the electron donating/accepting group in 4,4'-position of 2,2'-bipyridine ligand of the polymer utilised. The three-dimensional nature of redox hydrogels and their tunable $E^{o\prime}$ led to a large improvement in the effective number of enzymes that could be electronically linked to the electrode surface [157, 158]. In electrode preparation procedures, redox polymers and enzymes are crosslinked using homobifunctional crosslinkers, resulting in a matrix of an enzyme-containing redox hydrogel on the electrode surface. In the early 1990s Gregg *et al.* developed an approach to entrap enzymes and mediators on electrode surfaces using epoxide cross-linkers, forming a three dimensional matrix redox hydrogel [159]. Such hydrogels swell in aqueous solutions and allow for the facile diffusion of substrates and ions through the films while they do not leach mediator molecules into the surrounding environment which makes them applicable for *in vivo* purposes [160]. Redox hydrogels are capable of electrically wiring the enzyme's active centers to electrodes irrespective of the spatial orientation of the enzyme at the electrode surface and also connect multiple enzyme layers through MET. In the present study redox polymers were used for bioelectrochemical characterisation of BOd (chapter 4) and oxidoreductases (chapter 5). However the lack of commercial availability of PVI is a difficulty with the use of PVI as the polymer backbone for the preparation of redox polymers. Furthermore, the laboratory-scale synthesis of PVI involves bulk free radical polymerisation which leads to broad molecular weight distribution that affects the physical properties of redox polymers such as solubility and density [154]. To address these issues, Allen *et. al.* Recently reported on controlled radical polymerisation of *N*-vinylimidazole to produce mono-disperse homo-polymer [161].

1.7.2 Osmium polypyridyl complexes

Tetherable osmium polypyridyl redox complexes have been found to be effective mediators due to their stability to Os(II/III) transition states and rapid self-exchange constants [152, 153] and thus have a wide range of applications such as in research and development of biosensors and EFC electrodes. The starting osmium $[Os(N\text{-}N)_2Cl_2]$ complexes can be prepared by using a bidentate, mostly bipyridine-based ligand according to literature methods [20, 6]. The alternation of the 4 and 4′ positions of the bipyridine ligand attached to osmium metal center

with the electron accepting or electron withdrawing groups can tune the potential accordingly. The functional groups present in these complexes also enables them to easily anchor to the surface of electrodes or to the backbone of several different polymers. Consequently, a library of osmium based metal complexes with different functional groups and redox potentials could be created and potentially used as mediator for a variety of different enzymes. Rakesh Kumar *et al*. reported on direct grafting of osmium based redox complex with alkylamine functional group to glassy carbon surface by simple electro-oxidation methodology [162]. This process provides a simple route to prepare a monolayer of redox active complex on surfaces, however, a glucose oxidation current density of only 7 μA cm^{-2} was obtained which is due to the low amount of osmium redox centres at the surface to wire with biocatalyst. Therefore, in order to enhance the glucose oxidation current density for application as an anode in EFC, an alternative approach is used to form multiple layers of osmium complex and biocatalyst on the electrode surfaces as reported by Rakesh Kumar *et al.* [163]. Redox complexes and biocatalysts possessing amine functionality can be coupled to carboxylic acid functional groups of polymers via carbodiimide reagent, which offers greater versatility in preparation of multilayered films, as described in Chapter 3.

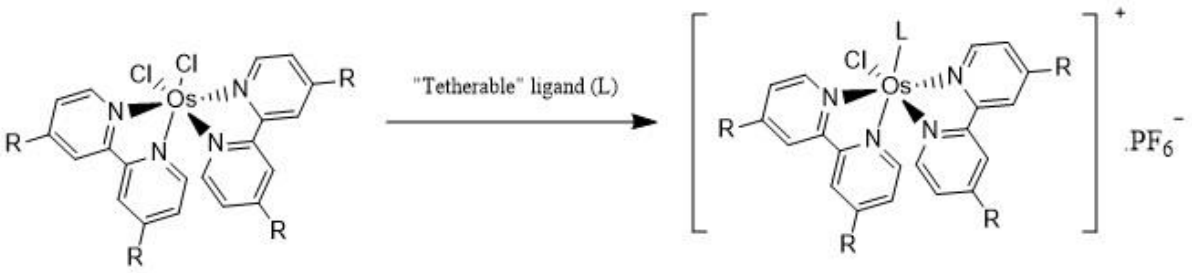

Figure 13: Structure of the "starting complex" [Os(2,2′-bipyridine)2Cl2] and tetherable osmium redox complexes formed by ligand substitution reaction.

1.8 Nanomaterials in enzyme electrodes

A wide variety of nanomaterials, especially nanoparticles with different properties have found broad application in many fields such as biosensors and biofuel cells. Incorporation of conductive nanomaterials within enzyme-containing films on electrodes may substantially

enhance current densities, due to improved surface area and/or electrical connections, and signal stability as reported on by many research groups in recent years. For example, reports have shown that addition of carbon micro-, meso- and nanostructured materials to enzymatic electrodes show improved current signal over those prepared without addition of such materials [48-165]. Addition of multi-walled carbon nanotubes (MWCNT) to the enzyme electrode preparation step results in increased surface area, improved operational output and stability under pseudo physiological conditions [166]. These nanostructures provide a support which acts as a scaffold for improved retention of enzymes and electron-shuttling mediators as reported on by many research groups in recent years [85, 14]. For example, recent studies have shown that the high electrical conductivity of CNTs promote electron transfer from proteins to electrode surfaces [167-171] as reported in chapter 3 of this thesis. In chapter 4, the fabrication and characterisation of a membrane-less glucose-O_2 EFC is described using a combination of an *Mv*BOd/osmium redox polymers/MWCNT-based enzyme electrode for oxygen reduction as a cathode, with glucose-oxidising anodes assembled from FADGDH as the enzyme, osmium redox complex as mediator and including MWCNT as support. CNTs are graphene sheets that are rolled up to form tubular structures. There are two basic types of CNTs, namely single-wall carbon nanotubes (SWCNTs) and multi-wall carbon nanotubes. SWCNTs consist of a single graphene sheet that is rolled up, whereas MWCNT consist of multiple rolled layers of tubes of graphene. The conductivity of CNTs is proportional to the number of carbon nanotube layers thus making MWCNT more conductive than SWCNTs [172]. The inclusion of other nanoparticles such as gold nanoparticles (AuNP) to enzyme electrodes also improves electrical contact between enzyme and electrode, displaying increased current and stability compared to planar electrodes [173,174]. Forexample, Fan *et al.* reported on the anodes decorated with Au nanoparticles produced current densities up to 20-fold higher than plain graphite anodes by *Shewanella oneidensis*. The Au decorated anodes generated a maximum current density ranging from 10.7 to 74.4 $\mu A/cm^2$, which was 2–20 times higher than the plain graphite anodes [175]. In another study conducted by German *et al.* shows that the application of Au-NPs increases the rate of mediated electron transfer [176].

1.9 Immobilisation strategies

For the ideal operation of EFCs, a major obstacle that has to be addressed is the leaching and the stability of the enzymes and redox mediators on the electrode surfaces in order to extend the EFC operational life-time [1]. One approach to resolve this issue is through effective immobilisation of the enzyme and other components on a solid surface. The effective immobilisation of enzyme at the electrode is necessary to develop a favourable environment for maintaining enzyme activity and thereby extending stability. There are a wide variety of immobilisation strategies such as simple physical adsorption, entrapment in polymeric or inorganic gels, covalent attachment and cross-linking [84] to name a few. The immobilisation approach can often be a combination of these and generally, multilayers or other three-dimensional (3D) structures tend to favor over monolayer configurations in order to increase current output, and provide suitable immobilisation matrices for enzymes to retain their activity. A traditional chemical immobilisation method is the coupling of the enzyme to polymer support [177, 178]. The biocatalysts are bonded to the surface of electrodes or support through functional groups that are not essential for their catalytic activity. Bifunctional reagents such as poly (ethylene glycol) diglycidyl ether (PEGDGE) and glutaraldehyde (Glut) or coupling chemicals such as carbodiimides are used to couple enzymes to the electrode/support. For example, Gregg and Heller developed a technique using PEGDGE (Figure 14) as a cross-linker to create a redox hydrogel to entrap enzyme and mediators in films [159]. In addition, Ohara *et al.* demonstrated the use of PEGDGE di-epoxide crosslinker to coimmobilise an osmium redox polymer and GOx on electrode surfaces. This study showed that the redox hydrogels were permeable to glucose and allowed diffusion of electrons [179].

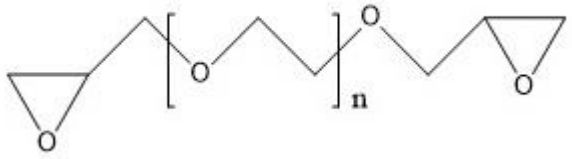

Figure 14: Structure of PEGDGE cross-linker.

The enzyme-mediator films are made by cross-linking the amine groups of the enzyme with the imidazole in a polymer backbone using poly (ethylene glycol) diglycidyl ether (PEGDGE) as illustrated in Figure 15 [152].

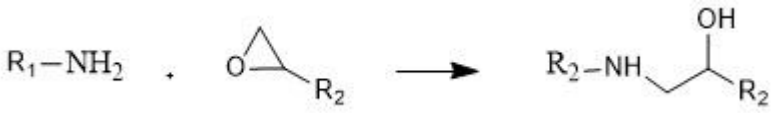

Figure 15: General reaction of PEGDGE with amine groups of the enzyme.

De Lumley-Woodyear *et al.* [180] compared PEGDGE crosslinking to that using suberic acid bis(N-hydroxysuccinimide ester), dimethyl suberimidate or glutaraldehyde (Glut) (Figure 16) in solution for co-immobilisation of enzyme with redox-polymer mediators. Although glutaraldehyde had a considerable negative effect on the resulting current density as compared to the current densities observed for the electrodes prepared using other crosslinkers, the application of Glut vapours as a crosslinking agent has proved to be effective for enzyme immobilisation [181-183], thus providing an alternate methodology to the di-epoxide solid-phase or Glut solution phase crosslinking reaction. Crosslinking occurs between the aldehydes in Glut and the amine groups of the enzymes.

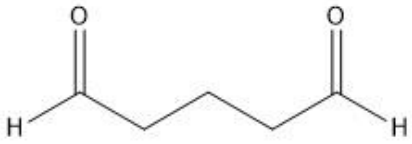

Figure 16: Structure of glutaraldehyde cross linker.

The carbodiimide coupling is widely used to develop enzymatic sensors [184-187]. The water-soluble carbodiimide reagent N-(3-dimethylaminopropyl) -N´-ethylcarbodiimide (EDC) couples carboxyl groups to amino functions. To increase the coupling efficiency, EDC is frequently used with an N-hydroxysuccinimide (NHS) reagent in order to stabilise the activated ester formed as an intermediate from the carboxylic acid by EDC as illustrated in Figure 17.

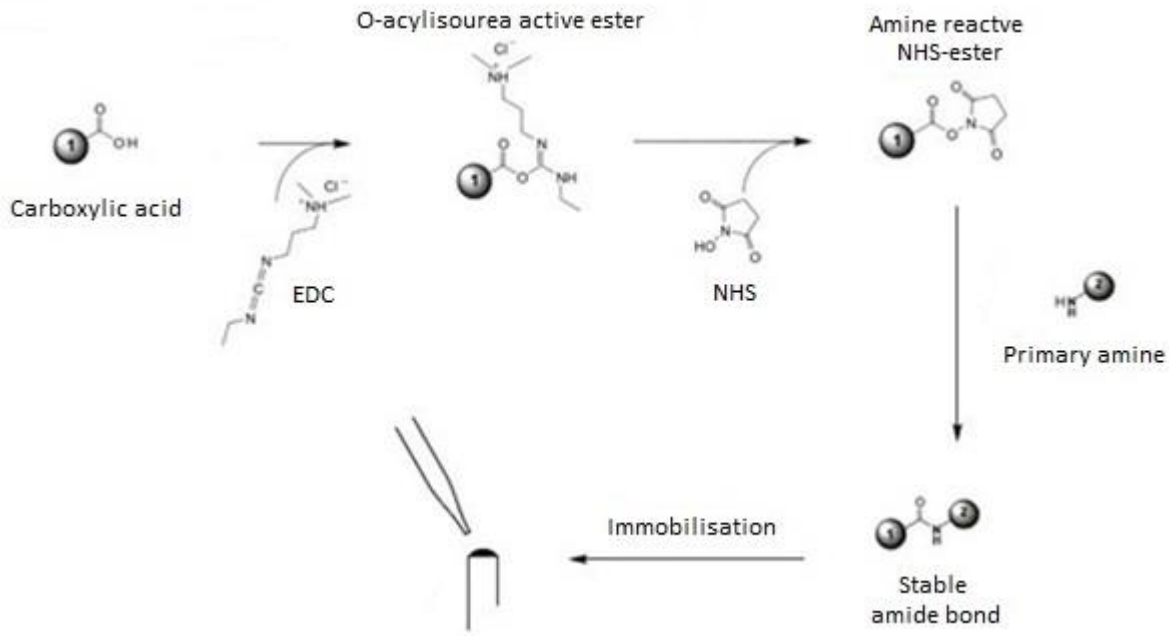

Figure 17: Immobilisation techniques with polymer bearing carboxylic functional group, as chemical support with amine-containing osmium redox complexes and enzyme (GOx) by EDC/NHS coupling where 1 is either the acid treated MWCNT or Carboxymethyl-dextran (CMD) and 2 is the redox mediator or the enzyme.

The use of an EDC/NHS coupling technique to crosslink enzyme and redox mediators in a polymer matrix, together with nanostructured CNT support, is reported in chapters 3 and 5. Chapter 5 of the thesis examines the effect of pH on immobilisation of redox complexes and enzymes in three-dimensional films at electrode surfaces.

1.10 Design of experiments

Design of experiment (DoE) is a systematic method to determine the relationship between factors affecting a process and the output of that process. In general, scientists are interested to determine the statistical significance of an effect that a particular factor exerts on the dependent variable of interest [188,189], but often each factor is evaluated by isolation, keeping all other factors constant. This experimental approach is termed one-factor-at-a-time (OFAT), however

OFAT is extremely time-consuming and is based on a trial-and-error method. Instead, design of experiment offers a more efficient type of experiment which considers all variables simultaneously leading to more effective improvements [190]. DoE provides a structure to experimental planning so that the data obtained can be analysed to yield valid and objective conclusions [191, 192]. After the execution of a purposefully designed experiment, cause-and-effect relationships in a process or system, between experimental output and experimental factors, are established. DoE is widely used in research as well as industrial settings for solving scientific and engineering problems [193-195]. For example Babanova *et al.* reported on a DoE approach for optimisation of the performance of an air-breathing bilirubin oxidase-based EFC cathode [196]. More recently Kumar and Leech reported on a design of experiment methodology to investigate and improve the performance of glucose oxidising enzyme electrodes. According to the report, components used to construct enzyme electrodes were optimised and validated using DoE, with a resulting glucose oxidation current density of 1.2 ± 0.1 mA cm^{-2} in PBS, significantly higher by 32% than the previously observed current density for enzyme electrodes optimised by varying one factor at a time. Therefore the application of DoE is useful for the optimisation of component amounts in enzyme electrodes for application to EFCs [197]. The initial step of the DoE approach begins with determining the objective of an experiment and selecting the process variables (factors) and the range over which each factor varies. It is desirable to identify all the important factors that may significantly influence the response variable (Output). The number of levels or range of each factor depends on types of experiment considered. Then depending on the number of factors and the number of levels in each factor, experimental design defines a total number of experimental runs. The next step involves running experiments to collect the raw data from the DoE designed experiment. Subsequently different statistical methods are used to analyse the data, for instance identifying the relative importance of each factor by numerical score using analysis of variance (ANOVA) method, estimating the regression coefficients in the model and validating the accuracy of model. Once the data analysis is completed, the conclusions about the experiment can be drawn [198, 199].

Response Surface Methodology (RSM) can be used to generate sufficient experimental design to understand and optimise desired response based on the combination of statistical and optimisation methods after one has determined important factors. The output is a mathematical

equation that attempts to fit an empirical model to the data collected in the experiment [200]. The input variables for the experiment are called factors and the measured outcome of the experiment are called responses. The experimental output, *y*, may be described by the following equation in relation to the experimental factors:

$$y = f(x_1, x_2, \dots, x_n) + \varepsilon \qquad \textit{Equation [10]}$$

Where ε is experimental error, and thereby implies that the functional relationship between the chosen experimental factors (x_1, x_2,…,x_n) and *y* may not be fully explained [201]. Figure 18 shows a model of a typical process. The process explains a system, either a chemical reaction or manufacturing process, with all associated variables that changes the input into an output that has one or more predicted response. Process variables and material properties are either controllable (x_1, x_2,…,x_n), or uncontrollable (z_1, z_2,…,z_n).

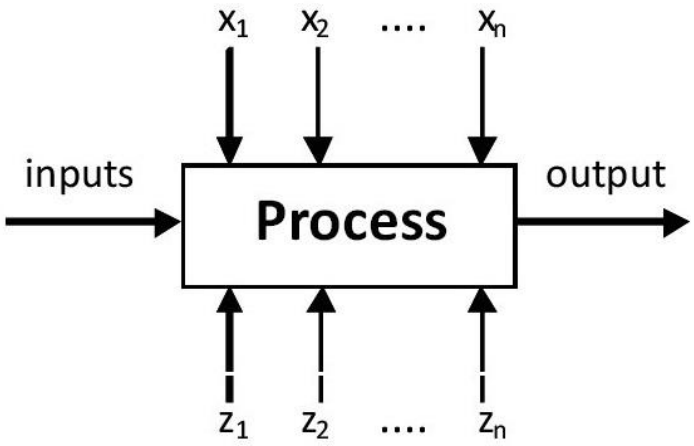

Figure 18: A model of a process or system.

In the DoE, it is important to recognise the uncontrollable and controllable input factors in order to understand how they may influence the response variable. Uncontrollable input factors (*z*) are those parameters that cannot be changed while controllable input factors (*x*) are those input parameters that can be modified in an experiment or process. Responses, or output measures, are the elements of the process outcome that gage the desired effect. When designing an

experiment, the initial step is recognition of the knowledge gap or problem in the process that needs to be solved [201]. Most commonly used response surface designs are the central composite design, Box-Behnken design and D-optimal design [202, 203]. The Box-Behnken Design (BBD) is a rotatable second order design based on a three-level factorial design and used to evaluate the interaction effects of components. BBD offers some advantage in that it requires a fewer number of runs in comparison to central composite design that can fit a full quadratic model [201]. BBD is less expensive to run in comparison to central composite design with the same number of factors and can efficiently estimate the first- and second-order coefficients. The Box-Behnken design requires an experiment number according to $N = 2k\ (k-1) + C_0$, [204] where k is the number of factors, and C_0 is the number of central points. The Box-Behnken design is a spherical, revolving design viewed as a cube as illustrated in Figure 19, where the experimental combinations are at the midpoints of edges of the process space and at the center.

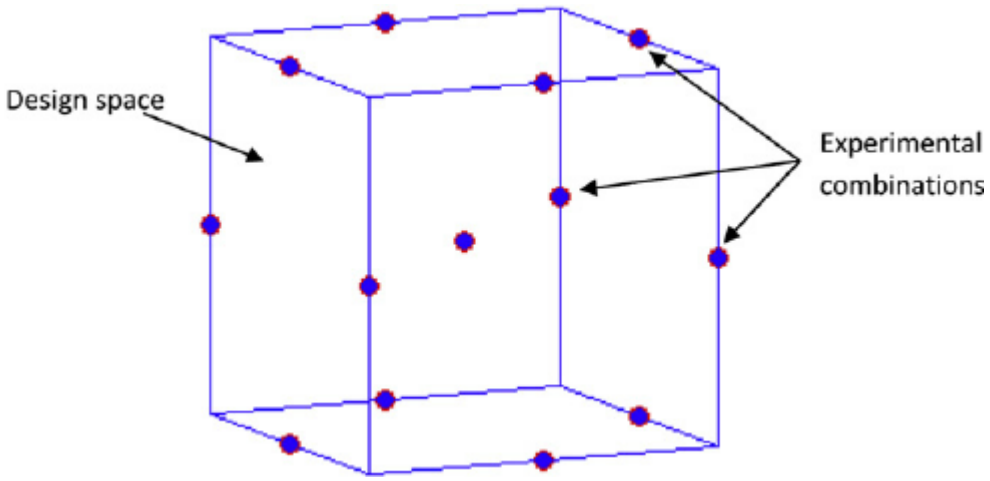

Figure 19: A Box-Behnken design for three factors.

The geometry of this design suggests a sphere within the process space such that the surface of the sphere protrudes through each face with the surface of the sphere tangential to the midpoint of each edge of the space. Chapter 4 of this thesis focuses on the use of DoE for the optimisation of the component amounts in preparation of an oxygen reducing biocathode enzyme electrode.

1.11 Electrochemical methods

Measurement of electrical quantities such as current, potential or charge and their relationship to chemical parameters forms a group of electrochemical techniques which combine the field of electricity with the field of chemistry. Such an interrelation provides a variety of useful applications [205, 206]. Depending on the type of electrochemical signal which is measured, all electrochemical techniques can be divided into two groups: potentiometric (zero-current) and potentiostatic or controlled-potential (non-zero current). The most widely used potentiometric applications are pH measurements or ion selective electrodes. The potentiostatic technique includes cyclic voltammetry (CV), chronoamperometry (CA) and CA in combination with flow injection analysis (FIA). Both of the techniques require at least two electrodes (conductors) and analyte solution (electrolyte) which forms an electrochemical cell. One of the electrode termed as working electrode (WE) where the reaction of interest occurs, the other one, termed as reference electrode (RE), has a constant potential independent of the properties of the solution. In practice three-electrode setup is more common. In this configuration, the potential of the WE is still monitored relative to the reference potential; however, the current passes between the working electrode and a separate auxiliary (counter) electrode (CE). Since no (or little) current passes to the reference electrode, it can maintain its potential [207]. Working electrodes are generally made of relatively electrochemically inert carbon such as glassy carbon and graphite or inert metals such as platinum and gold. The reference electrode utilised is usually the silver/silver chloride (Ag/AgCl) electrode or a saturated calomel electrode (SCE). A platinum wire is normally used as the counter electrode to measure the current at the working electrode. The basic reaction which underlies electrochemical process can be described as in equation 11.

$$Ox + ne^{-} = Red \qquad Equation\,[11]$$

Where Ox is the oxidised species, Red is the reduced species, and n is the number of electrons exchanged between Ox and Red. The potential of the electrochemical cell can be correlated

with the concentrations of the electroactive species through the Nernst equation as in Equation 12.

$$E = E^{o\prime} + \frac{RT}{nF} ln \frac{[Ox]}{[Red]} \qquad Equation\ [12]$$

where $E^{o\prime}$ is the formal potential of the redox reaction, R is the universal gas constant (8.3145 J mol^{-1} K^{-1}), n is a number of electrons involved in the reaction, F is Faraday's constant (96485.3 C mol^{-1}) and T is the temperature measured in Kelvin. The following section would focus on the voltammetry and amperometry techniques that are extensively used in this thesis.

1.11.1 Voltammetric and amperometric technique

Cyclic voltammetry (CV) belongs to the class of potentiostatic techniques which is the most widely used technique to study the electrochemical reaction mechanism and in acquiring qualitative information about the response. Cyclic voltammetry involves applying a linearly varying electrode potential, cycled between two limits, (V_1 and V_2) to the working electrode (WE), versus a reference electrode (RE), at a particular rate (scan rate) and recording the current versus potential [208], the potential serves as a controlled parameter utilised for derivation of the electron transfer. Shifting the potential into positive or negative directions forces the electroactive species to gain or lose electrons and generates the current flow either from or towards the working electrode. Resulting current indicates the rate at which the electrons are transported across the electrode-solution interface. At the WE, the electrons are transferred between reactant and electrode surface. The potential starts to scan from V_1 and reaches V_2, and then the scan is reversed back to V_1. In a first half-cycle, the potential applied to the WE is increased and the Red species become oxidised, starting at the applied potential higher than $E^{o\prime}$ of the redox couple involved in the reaction. This involves the diffusion of Red species from the bulk solution to the WE's surface and the transfer of electrons to the electrode surface and subsequently the production of the anodic current (I_{pa}). Switching potential into negative direction results in (re)reduction of the Ox species and production of the cathodic current (I_{pc}). Two waves plotted against the applied potential forms a vomtammogram. In a typical CV, the

potential waveform is triangular; if we consider a redox couple ($Fe^{2+/}Fe^{3+}$) then the following CV will represent its electrochemical properties (Figure 20 B).

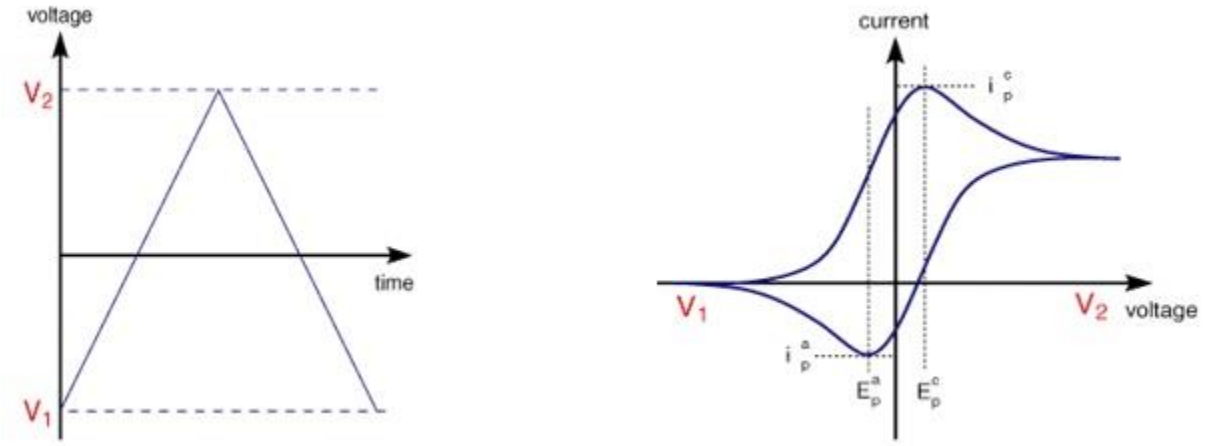

Figure 20: A graphical presentation of a CV. The potential waveform (A) and A typical cyclic voltammogram for a reversible redox couple showing parameters, the anodic peak potential and current (E_{pa} and i_{pa}) and the cathodic peak potential and current (E_{pc} and i_{pc}) (B).

An electrochemically reversible reaction is where the reaction kinetics are fast and the current is limited by the diffusion of Ox and Red to or from the electrode. The potential at which the peak current is reached its maximum value is called the peak potential. The peak potentials at maximum anodic current and maximum cathodic current are referred to as E_{pa} and E_{pc}, respectively. From voltammogram an estimation of reaction reversibility can be made by analysing the difference in peak potentials (ΔE_p). For an electrochemical reversible reaction, ΔE_p does not change with scan rate [209].

$$\Delta E_p = E_{pa} - E_{pc} = \frac{59}{n} mV \ [at\ 298\ K] \qquad Equation\ 12$$

For a system that is not reversible, electron transfer becomes the rate determining step and the Nernstian equilibrium is not maintained, i.e. the peak to peak separation is greater than $\frac{59}{n}$ mV and increases with increasing scan rate. In addition the ratio of the anodic peak current (i_{pa}) and

the cathodic peak current (i_{pc}) for an electrochemically reversible reaction is equal to one as in equation 13.

$$\frac{i_{pa}}{i_{pc}} = 1 \qquad Equation\ [13]$$

Whereas for a quasireversible and an irreversible reaction ΔE_p changes with an increased scan rate. The formal redox potential ($E^{0'}$) of a redox couple is determined by averaging the E_{pa} and E_{pc} as in equation 14.

$$E^{o\prime} = \frac{E_{pa} + E_{pc}}{2} \qquad Equation\ [14]$$

In a diffusion controlled reversible system, the peak current depends not only on the analyte concentration and diffusion coefficient but also on scan rate as expressed by the Randles-Sevčik equation as in equation 15 [210].

$$i_p = 0.4463\ n\ F \sqrt{\frac{nF}{RT}}\ AD^{1/2}Cv^{1/2} \qquad Equation\ [15]$$

Where n is the number of moles of electrons being transferred, A is the area of working electrode (cm^2), D is the diffusion coefficient of analyte ($cm^2\ s^{-1}$), C is the analyte concentration (mol cm^{-3}) and v is the scan rate ($V\ s^{-1}$). The symbols within $nFRT$ have their regular values stated above. Therefore, peak current increases linearly as a function of the square root of the scan rate of a reversible system.

$$i_p \propto i_c \propto \sqrt{v} \qquad Equation\ [16]$$

When the solution is at 25 °C equation 15 can be expressed as in equation 17.

$$i_p = (2.69 \times 10^5)n^{3/2}AD^{1/2}C^{1/2}V^{1/2} \qquad Equation\ [17]$$

The CV is said to show irreversible or quasi-reversible behavior if the rate of electron transfer is slow relative to the scan rate. A plot of *ip* and $v^{1/2}$ should be linear and pass through origin and thus the diffusion coefficient (*D*) can be calculated from the slope as in equation 18.

$$D = \frac{(Slope)^2}{n^3(2.69 \times 10^5 AC)^2} \qquad Equation\ [18]$$

However, if the redox species are adsorbed or immobilised on the surface of the working electrode, the diffusion coefficient will no longer control i_p. In this situation i_p vary linearly with scan rate rather than $v^{1/2}$ for scan rates less than 20 mVs^{-1}, indicative of a surface-controlled response and the peak current would be proportional to the surface coverage (Γ) [211] as in equation 19.

$$i_p = \frac{n^2F^2\Gamma Av}{4RT} \qquad Equation\ [19]$$

At higher scan rates, the peak currents scale linearly with the square root of scan rate, indicative of semi-infinite diffusion control of the response, as expected for multi-layered films on electrodes. An estimate of concentration of electronically addressed redox sites by the electrode is characterised as a surface coverage (Γ, in moles/cm^2) for confined species, and can be calculated from the integration of the Faradaic charge (*Q*) passed, usually under conditions of slow scan rate voltammetry.

$$\Gamma = \frac{Q}{nFA} \qquad Equation\ [20]$$

Where *Q* is the electrical charge involved in the reaction.

1.11.2 Amperometric flow-injection analysis

Amperometric flow-injection analysis belongs to the class of potentiostatic techniques where a constant potential is applied at the WE against the reference electrode and the current produced by electroactive species which is either adsorbed or bound to the electrode surface is measured with time. The applied potential of the working electrode is selected from CV measurement, where the $E^{o\prime}$of the redox couple is determined. For oxidation reactions a potential more positive than the $E^{o\prime}$of the electroactive couple is applied (E_{app}) and vice versa. To control the mass transfer of the analyte either to or from the electrode, two strategies can be considered. Either by moving the electrode with respect to the electrolyte, i.e., rotating disk electrode, where an electrode moves during the experiment to induce the flux of analyte to the electrode. Or in flow conditions where the solution is forced to pass the stationary electrode, e.g., in the wall-jet configuration where the electrolyte flows to the electrode by means of a pump [212]. For this thesis, amperometric flow-injection measurements utilising wall-jet type electrochemical cell was used in chapter 5 which will be described in details here. In 1975, Ruzicka and Hansen pioneered the idea of flow analysis based on injecting the samples into a rapidly flowing carrier [213]. The technique was named flow-injection analysis (FIA) and the influence of tubing length, tubing diameter, peak height, sampling rate and sample volume onto the detector response were carefully analysed [214]. FIA is based on the injection of a liquid sample into a moving, non-segmented continuous carrier stream of an electrolyte. FIA has been extensively used in different electro-analytical applications in agriculture, food industry, biochemical, clinical and environmental analysis due to the fact that compared to the stationary batch systems, FIA has an advantage of rapid solution exchange and an ability to perform on-line monitoring [215]. A demonstration of the FIA system is depicted in Figure 21.

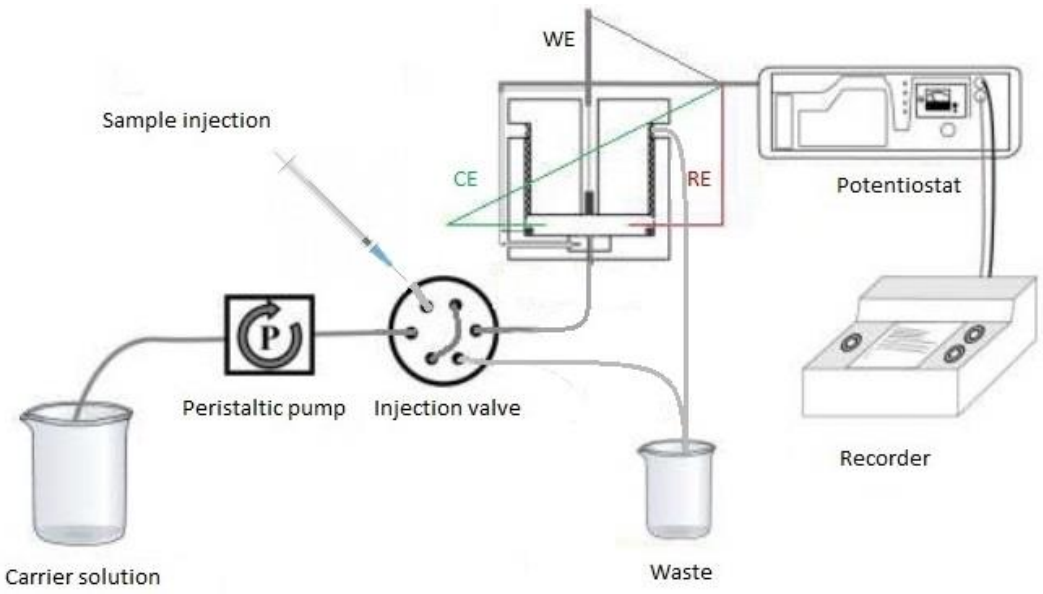

Figure 21: Flow-injection setup with wall-jet type amperometric electrochemical cell.

Combination of FIA with electrochemical detection gave a rise to hydrodynamic voltammetric techniques. Wall jet electrochemical cell inserted into a FIA system is one of the most commonly utilised setup in electrochemical experiments. The term "wall jet" was first introduced by Glauert to describe the flow due to a jet of fluid which spreads over the plane surface [216]. The cell, consist of two Plexiglas halves which can be screwed together in order to adjust the distance between the working electrode and the inlet. The WE usually consists of a graphite rod which is inserted into a Teflon holder so that only the circular surface is exposed to the solution. It is placed into the upper Plexiglas part, mounted onto the FIA system and brought into a close proximity to inlet (typically, 1-2 mm). The lower Plexiglas part is uncirculated with the Pt wire which serves as a counter electrode. The cell is supplied with the lower chamber filled up with 0.1 M KCl where the reference Ag/AgCl electrode is located. The carrier is transferred through the cell by a peristaltic pump and a sample is introduced as a plug through the six-way injection valve. The injection of the sample material in a carrier flow results in formation of the characteristic asymmetric peak with the height proportional to the analyte concentration (Figure 21). Each FIA system is characterised by a certain dispersion coefficient (D) which is defined as a ratio of the signal obtained from the undispersed and dispersed analyte. In practice dispersion coefficient can be calculated with the help of ferro/ferricyanide redox couple as a ratio of steady-state current measured when the sample is continuously pumped

through the system (I_{ss}) and peak current when the sample is injected as a plug (I_p) [217]. By knowing D true correlation between the concentration of the analyte and the detector signal can be maintained.

$$D = \frac{I_{ss}}{I_p} \quad (D \geq 1) \qquad Equation\ [21]$$

Using FIA has many advantages such as it is fast, precise, accurate, requires a low volume of sample for analysis, offers the possibility to control any drift in the background current of the WE with time, highly reproducible and tremendously versatile, simple in operation, cheap and with a low signal to noise ratio [218].

1.12 The effect of crosslinking on anti-calcification of bovine pericardium

One of the major causes of mortality worldwide is related to heart valve disease and heart valve replacement procedures have been performed successfully throughout the past 30 years. The roughly half a million cardiac valve procedures in a year, with nearly 100,000 valve replacements in the USA and twice that number in European countries, underscores their extensive application in the healthcare system worldwide [219]. Currently, defective heart valves are replaced either by mechanical or bioprosthetic valves. Advantages of bioprostheses include an extensive supply of donor tissue, superior hemodynamics and lower thromboembolic complications when compared to mechanical valves, which are associated with a significant risk of thromboembolism and require lifelong treatment with anti-coagulation drugs. Commonly, bioprosthetic heart valves are either from animal tissue, pericardium or aortic porcine valves, treated with Glut to preserve the tissue's structure [220]. Glut forms crosslinks between the collagen and thus enables maintenance of the valve structure, inhibits degradation by collagenases and other enzymes. However, the Glut crosslinked valves can fail because of leaflet stiffening or defects caused by intrinsic calcific deposits that develop over time in both children and adults [221-223]. As a result of tissue degradation, durability of bioprosthetic valves range from 5 to 20 years, which leads to reoperation for the recipient [224]. The life span of bioprosthetic valve implants could be significantly increased by inhibiting valve

calcification. Various factors have been suggested that may contribute to the onset and progress of the calcification process, including host and implant factors. The most important host factor has proven to be young age; children and young adults develop severe bioprosthetic calcification sooner in their postoperative course than do adults [225]. One of the most important implant factors potentiating calcification is Glut pretreatment. [226]. During the treatment process, Glut devitalises the cells by disrupting their membranes and exposing the cellular contents onto the interstitial space. These residual cells, then turned to cellular debris, become the primary sites for calcification. Calcium phosphate forms through the reaction of the calcium ion in extracellular fluid with the phosphorus ions from the phospholipids present in the cellular membrane. In addition, devitalisation of cells subsequent to tissue treatment disrupts their calcium regulation mechanisms. In living cells, the intracellular calcium level is approximately 10^{-7} M, and extracellular calcium is 10^{-3}M. This 10,000-fold gradient across the plasma membrane is maintained by energy-requiring metabolic pumps that extrude this ion, as well as intracellular buffering mechanisms. In cells modified by Glut crosslinking, the mechanisms for calcium extrusion are no longer functional, and calcium influx occurs unimpeded. The cell membranes and other intercellular structures are high in phosphorus (as phospholipids, especially phosphatidyl serine, and the phosphate backbone of the nucleic acids); they can bind calcium and serve as nucleators. Initial calcification deposits eventually enlarge and coalesce, resulting in grossly mineralised nodules that stiffen and weaken the tissue and thereby cause a prosthesis to malfunction [227, 228]. Glut crosslinks are also unstable, and this can lead to inflammation due to the leaching of Glut from treated tissue. Inflammation has also been associated with leaflet thicknening which again leads to stenosis and ultimately valve failure [229, 230]. The ideal crosslinking reagents should meet rigorous efficacy and safety requirements. The treatment should not impede normal valve performance and able to enhance stability and durability of the animal heart valves. Thus, different approaches have been taken towards reducing the calcification of bioprosthetic heart valves. They include pretreatment of the valves with polyepoxides [231, 232], water soluble carbodiimide [233], photooxidative crosslinking [234, 235] or by covalent attachment of other anti-calcification agents. However, these prior strategies have not been demonstrated to be effective for preparing durable bioprostheses with calcification resistance and ability to meet biomechanical and sterilisation requirements [236, 237]. Some polyepoxy crosslinkers have been previously studied for

treatment of bioprosthetic heart valves with comparable shrinkage temperature and significantly lower calcification rate in animal studies. However the approach hasn't been used in commercial valves – probably associated to mechanical performance, cost and sterilisation issues. In addition, the relatively poor water solubility of the polyepoxys studied is an important drawback [238-241]. The present study investigated epoxy functionalised PEP polymer, a highly polar, water-soluble polyepoxy crosslinking agent. We investigated the hypothesis that treatment with PEP confers calcification resistance because of its unique reactions with extracellular matrix (ECM) proteins forming irreversible bonds with structural proteins, thereby favorably altering collagen structure to mitigate pathological calcification. An *in vitro* method was used for the comparative testing of different anti-calcification treatments as the extent and progression of calcification *in vivo* (in animals) depends on many factors. These factors include animal species and age-with rats, sheep and pigs being the most commonly used; site of implantation, mainly subdermal versus orthotopic implant and length of implantation. Due to each species and age genetic predispositions and immunogical responses, no animal model has shown calcium levels directly translated to humans [242, 243]. In addition *in vivo* methods are costly and time-consuming. Therefore, *in vitro* methods which attemp to exclude these individual factors, are able to investigate the effectiveness of anti-calcification treatments more objectively with lower variability, shorter term and reduced costs. *In vitro* methods have their own drawbacks – their major focus is on calcium and phosphorous deposition, thus they do not include other biological components such as enzymes, immunological response, coagulation factors and so many others that may affect the calcification outcomes. However, by using controls for direct comparison, *in vitro* mothods are most valuable as screening tests. *In vitro* models include the technique of submerging the materials tested into buffer solutions mimicking some of the important parameters of human blood (e.g. concentration of electrolytes, pH, temperature) either in a stress free state or under different loading conditions [244-246].

1.13 Thesis proposition

The aim of this thesis is to investigate the integration of electron transfer mediators, enzymes and nanostructures to improve enzyme electrode performance for use in an enzymatic fuel cell and for application to biosensing. Chapter 2 will address the synthesis, characterisation and

purification of electron transfer mediators. These will be integrated with enzymes and incorporated into hydrogels on planar electrodes to provide bioelectrochemical systems. Chapter 3 focuses on a comparison of glucose oxidation by enzyme electrodes prepared using a range of conductive and non-conductive nanoparticles as supports. This study sought to probe whether the properties of different supports with similar sizes can improve current density and/or stability for these electrodes. Subsequently using a previously reported DoE-optimised anode, experiments are performed to produce the maximum glucose current in order to evaluate the role and effect of oxygen on enzyme electrodes. These enzymatic electrodes are prepared by co-immobilisation of the redox complex Os(dmobpy)$_2$4AMP with MWCNT, CMD as a polymer support and either GOx or FADGDH as enzyme. Chapter 4 focuses on optimisation of individual component amounts used to prepare biocatalytic redox films. These components are MWCNT, the *Mv*Bod enzyme and Os(dclbpy)PVI mediator. Optimisation is achieved using a response surface methodology in order to maximise current density provided by the enzyme electrode. The DoE model is developed and validated for enzyme electrode performance in pseudo-physiological conditions. The components were co immobilised using PEGDGE on a graphite electrode surface. The optimised enzyme electrode is used as a biocathode to assemble a membrane-less EFC operating in pseudo-physiological conditions (5 mM glucose, 50 mM phosphate buffered saline, pH 7.4, 37 °C) for application to power generation. Chapter 5 addresses a comparison of cross-linking reaction conditions for preparation of films of redox complexes, enzymes and supports on electrodes for application as biofuel cell anodes. Finally chapter 6 involves development of a bio-reactor that can be used to simulate calcification of bovine pericardium *in vitro* and its application to study cross-linkers to attempt to inhibit this calcification. The application of cross linkers is a link to this thesis that is enzyme electrode modification for biosensor and biofuel cell application.

1.14 Main goals and objectives

- To investigate the interaction between enzymes and redox mediators, to improve biocatalytic electrodes power outputs, ideally sufficient to power implantable devices.
- To develope a bio-reactor, to simulate calcification of bovine pericardium *in vitro* and to study the effect of different cross-linkers to inhibit this calcification.

1.15 References

[1] S. C. Barton, J. Gallaway and P. Atanassov, Chemical Reviews, 104 (2004) 4867-4886.

[2] P. Kavanagh, D. Leech, Wiley-VCH, 13 (2011) 229-267.

[3] R. A. Bullen, T. C. Arnot, J. B. Lakeman, F. C. Walsh, Biosensors and Bioelectronics, 21 (2006) 2015-2045.

[4] D. Leech, P. Kavanagh, W. Schuhmann, Electrochimica Acta, 84 (2012) 223-234.

[5] F. Davis, S. P. Higson, Biosensors and Bioelectronics, 22 (2007) 1224-1235.

[6] A.B.P. Lever, Inorganic Chemistry, 29 (1990) 1271-1285.

[7] H. Masui, A.B.P. Lever, Inorganic Chemistry, 32 (1993) 2199-2201.

[8] G.T.R. Palmore, H. Bertschy, S.H. Bergens, G.M. Whitesides, Journal of Electroanalytical Chemistry, 443 (1998) 155-161.

[9] T. Chen, S.C. Barton, G. Binyamin, Z. Gao, Y. Zhang, H.-H. Kim, A. Heller, Journal of the American Chemical Society, 123 (2001) 8630-8613.

[10] A. T. Yahiro, S. M. Lee, D. O. Kimble, Biochimica et Biophysica Acta, 88 (1964) 375-383.

[11] M. J. Moehlenbrock, S. D. Minteer, Chemical Reviews, 37 (2008) 1188-1196.

[12] A. Heller, B. Feldman, Chemical Reviews, 108 (2008) 2482-2505.

[13] A. Heller, Physical Chemistry Chemical Physics, 6 (2004) 209-216.

[14] I. Osadebe, D. Leech, ChemElectroChem, 1 (2014) 1988-1993.

[15] S. Boland, P. Kavanagh, D. Leech, Journal of the Electrochemical Society, 13 (2008) 77-87.

[16] P. Ó Conghaile, S. Kamireddy, D. MacAodha, P. Kavanagh, D. Leech, Analytical and Bioanalytical Chemistry, 405 (2013) 3807-3812.

[17] R. Kumar, D. Leech, Journal of the Electrochemical Society, 161 (2014) H3005-H3010.

[18] P. Kavanagh, D. Leech, Physical Chemistry Chemical Physics, 15 (2013) 4859-4869.

[19] S. Babanova, K. Artyushkova, Y. Ulyanova, S. Singhal, P. Atanassov, Journal of Power Sources, 245 (2014) 389-397.

[20] E.M. Kober, J.V. Caspar, B.P. Sullivan, T.J. Meyer, Inorganic Chemistry, 27 (1988) 4587-4598.

[21] R.J. Forster, J.G. Vos, Macromolecules, 23 (1990) 4372-4377.

[22] G. Hoogers, Fuel cell technology handbook, CRC Press, (2002).

[23] C.F. Schoenbein, The London, Edinburgh, and Dublin Philosophical Magazine and Journal of Science, 3 (1838) 43-45.

[24] W. Grove, The London, Edinburgh, and Dublin Philosophical Magazine and Journal of Science, 3 (1839) 127-130.

[25] J. Larminie, A. Dicks, Fuel Cell Systems Explained, John Wiley & Sons, Ltd, (2000).

[26] P. Atkins, J. De Paula, Physical Chemistry, Ninth Edit., W. H. Freeman and Company, New York, (2010).
[27] A. Morozan, B. Jousselme, S. Palacin, Energy & Environmental Science, 4 (2011) 1238-1254.
[28] S. Kerzenmacher, J. Ducree, R. Zengerle, F. von Stetten, Journal of Power Sources, 182 (2008) 1-17.
[29] P. Atanassov, C. Apblett, S. Banta, S. Brozik, S. C. Barton, M. Cooney, B. Y. Liaw, S. Mukerjee, S. D. Minteer, The Electrochemical Society Interface. 16 (2) (2007) 28-31.
[30] M. J. Moehlenbrock, S. D. Minteer, Chemical Society Reviews, 37 (2008) 1188-1196.
[31] R.A. Bullen, T.C. Arnot, J.B. Lakeman, F.C. Walsh, Biosensors and Bioelectronics, 21 (2006) 2015-45.
[32] J. Kim, H. Jia, P. Wang, Biotechnology Advances, 24 (2006) 296-308.
[33] R. Allen, H.P. Bennetto, Applied Biochemistry and Biotechnology, 39-40 (1993) 27-40.
[34] T. Catal, P. Kavanagh, V. O'Flaherty, D. Leech, Journal of Power Sources, 196 (2011) 2676-2681.
[35] M.A. Moqsud, K. Omine, N. Yasufuku, M. Hyodo, Y. Nakata, Waste Management, 33 (2013) 2465-2469.
[36] M. Zhou, J. Yang, H. Wang, T. Jin, D.J. Hassett, T. Gu, Bioenergy Research: Advances and Applications, Elsevier, Amsterdam, (2014) 131-152.
[37] D.R. Lovley, Current Opinion in Biotechnology, 19 (2008) 564-571.
[38] R.D. Milton, T. Wang, K. L. Knoche, S. D. Minteer, Langmuir, 32 (2016) 2291-2301.
[39] N. Yuhashi, M. Tomiyama, J. Okuda, S. Igarashi, K. Ikebukuro, K. Sode, Biosensors and Bioelectronics, 20 (2005) 2145-2150.
[40] F. Sato, M. Togo, M.K. Islam, T. Matsue, J. Kosuge, N. Fukasaku, S. Kurosawa, M. Nishizawa, Electrochemistry Communications, 7 (2005) 643-647.
[41] H.A.O. Hill, Coordination Chemistry Reviews, 151 (1996) 115-123.
[42] A. Merz, A.J. Bard, Journal of the American Chemical Society, 100 (1978) 3222-3223.
[43] R.W. Murray, Accounts of Chemical Research, 13 (1980) 135-141.
[44] G. Inzelt, Electrochimica Acta, 34 (1989) 83-91.
[45] N. Mano, F. Mao, A. Heller, Journal of the American Chemical Society 125 (2003) 6588.
[46] N. Mano, F. Mao, A. Heller, Journal of the American Chemical Society 124 (2002) 12962.
[47] N. Mano, F. Mao, W. Shin, T. Chen, A. Heller, Chemical Communications (2003) 518.
[48] F. Barrière, P. Kavanagh, D. Leech, Electrochimica Acta, 51 (2006) 5187-5192.
[49] S. Boland, D. Leech, Analyst, 137 (2012) 113-117.
[50] F.P. Cardoso, S. Aquino Neto, L.B. Crepaldi, S. Nikolaou, V.P. Barros, A.R. De Andrade, Journal of Electrochemical Society, 161 (2014) F445-F450.

[51] A. Pizzariello, M. Stred'ansky, S. Miertuš, Bioelectrochemistry, 56 (2002) 99- 105.
[52] Y. Kamitaka, S. Tsujimura, N. Setoyama, T. Kajino, K. Kano, Physical Chemistry Chemical Physics, 9 (2007) 1793-1801.
[53] N.L. Akers, C.M. Moore, S.D. Minteer, Electrochimica Acta, 50 (2005) 2521-2525.
[54] E. Simon, C.M. Halliwell, C.S. Toh, A.E.G. Cass, P.N. Bartlett, Bioelectrochemistry 55 (2002) 13-15.
[55] D. Bhatnagar, S.A. Xu, C. Fischer, R.L. Arechederra, S.D. Minteer, Physical Chemistry Chemical Physics 13 (2011) 86-92.
[56] P.K. Addo, R.L. Arechederra, S.D. Minteer, Electroanalysis 22 (2010) 807-812.
[57] D. Sokic-Lazic, R.L. Arechederra, B.L. Treu, S.D. Minteer, Electroanalysis 22 (2010) 757-764.
[58] R.L. Arechederra, S.D. Minteer, Fuel Cells 9 (2009) 63-69.
[59] R.L. Arechederra, K. Boehm, S.D. Minteer, Electrochimica Acta 54 (2009) 7268-7273.
[60] M.H. Schoenfisch, M. Ovadia, J.E. Pemberton, Journal of Biomedical Materials Research, 51 (2000) 209-215.
[61] R. Linford, W. Schlindwein, Solid State Ionics, 177 (2006) 1559-1565.
[62] C. Vincent, Solid State Ionics, 134 (2000) 159-167.
[63] S.M. Kurtz, J. a Ochoa, E. Lau, Y. Shkolnikov, B.B. Pavri, D. Frisch, A.J. Greenspon, Pacing and Clinical Electrophysiology, 33 (2010) 705-11.
[64] D. Ivnitski, B. Branch, P. Atanassov, C. Apblett, Electrochemistry Communications, 8 (2006) 1204-1210.
[65] P.P. Joshi, S.A. Merchant, Y. Wang, D.W. Schmidtke, Analytical Chemistry, 77 (2005) 3183-3188.
[66] B. Reuillard, A. Le Goff, C. Agnes, M. Holzinger, A. Zebda, C. Gondran, K. Elouarzaki, S. Cosnier, Physical Chemistry Chemical Physics, 15 (2013) 4892-4896.
[67] A. Zebda, S. Cosnier, J.P. Alcaraz, M. Holzinger, A. Le Goff, C. Gondran, F. Boucher, F. Giroud, K. Gorgy, H. Lamraoui, P. Cinquin, Scientific Reports, 3 (2013).
[68] M. Falk, C.W. Narváez Villarrubia, S. Babanova, P. Atanassov, S. Shleev, ChemPhysChem, 14 (2013) 2045-2058.
[69] L. Stryer, J.M. Berg, J.L. Tymoczko, Biochemistry (5th ed.), W.H. Freeman. ISBN 0-7167-4955-6 (2002).
[70] The Catalytic Site Atlas, The European Bioinformatics Institute. Retrieved 4 April (2007).
[71] H. Suzuki, How Enzymes Work: From Structure to Function, CRC Press. (2015) 117-140.
[72] J.D. Rozzell, Bioorganic & Medicinal Chemistry, 7 (1999) 2253-2261.
[73] T.S. Zhao, Micro Fuel Cells Principles and Applications, Academic Press, (2009).

[74] M.J. Cooney, V. Svoboda, C. Lau, G. Martin, S.D. Minteer, Energy and Environmental Science, 1 (2008) 320-337.
[75] K.S. Polonsky, B.D. Given, L. Hirsch, E.T. Shapiro, H. Tillil, C. Beebe, J.A. Galloway, B.H. Frank, T. Karrison, E. Van Cauter, The Journal of Clinical Investigation, 81 (1988) 435-441.
[76] A.C. Guyton, J.E. Hall, Textbook of Medical Physiology, 11th ed., Elsevier Saunders, (2006).
[77] C.M. Wong, K.H. Wong, X.D. Chen, Applied Microbiology and Biotechnology, 78 (2008) 927-938.
[78] R. Wilson, A.P.F. Turner, Biosensors and Bioelectronics, 7 (1992) 165-185.
[79] P.-R. Kommoju, Z.-w. Chen, R.C. Bruckner, F.S. Mathews, M.S. Jorns, Biochemistry, 50 (2011) 5521-5534.
[80] J. Gallaway, I. Wheeldon, R. Rincon, P. Atanassov, S. Banta, S.C. Barton, Biosensors and Bioelectronics, 23 (2008) 1229-1235.
[81] R.D. Milton, F. Giroud, A.E. Thumser, S.D. Minteer, R.C.T. Slade, Physical Chemistry Chemical Physics, 15 (2013) 19371-19379.
[82] R.D. Milton, F. Giroud, A.E. Thumser, S.D. Minteer, R.C.T. Slade, Electrochimica Acta, 140 (2014) 59-64.
[83] R.D. Milton, F. Giroud, A.E. Thumser, S.D. Minteer, R.C.T. Slade, Chemical Communication, 50 (2014) 94-96.
[84] D. MacAodha, M.L. Ferrer, P.O. Conghaile, P. Kavanagh, D. Leech, Physical Chemistry Chemical Physics, 14 (2012) 14667-14672.
[85] M. Holzinger, A. Le Goff, S. Cosnier, Electrochimica Acta, 82 (2012) 179-190.
[86] M. Wooten, S. Karra, M. Zhang, W. Gorski, Analytical Chemistry, 86 (2014) 752-757.
[87] J.M. Goran, S.M. Mantilla, K.J. Stevenson, Analytical Chemistry, 85 (2013) 1571-1581.
[88] M. Wooten, S. Karra, M. Zhang, W. Gorski, Analytical Chemistry, 86 (2013) 752-757.
[89] R. Antiochia, L. Gorton, Biosensors and Bioelectronics, 22 (2007) 2611-2617.
[90] S.C. Barton, Handbook of Fuel Cells, John Wiley & Sons Ltd, 5 (2009) 1-19.
[91] L.H. Yufeng Yang, Jufang Wang, Xiaoning Wang, Zhinan Xu, Journal of Microbiology and Biotechnology 24 (2014) 1516-1524.
[92] F. Sato, M. Togo, M.K. Islam, T. Matsue, J. Kosuge, N. Fukasaku, S. Kurosawa, M. Nishizawa, Electrochemistry Communications, 7 (2005) 643-647.
[93] V. Flexer, F. Durand, S. Tsujimura, N. Mano, Analytical Chemistry, 83 (2011) 5721-5727.
[94] T. Ikeda, K. Kano, Biochimica et Biophysica Acta, Proteins Proteomics, 1647 (2003) 121-126.
[95] H. Yoshida, G. Sakai, K. Mori, K. Kojima, S. Kamitori, K. Sode, Scientific Reports, 5 (2015) 13498.

[96] M.N. Zafar, N. Beden, D. Leech, C. Sygmund, R. Ludwig, L. Gorton, Analytical and Bioanalytical Chemistry, 402 (2012) 2069-2077.

[97] D. MacAodha, P. O'Conghaile, B. Egan, P. Kavanagh, C. Sygmund, R. Ludwig, D. Leech, Electroanalysis, 25 (2013) 94-100.

[98] C.F. Blanford, R.S. Heath, F.A. Armstrong, Chemical Communications, (2007) 1710–1712.

[99] S. Tsujimura, T. Nakagawa, K. Kano, T. Ikeda, Electrochemistry, 72 (2004) 437-439.

[100] S. V Shleev, A. Elkasmi, T. Ruzgas, L. Gorton, Electrochemistry Communications, 6 (2004) 934-939.

[101] E.I. Solomon, U.M. Sundaram, T.E. Machonkin, Chemical Reviews, 96 (1996) 2563-2606.

[102] T. Sakurai, K. Kataoka, The Chemical Record, 7 (2007) 220-229.

[103] R.M. Berka, P. Schneider, E.J. Golightly, S.H. Brown, M. Madden, K.M. Brown, T. Halkier, K. Mondorf, F. Xu, Applied and Environmental Microbiology, 63 (1997) 3151-3157.

[104] Ping-Yü Ho, Gwei-Djen Lu and Nathan Sivin, Science and Civilisation in China: Chemistry and chemical technology, Cambridge university press, 5 (1959) 209.

[105] F. Xu, W. Shin, S.H. Brown, J.A. Wahleithner, U.M. Sundaram, E.I. Solomon, Biochimica et Biophysica Acta, 1292 (1996) 303-311.

[106] H. Claus, Micron Journal, Elsevier, 35 (2004) 93-6.

[107] M. Ferraroni, I. Matera, A. Chernykh, M. Kolomytseva, L.A. Golovleva, A. Scozzafava, F. Briganti, Journal of Inorganic Biochemistry, 111 (2012) 203-209.

[108] A.M. Mayer, R.C. Staples, Phytochemistry, 60 (2002) 551-65.

[109] G. Alexandre, I.B. Zhulin, Trends in Biotechnology, 18 (2000) 41-42.

[110] M. Falk, C.W. Narváez Villarrubia, S. Babanova, P. Atanassov, S. Shleev, ChemPhysChem, 14 (2013) 2045-2058.

[111] M.C. Machczynski, E. Vijgenboom, B. Samyn, G.W. Canters, Protein science: a publication of the Protein Society, 13 (2004) 2388-2397.

[112] T. Skálová, J. Dohnálek, L.H. Østergaard, P.R. Østergaard, P. Kolenko, J. Dušková, A. Štěpánková, J. Hašek, Journal of Molecular Biology, 385 (2009) 1165-1178.

[113] S. Murao, N. Tanaka, Agricultural and Biological Chemistry, 45 (1981) 2383-2384.

[114] N. Tanaka, S. Murao, Agricultural and Biological Chemistry, 46 (1982) 2499-2503.

[115] A. Shimizu, J.H. Kwon, T. Sasaki, T. Satoh, N. Sakurai, T. Sakurai, S. Yamaguchi, T. Samejima, Biochemistry, 38 (1999) 3034-3042.

[116] S. Tsujimura, K. Kano, T. Ikeda, Journal of Electroanalytical Chemistry, 576 (2005) 113-120.

[117] S. Tsujimura, A. Kuriyama, N. Fujieda, K. Kano, T. Ikeda, Analytical Biochemistry 337 (2005) 325-331.

[118] Y. Kamitaka, S. Tsujimura, K. Kataoka, T. Sakurai, T. Ikeda, K. Kano, Journal of Electroanalytical Chemistry, 601 (2007) 119-124.
[119] S. Tsujimura, H. Tatsumi, J. Ogawa, S. Shimizu, K. Kano, Journal of Electroanalytical Chemistry, 496 (2001) 69-75.
[120] J.A. Cracknell, T.P. McNamara, E.D. Lowe, C.F. Blanford, Dalton transactions, 40 (2011) 6668-6675.
[121] S. Tsujimura, H. Tatsumi, J. Ogawa, S. Shimizu, K. Kano, T. Ikeda, Journal of Electroanalytical Chemistry, 496 (2001) 69-75.
[122] P. A. Jenkins, S. Boland, P. Kavanagh, D. Leech, Bioelectrochemistry 76 (2009) 162-168.
[123] N. Mano, H.-H. Kim, Y. Zhang, A. Heller, Journal of the American Chemical Society, 124 (2002) 6480-6486.
[124] N. Mano, H.-H. Kim, A. Heller, The Journal of Physical Chemistry, 106 (2002) 8842-8848.
[125] A.M. Kuznetsov, J. Ulstrup, John Wiley & Sons, Chichester, (1999).
[126] A.J. Appleby, Modern Aspects of Electrochemistry, 38 (2005) 175-301.
[127] R.A. Marcus, Journal of Electroanalytical Chemistry, 438 (1997) 251-259.
[128] V. Balzani, Electron transfer in chemistry, WILEY-VCH, (2001).
[129] F.A. Armstrong, H.A.O. Hill, N.J. Walton, Accounts of Chemical Research, 21 (1988) 407-413.
[130] J.E. Frew, H.A.O. Hill, European Journal of Biochemistry, 172 (1988) 261-269.
[131] M.J. Eddowes, H.A.O. Hill, Journal of the Chemical Society, Chemical Communications, (1977) 771-772.
[132] P. Yeh, T. Kuwana, Chemistry Letters, (1977) 1145-1148.
[133] L. Gorton, A. Lindgren, T. Larsson, F.D. Munteanu, T. Ruzgas, I. Gazaryan, Analytica Chimica Acta, 400 (1999) 91-108.
[134] D. Wang, L. Chen, Electrochimica Acta, 54 (2009) 4316-4320.
[135] A. Lindgren, T. Larsson, T. Ruzgas, L. Gorton, Journal of Electroanalytical Chemistry, 494 (2000) 105-113.
[136] Y. Liu, Y. Du, C.M. Li, Electroanalysis, 25 (2013) 815-831.
[137] J.T. Holland, C. Lau, S. Brozik, P. Atanassov, S. Banta, Journal of the American Chemical Society, 133 (2011) 19262-5
[138] S.C. Feifel, R. Ludwig, L. Gorton, F. Lisdat, Langmuir, 28 (2012) 9189-94
[139] O. Courjean, F. Gao, N. Mano, Angewandte Chemie International Edition, 48 (2009) 5897-9.
[140] S. Demin, E.A.H. Hall, Bioelectrochemistry, 76 (2009) 19-27.
[141] M.F. Cardosi, A.P.F. Turner, I. Karube, G.S. Wilson (Eds.), (1987) 257-275.
[142] L.C. Clark, C. Lyons, Annals of the New York Academy of Sciences, 102 (1962) 29-45.

[143] Guilbaul.Gg, G.J. Lubrano, Analytica Chimica Acta, 64 (1973) 439-455.
[144] A.E.G. Cass, G. Davis, G.D. Francis, H.A.O. Hill, W.J. Aston, I.J. Higgins, E.V. Plotkin, L.D.L. Scott, A.P.F. Turner, Analytical Chemistry, 56 (1984) 667-71.
[145] Y. Degani, A. Heller, The Journal of Physical Chemistry, 91 (1987) 1285-1289.
[146] Y. Degani, A. Heller, Journal of the American Chemical Society, 110 (1988) 2615-2620.
[147] W. Schuhmann, T.J. Ohara, H.L. Schmidt, A. Heller, Journal of the American Chemical Society, 113 (1991) 1394-1397.
[148] E. Katz, I. Willner, A.B. Kotlyar, Journal of Electroanalytical Chemistry, 479 (1999) 64-68.
[149] S.M. Zakeeruddin, D.M. Fraser, M.K. Nazeeruddin, M. Grätzel, Journal of Electroanalytical Chemistry, 337 (1992) 253-283.
[150] A. Heller, AIChE Journal, 51 (2005) 1054-1066.
[151] T. Chen, S.C. Barton, G. Binyamin, Z. Gao, Y. Zhang, H.-H. Kim, A. Heller, Journal of the American Chemical Society, 123 (2001) 8630-8631.
[152] T.J. Ohara, R. Rajagopalan, A. Heller, Analytical Chemistry, 65 (1993) 3512-3517.
[153] R.J. Forster, J.G. Vos, Electrochimica Acta, 37 (1992) 159-167.
[154] P. Kavanagh, D. Leech, Tetrahedron Letters, 45 (2004) 121-123.
[155] A. Heller, Current Opinion in Chemical Biology, 10 (2006) 664-672.
[156] F. Mao, N. Mano, A. Heller, Journal of the American Chemical Society, 125 (2003) 4951-4957.
[157] Y. Degani, A. Heller, Journal of the American Chemical Society, 111 (1989) 2357-2358.
[158] A. Heller, B. Feldman, Chemical Reviews, 108 (2008) 2482-2505.
[159] B.A. Gregg, A. Heller, The Journal of Physical Chemistry, 95 (1991) 5970-5975.
[160] M.T. Meredith, S.D. Minteer, in: R.G. Cooks, E.S. Yeung (Eds.), Annual Review of Analytical Chemistry, 5 (2012) 157-179.
[161] B.B. Dambatta, J.R. Ebdon, European Polymer Journal, 22 (1986) 783-786.
[162] R. Kumar and D. Leech, Electrochimica Acta 140 (2014) 209–216.
[163] R. Kumar and D. Leech, Journal of the Electrochemical Society, 13 (2014) 161.
[164] S.C. Barton, H.-H. Kim, G. Binyamin, Y. Zhang, A. Heller, Journal of the American Chemical Society, 123 (2001) 5802-5803.
[165] B. Tan, D.P. Hickey, R.D. Milton, F. Giroud, S.D. Minteer, Journal of the Electrochemical Society, 162 (2015) H102-H107.
[166] C.-M. Yu, M.-J. Yen, and L.-C. Chen, Biosensors and Bioelectronics, 25 (2010) 2515-2521.
[167] W. Yang, K.R. Ratinac, S.P. Ringer, P. Thordarson, J.J. Gooding, F. Braet, Angewandte Chemie International Edition, 49 (2010) 2114-2138.
[168] M.C. Weigel, E. Tritscher, F. Lisdat, Electrochemistry Communications, 9 (2007) 689-693.

[169] F. Tasca, L. Gorton, J.B. Wagner, G. Nöll, Biosensors and Bioelectronics, 24 (2008) 272-278.
[170] E. Nazaruk, M. Karaskiewicz, K. Żelechowska, J.F. Biernat, J. Rogalski, R. Bilewicz, Electrochemistry Communications, 14 (2012) 67-70.
[171] V. Švrček, C. Pham-Huu, J. Amadou, D. Begin, M.-J. Ledoux, F. Le Normand, O. Ersen, S. Joulié, Journal of Applied Physics, 99 (2006) 064306.
[172] B. Ha, J. Park, S.Y. Kim, C.J. Lee, the Journal of Physical Chemistry B, 110 (2006) 23742-23749.
[173] Y. Xiao, F. Patolsky, E. Katz, J.F. Hainfeld, I. Willner, Science, 299 (2003) 1877-1881.
[174] M. Zayats, E. Katz, R. Baron, I. Willner, Journal of the American Chemical Society, 127 (2005) 12400-12406.
[175] Yanzhen Fan, Shoutao Xu, Rebecca Schaller, Jun Jiao, Frank Chaplen, Hong Liu, Biosensors and Bioelectronics 26 (2011) 1908-1912
[176] N. German, A. Ramanaviciene, J. Voronovic, A. Ramanavicius, Microchim Acta 168 (2010) 221-229
[177] S. Boland, F. Barrière, D. Leech, Langmuir, 24 (2008) 6351-6358.
[178] S. Boland, P. Jenkins, P. Kavanagh, D. Leech, Journal of Electroanalytical Chemistry, 626 (2009) 111-115.
[179] T.J. Ohara, R. Rajagopalan, A. Heller, Polymer Materials Science and Engineering, 70 (1993) 182-183.
[180] T. de Lumley-Woodyear, P. Rocca, J. Lindsay, Y. Dror, A. Freeman, A. Heller, Analytical Chemistry, 67 (1995) 1332-1338.
[181] I. Migneault, C. Dartiguenave, M.J. Bertrand, K.C. Waldron, BioTechniques, 37 (2004) 790-796, 798-802.
[182] S. Nardecchia, M.C. Serrano, M.C. Gutiérrez, M.T. Portolés, M.L. Ferrer, F. del Monte, Advanced Functional Materials, 22 (2012) 4411-4420.
[183] K. Sirkar, A. Revzin, M.V. Pishko, Analytical Chemistry, 72 (2000) 2930- 2936.
[184] M.E. Fischer, N.J. Mol, M.J.E. Fischer (Eds.) Surface Plasmon Resonance, 627 (2010) 55-73.
[185] T. Lai, Q. Hou, H. Yang, X. Luo, M. Xi, Acta Biochimica et Biophysica Sinica, 42 (2010) 787-792.
[186] S. Nandini, S. Nalini, J. Sanetuntikul, S. Shanmugam, P. Niranjana, J.S. Melo, G.S. Suresh, Analyst, 139 (2014) 5800-5812.
[187] M. Moyo, J.O. Okonkwo, N.M. Agyei, Sensors (Basel, Switzerland), 12 (2012) 923-953.
[188] K. Yang, B. El-Haik, 2nd ed., McGraw-Hill, (2003).
[189] M. Anderson, the Industrial Physicist, (1997) 24-27.
[190] J. Antony, Design of Experiments for Engineers and Scientists Elsevier, (2003).

[191] R. Leardi, Analytica Chimica Acta, 652 (2009) 161-172.
[192] M. Anderson, the Industrial Physicist (1997) 24-27.
[193] S.M. Ghoreishi, M. Behpour, A. Khoobi, S. Masoum, Arabian Journal of Chemistry, (2014)
[194] O. Levi, B. Tal, S. Hileli, A. Shapira, I. Benhar, P. Grabov, N. Eliaz, Cytometry, Part B, 88 (2015) 338347.
[195] F. Galvanin, E. Cao, N. Al-Rifai, V. Dua, A. Gavriilidis, Chim. Oggi, 33 (2015) 51-56.
[196] S. Babanova, K. Artyushkova, Y. Ulyanova, S. Singhal, P. Atanassov, Journal of Power Sources, 245 (2014) 389-397.
[197] R. Kumar, D. Leech, Bioelectrochemistry 106 (2015) 41–46
[198] J. Antony, Design of Experiments for Engineers and Scientists Elsevier, (2003).
[199] L. Eriksson, E. Johansson, N.K. Wold, C. Wikstrom, S. Wold, Design of Experiments: Principles and Applications Umetrics Academy, (2008).
[200] S. Babanova, K. Artyushkova, Y. Ulyanova, S. Singhal, P. Atanassov, Journal of Power Sources, 245 (2014) 389-397.
[201] J. Anthony, Design of Experiments for Engineers and Scientists, (2003).
[202] K. Yang, B. El-Haik, design for Six Sigma: Roadmap to product development, 2nd ed., McGraw-Hill, (2003).
[203] L. Eriksson, E. Johansson, N.K. Wold, C. Wikstrom, S. Wold, Design of Experiments: Principles and Applications Umetrics Academy, (2008).
[204] B. Qi, X. Chen, F. Shen, Y. Su, Y. Wan, Industrial & Engineering Chemistry Research, 48 (2009) 7346 7353.
[205] A.J. Bard, L.R. Faulkner, Electrochemical Methods: Fundamentals and Applications, Wiley, (2000).
[206] J. Wang, Analytical electrochemistry, Wiley, (2006).
[207] C.G. Zoski, Handbook of electrochemistry, Elsevier Science & Technology Books, (2007).
[208] P. Kissinger, W.R. Heineman, Laboratory Techniques in Electroanalytical Chemistry, 2 ed., Marcel Dekker, Inc., (1996).
[209] C. C. Page, C. C. Moser and P. L. Dutton, Current Opinion in Chemical Biology, 7 (2003) 551.
[210] A. Ševčik, Collection of Czechoslovak Chemical Communications, 13 (1948) 349.
[211] Wopschal.Rh, I. Shain, Analytical Chemistry, 39 (1967) 1514.
[212] M. Glauert, Journal of Fluid Mechanics, 1956, 1, 625.
[213] J. Ṙužička, E.H. Hansen, Analytica Chimica Acta, 78 (1975) 145.
[214] J. Ruzicka, J.W.B. Stewart, Analytica Chimica Acta, 79 (1975) 79.
[215] M. Trojanowicz, Annali di Chimica, 95 (2005) 421.

[216] M.B. Glauert, Journal of Fluid Mechanics, 1 (1956) 625.
[217] J. Ružicka, E.H. Hansen, Flow injection analysis, Wiley, (1988).
[218] J. Ružicka and E. H. Hansen, in Flow Injection Analysis, John Wiley & Sons, New York, (1988).
[219] Friedewald, V. E., Bonow, R. O., Borer, J. S., Carabello, B. A., Kleine, P. P., Akins, C. W. & Roberts, W. C. American Journal of Cardiology 99 (2007) 1269-1278.
[220] Schmidt CE, Baier JM, Biomaterals, 21(2000) 2215-31.
[221] Ellsmere JC, Khanna RA, Lee JM, Biomaterials, 2 (1999) 1143–50.
[222] Trantina-Yates AE, Human P, Bracher M, Zilla P, Biomaterials, 22 (2001) 1837-46.
[223] Stock UA, Schenke-Layland K, Biomaterials, 27(2006) 1-2.
[224] G. Hoffmann, G. Lutter, J. Cremer, Deutsches Arzteblatt International, 105 (2008) 143-148.
[225] Schoen FJ, Levy RJ, The Annals of Thoracic Surgery, 79 (2005)1072-80.
[226] Brockbank KG, Song YC, Transplantation, 75(2003) 1133-5.
[227] Schoen FJ, Levy RJ, Nelson AC, Bernhard WF, Nashef A, Hawley M, Laboratory Investigation, 52 (1985) 523-532.
[228] Schoen FJ, Tsao JW, Levy RJ., American Journal of Pathology, 123 (1985)134-145.
[229] Schoen FJ., Cardiovasc Pathol, 14 (2005)189-94.
[230] Giachelli C., American Journal of Pathology, 154(1999) 671-5.
[231] ung, H. W., Shen, S.- H. Tu, R., Lin, D., Hata, C., Noishiki, Y., Tomizawa, Y., Quijano, R. C., American Society for Artificial Internal Organs, 39 (1993) M532-M536.
[232] Xi T, Ma J, Tian W, Lei X, Long S, Xi B., Journal of Biomedical Materials Research, 26 (1992) 1241-51.
[233] Alferiev I, Connolly JM, Levy RJ., Journal of Organometallic Chemistry, 690 (2005) 2543-7.
[234] Schoen FJ, Levy RJ., The Annals of Thoracic Surgery, 79 (2005) 1072-80.
[235] Bianco RW, Phillips R, Mrachek J, Witson J., The Journal of Heart Valve Disease, 5 (1996) 317-22.
[236] Vyavahare N., Chen W., Joshi R, Lee C., Hirsch D., Cardiovascular Pathology , 6 (1997) 219-29.
[237] Vyavahare N., Hirsch D., Lerner E., Baskin JZ., Schoen FJ., Bianco R., Kruth HS., Zand R., Levy RJ. Circulation, 95(1997) 479-88.
[238] Xi T, Ma J, Tian W, Lei X, Long S, Xi B., Journal of Biomedical Materials Research, 26 (1992)1241-1251.
[239] Tu R, Shen SH, Lin D, Hata C, Thyagarajan K, Noishiki Y, Quijano RC, Journal of Biomedical Materials Research, 28(1994) 677-684.
[240] Hendriks M, Everaerts F, Verhoeven M., Journal of Long-Term Effects of Medical Implants, 11 (2001)163-183.

[241] Sung HW, Shen SH, Tu R, Lin D, Hata C, Noishiki Y, Tomizawa Y, Quijano RC., American Society for Artificial Internal Organs, , 39 (1993) M532-M536

[242] Mako WJ, Vesely I., The Journal of Heart Valve Disease, 6 (1997) 316-23.

[243] Friedewald VE, Bonow RO, Borer JS, Carabello BA, Kleine PP, Akins CW, Roberts WC., American Journal of Cardiology, 1(2007) 1269-78.

[244] G.M. Bernacca, A.C. Fisher, T.G. Mackay, D.J. Wheatley, Journal of Materials Science: Materials in Medicine, 3 (1992) 293.

[245] G. Golomb, Journal of Materials Science: Materials in Medicine, 3 (1992) 272.

[246] B. Glasmacher, M. Deiwick, H. Reul, H. Knesch, D. Keus, G. Rau, The International journal of Artificial Organs, 20 (1997) 267.

[247] P. Kommoju, Z. Chen, R.C. Bruckner, F.S. Mathews, M.S. Jorns, Biochemistry, 50 (2011) 5521-34.

[248] M. Ferraroni, I. Matera, A. Chernykh, M. Kolomytseva, L.A. Golovleva, A. Scozzafava, F. Briganti, Journal of inorganic biochemistry, 111 (2012) 203-209.

[249] J.A. Cracknell, T.P. McNamara, E.D. Lowe, C.F. Blanford, Dalton transactions, 40 (2011) 6668-6675.

Chapter 2

Synthesis and characterisation of polypyridyl osmium complexes

2.1 Introduction

Polypyridyl transition metal complexes have been studied extensively due to their photochemical and photophysical properties, making them useful in diverse applications, including as catalysts for energy and electron transfer processes [1-5]. In order for energy and electron transfer processes to occur, the complexes should be relatively stable in both the oxidised and reduced states, thus the focus on the group 8 transition metals such as osmium and ruthenium based complexes [10-13]. Although the photophysical and photochemical properties of the polypyridyl complexes of Os are closely related to those of analogous complexes of Ru, osmium has many advantages over ruthenium and other group 8 metals due to differences in electronic structure. Os has lower third ionisation energy, leading to a lower redox potential for complexes of Os (II) and consequent stabilisation of higher oxidation states. In addition, the greater extension of the metal d orbitals enhances the metal-ligand back-bonding and thereby provides increased stability of the complexes [6]. The above advantages of Os over other group 8 metals has led to the application of osmium complexes in electrochemical biosensors [14-17] or as catalysts in bio-anodes of biocatalytic fuel cells [18-22] where low redox potentials are required for minimising the effects of interferences or maximising the power output. Moreover, the energy of the excited state is much lower for the Ru complexes than for their Os analogues, making Ru complexes photolabile, which can lead to decomposition, while osmium polypyridyl complexes tend to be photostable [9]. The redox potential of a redox couple is affected by the nature of its ligands. For instance, the presence of electron withdrawing substituents on ligands

of the same series results in an increase of redox potential of the complex, while the opposite occurs with electron donating substituents [23]. Figure 1 shows a clear example of the effect of ligand substituent on redox potential for the series of osmium polypyridyl complexes of 2, 2'-bipyridine (bpy) and its derivatives. The alteration of the 4 and 4' positions of bpy with an electron-donating substituent such as $–OCH_3$ leads to a shift in redox potential of −0.27 V, while the presence of an electron withdrawing substituent such as –Cl at the 4 and 4' positions leads to a shift in redox potential of 0.16 V [23].

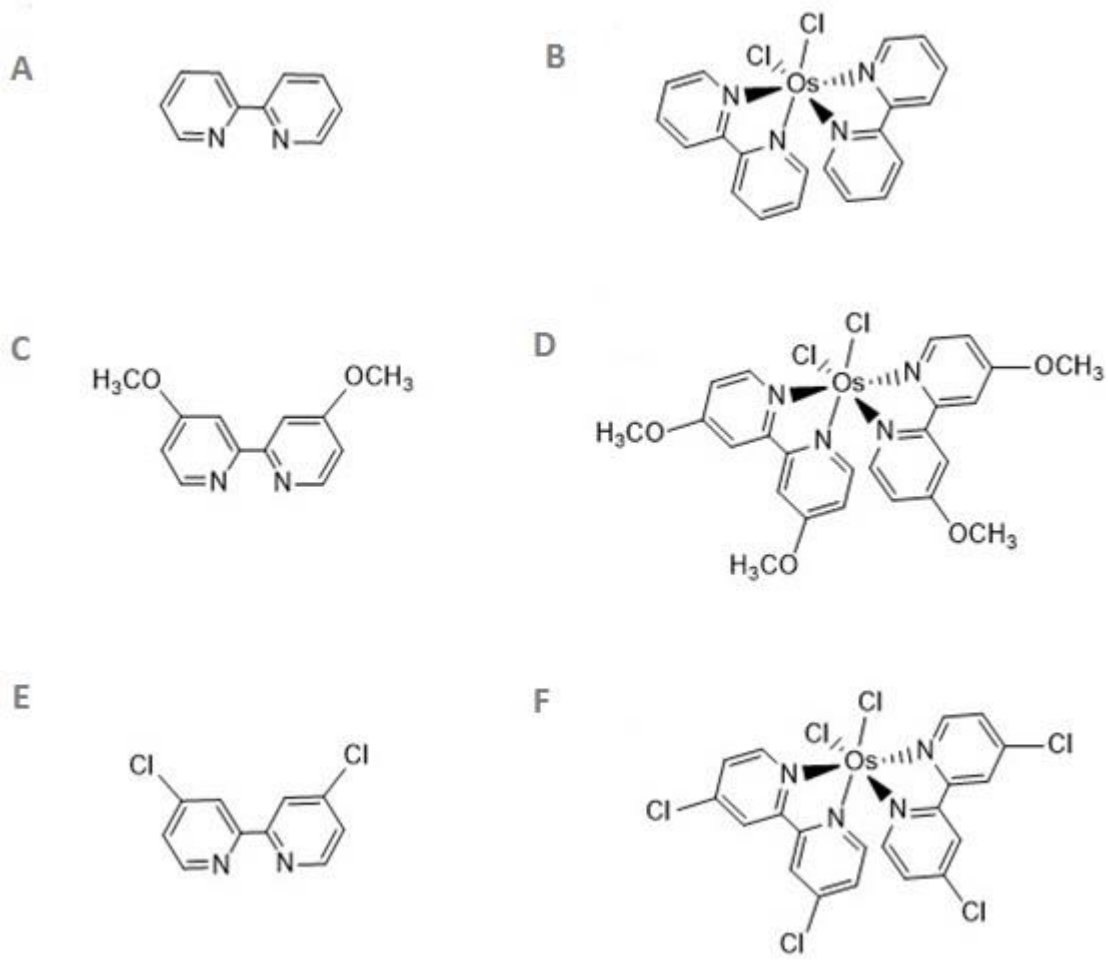

Figure 1: Structure of polypyridyl ligands and polypyridyl complexes of osmium: (A) bpy, (B) $Os(bpy)_2Cl_2$ ($E^{\circ\prime}$ = 0 V), (C) dmobpy, (D) $Os(dmobpy)_2Cl_2$ ($E^{\circ\prime}$ = −0.27 V), (E) dclbpy, (F) $Os(dclbpy)_2Cl_2$ ($E^{\circ\prime}$ = 0.16 V). All potentials quoted vs Ag/AgCl (3 M KCl).

Dwyer and co-workers were among the first scientists to develope the synthesis and characterisation of polypyridyl complexes of both Os and Ru [24]. The first reported Os polypyridyl complex was among the products of pyrolysis of mixtures of potassium hexachloroosmate and bipyridine [25]. Successive synthetic methods which have been developed provide an efficient high-yielding synthesis of complexes of general formula cis-$[Os(N\text{-}N)_2Cl_2]$ (where N-N = bipyridyl ligand) [6, 26]. In this chapter, the synthesis, characterisation and purification of a range of osmium polypyridyl complexes is described, which can subsequently be applied for development of biosensor and enzymatic fuel cell devices.

2.2 Experimental

2.2.1 Materials and methods

Ammonium hexachloroosmate, 2,2′-bipyridine, 4,4′-dichloro-2,2′-bipyridine, 4,4′-dimethoxy-2,2′-bipyridine, ethylene glycol, acetonitrile, sodium dithionite, N–vinylimidazole, ethanol, toluene, methanol, aluminium oxide (activated, neutral, STD grade, 150 mesh), Poly(ethylene glycol) diglycidyl ether (PEGDGE) (average molecular weight of 500) and diethyl ether were purchased from Sigma and used as received. MWCNT (Sigma-Aldrich) were treated by stirring under reflux in nitric acid for 6 h and isolated by filtration.

2.2.2 Instrumentation and techniques

Electrochemical measurements were carried out using a CH Instruments 600 potentiostat (IJ Cambria) in a three electrode cell containing 50 mM phosphate buffer and 150 mM NaCl (henceforth referred to as phosphate buffered saline, PBS) pH 7 at room temperature purged with nitrogen, using a 3 mm diameter graphite or glassy carbon (GC, CH Instruments) working electrode, a platinum mesh counter electrode (Goodfellow) and a custom built Ag/AgCl reference electrode (3 M KCl), abbreviated to Ag/AgCl throughout the thesis. Graphite disc electrodes were prepared by shrouding graphite rods (Graphite store, part # NC001295) in heat-

shrinkable tubing and polishing the exposed disk on 1200 grit silicon carbide paper (Buehler) followed by thorough rinsing with Milli-Q water. Prior to modification, GC disk electrodes were polished with 1 µm, 0.3 µm, and 0.05 µm of alumina slurry on microcloth pads (Buehler) followed by rinsing with MilliQ-water and drying with nitrogen gas stream. C, H, N elemental microanalyses were carried out in the NUIG micro analytical laboratory. Electrospray mass spectrometry (ESI-MS) was performed on a tandem quadrupole mass spectrometer in conjunction with tandem mass spectrometry using a micromass Qtof 1 spectrometer. The complexes were delivered to the gas phase by electrospraying 0.1 mM sample solutions of the complexes, dissolved in acetonitrile, at a flow rate of 30 µL min^{-1}. Spectra were recorded, in the positive ion mode over, typically, an average of 30 scans, using a cone voltage of 40 V, while keeping capillary voltage constant at 3500 V.

2.2.3 Synthesis

2.2.3.1 Synthesis of osmium polypyridyl complexes

The synthesis of the osmium complexes of general formula cis-$Os(N\text{-}N)_2Cl_2$ was conducted in a modification to a published procedure [6]. In order to synthesise the complexes, $(NH_4)_2OsCl_6$ and a slight excess of twice the molar equivalent of the polypyridine ligand (N-N) were dissolved in ethylene glycol and held at reflux for 45 minutes. After cooling to room temperature an appropriate amount of aqueous sodium dithionite was added to reduce Os(III) to Os(II). The mixture was stirred in ice for 30 minutes before filtering. The precipitate was then washed with water and large volumes of diethyl ether. Yields in excess of 88 % were consistently obtained. Complexes were characterised using cyclic voltammetry (CV), CHN and ESI-MS.

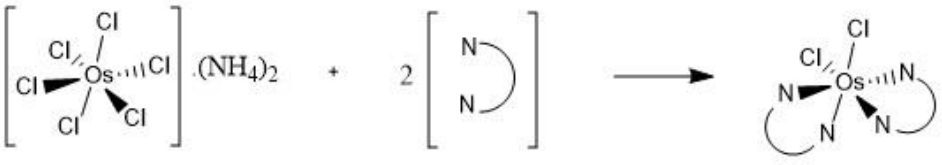

Figure 2: Simplified reaction scheme for synthesis of Os polypyridyl complexes of general formula cis-$[Os(N\text{-}N)_2Cl_2]$.

2.2.3.2 Synthesis of cis-[Os(dmobpy)$_2$(4AMP)Cl].PF$_6$ polypyridyl complex

Following the successful synthesis of Os(dmobpy)$_2$Cl$_2$, the Os(dmobpy)$_2$4AMP complex was synthesised by ligand substitution of a Cl with 4AMP according to literature methods [7, 8], with progress of the ligand substitution reaction monitored by cyclic voltammetry and differential pulse voltammetry, as reported on previously [9, 6] (Figure 3). In the procedure, 500 mg of Os(dmobpy)$_2$Cl$_2$ and a 1.05 molar equivalent of the ligand 4AMP was stirred in ethylene glycol in a 50 mL round-bottomed flask for 10 minutes to allow for complete dissolution of the complex while bubbling N_2 through the mixture. The mixture was then held at reflux while stirring under a N_2 atmosphere. CVs and DPVs were performed every 30 minutes to monitor reaction progress. To halt the reaction, the mixture was allowed to cool to room temperature. After cooling, an excess amount of aqueous ammonium hexafluorophosphate was added to form the insoluble .PF$_6$ adduct of the complex. The mixture was stirred in ice for 45 minutes before filtering with Whatman filter paper (0.45 µm). The precipitate was washed with water followed by washing with large volumes of diethyl ether. The resulting complex was then dried under vacuum and in an oven at 50°C overnight. A yield of 78% of Os(dmobpy)$_2$4AMP was obtained.

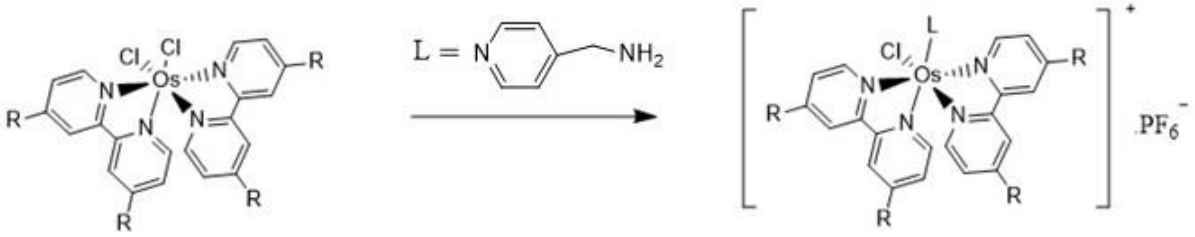

Figure 3: Simplified reaction for synthesis of "tetherable" complexes of general formula *cis*-[Os(N-N)$_2$(L)Cl].PF$_6$, where R represents the 4, 4' group on the bpy ligand and L is 4AMP.

2.2.3.3 Synthesis of poly(N-vinylimidazole) redox polymers containing cis-Os(N-N)$_2$Cl$_2$ redox centre

Poly(N-vinylimidazole) (PVI) polymers containing cis-Os(N-N)$_2$Cl$_2$ redox centres were synthesised according to literature procedures described by Forster and Vos [9]. The osmium complex, of general formula Os(N-N)$_2$Cl$_2$, was allowed to reflux in ethanol for 20 minutes to ensure complete dissolution of the complex. A ten molar equivalent of PVI dissolved in ethanol was added slowly to the ethanol solution in 1 ml aliquots. The mixture was allowed to reflux for ~ 3 days and the reaction monitored at regular intervals using cyclic voltammetry. After the reaction reached completion the product was precipitated by adding the solution drop-wise to a solution of stirring diethyl ether. The product was then suction filtered and allowed to air-dry. It was then further dried at 50 °C in a pre-heated oven overnight.

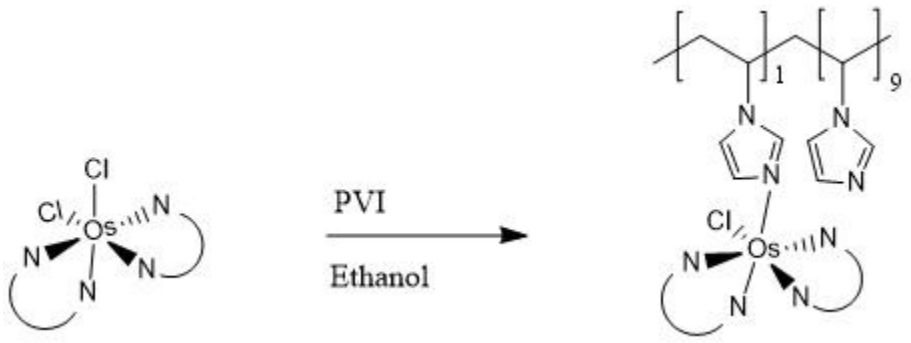

Figure 4: Simplified reaction for synthesis of Os polymer complexes of general formula cis-[(Os(N-N)$_2$(PVI)$_{10}$Cl]$^+$.

2.3 Results and Discussion

2.3.1 Characterisation and purification

2.3.1.1 Characterisation of cis-[Os(N-N)$_2$Cl$_2$] complexes

Following the synthesis of a range of *cis*-osmium polypyridyl complexes they were dissolved in appropriate solutions for further characterisation. Characterisation of the osmium complexes

was achieved using CV, ESI-MS and CHN microanalysis. Films of complexes on electrodes, for CV characterisation, were prepared by drop coat deposition of 3 μL of an 8 mg ml^{-1} solution of redox complex in ethanol onto the surface of 3 mm diameter GC electrodes. Cyclic voltammograms were recorded in 50 mM, PBS pH 7 at room temperature. As a result of limited structural data produced by electrochemical and photochemical analysis, the structural characterisation of cis-osmium compounds has heavily depended on methods such as ESI-MS and CHN. The ESI-MS characterisation involves a gentle ionisation process using an electrospray, yielding multiply charged molecular ions with little or no fragmentation. Table 1 shows the redox potentials and molecular ion (m/z) evaluated for each of the Os(II) complexes. Formal redox potentials (E°′) were calculated from the mean of the oxidation and reduction peak potentials, corresponding to the Os(II) and Os(III) redox couple, evaluated by CVs, as shown in Figure 5. Depending on the nature of the substituent group, the value of E°′ varies between -270 and 160 mV (vs Ag/AgCl) consistent with previously reported results [6, 9].

Complex	**E°′ (vs Ag/AgCl)**	**m/z**
$Os(bpy)_2Cl_2$	0 mV	574
$Os(dmobpy)_2Cl_2$	-270 mV	694
$Os(dclbpy)_2Cl_2$	160 mV	711

Table 1: Redox potentials and molecular ion m/z values evaluated for osmium complexes.

The highest m/z value observed in the ESI-MS was consistent with the molecular ion ($[Os(N-N)_2Cl_2]^+$) of the complex under analysis. In addition, an isotopic distribution calculator (Sheffield chemputer) was utilised to generate the theoretical isotopic distribution of the osmium complexes, for comparison to the observed distribution in the ESI-MS. As shown in Figure 5, comparison between experimental and calculated isotopic distribution patterns show good correlation, confirming the presence of the osmium complex.

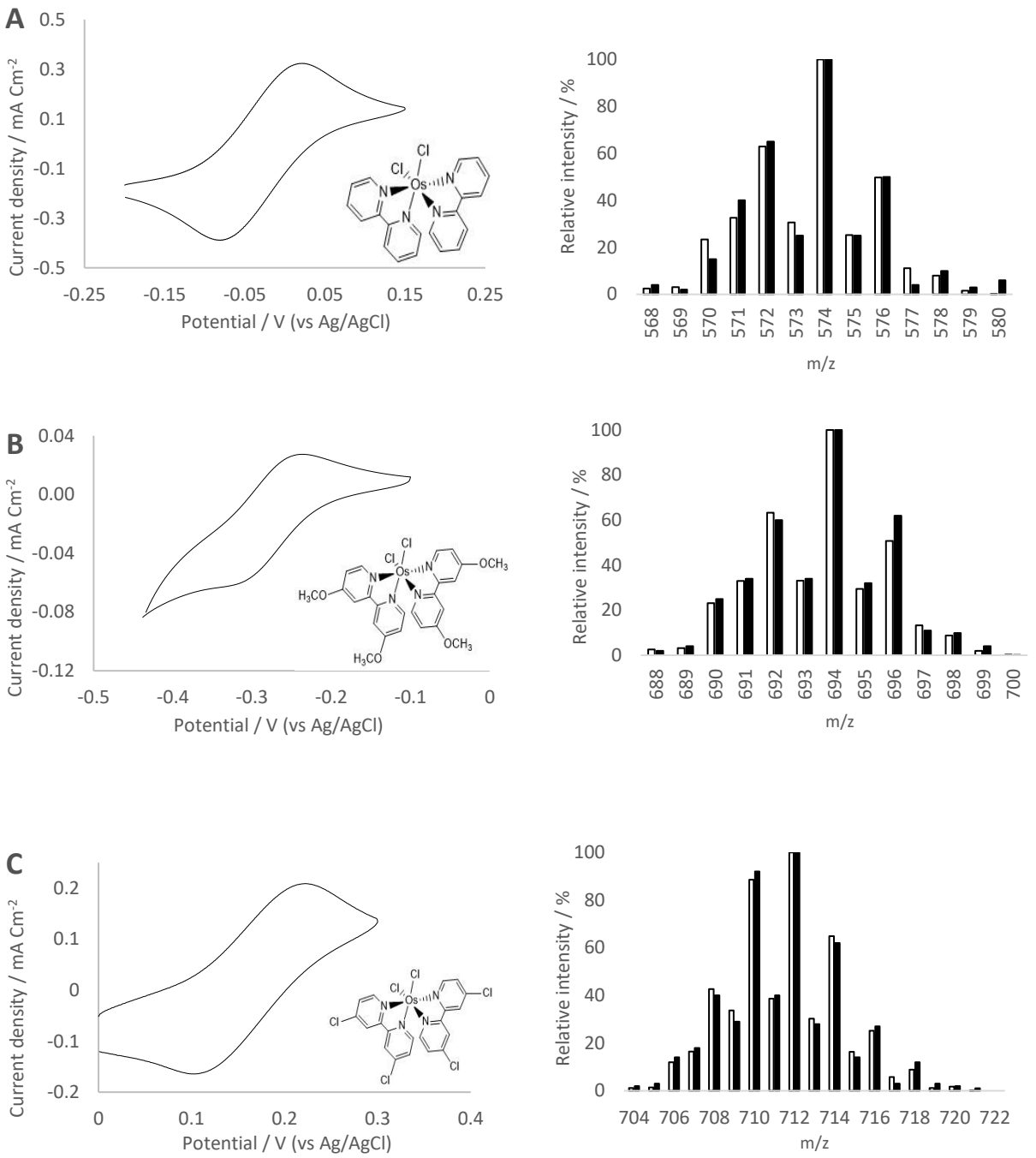

Figure 5: Proposed structure, CVs (at left) and bar graph (at right) representing experimental (black) and calculated (white) isotopic distribution pattern for (A) $Os(bpy)_2Cl_2$, (B) $Os(dmobpy)_2Cl_2$ and (C) $Os(dclbpy)_2Cl_2$ in acetonitrile. CVs recorded at GC electrodes in 50 mM, PBS pH 7 at room temperature at 100 mV s^{-1} scan rate. Inset: structure of the Os complexes.

Further characterisation of the cis-$Os(N\text{-}N)_2Cl_2$ complexes was undertaken using elemental analysis, with results shown in Table 2.

	% C		% H		% N	
Complex	**T**	**Obs**	**T**	**Obs**	**T**	**Obs**
$Os(dmobpy)_2Cl_2.2H_2O$	39.5	37.3	3.3	3.3	7.7	7.7
$Os(dclbpy)_2Cl_2.2H_2O$	32.1	33.6	1.6	1.4	7.5	7.2
$Os(bpy)_2Cl_2.2H_2O$	39.4	35.2	3.3	3.2	9.2	9.9

Table 2: Elemental analysis for osmium complexes, containing water of crystallisation, showing theoretical (T) and observed (Obs) values.

The differences in theoretical and observed values are as a result of impurities or solvent contained within these crude samples. Nonetheless, the crude complexes can be used for the follow-on ligand substitution reaction, as the required product is present in the crude sample, as evident from the MS and CV results.

2.3.1.2 Characterisation of poly(N-vinylimidazole)-based redox polymers

Following the successful synthesis of a range of Os polymer complexes of general formula cis-$[(Os(N\text{-}N)_2(PVI)_{10}Cl]^+$, aqueous solutions of the product were used for further characterisation. Proposed structure and the redox potentials of the polymer bound complexes, determined using CV of films immobilised at the surface of GC electrodes, is provided in Figures 6, 7 and 8. These films were prepared by drop coat deposition of 3 μL of an 8 mg ml^{-1} aqueous solution of redox polymer and 3 μL of a 15 mg ml^{-1} aqueous solution of epoxy crosslinker (polyethylene glycol didiglycidyl ether, PEGDGE). Cyclic voltammograms were recorded in 50 mM, PBS pH 7 at room temperature. The redox potentials observed for each of the different redox polymers are comparable to results already determined by others [9-30].

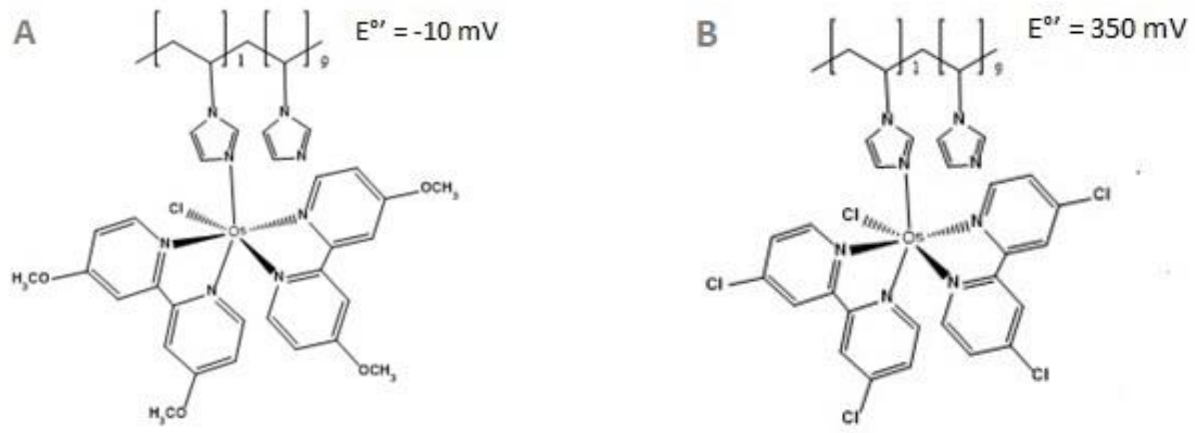

Figure 6: Proposed structures and redox potential of (A) [Os(4,4'- dimethoxy -2,2'-bipyridine)$_2$(PVI)$_{10}$Cl]$^+$ (Os(dmobpy)$_2$PVI) and (B) [Os(4,4'-dichloro-2,2'-bipyridine)$_2$(PVI)$_{10}$Cl]$^+$ (Os(dcbpy)$_2$PVI).

In order to purify the redox polymers, the crude polymer-bound complexes were dissolved in methanol and were allowed to centrifuge at 4000 rpm for ~ 30 minutes in Vivaspin ultrafiltration spin columns. For this Vivaspin columns with membrane size of 5000 MWCO were used, that allows removal of contaminating low molecular weight species such as un-reacted complexes. Cyclic voltammetry was used to monitor the progress of the ultrafiltration at regular intervals. After the required result was reached, the product was precipitated and allowed to air-dry. It was then further dried at 50 °C in a pre-heated oven overnight.

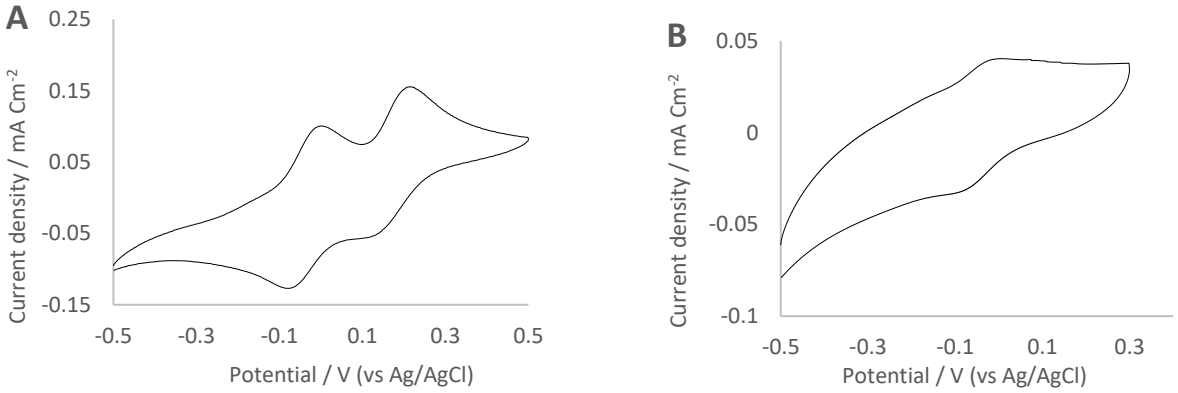

Figure 7: CVs of (A) crude Os(dmobpy)$_2$PVI and (B) purified Os(dmobpy)$_2$PVI. CVs recorded on films of redox polymer at GC electrodes in 50 mM, phosphate buffer pH 7 at room temperature at 100 mV s^{-1} scan rate.

Figures 7 and 8 shows the CVs for the crude and purified polymer complexes of Os(dmobpy)$_2$PVI and Os(dcbpy)$_2$PVI respectively, where the obvious presence of double substitution is apparent in Figures 7A, compared to 7B. In addition, the presence of unreacted, non-polymer-bound, starting material redox complex is apparent in Figure 8A compared to 8B.

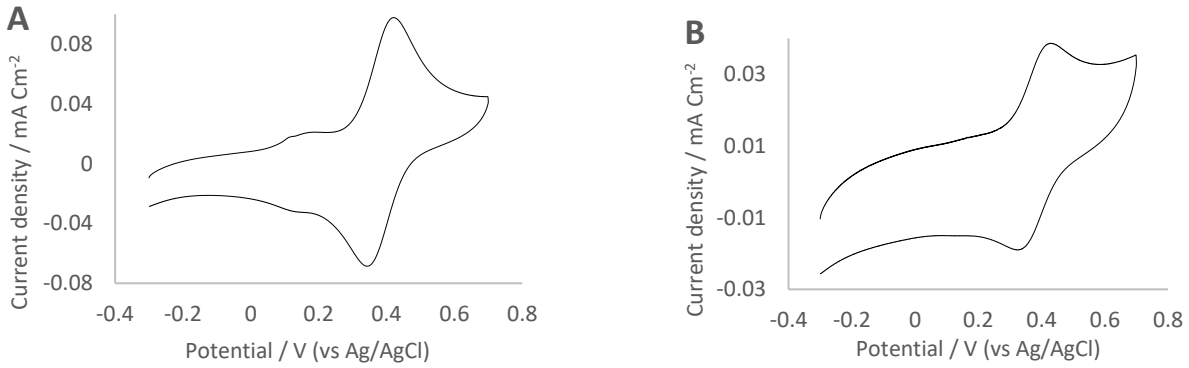

Figure 8: CVs of (A) crude Os(dcbpy)$_2$PVI and (B) purified Os(dcbpy)$_2$PVI . CVs recorded on films of redox polymer at GC electrodes in 50 mM, phosphate buffer pH 7 at room temperature at 100 mV s^{-1} scan rate.

2.3.1.3 Characterisation and purification of Os(dmobpy)$_2$4AMP complex

Following the successful synthesis of Os(dmobpy)$_2$4AMP complex with a yield of 78%, solutions of the complex were used for further characterisation. Films of the complex were prepared by drop coat deposition of 3 μL of an 8 mg ml^{-1} solution of redox complex in ethanol onto the surface of GC electrodes and allowing to dry, with CVs of the films provided in Figure 9. Cyclic voltammograms (100 mV s^{-1}) were recorded in 50 mM, PBS pH 7 at room temperature. The formal redox potential observed for Os(dmobpy)$_2$4AMP redox complex of 40 mV versus Ag/AgCl is comparable to results already reported by others [32]. The solid product was purified by column chromatography using aluminium oxide as stationary phase and a mobile phase of acetonitrile:toluene (1:1 volume ratio). The initial method to attempt to purify crude osmium complexes using column chromatography on aluminium oxide as stationary phase and 30:1 acetonitrile:methanol as eluent was unsuccessful. The relative components of

the mobile phase were changed gradually to 1:1 acetonitrile-methanol to provide the CV result shown in Figure 9B. The crude complex was compared with the purified Os(dmobpy)$_2$4AMP using CV, ESI-MS, HPLC and CHN characterisation methods.

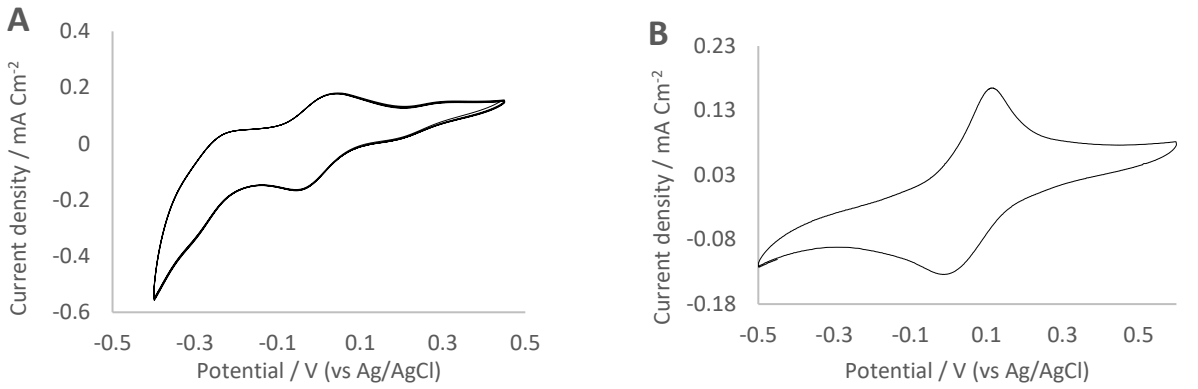

Figure 9: CVs of (A) crude Os(dmobpy)$_2$4AMP and (B) purified Os(dmobpy)$_2$4AMP. CVs recorded on films of redox polymer at GC electrodes in 50 mM, phosphate buffer, pH 7 at room temperature at 100 mV s^{-1} scan rate.

Analytical reversed phase HPLC was performed to characterise the pure versus the crude osmium complex based on ion-pair chromatography with 0.1% trifluoroacetic acid (TFA) in solvent for ion-pairing, with the results shown in Figure 10 [31].

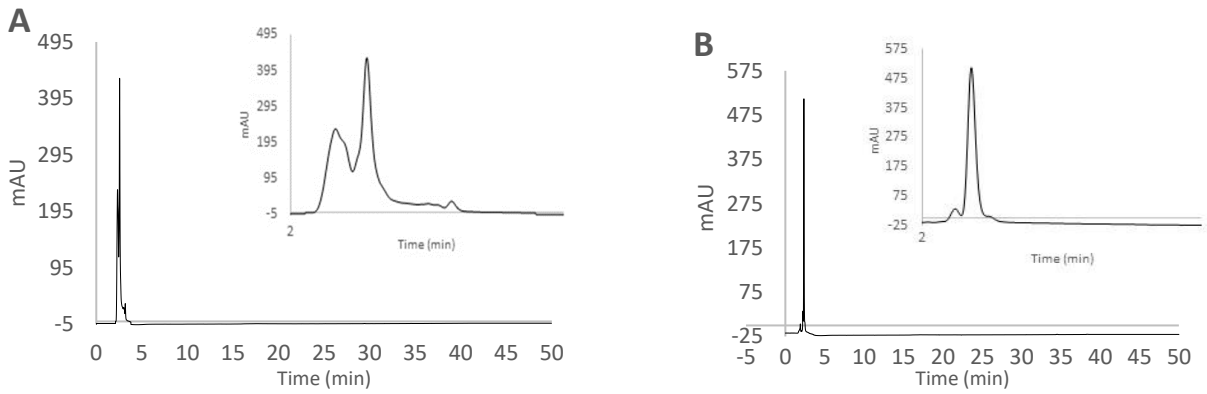

Figure 10: HPLC traces of (A) crude Os(dmobpy)$_2$4AMP and (B) purified Os(dmobpy)$_2$4AMP. HPLC results obtained with stationary phase of Luna 5 µm C18 and mobile phase of A=0.1% TFA in H_2O, B=0.1% TFA in CH_3CN, Gradient: 0-5 min: 10% B, 5-45 min: 10% B→50% B at 1%/min, 45-50 min: 100% B, 1 ml/min flow rate, 254 nm detection wavelength [31]. Inset: chromatogram from time 2 to 4 minutes.

In order to characterise the complexes further, ESI-MS was applied. The highest mass ion observed by the ESI-MS was consistent with the molecular ion of the complex under analysis. As illustrated in Figure 11, comparison between experimental and calculated isotopic distribution patterns show good correlation for the purified complex. The differences in experimental and calculated values are as a result of traces of starting complex, mass 694, contained within these samples.

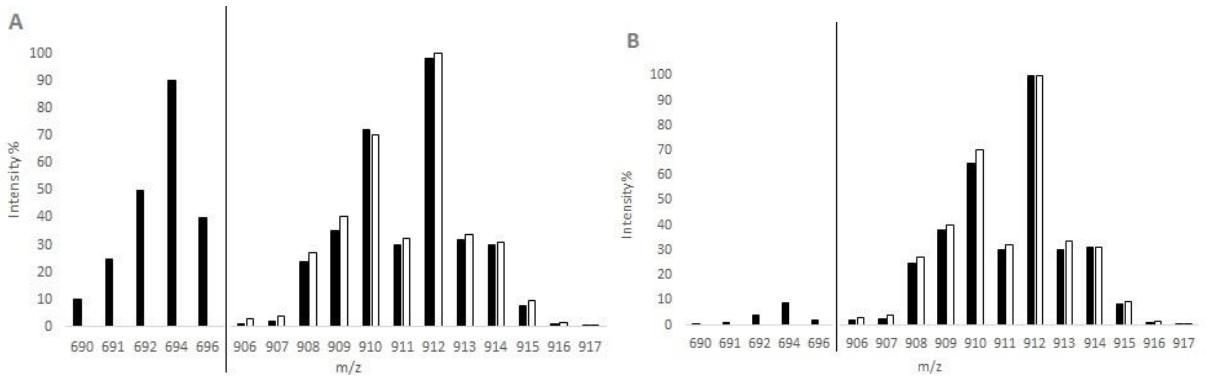

Figure 11: Bar graph representing experimental (black) and calculated (white) isotopic distribution pattern for (A) crude Os(dmobpy)$_2$4AMP and (B) purified Os(dmobpy)$_2$4AMP.

In addition, CHN was performed as with results presented in Table 3. The CHN results for the purified complex show improved correlation between the experimental and calculated results, compared to those for the crude product providing further evidence that the desired complex was synthesised and purified.

	% C		% H		% N	
Complex	**T**	**Obs**	**T**	**Obs**	**T**	**Obs**
Crude Os(dmobpy)$_2$4AMP	38	37	3.4	3	8.9	7.9
Purified Os(dmobpy)$_2$4AMP	38	38.2	3.4	3.2	8.9	8.8

Table 3: Elemental analysis for osmium complexes showing theoretical (T) and observed (Obs) values.

2.4 Conclusion

The synthesis, characterisation and purification of a range of osmium polypyridyl complexes and redox polymers is described. Subsequent to the production of cis-[$Os(N\text{-}N)_2Cl_2$], one of the Cl ligands was substituted with either a 4AMP ligand or a pendant monomer of a PVI polymer to form tetherable redox complexes or polymer bound complexes, respectively. Subsequently the products were characterised and purified using the relevant techniques. The purified osmium polypyridyl complexes and redox polymers are ready to be utilised as redox mediators in chapters 3, 4 and 5 of this thesis.

2.5 References

[1] W.W. Brandt, F.P. Dwyer, E.D. Gyarfas, Chemical Reviews, 54 (1954) 959-1017.

[2] K. Kalyanasundaram, Coordination Chemistry Reviews, 46 (1982) 159-244.

[3] A. Juris, V. Balzani, F. Barigelletti, S. Campagna, P. Belser, A. von Zelewsky, Coordination Chemistry Reviews, 84 (1988) 85-277.

[4] V. Balzani, A. Juris, Coordination Chemistry Reviews, 211 (2001) 97-115.

[5] T.J. Meyer, M.H.V. Huynh, Inorganic Chemistry, 42 (2003) 8140-8160.

[6] E.M. Kober, J.V. Caspar, B.P. Sullivan, T.J. Meyer, Inorganic Chemistry, 27 (1988) 4587-4598.

[7] P. Ó Conghaile, S. Kamireddy, D. MacAodha, P. Kavanagh, D. Leech, Analytical and Bioanalytical Chemistry, 405 (2013) 3807-3812.

[8] A.B.P. Lever, Inorganic Chemistry, 29 (1990) 1271-1285.

[9] R.J. Forster, J.G. Vos, Macromolecules, 23 (1990) 4372-4377.

[10] J.P. Paris, W.W. Brandt, Journal of the American Chemical Society, 81 (1959) 5001-5002.

[11] W.J. Vining, T.J. Meyer, Inorganic Chemistry, 25 (1986) 2023-2033.

[12] Y. Chen, M. Wang, K. Jin, D. Wang, Y. Na, L. Sun, Inorganic Chemistry Communications, 8 (2005) 606-609.

[13] M.K. Nazeeruddin, C. Klein, P. Liska, M. Grätzel, Coordination Chemistry Reviews, 249 (2005) 1460-1467.

[14] K. Kalyanasundaram, S.M. Zakeeruddin, M.K. Nazeeruddin, Coordination Chemistry Reviews, 132 (1994) 259-264.

[15] P. Kavanagh, D. Leech, Analytical Chemistry, 78 (2006) 2710-2716.

[16] S. Boland, F. Barrière, D. Leech, Langmuir, 24 (2008) 6351-6358.

[17] M. Pellissier, F. Barrière, A.J. Downard, D. Leech, Electrochemistry Communications, 10 (2008) 835-838.

[18] F. Gao, Y. Yan, L. Su, L. Wang, L. Mao, Electrochemistry Communications, 9 (2007) 989-996.

[19] A. Heller, Physical Chemistry Chemical Physics, 6 (2004) 209-216.

[20] N. Mano, F. Mao, A. Heller, ChemBioChem, 5 (2004) 1703-1705.

[21] E. Katz, I. Willner, A.B. Kotlyar, Journal of Electroanalytical Chemistry, 479 (1999) 64-68.

[22] D. MacAodha, P.O. Conghaile, B. Egan, P. Kavanagh, D. Leech, ChemPhysChem, 14 (2013) 2302-2307.

[23] S. Boland, P. Kavanagh, D. Leech, ECS Transactions, 13 (2008) 77-87.

[24] F. P. J. Dwyer, D. P Mellor. Chelating Agents and Metal Chelates. New York: Academic press (1964).

[25] F.H. Burstall, F.P. Dwyer, E.C. Gyarfas, Journal of the Chemical Society, (1950) 953-955.
[26] D.A. Buckingham, FP Dwyer, H. A. Goodwin, A. M. Sargeson, Australian Journal of Chemistry, 17 (1964) 325.
[27] P. Kavanagh, D. Leech, Physical Chemistry Chemical Physics, 15 (2013) 4859-4869.
[28] D. MacAodha, M.L. Ferrer, P. O'Conghaile, P. Kavanagh, D. Leech, Physical Chemistry Chemical Physics, 14 (2012) 14667-14672.
[29] D. MacAodha, P. O'Conghaile, B. Egan, P. Kavanagh, C. Sygmund, R. Ludwig, D. Leech, Electroanalysis, 25 (2013) 94-100.
[30] R. Antiochia, L. Gorton, Biosensors and Bioelectronics, 22 (2007) 2611-2617.
[31] H.B. Buck Jr., Z.D. Deng (2001) US Patent 6262264 B1
[32] R. Kumar, D. Leech, Bioelectrochemistry, 106 (2015) 41-46.

Chapter 3

Glucose oxidation in mediated enzymatic fuel cell anodes: effect of nanoparticle support and addition of oxygen

3.1 Introduction

Advances in electrical communication between enzymes and electrodes make it possible to fabricate miniaturised implantable power generation and sensing devices. Enzymatic fuel cells (EFCs) use enzymes as specific catalysts to oxidise glucose at the anode and reduce oxygen at the cathode, converting chemical energy into electrical power [1]. This specificity of enzyme catalyst eliminates the need for casings and ion-exchange membranes, making enzyme catalysts a good alternative to traditional metal catalysts in anode and cathode compartments and has led to renewed interest in the development of potentially implantable or portable, miniaturised, membrane-less EFCs operating under moderate ambient conditions and on sugars as fuel [2-4]. However, challenging issues such as low power and signal output and instability of the signal remain for the development of miniaturised implantable devices e.g. enzyme based biosensors and biofuel cells, pacemakers, and artificial sensors etc., which have thus instigated a range of studies to seek to improve the performance of EFCs. Research is mainly focused on finding a combination of enzyme electrodes that will deliver sufficient current at high enough cell voltages to power electric devices. A wide variety of nanomaterials, especially nanoparticles with different properties have found broad application in many fields such as biosensors and biofuel cells. Owing to their small size (normally in the range of 1–100 nm), nanoparticles

exhibit unique chemical, physical and electronic properties that are different from those of bulk materials, and can be used to construct novel and improved sensing devices and biofuel cells. Many types of nanoparticles of different sizes and compositions are now available, which facilitate their application. Generally, metal nanoparticles have excellent conductivity which make them suitable for acting as "electronic wires" to enhance the electron transfer between redox centres in proteins and electrode surfaces [5]. Nanoparticles are suitable for enzyme immobilisation, in some particular cases nanoparticles could not only increase electron transfer rate between enzyme and an electrode surface, but could act like a nano-scaled electrode [6]. Addition of multi-walled carbon nanotubes (MWCNT) to the enzyme electrode preparation step results in increased surface area, improved operational output and stability under pseudo-physiological conditions [7]. These nanostructures provide a support which acts as a scaffold for improved retention of enzymes and electron-shuttling mediators as reported on by many research groups in recent years [8, 9]. For example, it has been reported that the addition of CNTs to the enzyme electrode preparation step has resulted in improved performance of these electrodes over those prepared without addition of such materials, due to provision of highly conductive, mechanically strong, high surface area and chemically stable films on electrodes [10,11]. However, no comprehensive study has been performed on the effects of nanoparticles with different chemical composition on the anode performance. Mediated electron transfer achieved by the co-immobilisation of enzymes with electron-shuttling mediators on solid electrodes can enhance current capture via electron-hopping between redox active sites of enzymes and mediator, and subsequent mediator self-exchange redox reactions to transfer electrons between enzyme and electrode surfaces [4-13]. For example, over the past two decades, Heller and co-workers [14] have pioneered the use of osmium redox polymers in films on electrodes prepared by epoxy cross-linking of electrostatic adducts of glucose oxidase (GOx) enzyme and redox polymer, using PVI as the polymer backbone, to provide "wired" enzyme electrodes capable of producing glucose oxidation current. However, a difficulty with use of PVI as the polymer backbone for preparation of redox polymers is the lack of commercial availability of PVI, and laboratory-scale synthesis of PVI by bulk free radical polymerisation [15] results in wide molecular weight distribution which affects the physical properties of polymers such as solubility, density etc. In addition, osmium complex loading on the PVI backbone by ligand substitution is also difficult to control and replicate, leading to batch-to-

batch variation in enzyme electrode performance using these redox polymers [16, 17]. Alternatively, commercially available and well characterised polymer supports for preparation of enzyme electrodes can be used. Danilowicz *et. al.* [18] reported on coupling of osmium complexes that contain an aldehyde functional group distal to the metal co-ordinating site to amine-based polymers and enzymes in films on electrodes to provide enzyme electrodes. Osmium based polypyridyl complexes are broadly explored for a range of applications as redox catalysts and mediators, owing to the ability to modulate the mediator redox potential of the central Os metal by using coordinating ligands and the relative stability of the resulting complexes in the reduced/oxidised states Os(II/III), [19]. For example, the redox potential of osmium based complexes can be tuned across a wide potential window by altering the ligand of a complex [20, 21]. Surface confined osmium based complexes are capable of mediating electron transfer to/from enzymatic [22, 23] as well as microbial systems on electrodes [24, 9]. In MET, for biocatalytic electrodes, it has been proposed that mediators should have redox potentials approximately 50 mV downhill from the redox potential of the enzyme in order to provide a driving force for electron transfer for an effective electron exchange. For the fuel cell application, as the power is dependent on differences of potentials by the current generated, there has to be a compromise between the need to have a high cell voltage and a high current, hence the synthesis and application of low potential osmium complexes such as $Os(dmobpy)_2$4AMP with redox potential of 40 mV versus Ag/AgCl for application to anodes. This chapter presents a comparison of glucose oxidation by enzyme electrodes prepared by coupling glucose-oxidising enzyme and an amine-functionalised osmium complex to carboxymethyl dextran (CMD) on electrode surfaces in the presence of a range of conductive and non-conductive nanoparticles as supports. The size and property of the nanoparticle supports may improve current density and/or stability for these electrodes. Glucose oxidase is a widely used glucose oxidising enzyme due to its high turnover rate and commercial availability, thus becoming a benchmark for comparison of glucose oxidising enzyme electrodes. However, the main disadvantage to use of GOx is its sensitivity to oxygen, which can diminish the power output of EFCs [26-28] through oxygen competition for electrons [13]. In order to address this issue, oxygen-insensitive glucose oxidising enzymes, such as the glucose dehydrogenases (GDH) can be utilised. As described in section 1.4.2, GDH belongs to

the family of oxidoreductase capable of oxidising glucose by transferring one or more electrons and protons to their respective acceptor such as NAD, PQQ co-factor or a flavin such as FAD.

3.2 Experimental

3.2.1 Materials

$Os(dmobpy)_2$4AMP complex was synthesised, as described in Chapter 2, by ligand substitution of one Cl ligand of $Os(dmobpy)_2Cl_2$ with 4-aminomethylpyridine by heating of the complex in an ethylene glycol solution containing 1.1 mole equivalents of ligand at reflux, with ligand substitution monitored by cyclic voltammetry and differential pulse voltammetry, as reported on previously, and in Chapter 2 [31, 31]. The $Os(dmobpy)_2Cl_2$ complex was prepared from $(NH_4)_2OsCl_6$ according to modified literature methods, as described in Chapter 2 [31, 21]. All chemicals were purchased from Sigma–Aldrich and all solutions were prepared from Milli-Q (18.2 MΩ cm) water, unless otherwise stated. GOx from *Aspergillus niger*, CMD (average molecular mass of 15,000 Da) and an FAD-dependent glucose dehydrogenase (FADGDH) from *Aspergillus sp.* (Sekisui, Cambridge) were used as received. MWCNT, DXL 110-170 nm X 5-9μm (Sigma-Aldrich) were treated by stirring in nitric acid at reflux for 6 h, and were isolated by filtration.

3.2.2 Methods

The GOx average activity was calculated as 221 ± 33 U mg^{-1} using the o-dianisidine and horseradish peroxidase coupled spectrophotometric assay by monitoring absorbance changes at 460 nm on an Agilent 8453 UV/Vis spectrophotometer. This activity correlated well with the activity reported by Sigma Aldrich (100 – 250 U mg^{-1}) [32]. The FADGDH activity was determined to be 242 ± 45 U mg^{-1} using a nitrotetrazolium blue with phenazine methosulfate coupled spectrophotometric assay by monitoring absorbance changes at 570 nm [33]. Working electrodes (3 mm diameter) were prepared from graphite rods (NC001295; GraphiteStore.com,

Inc., Buffalo Grove, IL) shrouded with heatshrink tubing and polished on fine grit paper followed by thorough rinsing with Milli-Q water to create a working geometric surface area of 0.0707 cm^2. Working electrodes were sonicated in Milli-Q water for 10 min and dried under nitrogen gas prior to use. Custom built Ag/AgCl reference electrodes (3 M KCl) and platinum foil counter electrodes (Goodfellow) were used in the cell. CH Instruments 600 series or 1030 multichannel potentiostat (IJ Cambria, Llanelli, UK) coupled to a thermostated electrochemical cell was used to perform all electrochemical measurements. All electrochemical measurements were performed in phosphate buffered saline (PBS, 0.05 M phosphate, pH 7.4, 0.15 M NaCl) at 37°C. To prepare the anodes, the carboxylic acid functional groups of the polymer and the acid treated MWCNT were activated for coupling to amine functional groups. The activation was performed by incubation of 10 μL of CMD (5 mg ml^{-1}) and 8.7 μL aqueous suspension 2.8 mg mL^{-1} of functionalised nanoparticles (for the studies in section 3.3.1) or 46.25 mg mL^{-1} of acid treated MWCNT (for the studies in sections 3.3.2 and 3.3.3) with 4 μL of an aqueous solution of 40 mM N-[3-dimethylaminopropyl]-N'-ethylcarbodiimide (EDC) and 10 mM N-hydroxysuccinimide (NHS) in an eppendorf for 12 minutes. This was followed by addition of GOx (5 μL of 10 mg ml^{-1}) and redox complex (7.32 μL of 4.5 mM aqueous solution) to the eppendorf. Enzyme electrodes were prepared by drop coating 39 μL of the resulting solution onto the graphite disk, with the dropcoat dried for 18 hr at room temperature to allow crosslinking, followed by rinsing of the enzyme electrode with PBS before testing commenced.

3.2.3 Selection of nanomaterial

Three different nanoparticle types were selected for comparison: carboxylic acid functionalised gold nanoparticles (5 nm diameter, PEG 5000 coated, dispersion in H_2O), 3-aminopropyl functionalised silica nanoparticles (100 nm particle size, dispersion 3% (W/V) in ethanol) and acid treated MWCNT (DXL 110-170 nm X 5-9μm). In addition the same system with no nanoparticles was used as control. The morphology of the nanoparticle-decorated electrodes was examined using a Hitachi S-4700 scanning electron microscope with amplification ranging from 30X to 500,000X. Figure 1 illustrates the SEM images of the nanoparticles.

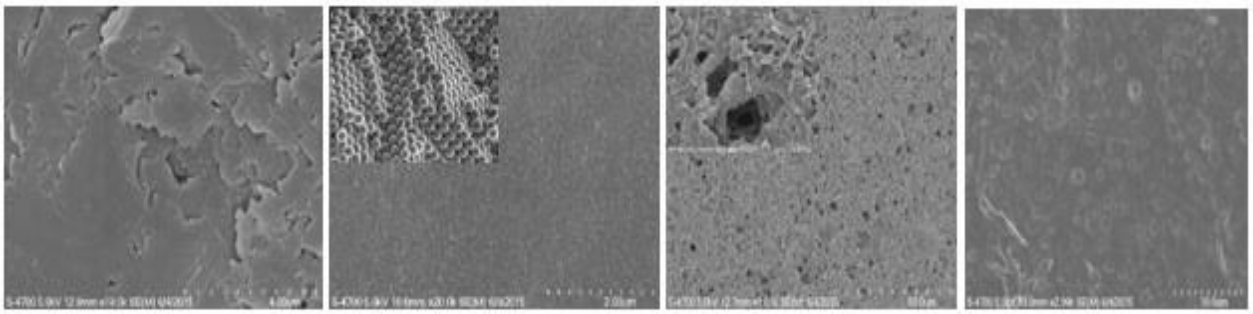

Figure 1: SEM image (Left to right) of bare graphite disk electrode 10000x magnification, graphite anodes decorated with Os(dmobpy)$_2$4AMP, GOx, CMD and either 3-aminopropyl functionalised silica 1000x and 10000x (Inset) magnification, acid treated MWCNT 1000x and 10000x (Inset) magnification or carboxylic acid functionalised AuNPs 1000x magnification.

3.3 Results and Discussion

3.3.1 Effect of nanoparticles on enzyme electrodes

Enzymatic electrodes for glucose oxidation were prepared initially by co-immobilisation of Os(dmobpy)$_2$4AMP with GOx, CMD as a polymer support, with a range of conductive and non-conductive nanoparticles as supports, to probe whether the properties of different supports with similar sizes can improve current density and/or stability for these electrodes. The relative amounts of components (redox complex, enzyme, nanoparticle and polymer support) used to prepare a previously reported DoE-optimised anode were initially selected to test the effect of adding different types of nanoparticles to the enzymatic electrodes. These amounts were reported to provide maximum glucose-oxidation current [29]. However, a lower amount of the nanoparticle than the DoE-optimised amount of 46.25 mg mL^{-1} (optimised using MWCNT) was subsequently selected to permit comparison of electrode performance using different nanoparticles as the maximum amount available in the commercial sample of the carboxylic acid functionalised Au NPs dispersion is 2.8 mg mL^{-1}; this amount of nanoparticle was therefore used for comparison. To identify differences between the anodes with different nanoparticles, a high current density is needed, thus the concentration of the polymer, mediator and enzyme was not altered proportionally so as to retain relatively high current output. In

addition a lower concentration of polymer decreased the stability of the components on the electrode surfaces and led to leaching of component from the surfaces. The enzymatic electrodes were characterised using CV and amperometry in the presence and absence of the substrate glucose in the absence of oxygen. Cyclic voltammograms recorded for all enzymatic electrodes in the absence of glucose display peaks for oxidation and reduction centred at 0.05 V vs Ag/AgCl (Figure 2), which can be assigned to the Os(II/III) transition of the redox complex, as this value is similar to the redox potential previously observed for an $Os(dmobpy)_2$4AMP complex in solution [34, 35]. The similarity of redox potential between solution-phase and immobilised complex indicates that the Os(II/III) redox transition is generally not affected by the immobilisation procedure. In addition, the difference in oxidation and reduction peak potentials (ΔE_p) for all enzymatic electrodes is 0.055 ± 0.004 V, which is less than the 0.059 V separation expected for a one electron redox process under semi-infinite diffusion control, but greater than 0 mV as expected for surface-confined redox species [36].

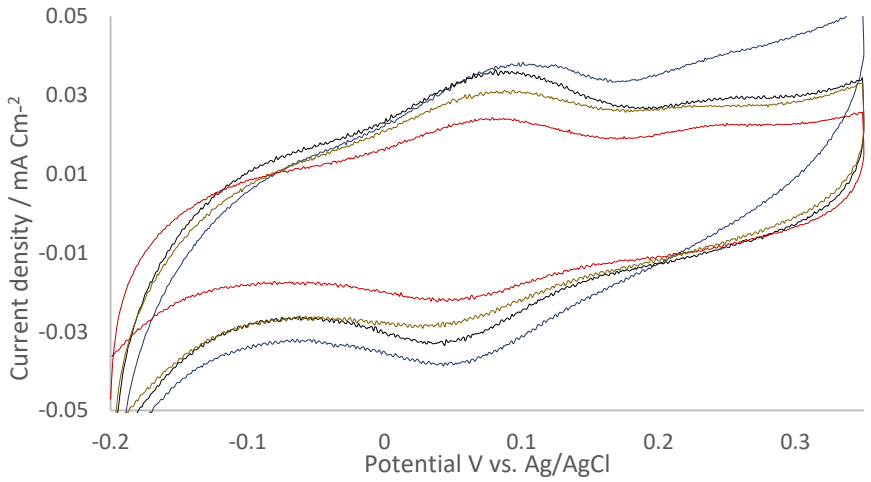

Figure 2: CVs recorded at 1 mV s^{-1} in the absence of air and glucose in PBS (pH 7.4, 37°C) for enzyme electrodes prepared from $Os(dmobpy)_2$4AMP, GOx, CMD and either with 3-aminopropyl functionalised silica (blue), acid treated MWCNT (black), carboxylic acid functionalised AuNPs (golden) and without nanoparticles (red).

In the absence of substrate, peak currents vary linearly with scan rates (< 20 mVs^{-1}), indicative of a surface controlled response [36]. As shown in Figure 3, at higher scan rates (> 20 mV s^{-1}), the peak currents scale linearly with the square root of scan rate, indicative of semi-infinite diffusional charge transport limitations within the films, as expected for multi-layered films [17].

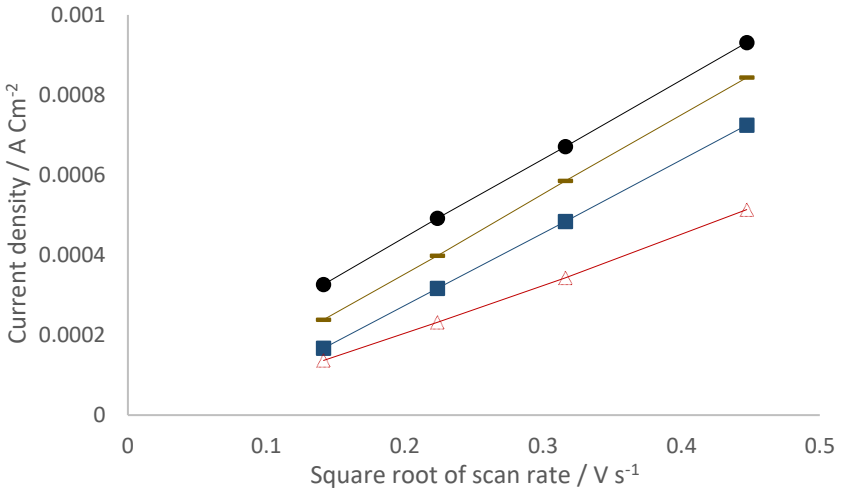

Figure 3: Plot of anodic peak currents, extracted from cyclic voltammograms versus square root of scan rates for enzyme electrodes decorated with $Os(dmobpy)_2$4AMP, GOx, CMD and either 3-aminopropyl functionalised silica (▪), acid treated MWCNT (●), carboxylic acid functionalised AuNPs (-) or control (Δ) (no NPs).

The area under the peak for CV recorded at slow scan rates in the absence of substrate can be integrated to provide an estimate of the redox complex surface coverage (Γ_{Os}) [17]. For example, Γ_{Os} values of 53 ± 2 nmol cm^{-2} and 37 ± 3 nmol cm^{-2} were obtained for enzymatic electrodes containing CMD and GOx in the presence and absence of MWCNT, respectively. These values are characteristic of multilayer formation (~500 layers) [36] and are comparable to the values obtained previously for enzyme electrodes prepared by co-immobilisation of osmium redox complexes or polymers and enzymes [17, 39]. Upon the addition of high concentrations (100 mM) of glucose, sigmoidal-shaped cyclic voltammograms, characteristic of catalytic oxidation of glucose by the enzyme, were obtained for all enzyme electrodes [39], as shown in Figure 4. Performance of enzyme electrodes is compared using either CV or constant potential amperometry at an applied potential of 0.2 V vs Ag/AgCl, selected to be 150 mV positive of the Os(II/III) oxidation to ensure steady-state mediated glucose oxidation

current. The amperometric responses show glucose oxidation currents that are similar to the catalytic current observed in slow scan CVs, with slight increases in current density for amperometry over CV due to use of convection (150 rpm) of solutions in amperometry to avoid substrate depletion over the course of the experimental timescale. For example, the 1 mV s^{-1} CV current density of 0.2 ± 0.05 mA cm^{-2} for oxidation of 100 mM glucose at enzyme electrodes prepared from $Os(dmobpy)_2$4AMP co-immobilised with GOx, MWCNT and CMD as a polymer support compares well with the amperometric 0.23 ± 0.01 mA cm^{-2} current density obtained at 0.2 V applied potential (Figures 4 and 5).

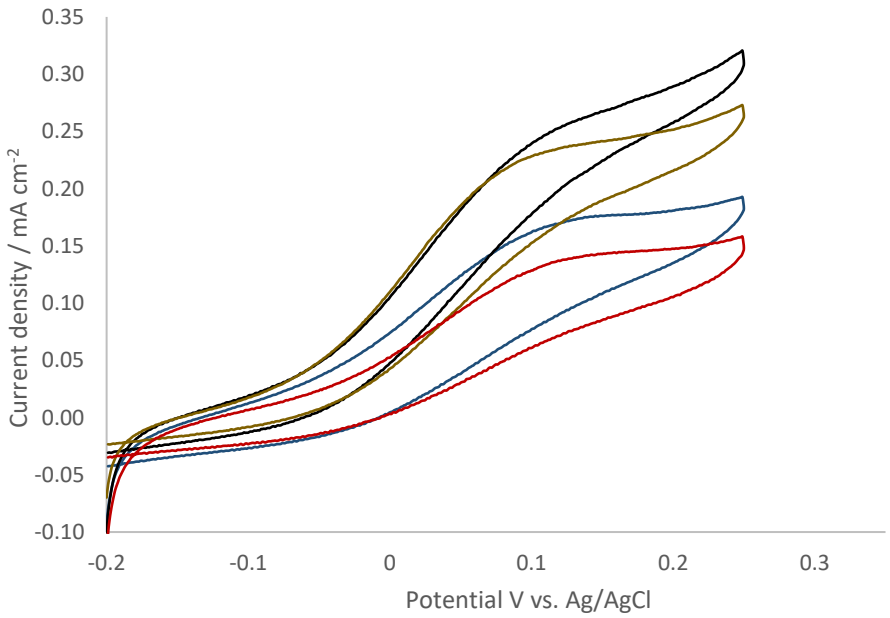

Figure 4: CVs recorded at 1 mV s^{-1} in the absence of air and presence of 100 mM glucose in PBS (pH 7.4, 37°C) for enzyme electrodes prepared from $Os(dmobpy)_2$4AMP, GOx, CMD and either with 3-aminopropyl functionalised silica (blue), acid treated MWCNT (black) and carboxylic acid functionalised AuNPs (golden) and without nanoparticles (red).

A comparison of glucose oxidation current density, extracted from amperometric measurements at 0.2 V vs. Ag/AgCl, as a function of glucose concentration when the nanoparticle type was varied is shown in Figure 5. Initial comparison shows higher current from amperometry for electrodes prepared using nanoparticles (MWCNT>AuNP>silica) over that obtained using no nanoparticles. For all enzymatic electrodes, the increase in glucose-oxidation current density

as a function of glucose concentration followed the trend expected for the steady-state approximation of Michaelis–Menten enzyme kinetics, with an initial linear increase in current density that subsequently approached a maximum at high glucose concentrations. An estimate of apparent Michaelis constant, K_m^{app}, and apparent maximum saturated currents j_{max}^{app} is obtained by non-linear least-squares fitting of the data, recorded in the absence of oxygen in Figure 5, to a Michaelis-Menten model and using the Lineweaver-Burke plots of the transformed data to verify the fit. The Michaelis-Menten constant represents the concentration of the substrate when the reaction velocity is equal to one half of the maximal velocity for the reaction. Low K_m^{app} values could indicate a high binding affinity, as the reaction will approach j_{max}^{app} more rapidly and a high K_m^{app} could indicate that the enzyme does not bind as efficiently with the substrate. When all the active sites of the enzymes have been occupied due to the high concentration of substrate, the reaction is saturated, which means that the enzyme is at its maximum capacity and increasing the concentration of substrate will not increase the rate of turnover and the current reaches plateau. Glucose oxidase is relatively specific for D-glucose with a K_m of 33-110 mM in solution [50,51].

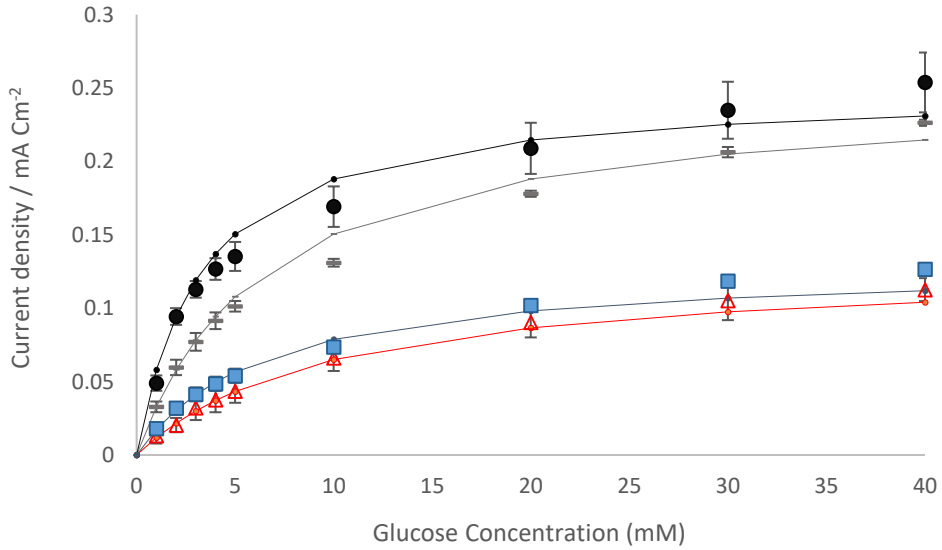

Figure 5: Average glucose oxidation current density recorded in PBS (37 °C) at 150 rpm at an applied potential of 0.2 V, as a function of glucose concentration for enzyme electrodes decorated with $Os(dmobpy)_2$4AMP, GOx, CMD and either 3-aminopropyl functionalised silica (▪), acid treated MWCNT (●), carboxylic acid functionalised AuNPs (-) or control (Δ) (no NPs) and Michaelis-Menten steady state approximation (solid line) for each enzyme electrode (n=3).

As shown in table 1, the K_m^{app} values obtained for all enzymatic electrodes are similar, although values for the MWCNT-based electrodes are slightly lower, at 3.3 ± 0.4 mM compared to 10.0 ± 3.4 mM with no nanoparticles. Reports have suggested that mass transport can be a limiting factor for enzyme electrodes and the K_M^{app} may therefore reflect instead a difference in mass transport and not affinity [45, 46].

Nanoparticle	j_{max}^{app} **(mA cm^{-2})**	**Surface coverage (Γos nmoles cm^{-2})**	**% Enzyme activity on surface**	K_m^{app} **(mM)**	**Initial current density in 100 mM glucose (mA cm^{-2})**	**Final current density in 100mM (mA cm^{-2}) After 24 hr**	**% initial current density after 24 h**
None	0.13 ± 0.01	37 ± 3	32	10.0 ± 3.4	0.11 ± 0.01	0.010 ± 0.002	8.9 ± 1
MWCNT (acid treated)	0.25 ± 0.02	53 ± 2	38	3.3 ± 0.4	0.23 ± 0.01	0.031 ± 0.003	13.5 ± 1
AuNPs carboxylic acid functionalised	0.25 ± 0.01	48 ± 3	43	6.6 ± 0.1	0.24 ± 0.01	0.007 ± 0.001	3.0 ± 0.3
Silica 3-aminopropyl functionalised	0.13 ± 0.01	49 ± 2	38	6.5 ± 0.90	0.12 ± 0.01	0.010 ± 0.001	8.5 ± 0.1

Table 1: Enzyme electrode performance for electrodes prepared using redox complex, GOx, CMD and conducting or non-conducting nanoparticles in the presence of 100 mM glucose. Maximum enzyme activity, if all added enzyme activity is retained, is 11.07 ± 0.17 U.

Enzyme electrodes prepared with MWCNT and AuNPs display higher saturated current densities compared to those prepared with silica and without nanoparticles (control) (Figure 4 and Table 1). As expected, use of conductive nanoparticles results in higher current density than the use of non-conductive silica nanoparticles as well higher current density than the control. The conductive paths to the electrode [40] enhance charge transport towards the graphite [40, 42]. A charge transport diffusion parameter ($D^{1/2}C$, where D is a diffusion co-efficient and C is

the concentration of redox complex within the enzyme electrode films) can be estimated from the slopes of the plots in Figure 3, using the Randles-Sevçik equation. This parameter is higher, with a value of 1.06×10^{-7} mol cm $^{-2}$ s $^{-1/2}$ in the presence of AuNPs and MWCNT compared to 9.8×10^{-8} for silica and 6.6×10^{-8} mol cm $^{-2}$ s $^{-1/2}$ in the absence of nanoparticles (control). The value observed for the control is similar to the value reported previously for an enzyme electrode prepared by co-immobilisation of an osmium redox polymer with a laccase enzyme on electrodes [49]. Interestingly for all enzyme electrodes prepared with a nanoparticles as support surface, redox site surface coverage and enzyme activity are similar, indicating that the higher saturated current densities for MWCNT and AuNPs are due to contribution of increased charge transport and/or conductivity (Table 1). Percentage remaining for enzyme activity on electrode surface was calculated from the intial and final enzyme activity after 24 hr.

Operational stability of glucose-oxidation current generation is important for the application of such enzymatic electrodes to continuous glucose monitoring, or electricity generating, devices. Testing for stability of glucose oxidation current generation for selected enzyme electrodes was evaluated from constant potential amperometry at 0.2 V vs. Ag/AgCl for 24 h in saturated glucose (100 mM) solution in PBS at 37 °C, with stirring at 150 rpm, as shown in Figure 6. Approximately 13.5% of initial current density response remains after a 24 h period for enzyme electrodes prepared from Os(dmobpy)$_2$4AMP, GOx, MWCNT and CMD compared to 8.9 % remaining for the control. The improved operational stability of MWCNT based enzyme electrodes may be as a result of improved retention of glucose oxidase activity over time, as these electrodes retained 12% of initial enzyme activity compared to 5.7% and 2.4% for silica NPs and control and only 1.5% for the AuNPs enzyme electrodes, respectively, after 24 h. The decrease in current density correlates well with the decrease in retained enzyme activity within the enzymatic electrode films, suggesting that retention of enzyme activity is the key parameter that controls the operational stability for these electrodes. However, in this study AuNPs-based electrodes provide lower stability of response in comparison with control electrodes prepared without addition of nanoparticles. Such decrease in stability of AuNPs based electrode could be explained by higher leakage of AuNPs from the electrode surface as AuNPs have higher density as a solid (approximately 500%) than MWCNT and silica NPs. A similar decrease of analytical signal of up to 96% after 2 weeks has been previously reported by German *et al.* [42]

for enzyme electrodes based on glucose oxidase immobilised on a graphite rod electrode modified by gold nanoparticles.

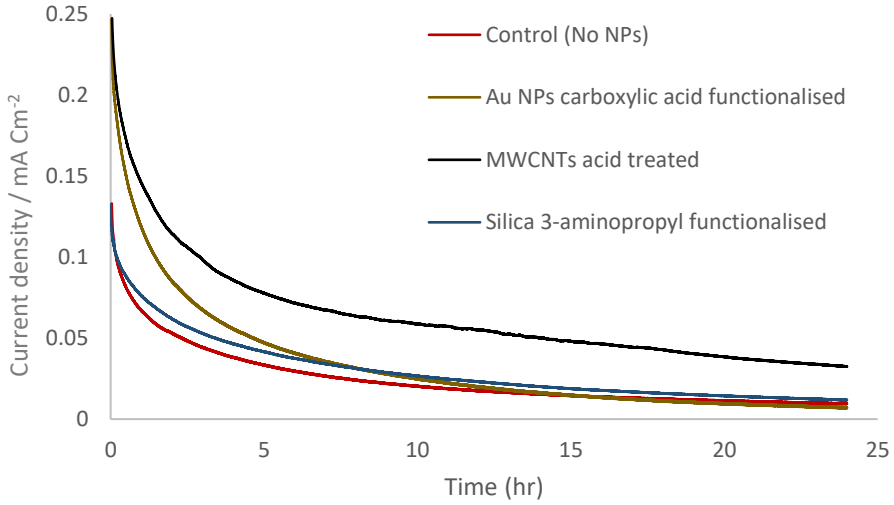

Figure 6: Operational stability recorded in PBS (37 °C) at 150 rpm at an applied potential of 0.2 V vs. Ag/AgCl in 100 mM glucose. The mean values of three independent measurements by three same type electrodes are presented (standard deviations as in Table 1).

3.3.2 Effect of amount of MWCNT on enzyme electrode response

As demonstrated in section 3.3.1, the inclusion of MWCNT compared to other nanoparticles resulted in improved catalytic current and operational stability of the enzyme electrodes. These electrodes were thus selected for comparison to enzyme electrode performance with previously reported DoE-optimised amounts of the MWCNT, enzyme and polymer support. The enzyme electrodes were thus prepared by co-immobilisation of the redox complex $Os(dmobpy)_2$4AMP, GOx as enzyme with CMD as a polymer support and either 2.8 mg mL^{-1} (amount used in section 3.3.1) or 46.25 mg mL^{-1} of MWCNT (DoE-optimised amount). The enzyme electrodes were characterised using CV and amperometry in the presence and absence of the substrate glucose. Upon addition of high concentrations (100 mM) of glucose in the absence of oxygen, sigmoidal-shaped cyclic voltammograms, characteristic of catalytic oxidation of glucose by the enzyme were obtained for all enzyme electrodes. Based on the optimised amount of components, enzyme electrodes immobilised with GOx display current density of 4.7 ± 0.2 at

0.2 V vs. Ag/AgCl in buffer containing 100 mM glucose that compares well with the previously reported 5.2 ± 0.2 mA cm^{-2} [29]. Initial comparison of slow-scan cyclic voltammograms show current density of 2.7 ± 0.2 mA cm^{-2} compared to 0.2 ± 0.05 mA cm^{-2} for oxidation of 100 mM glucose at enzyme electrodes prepared from $Os(dmobpy)_2$4AMP co-immobilised with GOx and CMD and 46.25 mg mL^{-1} or 2.8 mg mL^{-1} of MWCNT, respectively (Figure 7). For all enzyme electrodes, the increase in glucose-oxidation current density as a function of glucose concentration followed the trend expected for the steady-state approximation of Michaelis–Menten enzyme kinetics as explained previously. The K_m^{app} obtained from amperometric current density at 0.2 V applied potential (Figure 8) for GOx-based electrodes with 46.25 mg mL^{-1} of MWCNT was higher at 20.7 ± 1.2 compared to 3.3 ± 0.4 for lower amounts of MWCNT (2.8 mg mL^{-1}). As reported previously the K_M ^{app} obtained for these enzyme electrodes may reflect a difference in mass transport and not affinity as mass transport can be the limiting factor [45, 46]. In addition, the stability after 24 h for GOx-based electrodes with 46.25 mg mL^{-1} of MWCNT is 51 %: considerably higher compared to 13.5 % for the enzyme electrodes prepared using 2.8 mg mL^{-1} of MWCNT.

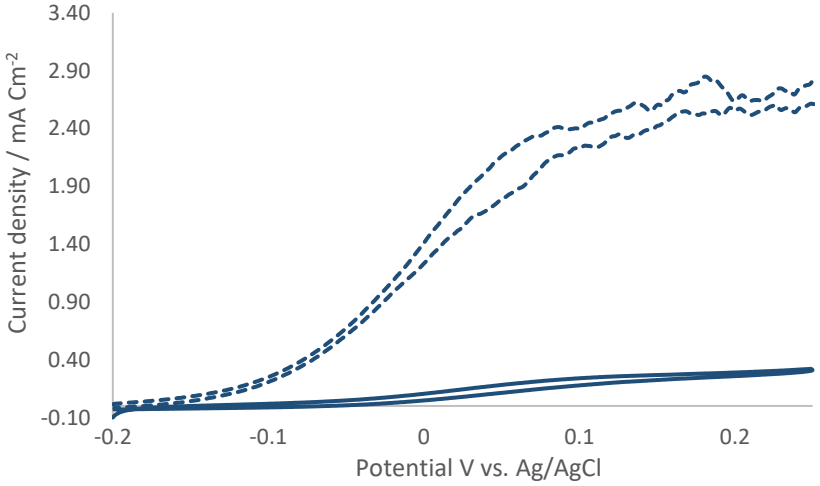

Figure 7: CVs recorded at 1 mV s^{-1} in the absence of oxygen and presence of 100 mM glucose in PBS (pH 7.4, 37°C) for enzyme electrodes prepared from $Os(dmobpy)_2$4AMP, CMD, GOx and either 2.8 mg mL^{-1} (solid line) or 46.25 mg mL^{-1} (dotted line) of MWCNT.

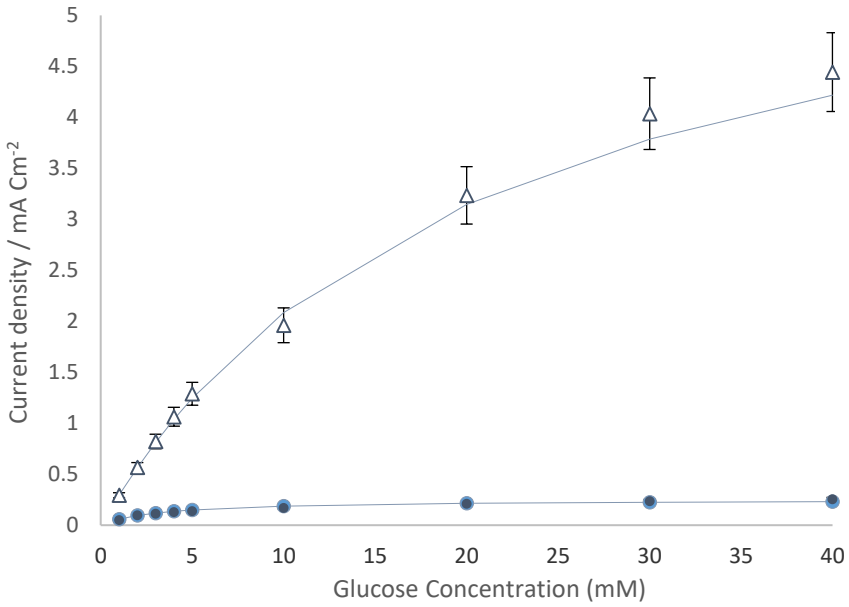

Figure 8: Average glucose oxidation current densities (n=3) as a function of glucose concentration, measured in PBS at 37 °C with stirring at 150 rpm in the absence of air at an applied potential of 0.2 V, for enzymatic electrodes using GOx co-immobilised with Os(dmobpy)$_2$4AMP, CMD and either 2.8 mg mL^{-1} (●) or 46.25 mg mL^{-1} (Δ) MWCNT. Solid lines show the Michaelis-Menten steady state approximation for each type of enzyme electrode.

3.3.3 Effect of oxygen on enzyme electrodes

Further experiments were conducted in order to evaluate the role and effect of oxygen on the enzyme electrodes that produced the highest current densities (those prepared using the 46.25 mg mL^{-1} acid treated MWCNT dispersion). To study this enzyme electrodes were prepared by co-immobilisation of the redox complex Os(dmobpy)$_2$4AMP with MWCNT, CMD as a polymer support and either GOx or FADGDH as enzyme. The enzyme electrodes were characterised using CV and amperometry at an applied potential of 0.2 V vs Ag/AgCl in the presence and absence of the substrate glucose. Upon addition of high concentrations (100 mM) of glucose, sigmoidal-shaped cyclic voltammograms, characteristic of catalytic oxidation of glucose by the enzyme were obtained for all enzyme electrodes [41] prepared from Os(dmobpy)$_2$4AMP, acid treated MWCNT, CMD and either GOx or FADGDH as shown in Figure 9. Initial comparison of the effect of oxygen on enzyme electrode response shows a

decrease in glucose oxidation current density for all systems in the presence of oxygen. For example, in air saturated electrolyte, the enzyme electrodes in solutions containing 100 mM glucose show a decrease in current density of 20% in air as compared to N_2 saturated condition for those prepared using FADGDH, and a 32% decrease in current density for those prepared using GOx. The decrease in catalytic currents evident in the CVs (Figure 9) in the presence of oxygen suggest that reduction of molecular oxygen by the osmium redox mediator, which in turn lowers the amount of osmium redox centres that can be accessed by the electrons from glucose substrate, is a reason for a decrease in current density for all enzyme electrodes in the presence of oxygen, including those based on FADGDH. This has been previously reported on by Prévoteau *et al.* who demonstrated that molecular oxygen could be reduced by osmium based redox mediators with a formal redox potential $\leq +0.07$ V vs Ag/AgCl [26, 33].

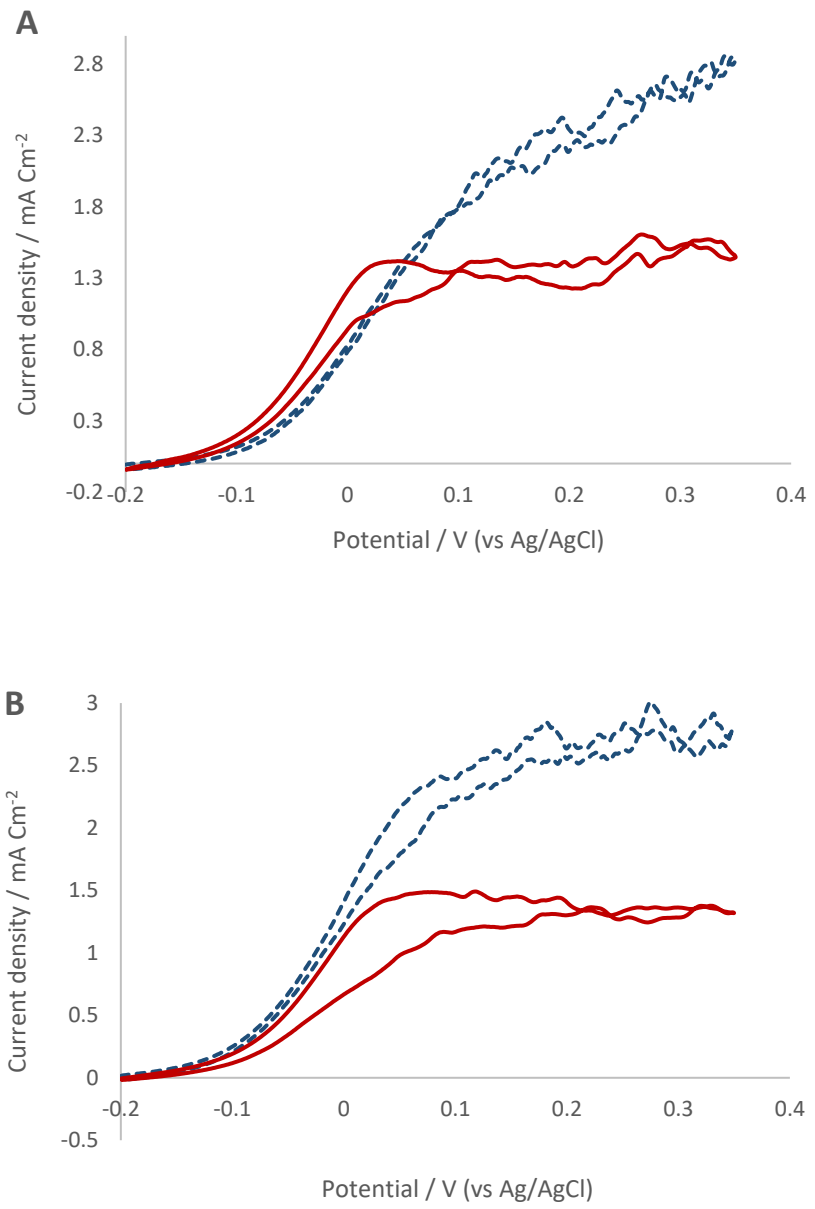

Figure 9: CVs recorded at 1 mV s^{-1} in the presence of 100 mM glucose in PBS (pH 7.4, 37°C) for enzyme electrodes prepared from $Os(dmobpy)_2$4AMP, CMD and acid treated MWCNT and either FADGDH (A) or GOx (B) in the presence (solid line) or absence (dotted line) of air.

For all enzyme electrodes, an initial linear increase in current density as a function of glucose concentration is observed, that subsequently approaches a maximum at high glucose concentrations. The increase in glucose-oxidation current density as a function of glucose concentration followed the trend expected for the steady-state approximation of Michaelis–Menten enzyme kinetics, as explained previously. The overall results are in Table 2. The current

responses show slight increases for amperometry over CV due to use of convection (150 rpm) of solutions in amperometry to avoid substrate depletion over the course of the experimental timescale. For example, the 1 mV s^{-1} CV current density of 2.4 ± 0.2 mA cm^{-2} for oxidation of 100 mM glucose at enzyme electrodes prepared from $Os(dmobpy)_2$4AMP co-immobilised with FADGDH, acid treated MWCNT and CMD as a polymer support compares well with the amperometric 3.2 ± 0.2 mA cm^{-2} current density obtained at 0.2 V applied potential in the absence of oxygen (Figures 9 and 10). The K_m^{app} values obtained for the FADGDH-based electrodes are lower than GOx-based electrodes in both presence and absence of oxygen. For example FADGDH shows a K_m^{app} of 9.3 ± 1.5mM, compared to 26.0 ± 1.7 mM obtained for GOx based electrodes in air-saturated electrolyte condition and suggests that FADGDH has a better affinity for glucose compared to GOx. Reports have suggested that mass transport can be a limiting factor for these enzyme electrodes and the K_m^{app} may therefore reflect instead a difference in mass transport and not affinity [45, 46], in addition, deviations from the simple Michaelis-Menten model are observed at higher glucose concentrations.

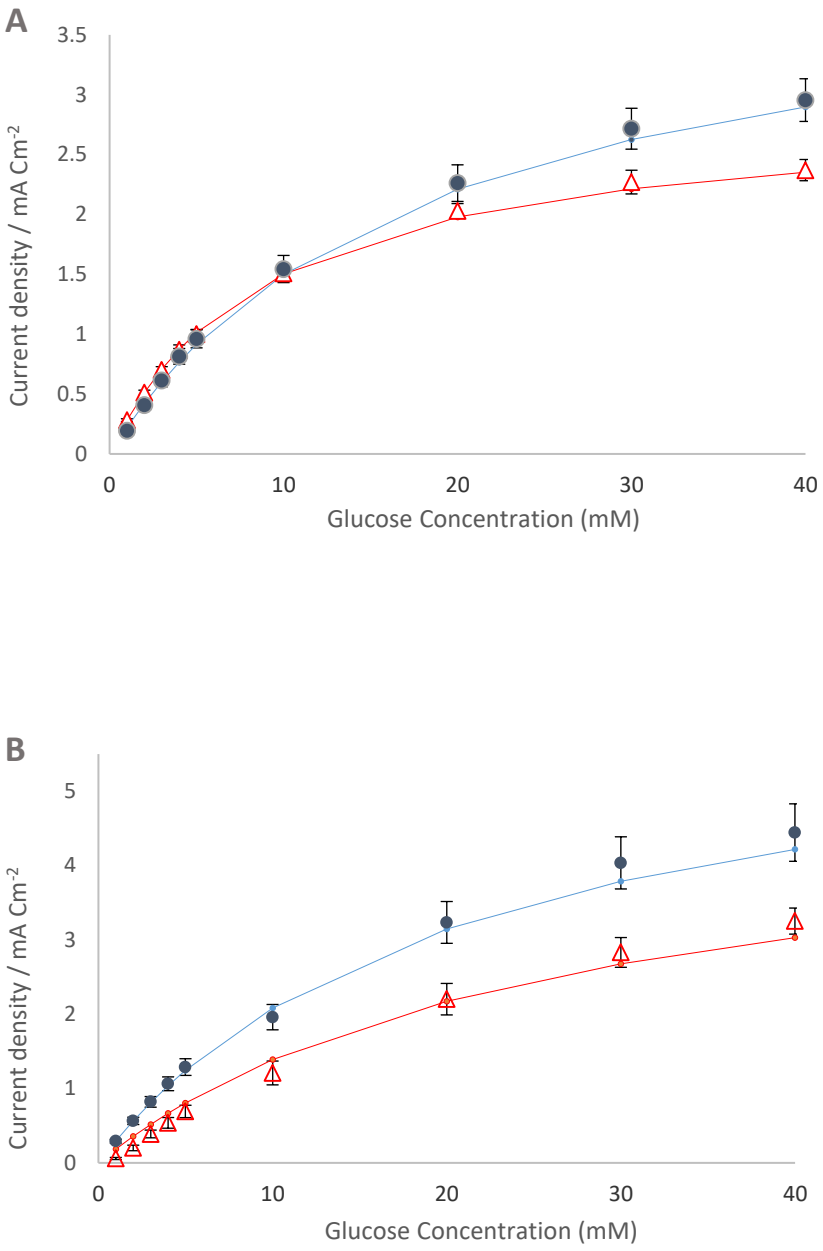

Figure 10: Average glucose oxidation current densities as a function of glucose concentration, measured in PBS at 37 °C with stirring at 150 rpm at an applied potential of 0.2 V, for enzymatic electrodes using FADGDH (A) and GOx (B) co-immobilised with $Os(dmobpy)_2$4AMP, CMD, and acid treatd MWCNT in air (Δ) and absence of oxygen (●) and Michaelis-Menten steady state approximation (solid line) for each enzyme electrode (n=3).

Enzyme electrodes	j_{max}, app (mA cm^{-2})	K_M^{app} (mM)	Initial current density) in 100 mM (mA cm^{-2})	Final current density in 100mM after 24 hr (mA cm^{-2})	% j_{max} in 100 mM glucose after 24 hr
FADGDH In nitrogen	4.2 ± 0.1	18.0 ± 1.0	3.2 ± 0.1	1.6 ± 0.1	50 ± 1
FADGDH In air	2.9 ± 0.2	9.3 ± 1.5	2.5 ± 0.1	1.5 ± 0.01	60 ± 2
GOx In nitrogen	6.4 ± 0.8	20.7 ± 1.2	4.7 ± 0.2	2.4 ± 0.2	51 ± 2
GOx In air	5.0 ± 0.2	26.0 ± 1.7	3.2 ± 0.1	1.0 ± 0.1	31 ± 2

Table 2: Enzyme electrode performance for electrodes prepared using Os(dmobpy)$_2$4AMP redox complex, acid treated MWCNT, CMD and either FADGDH or GOx in the presence of 100 mM Glucose.

Operational stability tests carried out in 100 mM glucose solutions in PBS using amperometry at 0.2 V, show approximately 60% retained glucose oxidation current after 24 h for FADGDH-based enzyme electrodes compared to only 31 % retained glucose oxidation current after 24 h for GOx-based enzyme electrodes, both in air saturated electrolyte condition. Previous reports have demonstrated that H_2O_2 is produced as a result of the reduction of molecular oxygen by osmium complexes in the presence of oxygen [43]. In addition the higher loss of current for GOx-based enzyme electrodes as compared to oxygen insensitive FADGDH electrodes is proposed to be as a result of the competition for electrons from the oxygen co-substrate for GOx [33, 43, 44], forming more H_2O_2 in the process that damages the GOx enzyme under air saturated electrolyte conditions.

3.3.4 Fuel cell operating in pseudo-physiological buffer

A potential application for EFCs is to supply power to medical implants relying on the electrochemical reactions of glucose and oxygen as fuel and oxidant which are present *in vivo*. Thus an EFC was assembled for testing under pseudo-physiological conditions using anodes prepared by co-immobilisation of Os(dmobpy)$_2$4AMP redox complex, acid treated MWCNT,

CMD and FADGDH in the presence of 100 mM glucose. An oxygen-reducing cathode was selected based on DOE-optimised amounts of Os(dcbpy)$_2$PVI redox polymer co-immobilised with a bilirubin oxidase from *Myrothecium verrucaria* (*Mv*BOd) and MWCNT, as presented in chapter 4 of this thesis. As the glucose oxidation current density is higher than the current at the cathode, the cathode would limit power output if the same areas of electrode for cathodes and anode were to be used. Thus to ensure that the anode limits the current in the EFC, the assembled EFC consists of graphite cathodes of higher geometric area than the anode. Assembled EFC based on anodes of Os(dmobpy)$_2$4AMP co-immobilised with FADGDH and MWCNT yield power output of 74 ± 7 μW cm^{-2} and 42 ± 8 μW cm^{-2} in air and oxygen saturated electrolyte condition, respectively (Figure 11). The lower power output observed for the EFC in oxygen saturated electrolyte condition is as a result of the reduction of molecular oxygen by the osmium redox mediator, which in turn decreases the amount of osmium redox centres that can be accessed by the electrons from glucose substrate under the low (5 mM) glucose concentrations.

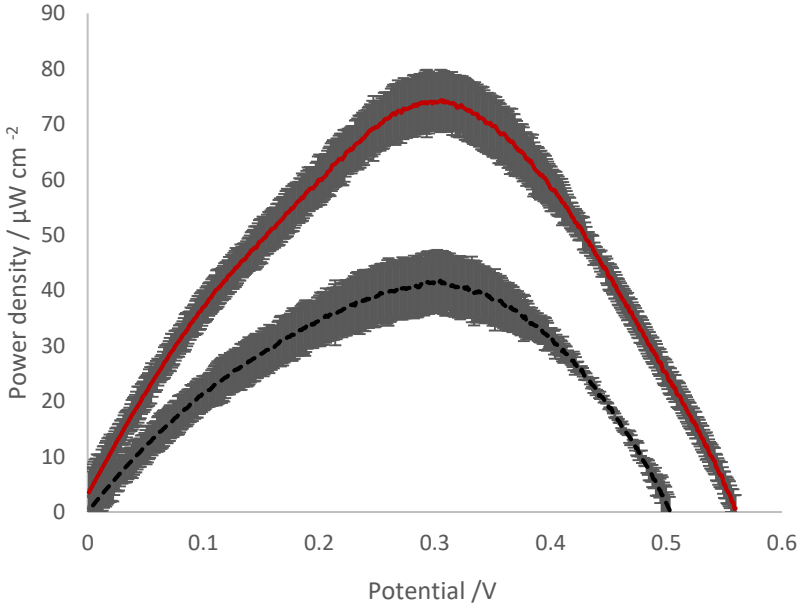

Figure 11: Average power curves (n=3) with error bars, recorded by 1 mV s^{-1} linear sweep voltammetry in 50 mM PBS containing 5 mM glucose for membrane-less EFCs based on *Mv*BOd, Os(dc bpy)PVI and MWCNT as a cathode combined with Os(dmobpy)$_2$4AMP redox complex, acid treated MWCNT, CMD and FADGDH as anode in the air (solid line) and oxygen saturated (dotted line) electrolyte conditions.

In order to investigate the factors limiting the power output for the EFCs, polarisation curves were computed from linear sweep voltammetry at 1 mV s^{-1} scan rate for the EFC anode and cathode enzyme electrodes. The polarisation curves in Figure 12 indicate that the current at the anode limits power produced at the assembled fuel cell for the EFC, as expected.

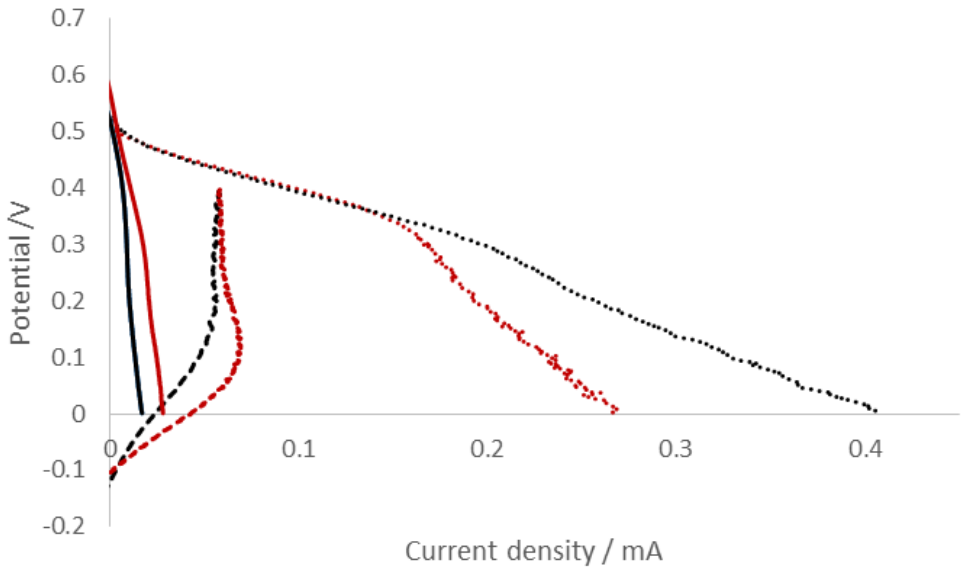

Figure 12: Polarisation curves recorded in PBS containing 5 mM glucose in air (red) and in saturated O_2 (black) at 37 °C for enzyme electrodes prepared by co-immobilisation of $Os(dmobpy)_2$4AMP redox complex, acid treated MWCNT, CMD and FADGDH (dashed line) or *Mv*BOd, $Os(dcbpy)_2$PVI and MWCNT (dotted line) reported vs Ag/AgCl, and for the cell voltage of enzyme electrodes assembled as a membrane-less fuel cell (solid line). Geometric areas are anode: 0.0707 and cathode: 0.2121 cm^2.

Comparison of the results obtained here with other EFC results is difficult due to differences in operating conditions, such as electrode preparation methodologies, glucose concentrations and pH. The maximum power density for the EFC assembled in this study is observed at 0.3 V while, for example, Kim *et al.* [47] reported on a membrane-less EFC generating a power density of 50 µW cm^{-2} at a 0.5 V cell voltage in air saturated electrolyte condition at pH 7.4, 140 mM NaCl, 37.5 °C in 15 mM glucose concentration. In addition, Soukharev *et al.* reported an EFC using GOx and fungal laccase, co-immobilised with osmium redox polymers on 7 µm diameter, 2 cm long, carbon fibres that produced a power density of 350 µW cm^{-2} in 15 mM

glucose solutions. The highest maximum power densities reported to date under similar conditions for an EFC operating in 5 mM glucose, pH 7.4 PBS, is of 275 μW cm^{-2} for an EFC based on osmium redox polymers as mediators but using a de-glycosylated pyranose dehydrogenase sourced from *Pichia pastoris* as anode enzyme [48].

3.4 Conclusions

A comparison of glucose oxidation by enzyme electrodes based on coupling of GOx and an amine-functionalised osmium complex to CMD and a range of conductive and non-conductive nanoparticles as alternate supports was undertaked to probe whether the properties of different supports with similar sizes can improve current density and/or stability for these electrodes. Firstly MWCNT, silica and AuNPs provide a large surface area for abundant loading of redox mediators and enzymes for catalytic reactions. Secondly, the nanotopographic surface and chemical functional gruops provided by nanostructures are proposed to facilitate anchoring of enzymes at the sufaces. The anodes decorated with MWCNT and AuNPs produced current densities more than 100% higher than that observed for films prepared without nanoparticles on graphite anodes as control, while those of silica-decorated anodes with similar morphologies produced 3.5 % higher than the control. For all enzyme electrodes with the nanoparticles support, redox site surface coverage and enzyme activity are similar which indicates that the higher saturated current densities for MWCNT and AuNPs are due to their higher conductivity. Although AuNPs might be too expensive to be used in practical application for energy generation, the results of this study highlight the importance of the chemical properties and morphologies of the electrode surface on current generation. In addition, performances of glucose oxidising enzyme electrodes prepared using an anode system with optimised DoE amounts with either FADGDH or GOx co-immobilised with a low potential osmium-based redox complex on graphite electrodes were compared. A more substantial decrease in current density is observed for GOx-based electrodes when operated in the presence of oxygen, in comparison to the FADGDH-based electrodes. In addition, oxygen reduction by the mediator contributes to decreased current density for glucose oxidationfor all enzyme electrodes, including FADGDH-based electrodes, in air saturated electrolyte conditions compared to

operation in the absence of oxygen. EFCs assembled from anodes prepared by co-immobilisation of Os(dmobpy)$_2$4AMP redox complex, acid treated MWCNT, CMD and FADGDH and cathodes consisting of *Mv*BOd, Os(dcbpy)$_2$PVI and MWCNT were tested for power generation under pseudo-physiological conditions. A maximum power output of 80 μW cm^{-2} in air saturated, 5 mM glucose solutions was generated. Such information might be valuable for the selection and development of anode materials for EFCs.

3.5 References

[1] A. T. Yahiro, S. M. Lee, D. O. Kimble, Biochimica et Biophysica Acta, 88 (1964) 375-383.

[2] A. Heller, Physical Chemistry Chemical Physics, 6 (2004) 209-216.

[3] S. C. Barton, J. Gallaway, P. Atanassov, Chemical Reviews, 104 (2004) 4867-4886.

[4] P. Kavanagh, D. Leech, Physical Chemistry Chemical Physics, 15 (2013) 4859-4869.

[5] X. Luo, A. Morrin, J. Killard, R. Smyth Electroanalysis 18 (2006) 319-326.

[6] Zhang S, Wang N, Yu H, Niu Y, Sun C. Bioelectrochemistry (2005) 675-680.

[7] C.-M. Yu, M.-J. Yen, and L.-C. Chen, Biosensors and Bioelectronics, 25 (2010) 2515-2521.

[8] M. Holzinger, A. Le Goff, and S. Cosnier, Electrochimica Acta, 82 (2012) 179-190.

[9] I. Osadebe and D. Leech, ChemElectroChem, 1 (2014) 1988-1993.

[10] S. Cosnier, M. Holzinger, A. Le Goff, Frontiers in Bioengineering and Biotechnology, 2 (2014) 45-50.

[11] Y. Yan, W. Zheng, L. Su, L. Mao, Advanced Materials, 18 (2006) 2639-2643.

[12] A. E. G. Cass, G. Davis, G. D. Francis, H. A. O. Hill, W. J. Aston, I. J. Higgins, E. V. Plotkin, L. D. L. Scott, A. P. F. Turner, Analytical Chemistry, 56 (1984) 667-671.

[13] A. Heller, B. Feldman, Accounts of Chemical Research, 43 (2010) 963-973.

[14] A. Heller, B. Feldman, Chemical Reviews, 108 (2008) 2482-2505.

[15] B.B. Dambatta, J.R. Ebdon, European Polymer Journal, 22 (1986) 783-786.

[16] J.W. Gallaway, S.A. Calabrese Barton, Journal of Electroanalytical Chemistry, 626 (2009) 149-155.

[17] D. MacAodha, M.L. Ferrer, P. ÓConghaile, P. Kavanagh, D. Leech, Physical Chemistry Chemical Physics, 14 (2012) 14667-14672.

[18] C. Danilowicz, E. Cortón, F. Battaglini, E.J. Calvo, Electrochimica Acta, 43 (1998) 3525-3531.

[19] D. Leech, P. Kavanagh, W. Schuhmann, Electrochimica Acta, 84 (2012) 223-234.

[20] P. Ó Conghaile, D. MacAodha, B. Egan, P. Kavanagh, D. Leech, Journal of the Electrochemical Society, 160 (2013) G3165-G3170.

[21] A.B.P. Lever, Inorganic Chemistry, 29 (1990) 1271-1285.

[22] K. Habermüller, A. Ramanavicius, V. Laurinavicius, W. Schuhmann, Electroanalysis, 12 (2000) 1383-1389.

[23] P. Kavanagh, S. Boland, P. Jenkins, D. Leech, Fuel Cells, 9 (2009) 79-84.

[24] S.Timur, U. Anik, D. Odaci, L. Gorton, Electrochemistry Communications, 9 (2007) 1810-1815.

[25] I. Vostiar, E.E. Ferapontova, L. Gorton, Electrochemistry Communications, 6 (2004) 621-626.

[26] A. Prévoteau, N. Mano, Electrochimica Acta, 112 (2013) 318-326.

[27] R.D. Milton, F. Giroud, A.E. Thumser, S.D. Minteer, R.C.T. Slade, Physical Chemistry Chemical Physics, 15 (2013) 19371-19379.

[28] R.D. Milton, F. Giroud, A.E. Thumser, S.D. Minteer, R.C.T. Slade, Electrochimica Acta, 140 (2014) 59-64.

[29] R. Kumar and D. Leech. Bioelectrochemistry, 106 (2015) 41-46.

[30] R.J. Forster, J.G. Vos, Macromolecules, 23 (1990) 4372-4377.

[31] E.M. Kober, J.V. Caspar, B.P. Sullivan, T.J. Meyer, Inorganic Chemistry, 27 (1988) 4587-4598.

[32] F. Barigelletti, L. De Cola, V. Balzani, R. Hage, J. G. Haasnoot, J. Reedijk, J.G. Vos, Inorganic Chemistry, 30 (1991) 641-645.

[33] B.H. Ginsberg, Journal of Diabetes Science and Technology, 3 (2009) 903-913.

[34] K. Matsushita, E. Shinagawa, O. Adachi, M. Ameyama, Federation of European Microbiological Societies Microbiology Letters, 55 (1988) 53-57.

[35] P. Ó Conghaile, S. Kamireddy, D. MacAodha, P. Kavanagh, D. Leech, Analytical and Bioanalytical Chemistry, 405 (2013) 3807-3812.

[36] S. Boland, K. Foster, D. Leech, Electrochimica Acta, 54 (2009) 1986-1991.

[37] A.J. Bard, L.R. Faulkner, Electrochemical Methods: Fundamentals and Applications, 2 ed., Wiley & Sons, New York, (2001).

[38] T.J. Ohara, R. Rajagopalan, A. Heller, Analytical Chemistry, 65 (1993) 3512-3517.

[39] Bakker E, Qin Y. Analytical Chemistry, 78 (2006) 3965-3984.

[40] Willner I, Willner B, Katz E. Bioelectrochemistry, 70 (2007) 2-11.

[41] Yang W, Wang J, Zhao S, Sun Y, Sun C. Electrochemistry Communications, 8 (2006) 665-672.

[42] N. German, A. Ramanaviciene, J. Voronovic, A. Ramanavicius, Microchimica Acta, 168 (2010) 221-229.

[43] A. Prévoteau, N. Mano, Electrochimica Acta, 68 (2012) 128-133.

[44] C. Taylor, G. Kenausis, I. Katakis, A. Heller, Journal of Electroanalytical Chemistry, 396 (1995) 511-515.

[45] B. Limoges, J. Moiroux, J.M. Savéant, Journal of Electroanalytical Chemistry, 521 (2002) 8-15.

[46] P.N. Bartlett, K.F.E. Pratt, Journal of Electroanalytical Chemistry, 397 (1995) 61-78.

[47] H.-H. Kim, N. Mano, Y. Zhang, A. Heller, Journal of Electrochemical Society, 150 (2003) 209-13.

[48] P. Ó Conghaile, M. Falk, D. MacAodha, M. E. Yakovleva, C. Gonaus, C.K. Peterbauer, L. Gorton, S. Shleev and D. Leech, Analytical Chemistry, 88 (2016) 2156-2163.

[49] D. Leech and F. Daigle, Analyst, 123 (1998) 1971-1974.

[50] B.E.P. Swoboda and V. Massey, The Journal of Biological Chemistry, 240 (1965) 2209-2215.

[51] Q.H.Gibson, B.E.P.Swoboda, V.Massey, The Journal of Biological Chemistry, 239(1964)3927-34.

Chapter 4

An oxygen biocathode for enzymatic fuel cells optimised for current production under physiological conditions using a design of experiment approach

4.1 Introduction

Enzymatic fuel cells (EFCs) are electrochemical devices that utilise biocatalysts such as enzymes for converting chemical energy into electrical energy [1, 2]. In EFCs, enzymes are used as biocatalysts as a replacement for the conventional metal catalyst, due to their specificity towards reactions they catalyse [2 - 4]. The specificity of enzymes immobilised at electrodes allows for elimination of the need for casings and separating membranes that paves the way for developing a miniaturised and potentially implantable membrane-less configuration of fuel cell [2, 5]. Another potential advantage of the use of enzyme catalyst over metal catalyst is its ability to operate under relatively mild conditions (20-40 °C, neutral pH), making them attractive for power generation *in vivo* that can deliver power using oxidation of fuel such as glucose present in the bloodstream at an anode and oxygen reduction at a cathode [6, 7]. In recent years electrode modification with copper oxygenases has attracted considerable attention due to potential applications as cathodes for reduction of O_2 to water in biofuel cells [7, 8]. Some oxygen reducing enzymes such as *Trametes versicolor* laccase (*Tv*L) are not suitable for utility as oxygen biocathodes in a biofuel cell for implantable power production since they show diminished currents at neutral pH compared to pH 4.5, however other oxygen reducing 'blue'

copper oxygenase biocatalysts have been produced that display optimal activity closer to neutral pH such as the bilirubin oxidases (BOd) [9, 10]. The application of redox mediators in hydrogel films on electrode improves shuttling of electrons between the redox active sites of enzymes and electrode surface by electron-hopping self-exchange mechanism within the hydrogels [5], thereby making electron transfer independent of orientation or proximity of the enzyme active site to the electrode surface, in comparison to that for direct electron-transfer mechanisms between enzyme and electrode [2, 4]. Moreover, osmium based systems possess advantages over iron and ruthenium based systems due to the low redox potential of Os(II/III) redox transition and relative stability of complexes in both oxidation states [11, 12]. Current output from enzyme electrodes depends on selection of a mediator with appropriate structure (enzyme affinity) and suitable redox potential (driving force) for rapid electron transfer between the enzyme active site and the electrode surface [13,14]. The inclusion of multiwalled carbon nanotube (MWCNT) in enzyme electrode films provides a conductive support which acts as scaffold for retention of enzyme activity, resulting in improved catalytic current and operational stability of the enzyme electrodes [15,16,17]. In order to further enhance current output of an enzymatic fuel cell (EFC), optimisation of the constituting components such as the mediator, polymer, crosslinker and MWCNT is of crucial importance. Considering the number of different components, and the range of amounts and methods that can be used to prepare an enzyme electrode, a study is required on optimisation of each component used in an enzyme electrode in order to increase the performance of enzyme electrodes. A design-of-experiment (DoE) approach can be used to determine optimal enzyme electrode performance. Unlike the classical method of varying one factor at a time (OFAT), DoE adopt an optimisation approach based on alteration of several factors at a time. DoE application is necessary in an optimisation strategy that consists of various independent variables affecting the responding factors. For example, Babanova *et al.* used a design of experiment approach for optimisation of performance of an air-breathing bilirubin oxidase-based EFC cathode [18]. In addition Kumar and Leech [20] reported on use of a response surface methodology (RSM) technique to optimise components used to construct enzyme electrodes. They reported a 32% increase in glucose oxidation current density compared to previously reported values for the system optimised by variation of one factor at a time [19, 20]. Here the use of a response surface methodology (RSM) technique for optimisation of biocathode enzyme electrodes is examined to seek to achieve

increased current production at EFC cathodes. This DoE model is developed and validated for enzyme electrode performance in pseudo-physiological conditions (50 mM phosphate buffered saline, PBS, pH 7.4, 37 °C). The enzyme electrodes are prepared by co-immobilisation of $Os(dcbpy)_2PVI$, *Mv*BOd, PEGDGE and acid treated MWCNT. The $Os(dcbpy)_2PVI$ polymer was selected for screening due to its higher redox potential ($E^{o'}$ = 0.35 V vs. Ag/AgCl) compared to $[Os(2,2'\text{-bipyridine})_2(polyvinylimidazole)_{10}Cl]^{+/2+}$ (Os $(bpy)_2PVI$) ($E^{o'}$ = 0.22 V vs. Ag/AgCl) [21] and $[Os(4,4'\text{-dimethyl-}2,2'\text{-bipyridine})_2(polyvinylimidazole)_{10}Cl]^{+/2+}$ ($Os(dmbpy)_2PVI$) ($E^{o'}$ = 0.12 V vs. Ag/AgCl) [23]. The higher redox potential provides increased power output for EFC application due to greater potential difference between the anode and the cathode.

4.2 Experimental

4.2.1 Materials

All chemicals and biochemicals were purchased from Sigma Aldrich and used as received, unless otherwise stated. Bilirubin oxidase from Myrothecium verrucaria (*Mv*BOd) (2.06 U/mg) was a generous gift fromAmano Enzyme Inc. (Nagoya, Japan). *Mv*BOd activity is measured by a spectrophotometric assay with 2,2′-azinobis-(3-ethylbenzthiazoline-6-sulfonate) as a substrate in acetate buffer pH 4.5 [33]. Synthesis of the redox systems was achieved using $(NH_4)_2OsCl_6$ as starting material to prepare the *cis*-$Os(dcbpy)_2Cl_2$ complex (where, dcbpy is 4,4′-dichloro-2,2′-bipyridine), and the subsequent ligand substitution of one Cl with polyvinylimidazole (PVI) to yield the desired redox system, according to literature methods [21,23]. Poly(ethylene glycol) diglycidyl ether (average Mn~526) was purchased from Aldrich. The MWCNT (product 659258; Sigma-Aldrich) were pre-treated under reflux in concentrated nitric acid for 6 h at ~150 °C [24] and isolated by filtration. All solutions were prepared in Milli-Q (18.2 MΩ cm) water unless otherwise stated.

4.2.2 Methods

All electrochemical experiments were performed by a CH Instruments 1030 multichannel potentiostat (IJ Cambria) coupled to a thermostated electrochemical cell. Custom built Ag/AgCl reference electrode (3 M KCl) and platinum foil counter electrode (Goodfellow) were used in the cell. Graphite disk electrodes (3 mm diameter) were prepared by shrouding graphite rods (Graphite store, part # NC001295) in heat-shrinkable tubing and polishing the exposed disk on 1200 grit silicon carbide paper (Buehler) followed by thorough rinsing with Milli-Q water. Working electrodes were sonicated in Milli-Q water for 10 min and dried under nitrogen gas prior to use. All electrochemical measurements were performed in 0.05 M phosphate buffered saline containing 0.15 M NaCl adjusted to the physiological pH (pH 7.4 at 37 °C). Oxygen concentration was estimated by using a dissolved oxygen electrode and meter (EUTech Instruments). Currents are normalised to the two-dimensional projected area of the graphite disk electrodes to provide current density data.

4.2.3 Enzyme electrode preparation

Immobilisation of films was performed by depositing solutions of 5 mg mL^{-1} $Os(dcbpy)_2PVI$ redox polymer aqueous solution, 10 mg mL^{-1} *Mv*BOd (2.06 U/mg), aqueous solution and 46 mg mL^{-1} aqueous dispersion of acid treated MWCNT on the surface of the graphite working electrode. Crosslinking of the biocatalytic redox films was achieved by addition of 2 µL of a 15 mg mL^{-1} PEGDGE aqueous solution on the surface of the graphite working electrode and allowing the subsequent mixture to cross-link and dry for 24 h prior to use. The amount of different components of acid treatd MWCNT, $Os(dcbpy)_2PVI$ and *Mv*BOd to be added in the enzyme electrode preparation step is determined by the Design Expert Software (version 9, STAT-EASE Inc., Minneapolis, USA).

4.3 Results and discussion

4.3.1 Enzyme electrode electrochemistry

The electrodes were initially prepared by the co-immobilisation of Os(dcbpy)$_2$PVI redox polymer, *Mv*BOd and acid treated MWCNT using a PEGDGE as cross-linker on graphite electrode. The crosslinking of enzymes with redox polymer hydrogels consisting of electron shuttling mediators attached to water soluble polymer backbones enhances the electrical communication between the enzyme active site and the electrode surface [25]. For application to EFC, in order to have high power, the oxygen biocathode redox potential should be as high as possible in order to maximise the cell voltage while the bioelectrocatalytic process should display relatively fast electron transfer kinetics to generate sufficient current. An oxygen reducing enzyme (*Mv*BOd) with reasonably high standard reduction potential of T1 copper site (0.47 V vs. Ag/AgCl) [9] is selected as cathode catalyst. *Mv*BOd functions best at physiological conditions, thereby making it attractive for use in EFCs compared to other multi-copper oxygenases [26]. In order to have an efficient electron transfer between a redox mediator and the active site of a biocatalyst the redox potential of the mediator should be located thermodynamically downhill to that of the standard reduction potential of the biocatalyst [27]. In this case thus, for efficient O_2 reduction, the redox potential of the mediator should be negative of the T1 substrate oxidising site of *Mv*BOd. Cyclic voltammetry is used to evaluate the Os(II/III) redox potential of the Os(dcbpy)$_2$PVI in the enzyme electrodes in the presence and absence of substrate. Cyclic voltammograms and amperometric measurements of the enzyme electrode in the absence of oxygen, pseudo-physiological and oxygen saturated conditions at applied potential of 0.1 V vs. Ag/AgCl in PBS are shown in Figure 1.

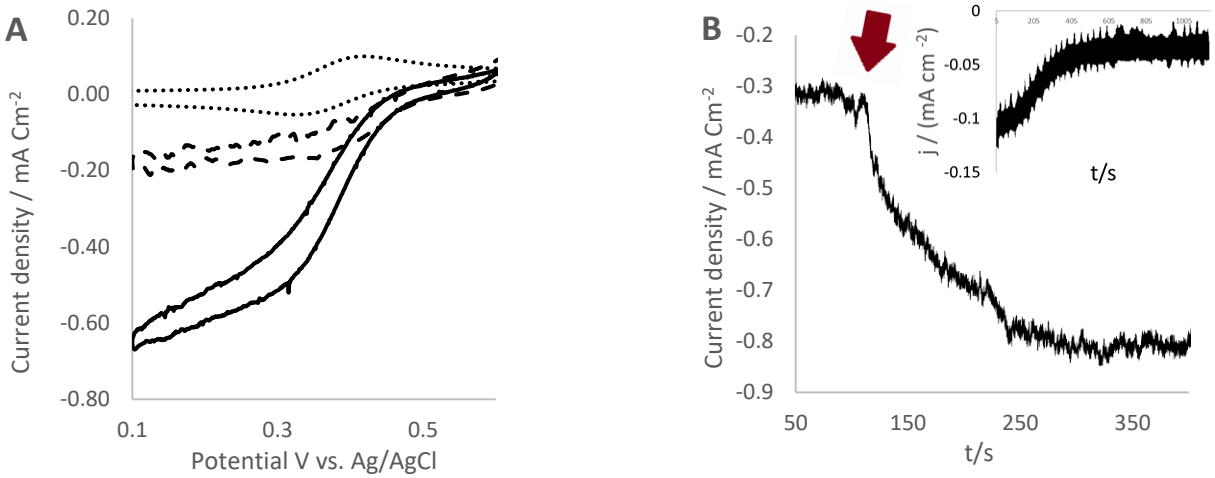

Figure 1: (A) CVs recorded at 1 mV s^{-1} in the absence of oxygen (dotted line), oxygen saturated (1 mM O_2) (solid line) and in (0.2 mM O_2) (dashed line) non-stirred PBS (37 °C). **(B)** Amperometric current density recorded for enzyme electrodes, prepared by cross-linking *Mv*BOd (11.1 µL), acid treated MWCNT (18.2 µL) and $Os(dcbpy)_2PVI$ (25.8 µL) with PEGDGE on graphite electrodes in PBS (37 °C), at 150 rpm at an applied potential of 0.1 V vs. Ag/AgCl, in initially 0.2 mM oxygen and, at time 114 seconds (indicated by the red arrow) upon commencement of oxygen sparging. Inset: sparging nitrogen after 24 h stability test.

All prepared enzyme electrodes, in the absence of oxygen substrate, exhibit reduction and oxidation peaks at 0.35 ± 0.01 V (vs. Ag/AgCl), which is similar to the redox potential previously reported for the osmium redox polymer in solution and on an electrode surface [28]. At slow scan rates (< 20 mV s^{-1}) in the absence of substrate, redox peak currents vary linearly with scan rate, indicative of a surface-controlled response [29]. At higher scan rates the peak currents scale linearly with the square root of scan rate which indicates semi-infinite diffusion control as expected for multi-layered films on electrodes [30, 31]. Oxygen reduction current for enzyme electrodes is extracted from amperometric measurements at 0.1 V vs. Ag/AgCl applied potential, selected to be 250 mV more negative of the redox potential of the osmium complex to ensure steady-state mediated oxygen reduction current is achieved. Amperometric response of enzyme electrodes displays slightly higher current density over the current density observed in slow scan CVs, due to use of convection (150 rpm) of solutions in amperometry implemented to have a homogenous oxygen saturated condition in the buffer solution, as depicted in Figure 1.

4.3.2 Design of experiment

A DoE approach can provide information about response and interaction of inter-connected factors over a wide range of values [32]. Here, for the optimisation of biocathodes, a DoE approach based on response surface factorial Box–Behnken Design (BBD) with a 3-level factorial design is used to evaluate the main effect and interaction between the MWCNT, osmium redox polymer and *Mv*BOd components required to prepare oxygen cathode electrodes as in Table 1 and 2.

Factor	**Low level (-1)**	**Central point (0)**	**High level (+1)**
$Os(dcbpy)_2PVI$	9.6 µL (48 µg)	18.2 µL (91µg)	26.8 µL (134 µg)
*Mv*BOd	11 µL (110 µg)	16 µL (160 µg)	21 µL (210 µg)
MWCNT	0	9.6 µL (442 µg)	19.2 µL (883µg)

Table 1. The range and level of components used in the enzyme electrode preparation step for biocathode optimisation.

For the 3-level three factorial, the BBD requires a minimum of 16 experimental runs according to $N = 2k(k-1) + C_0$ [34], where k is the number of factors and C_0 is the number of central points.

Run	Os(dcbpy)$_2$PVI	*Mv*BOd	MWCNT	Current density in 0.2 mM O_2/ mA cm^{-2}	SD
1	1	0	1	0.24	0.03
2	-1	-1	0	0.15	0.02
3	0	1	-1	0.05	0.02
4	-1	1	0	0.12	0.04
5	0	-1	-1	0.06	0.02
6	0	-1	1	0.27	0.01
7	-1	0	-1	0.03	0.01
8	-1	0	1	0.22	0.01
9	0	0	0	0.22	0.02
10	0	0	0	0.20	0.02
11	0	1	1	0.27	0.04
12	0	0	0	0.24	0.02
13	1	-1	0	0.28	0.02
14	1	0	-1	0.10	0.02
15	1	1	0	0.16	0.01
16	0	0	0	0.22	0.01

Table 2. Box-Behnken design arrangement demonstrating the amount of relative components and measured amperometric current density responses under pseudo-physiological conditions.

By default, the high levels of the factors are coded as +1 and the low levels of the factors are coded as -1. The design arrangement and response is shown in Table 2. The mathematical relationship between the enzyme electrode response and variables can be presented by a second-degree quadratic equation (Equation 1) [34],

$Equation$ [1] $$y = b_0 + b_1x_1 + b_2x_2 + b_3x_3 + b_{11}x_1^2 + b_{22}x_2^2 + b_{33}x_3^2 + b_{12}x_1x_2 + b_{13}x_1x_3 + b_{23}x_2x_3$$

Where y is the predicted current response value in mA cm^{-2}, x_1, x_2 and x_3 are the MWCNT,

redox polymer and enzyme amounts in µl used in the enzyme electrode preparation, b_0 is the constant coefficient (intercept), b_1, b_2, b_3 and b_{12}, b_{13}, b_{23} are linear and cross product coefficients, respectively, and the quadratic coefficients are b_{11}, b_{22} and b_{33}. On the basis of this equation, the design model provides a tool for improvement of experimental outcome by finding the best combination of component levels within the test set. Further, the model generated can be validated using confirmatory experiments. In this BBD design, the low level of *Mv*BOd and $Os(dcbpy)_2PVI$ is selected to be 11 µL and 9.6 µL, respectively. The levels are those reported previously [40] for optimised bioelectrocatalyic oxygen reduction close to the maximum current density established by OFAT. In addition, lower levels of redox polymer decreases the stability of the components on the electrode surface justifying the selected minimum level for the low level of redox polymer. The high levels selected for *Mv*BOd, $Os(dcbpy)_2PVI$ and MWCNT are as a result of the difficulties that may be accompanied in co-immobilisation of higher amounts on electrode surface. For example, if higher amounts of the components are added it is difficult to control the drop-coat on the electrode surface. For the responses of the designed combinations in Table 2, analysis of variance (ANOVA) is used for statistical testing and the data extracted shows whether or not the model is statistically significant, with results provided in Table 3. The coefficient of variation (R^2), Fisher's test (F-value) and probability (P-value) are used to verify the appropriateness of the model [35]. The ANOVA implies that the model data is statistically significant, as indicated by calculated F-value of 12.54 and a low calculated P-value of 0.003 (Table 3). P-value less than 0.05 shows that at least one of the components is significantly different.

Source	Sum of Squares	Degree of freedom	Mean Squares	F-value	p-value Prob > F	R^2	
Model	0.098	9	0.011	12.54	0.003	0.95	significant
Residual	0.005	6	0.0008				
Lack of fit	0.004	3	0.001	5.96	0.088		
Pure error	0.0007	3	0.0002				
Total	0.1	15					

Table 3. Analysis of variance (ANOVA) for response surface quadratic model of the enzyme electrode response.

The higher the F value the more likely the rejection of the null hypothesis and that the data show more variation between the three components. In addition, the coefficient of determination (R^2) between predicted and observed responses was evaluated to be 0.95, thereby suggesting significant correlation between predicted and observed responses [36, 37, 38] as depicted in Figure 2. The results obtained for statistical tests here are similar to those observed previously by Kumar and Leech [20] on enzyme electrodes prepared by co-immobilisation of MWCNT, GOx, osmium redox complex and carboxymethylated dextran and tested for current response to glucose under physiological conditions.

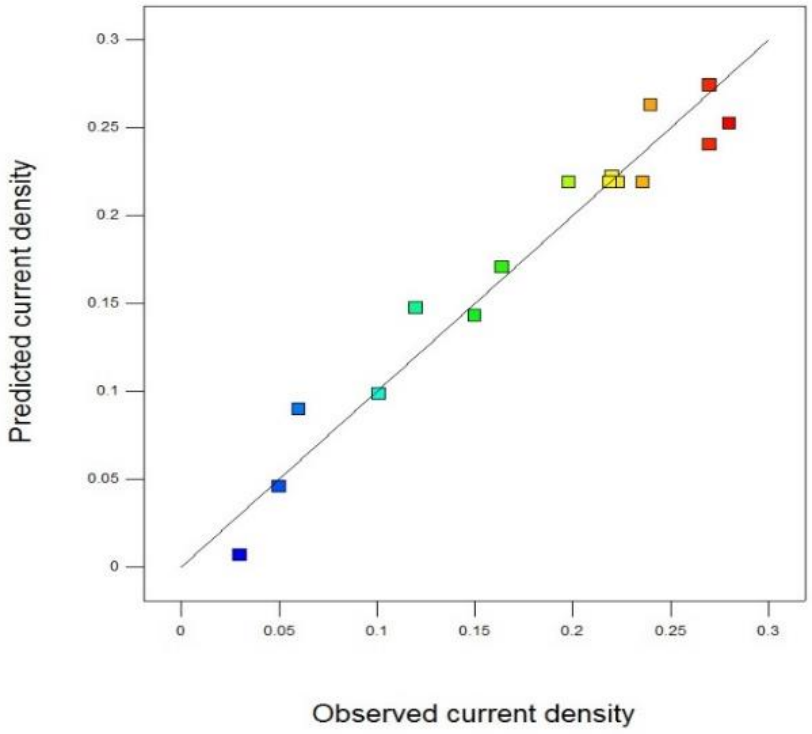

Figure 2: Observed amperometric oxygen reduction current densities (mA cm^{-2}) vs. the predicted current densities (mA cm^{-2}) at 0.1 V vs. Ag/AgCl under pseudo-physiological conditions.

4.3.3 Validation of model

Initial model validation was undertaken based upon preparation of test electrodes with component amounts of random values, provided by the software, in order to demonstrate that the model is a reasonable representation of the actual system. For instance, enzyme electrodes prepared using $Os(dcbpy)_2PVI$ (22.8 µl), *Mv*BOd (14.4 µl) and MWCNT (17.8 µl) are predicted to display current density of 0.28 ± 0.01 mA cm^{-2} in conditions which was tested using such enzyme electrodes, with the CV response for enzyme electrodes at 1 mV s^{-1} scan rate in PBS (37 °C) in pseudo-physiological and oxygen saturated conditions as in Figure 3. A current density of 0.28 ± 0.02 mA cm^{-2} (n=3) is obtained in pseudo-physiological condition in PBS, consistent with the predicted values of 0.28 ± 0.01 mA cm^{-2}. Results from further test set enzyme electrodes, prepared through the co-immobilisation of different component randomised amounts with experiments carried out under pseudo-physiological (0.2 mM O_2) conditions, are shown in Table 4.

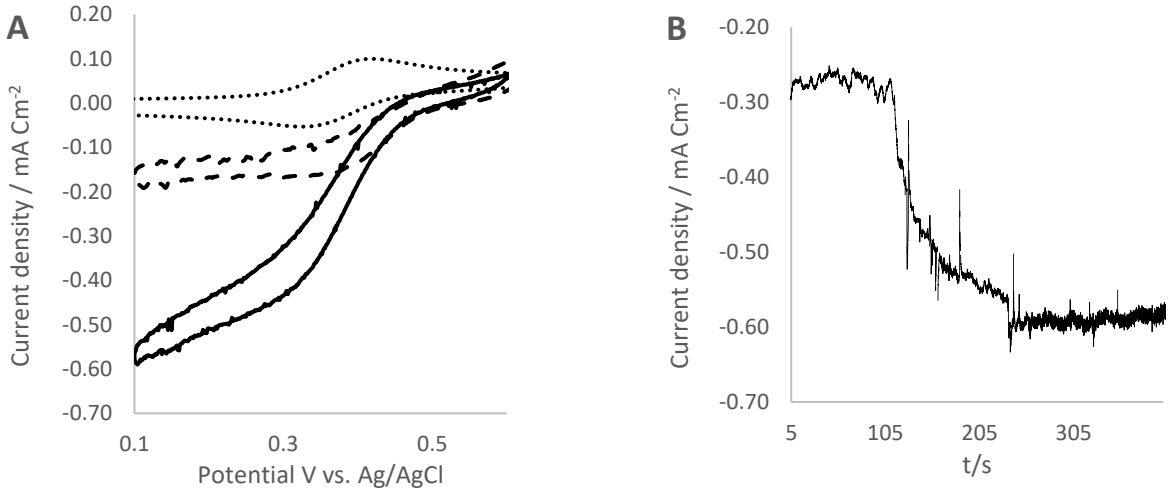

Figure 3. (A) CVs recorded at 1 mV s^{-1} in the absence of oxygen (dot line), oxygen saturated (1 mM O_2) (solid line) and in pseudo-physiological (0.2 mM O_2) (dashed line) non-stirred PBS (37 °C). **(B)** Amperometric current density recorded in PBS (37 °C) at 150 rpm at an applied potential of 0.1 V vs. Ag/AgCl, in pseudo-physiological and oxygen saturated conditions for enzyme electrodes.

Os(dclbpy)$_2$ PVI (µL)	**MWCNT (µL)**	***Mv*BOd (µL)**	**Predicted Current density (mA cm^{-2})**	**Actual Current density (mA cm^{-2})**
9.6 (48 µg)	6 (60 µg)	9.6 (442 µg)	0.24 ± 0.01	0.27 ± 0.02
18.2 (91 µg)	1 (10 µg)	9.6 (442 µg)	0.23 ± 0.01	0.19 ± 0.03
9.6 (48 µg)	1 (10 µg)	19.2(883 µg)	0.12 ± 0.01	0.14 ± 0.02
1 (5 µg)	6 (60 µg)	19.2 (883 µg)	0.12 ± 0.01	0.10 ± 0.01
1 (5 µg)	6 (60 µg)	0	0.02 ± 0.01	0.01 ± 0.01
1 (5 µg)	1 (10 µg)	9.6 (442µg)	0.04 ± 0.01	0.05 ± 0.01
9.6 (48 µg)	1 (10 µg)	0	0.03 ± 0.01	0.06 ± 0.02
18.2 (91 µg)	6 (60 µg)	0	0.06 ± 0.01	0.05 ± 0.01
9.6 (48 µg)	11 (110 µg)	0	0.05 ± 0.01	0.03 ± 0.01

Table 4: Model validation demonstrates predicted and experimental values of the enzyme electrode response at pseudo physiological conditions (n=3).

Predicted current density vs observed current density by the model is plotted to show the linear relationship using the above results (Table 2 and Table 4) as shown in Figure 4.

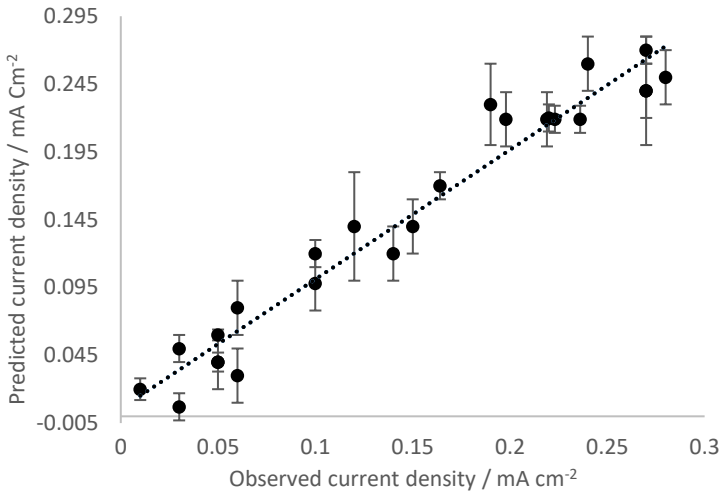

Figure 4: A plot of predicted current density vs observed current density for enzyme electrodes prepared according to results from table 2 and 4 (n=3).

A correlation (R^2) of 0.95 is achieved suggesting that the model is valid. Minor deviations on certain points in the model might be as a result of human error during experiments, and in particular in the enzyme electrode manual preparation steps.

4.3.4 Optimisation of biocathode

According to the current densities achieved from enzyme electrode preparation using the model, MWCNT and $Os(dcbpy)_2PVI$ appear to be the main contributing factors to the current densities. To confirm this, a perturbation diagram for enzyme electrode performance with respect to the three different factors is shown in Figure 5, where the influence of each factor around a specific point in the design range is plotted. In this method, the current density is plotted with respect to only one variable of the overall process, one at a time over its range, considering the other variables as constant at their centre point. A steep slope or curvature in a factor shows that current density response is sensitive to that factor and a flatter line therefore represents insensitivity to modification of that factor. A steep slope for MWCNT and $Os(dcbpy)_2PVI$ is

obtained compared to *Mv*BOd factor, indicating that the MWCNT and Os(dcbpy)$_2$PVI factors have a larger impact on current density of enzyme electrodes, in the ranges tested.

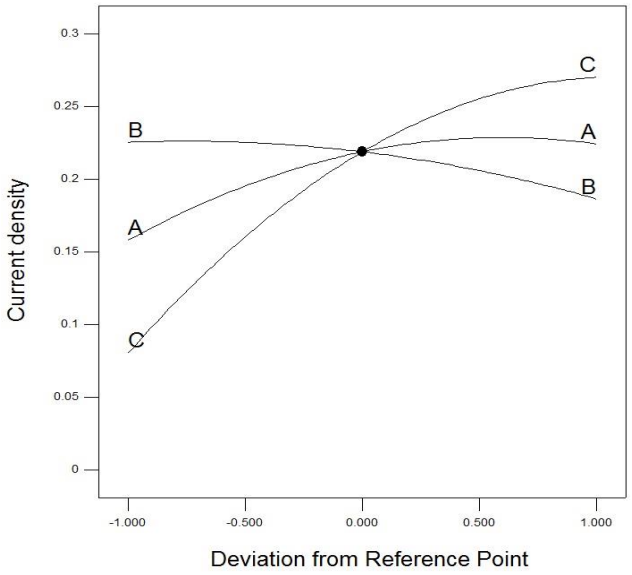

Figure 5: Deviation graph of predicted current density (mA cm^{-2}) versus the deviation from reference point, where A: Os(dcbpy)$_2$PVI, B: *Mv*BOd, C: MWCNT.

The MWCNT provide a scaffold that increases the surface area contributing to retention of enzyme activity which results in higher current density for enzyme electrodes [24, 39]. Increasing the Os(dcbpy)$_2$PVI loading in the enzyme electrode preparation step also displays a positive effect on the observed current density. It has also been previously reported by Osadebe *et al.* that the addition of MWCNT on the enzyme electrode increased the amount of redox polymer that is co-immobilised and electronically coupled within the enzyme films [17]. The three-dimensional response surface plots of the relationship between Os(dcbpy)$_2$PVI and MWCNT, on the current density response of enzyme electrodes are presented in Figure 6. In order to achieve the highest current density based on the model, an optimisation study was carried out from the validated DoE model to evaluate the experimental parameters for enzyme electrode preparation. The resulting response model from the 16 runs is:

Equation [2] $y = -0.34735 + 0.020949\,x_1 + 0.026930\,x_2 + 0.021180\,x_3 - 4.73362 \times 10^{-4}\,x_1^2 - 3.7351 \times 10^{-4}\,x_2^2 - 5.15 \times 10^{-4}x_3^2 - 1.54433 \times 10^{-4}x_1x_2 + 5.2083 \times 10^{-5}x_1x_3 - 5.0 \times 10^{-4}x_2x_3$

The DoE optimum component amounts, based on maximising the predicted current density using equation 2, are 25.8 µL redox polymer, 18.2 µL MWCNT and 11.1 µL of *Mv*BOd, predicted to deliver 0.29 ± 0.01 mA cm^{-2}. Table 5 shows the optimum of these components based on the combination of the response surface model and contours, with the predicted and experimentally determined response for the enzyme electrodes prepared and tested in pseudo-physiological conditions.

$Os(dcbpy)_2PVI$ (µL)	***Mv*BOd (µL)**	**MWCNT (µL)**	**Predicted current density mA cm^{-2}**	**Actual current density mA cm^{-2}**
25.8 (129 µg)	11.1 (111 µg)	18.2 (837.2 µg)	0.29 ±0.01	0.32 ± 0.03

Table 5: Predicted and experimental values of the enzyme electrode response at optimum conditions (n=3).

A

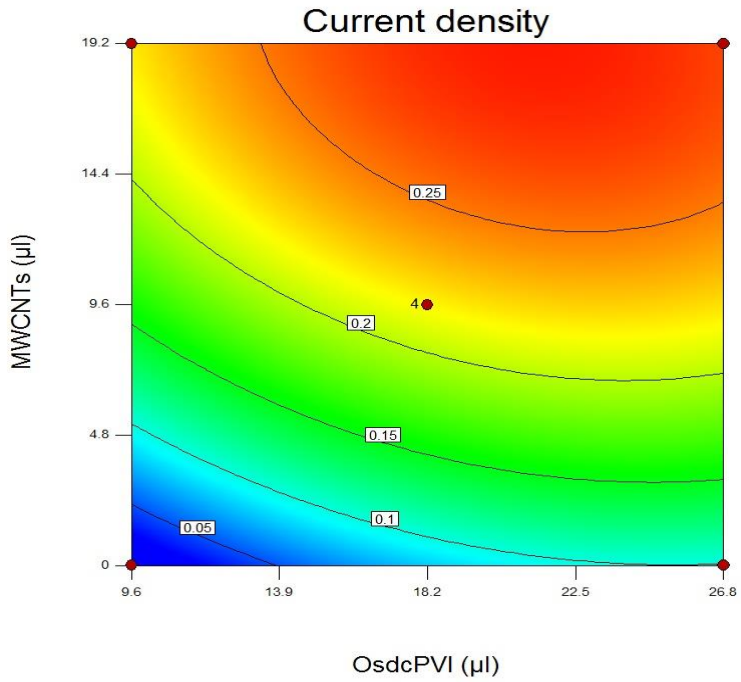

B

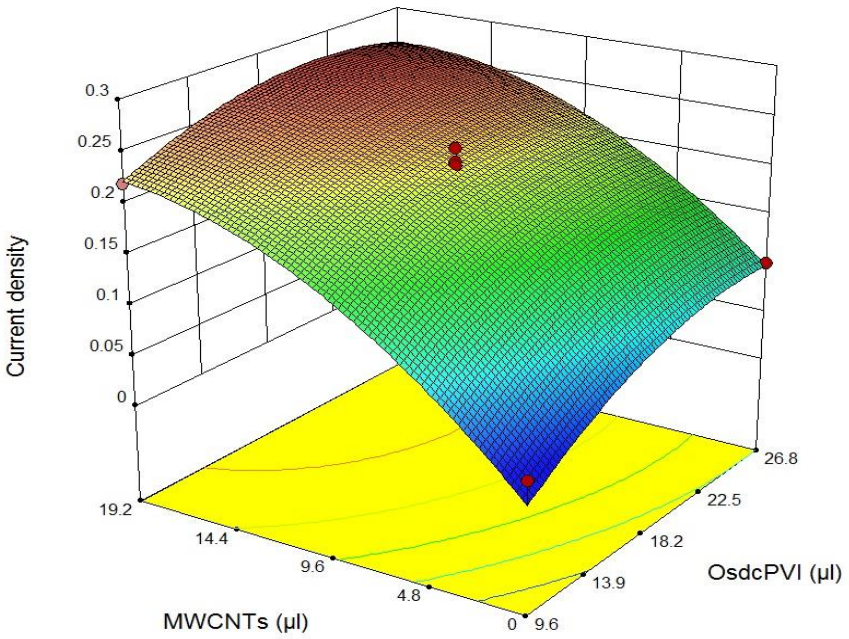

Figure 6: Contour plot (A) and Response surface (B) of the oxygen reduction current density (mA cm^{-2}) for MWCNT vs $Os(dcbpy)_2PVI$ amounts.

Current density of 0.32 ± 0.03 mA cm^{-2} is obtained in pseudo-physiological condition for the DoE optimised enzyme electrodes. This is higher than previously obtained (0.064 mA cm^{-2}) for enzyme electrodes under similar conditions but using the OFAT approach, and without MWCNT [40]. Addition of MWCNT is shown to increase the surface coverage of osmium on enzyme electrodes subsequently leading to improved enzyme retention and/or addressing the redox polymer on the electrode surface and improved oxygen reduction current density [41]. For comparison to other enzyme electrodes, an oxygen reduction current density of 0.12-0.22 mA cm^{-2} was reported for enzyme electrodes based on co-immobilisation of *Mv*BOd and multiwall carbon nanotube buckypaper (carbon nanotube grid paper) operating in pseudo-physiological condition [42]. In addition Schubert *et al.* reported that reduction of O_2 on *Mv*BOd covalently linked to a MWCNT-modified gold electrode generated up to 500 µAcm^{-2} at pH 7 and 25°C. Air breathing gas diffusion cathodes have also been investigated as illustrated by the work of Babanova *et al.* with an improved oxygen reduction current density of 755 µA cm^{-2} at

0.3 V vs. Ag/AgCl for enzyme electrodes based on immobilisation of *Mv*BOd in 0.1 M phosphate buffer (PBS)) on buckypaper by physical adsorption utilising DOE method [18].

4.3.5 Fuel cells operating in pseudo-physiological buffer

A potential application for an EFC system is to power implantable medical devices *via* the oxidation of glucose as fuel and the reduction of oxygen as oxidant due to their relatively high concentrations of 5-8 mM and 0.05-0.13 mM, respectively, available in the bloodstream (44-46). Following this approach, a membrane-less enzymatic fuel cell is assembled based on the utilisation of glucose as fuel and oxygen as oxidant for testing under pseudo-physiological conditions using cathodes prepared by co-immobilisation of $Os(dcbpy)_2PVI$ redox polymers with *Mv*BOd and MWCNT using amounts optimised from the DoE approach. Enzyme electrodes chosen as anodes are based on previous reports [17] of $Os(dmobpy)_2PVI$ redox polymer co-immobilised with FADGDH and MWCNT. The assembled EFC is tested in pseudo-physiological buffer conditions in 5 mM glucose and 0.2 mM O_2 in an attempt to mimic *in vivo* human conditions. To evaluate the factors limiting the power output for the EFCs, polarisation curves at the anode and cathode were investigated. Enzyme electrodes from the 1 mV s^{-1} slow scan CVs are used to compute cell polarisation curves for each EFC as shown in Figure 7. The polarisation curves indicate that the current at the cathode limits power produced at the assembled fuel cell for the EFC under both pseudo-physiological and saturated oxygen conditions. A maximum power density of 76 ± 10 μW cm^{-2} is achieved, according to Figure 7, while in O_2 saturated conditions, the maximim power density increased to 92 ± 9 μW cm^{-2}. The maximum power density for the EFC assembled is observed at ~0.3 V in saturated oxygen electrolyte condition and is similar to that obtained previously [46].

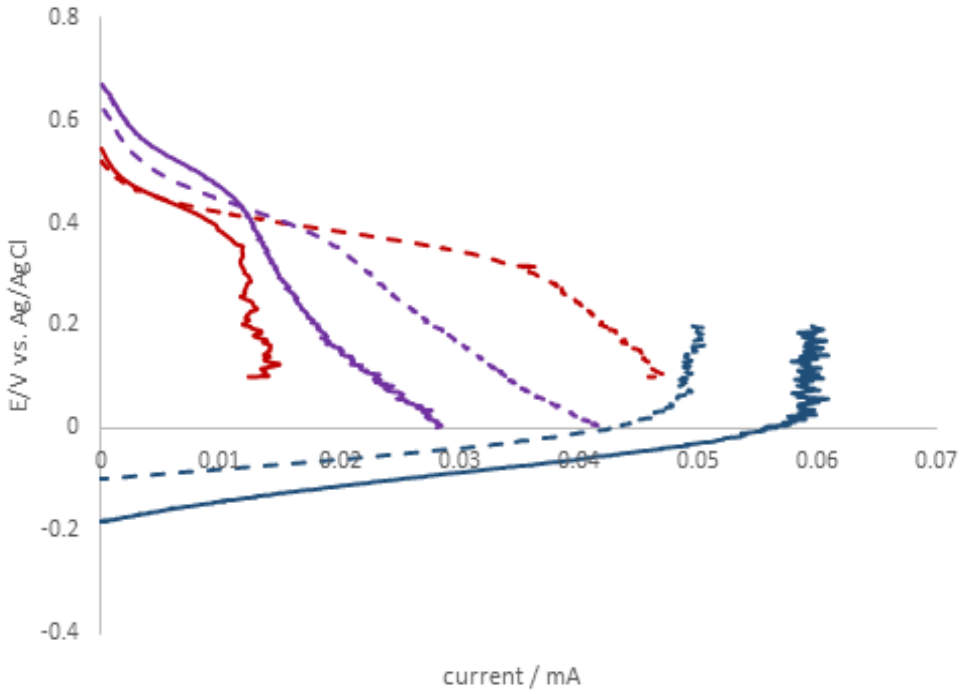

Figure 7: Polarisation curves recorded in PBS containing 5 mM glucose at 37 °C for enzyme electrodes prepared by co-immobilisation of MWCNT with either FADGDH and Os(dmobpy)$_2$PVI (blue) or *mv*BOd and Os(dcbpy)$_2$PVI (red) reported vs Ag/AgCl, and for the enzyme electrodes assembled as a membrane-less fuel cell (purple) in air (solid line) and in O_2 (dashed line). Geometric areas are anode: 0.2121 and cathode: 0.0707 cm^2.

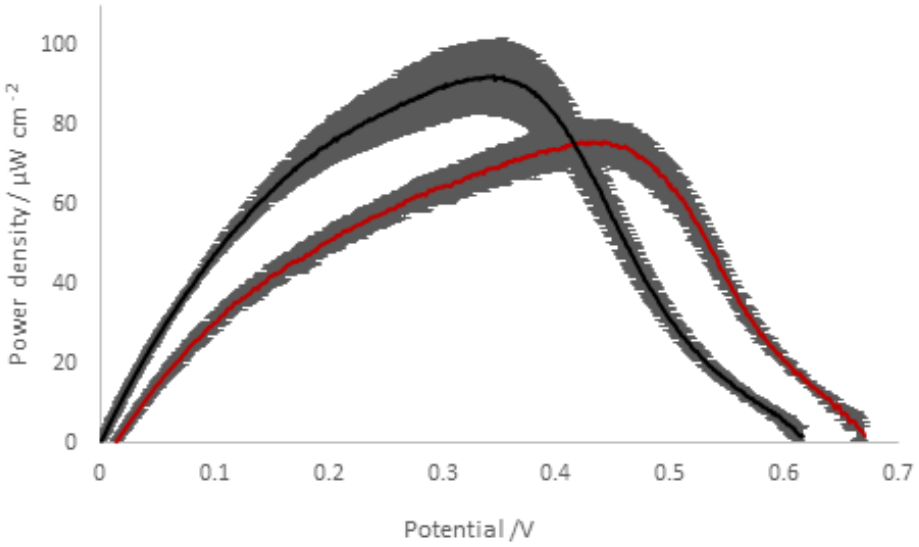

Figure 8: Power curves recorded for fully membrane-less enzymatic fuel cells by 1 mV s^{-1} linear sweep voltammetry in 50 mM PBS at 37 °C in air (red) and in saturated O_2 (black) containing 5 mM glucose for optimised biocathode prepared by co-immobilisation of $Os(dcbpy)_2PVI$ 25.8 µL, coimmobilised with *Mv*BOd 11.1 µL and MWCNT 18.2 µL. Anode enzyme electrodes prepared by co-immobilisation of $Os(dmobpy)_2PVI$, MWCNT and FADGDH. Power densities normalised to the geometric area of the cathode, as current-limiting electrode (n=3).

Comparison of EFC results has proven to be difficult considering the differences in operating conditions such as limiting factors, glucose concentrations, pH and also electrode preparation methodologies. For example, Kim *et al.* [47] have reported on a membrane-less EFC operating at higher cell voltages; producing a power density of 50 µW cm^{-2} at a 0.5 V cell voltage under physiological conditions (air saturated pH 7.4, 140 mM NaCl, 37.5 °C in 15 mM glucose concentration) with the increased voltage probably due to the differences in redox potential of the osmium redox polymers selected. In addition, Heller reported a power density of 4.4 µW cm^{-2} in physiological buffer solution produced by a membrane-less EFC operating in 15 mM glucose-containing stagnant. The EFC was constructed by GOx wired by [Os(N,N'-dialkylated-2,2'bi-imidazole)$_3$]$^{2+/3}$ redox polymer as anode and bilirubin oxidase wired by poly(N-vinylimidazole)-[Os-2,2',6',2''-terpyridine-4,4'-dimethyl-2,2' bipyridine)$_2$Cl]$^{2+/3+}$ polymer as cathode [28].

4.4 Conclusion

Enzyme electrodes component amounts were optimised to generate higher current densities and verified by response surface methodology. The MWCNT and Os(dcbpy)$_2$PVI were identified as the most significant contributing factors to cathode performance, although the oxygen reduction current also displayed a dependency on the level of *Mv*BOd used. The oxygen reduction current generated in pseudo-physiological conditions using the DoE approach and MWCNT was 4.3 fold higher than that previously observed for enzyme electrodes optimised by varying one factor at a time and prepared without addition of such nanostructures [40]. DoE optimised enzyme electrodes result in oxygen reduction current density of 0.32 ± 0.03 mA cm^{-2} in pseudo-physiological conditions and 0.8 ± 0.05 mA cm^{-2} in saturated oxygen solutions, at an applied potential of 0.1 V vs. Ag/AgCl, showing promise for application as oxygen reducing cathode in enzymatic fuel cells. EFCs were assembled and tested for power generation under pseudo-physiological buffer conditions using the optimised biocathode and an anode containing Os(dmobpy)$_2$PVI redox polymer co-immobilised with FADGDH and MWCNT. EFCs produced power densities of 76 ± 10 μW cm^{-2} under conditions mimicking those of a physiological environment and a maximum power output of 92 ± 9 μW cm^{-2} in oxygen saturated conditions.

4.5 References

[1] A. Heller, B. Feldman, Accounts of Chemical Research, 43 (2010) 963-973.

[2] A. Heller, Physical Chemistry Chemical Physics, 6 (2004) 209-216.

[3] S.C. Barton, J. Gallaway, P. Atanassov, Chemical Reviews, 104 (2004) 4867-4886.

[4] D. Leech, P. Kavanagh, W. Schuhmann, Electrochimica Acta, 84 (2012) 223-234.

[5] N. Mano, F. Mao, A. Heller, Journal of the American Chemical Society, 124 (2002) 12962-12963.

[6] R.D. Milton, K. Lim, D.P. Hickey, S.D. Minteer, Bioelectrochemistry, 106, Part A (2015) 56-63.

[7] S. Tsujimura, M. Fujita, H. Tatsumi, K. Kano, T. Ikeda, Physical Chemistry Chemical Physics, 3 (2001) 1331-1335.

[8] S.C. Barton, M. Pickard, R. Vazquez-Duhalt, A. Heller, Biosensors & Bioelectronics 17 (2002) 1071-1074.

[9] F. Xu, W. Shin, S.H. Brown, J.A. Wahleithner, U.M. Sundaram, E.I. Solomon, Biochimica et Biophysica Acta. 1292(1996) 303-311.

[10] S. Tsujimura, H. Tatsuni, J. Ogawa, S. Shimizu, K. Kano, T. Ikeda, Journal of Electroanalytical Chemistry 496 (2001) 69-75.

[11] E.J. Calvo, C. Danilowicz, L. Diaz, Journal of the Chemical Society, 89 (1993) 377-384.

[12] C. Danilowicz, E. Cortón, F. Battaglini, E.J. Calvo, Electrochimica Acta, 43 (1998) 3525-3531.

[13] A.E.G. Cass, G. Davis, G.D. Francis, H.A.O. Hill, W.J. Aston, I.J. Higgins, E.V. Plotkin, L.D.L. Scott, A.P.F. Turner, Analytical Chemistry, 56 (1984) 667-671.

[14] S.M. Zakeeruddin, D.M. Fraser, M.K. Nazeeruddin, M. Grätzel, Journal of Electroanalytical Chemistry, 337 (1992) 253-283.

[15] S.D. Minteer, B.Y. Liaw, M.J. Cooney, Current Opinion in Biotechnology, 18 (2007) 228-234.

[16] S.D. Minteer, P. Atanassov, H.R. Luckarift, G.R. Johnson, Materials Today, 15 (2012) 166-173.

[17] I. Osadebe, D. Leech, ChemElectroChem, 1 (2014) 1988-1993.

[18] S. Babanova, K. Artyushkova, Y. Ulyanova, S. Singhal, P. Atanassov, Journal of Power Sources, 245 (2014) 389-397.

[19] R. Kumar, D. Leech, Bioelectrochemistry, 106 (2015) 41-46.

[20] R. Kumar, D. Leech, Journal of the Electrochemical Society, 161 (2014) H3005-H3010.

[21] E.M. Kober, J.V. Caspar, B.P. Sullivan, T.J. Meyer, Inorganic Chemistry 27 (1988) 4587-4598.

[22] T.J. Ohara, R. Rajagopalan, A. Heller, Analytical Chemistry 66 (1994) 2451-2457.

[23] R.J. Forster, J.G. Vos, Macromolecules, 23 (1990) 4372-4377.

[24] D. MacAodha, M.L. Ferrer, P.O. Conghaile, P. Kavanagh, D. Leech, Physical Chemistry Chemical Physics, 14 (2012) 14667-14672.

[25] E. Katz, K. MacVittie, Energy & Environmental Science, 6 (2013) 2791-2803.
[26] S. Tsujimura, M. Kawaharada, T. Nakagawa, K. Kano, T. Ikeda. Electrochemistry Communications, 5 (2003) 138-141.
[27] J.W. Gallaway, S.C. Barton, Journal of the American Chemical Society 130 (2008) 8527-8536.
[28] H.H. Kim, N. Mano, Y. Zhang, A. Heller, Journal of the Electrochemical Society 150 (2003) A209-A213.
[29] A.B.P. Lever, Inorganic Chemistry, 29 (1990) 1271-1285.
[30] R.J. Forster, J.G. Vos, Langmuir, 10 (1994) 4330-4338.
[31] A.J. Bard, L.R. Faulkner, Electrochemical Methods: Fundamentals and Applications, 2 ed., Wiley & Sons, New York, (2001).
[32] L. Eriksson, E. Johansson, N. Kettaneh-Wold, C. Wikstrom, S. Wold, Design of Experiments, 3 ed., MKS Umetrics AB, (2008).
[33] R. Bourbonnais, M.G. Paice, B. Freiermuth, E. Bodie, S. Borneman, Applied & Environmental Microbiology 63 (1997) 4627-4632.
[34] B. Qi, X. Chen, F. Shen, Y. Su, Y. Wan, Industrial & Engineering Chemistry Research, 48 (2009) 7346-7353.
[35] G. Chen, J. Chen, C. Srinivasakannan, J. Peng, Applied Surface Science, 258 (2012) 3068-3073.
[36] H.-Y. Fu, P.-C. Xu, G.-H. Huang, T. Chai, M. Hou, P.-F. Gao, Desalination, 302 (2012) 33-42.
[37] J. Ren, M. Zhao, J. Shi, J. Wang, Y. Jiang, C. Cui, Y. Kakuda, S.J. Xue, Food Science and Technology, 41 (2008) 1624-1632.
[38] K. Shabbiri, A. Adnan, B. Noor, S. Jamil, Annals of Microbiology, 62 (2012) 523-532.
[39] P. Ó Conghaile, D. MacAodha, B. Egan, P. Kavanagh, D. Leech, Journal of the Electrochemical Society, 160 (2013) G3165-G3170.
[40] P. A. Jenkins, S. Boland, P. Kavanagh, D. Leech, Bioelectrochemistry 76 (2009) 162-168.
[41] P.P. Joshi, S.A. Merchant, Y. Wang, D.W. Schmidtke, Analytical Chemistry, 77 (2005) 3183-3188.
[42] D. V. Pankratov, Y. S. Zeifman, O. V. Morozova, G. P. Shumakovich, I. S. Vasil'eva, S. Shleev, V. O. Popov and A. I. Yaropolov, Electroanalysis, 25 (2013) 1143-1149.
[43] K. S. Polonsky, B. D. Given and E. Van Cauter, The Journal of Clinical Investigation, 81 (1988) 442-448.
[44] M. Falk, Z. Blum and S. Shleev, Electrochimica Acta, 82 (2012) 191-202.
[45] A. C. Guyton and J. E. Hall. Textbook of Medical Physiology, 11th ed., Elsevier Saunders, (2006).
[46] I. Osadebe, P.Ó. Conghaile, P. Kavanagh, D. Leech, Electrochimica Acta, 182 (2015) 320-326.
[47] H.-H. Kim, N. Mano, Y. Zhang, A. Heller, Journal of the Electrochemical Society, 150 (2003) A209-A213.

Chapter 5

Effect of pH on immobilisation and performance of sugar oxdising enzyme electrodes based on osmium redox mediation

5.1 Introduction

The co-immobilisation of enzymes and electron-shuttling mediators within redox-conducting hydrogels on solid electrodes is a promising approach for improving the catalytic current capture as a result of enzyme redox reactions. Mediators are incorporated to allow electron shuttling from the enzyme active site to electrodes, as active sites are buried within a proteinaceous insulating envelope too distant from the electrode surface to permit rapid electron transfer to occur [1]. As mediators, osmium based polymers and complexes are broadly explored [2-5], as these redox mediators possess advantages over iron and ruthenium based systems [6,7], as outlined in previous chapters. In addition application of multiwalled carbon nanotube (MWCNT) as components of enzyme electrodes provides an increased current capture and stability, attributed to improved retention of enzyme activity [8-10]. Furthermore, the utilisation of crosslinkers provides higher current densities and an improved signal stability by addressing the leaching and the stability of the enzymes and redox mediators on the electrode surfaces. Several cross-linking methods have been reported and in principle they can be divided into two groups. First, bifunctional reagents can be used to bridge amine groups of glycine or histidine residues of different polypeptide chains by monomeric or oligomeric cross-links. Second, amide-type cross-links can be formed by activation of the carboxylic acid functional

groups of residues followed by reaction of these activated carboxylic acid groups with amine groups of another polypeptide chain. As an example of the first approach, Gregg and Heller [11] demonstrated the use of a di-epoxide crosslinker, poly(ethylene glycol) diglycidyl ether (PEGDGE) to create a redox hydrogel to entrap enzyme and mediators in a 3-D structure with a very high concentration of both enzyme and mediator. This study showed that the redox hydrogels were permeable to both substrates and products and allowed diffusion of electrons [12]. Ohara *et al.* [12] reported on enzyme electrodes formed by co-immobilising osmium based redox polymer and GOx on electrode surfaces using PEGDGE, for sensing glucose. An example of the second approach is the use of the water-soluble carbodiimide reagent N-(3 dimethylaminopropyl)-N′ethylcarbodiimide (EDC) to couple carboxyl groups to amino functions, which involves the activation of carboxylic acid groups. This is frequently used with an N-hydroxysuccinimide reagent (NHS), used to stabilise the activated ester formed as an intermediate from the carboxylic acid by EDC, to increase the coupling efficiency. The EDC/NHS coupling procedure is widely used to develop enzymatic sensors [13, 14-17].

The pH of immobilisation and the operating electroyte pH can affect the current output by altering enzyme activity, crosslinking kinetics and charge transport rates through the enzyme electrodes under operational conditions [18]. *Trametes villosa* CDH (*Tv*CDH) and D-fructose dehydrogenase from alphaprotobacteria (FDH) are respectively monomeric and heterotrimeric oxidoreductases consisting of two domains: the catalytic dehydrogenase domain (DH) contains one strongly but non-covalently bound flavin adenine dinucleotide (FAD) molecule as cofactor and is connected to an electron-mediating cytochrome domain (CYT) featuring a *b*-type and *c*-type heme cofactor for *Tv*CDH and FDH respectively. D-fructose dehydrogenase is a membrane-bound enzyme commonly seen in various *Gluconobacter sp.* especially in *Gluconobacter japonicus* (*Gluconobacter industrius*) that catalyses the oxidation of D-fructose to produce 5-keto-D-fructose. *Tv*CDH is a Class I CDH with pH optimum in the acidic pH range [41]. Class I CDHs are produced by wood-degrading fungi of the Basidiomycota: e.g. *Trametes villosa* [42-44]. Class II CDHs produced by the fungi of the *phyla Ascomycota* can have pH optima also in the human physiological pH range [19]. The catalytic cycle of CDH is similar to FDH and can be described briefly by the following. After the FAD domain is reduced by cellobiose, a wide spectrum of compounds can reoxidise the enzyme to its oxidised form, acting as electron acceptors. Both one electron-no-proton as well as two electron–proton

acceptors can perform this function [20, 21]. When one-electron acceptors are used, the heme and DH both play an important role in the re-oxidation of the enzyme, whereas two electron acceptors are preferentially active with the DH part [21, 22]. In addition the electrons stored in the reduced DH domain can be transferred via an internal electron transfer (IET) step to the CYT domain and then to a redox mediator or an electrode surface. In order to investigate the effect of the CYT domain and IET, GOx consisting of FAD and no CYT domain was used as control. FDH, *Tv*CDH and GOx all belong to the group of oxidoreductases with a non-covalently bound flavin in the catalytic domain. GOx is a dimeric oxido-reductase that is produced by certain species of fungi (*Aspergillus niger*) and catalyses the oxidation of β -D-glucose to D-gluconolactone, coupled to oxygen reduction to hydrogen peroxide. This chapter reports on a comparison of the catalytic current out-put of enzyme electrodes prepared from *Tv*CDH, FDH and GOx and two different mediators. The mediatros selected for comparison are the $Os(dmobpy)_2PVI$ redox polymer and the $Os(dmobpy)_24AMP$ redox complex previously used in Chapters 3 and 4. The current for enzyme electrode response is studied using flow injection analysis (FIA). Optimised conditions for the operation of the enzyme electrodes are obtained upon investigation of the effect of factors such as pH of immobilisation and electrolyte pH on the mediated oxidation of substrate.

5.2 Experimental

5.2.1 Materials

All chemicals and biochemicals were purchased from Sigma-Aldrich and used as received. All aqueous solutions unless otherwise stated were prepared in Milli-Q water (18 MΩ cm), Multiwalled carbon nanotube (MWCNT, from Sigma-Aldrich) were pre-treated under reflux in concentrated nitric acid for 6 h and isolated by filtration and washed repeatedly with distilled water until nitric acid removal was complete. Synthesis of the redox polymer ($Os(dmobpy)_2PVI$) and redox complex $Os(dmobpy)_24AMP$ was achieved by adapting literature procedures, as described in Chapter 2 [23-27]. GOx was from *Aspergillus niger* (Sigma Aldrich) with an average activity of 240 U mg^{-1}. D-Fructose dehydrogenase from the culture supernatant of *Gluconobacter japonicus* NBRC 3260 (FDH; EC 1.1.99.11) was obtained from

the National Institute of Technology and Evaluation (Nishinomiya, Hyogo Pref., Japan), (specific activity measured with potassium ferricyanide at pH 4.5 = 250 ± 30 U mg^{-1}). Cellobiose dehydrogenase (CDH; cellobiose: (acceptor) 1-oxidoreductase; EC 1.1.99.18) from *T. villosa* was provided by the University of Natural Resources and Applied Life Sciences Vienna, Austria (specific activity (DCIP assay, pH 4.5, 308) = 6.5 U mg^{-1}). The enzymes were in aqueous solution with the concentrations of 10, 1.7 and 11.2 mg mL^{-1} for GOx, FDH and *Tv*CDH respectively. Carboxymethyl-dextran (CMD) (average molecular mass of 15,000 Da) and polyethylene glycol diglycidyl ether (PEGDGE) was purchased from Sigma-Aldrich (average Mn 526). Substrate solutions of D-fructose, D-glucose and D-lactose were prepared at pH 4.5 and 5.5 in 50 mM sodium acetate buffer and at pH 6.5 and 7.5 in 50 mM phosphate buffered saline (0.1 M KCl) and allowed 24 h for mutarotation.

5.2.2 Preparation of anodes

Electrodes were prepared from graphite rods (3.05 mm diameter AGKSP grade, Ultra "F" purity, Alfa aesar, GmbH & Co KB (Karlsruhe, Germany)), polished on emery paper, rinsed with Milli-Q water and dried at room temperature. Deposition of solutions to prepare enzyme electrode films with the osmium redox polymer was achieved by initially pipetting 3 µL of a 46.25 mg mL^{-1} dispersion of acid-treated MWCNT followed by 4 µL of a 5 mg mL^{-1} $Os(dmobpy)_2PVI$ aqueous solution, 1.6 µL of enzyme solution and finally 0.5 µL of 15 mg/mL PEGDGE as crosslinker on the surface of the graphite working electrode and allowing the deposition to dry for 24 h. In the case of osmium complex, enzyme electrode assemblies were achieved by depositing 2.17 µL of a 46.25 mg mL^{-1} dispersion of acid-treated MWCNT, 1.83 µL of 4.25 mg mL^{-1} $Os(dmobpy)_24AMP$ aqueous solution, 1.25 µL of enzyme, 2.5 µL of CMD as polymer and 1 µL of an aqueous solution of 40 mM N-[3-dimethylaminopropyl]-N'-ethylcarbodiimide (EDC) and 10 mM N-hydroxysuccinimide (NHS) as crosslinker on the surface of the graphite electrode and allowing the deposition to dry for 18 hr. All current densities are normalised to their corresponding added enzyme activity (U) and geometric surface of the electrode.

5.2.3 Electrochemical measurements

Flow injection measurements were performed with a flow-through amperometric cell of the wall-jet type [28]. The carrier flow was maintained at a constant flow rate of 0.5 mL min^{-1} by a peristaltic pump. The injection loop volume was 50 μL. These experiments were performed with air saturated solutions. The response of graphite disc working electrodes was registered with a recorder (BD 112, Kipp & Zonen, Utrecht, the Netherlands).

5.3 Results and discussion

Enzyme electrodes as anodes for biofuel cells are developed based on optimum amounts from previous immobilisation strategies but by a 4-fold lower overall total amount, [29, 30] by co-immobilisation of MWCNT with one of either *Tv*CDH, FDH or GOx and one of either $Os(dmobpy)_2$PVI or $Os(dmobpy)_2$4AMP redox mediators on graphite disk electrodes. The 4-fold lower overall total amount was selected because of the difficulty to control drop-casting of higher amounts to the graphite rod surfaces used in this part with FIA and in addition to decrease the amount of mediator used due to low amounts available from the synthesis (described in Chapter 2). As depicted in Figure 1, the electron-shuttling redox mediators are proposed to electrically connect the enzyme active site cofactor to the surface of the electrode via electron transfer from co-factor followed by self-exchange mechanism by collisions between the reduced and oxidised forms of the mobile osmium redox centers [31, 32].

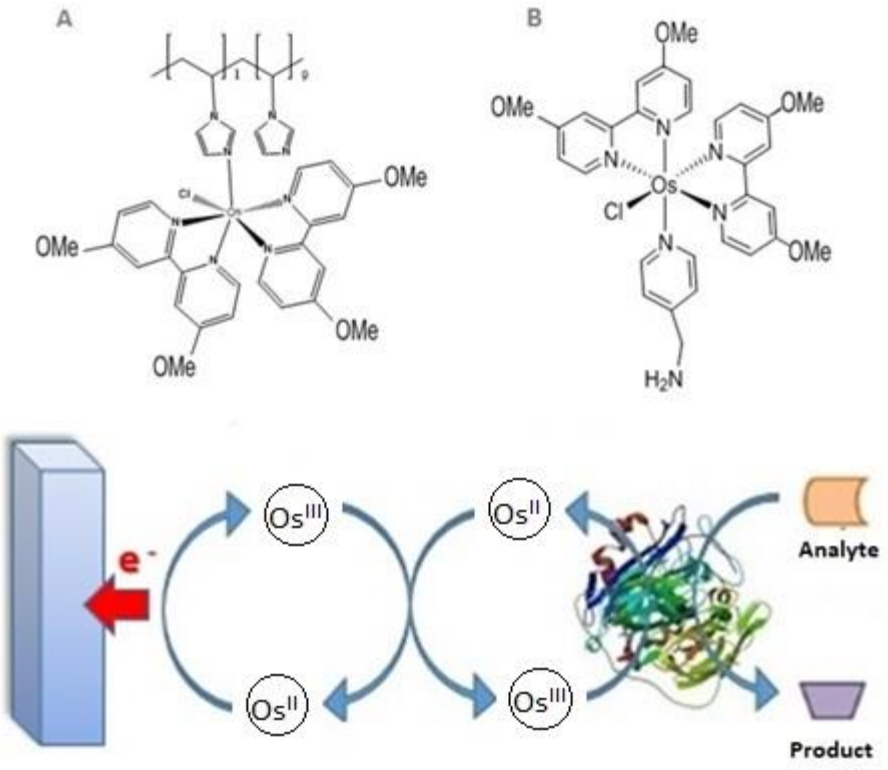

Figure 1. Scheme depicting the enzyme mediated electron transfer between an enzyme active site and the electrode surface via Os(dmobpy)$_2$PVI (A) or Os(dmobpy)$_2$4AMP (B)

The redox polymer Os(dmobpy)$_2$PVI and redox complex Os(dmobpy)$_2$4AMP are selected as mediators in films on carbon electrodes because of their relatively low redox potentials of -10 and 40 mV vs. Ag/AgCl, respectively, since lower potentials prevent the oxidation of interfering compounds and increase the overall obtained cell voltage on application to biofuel cells.

5.3.1 Selection of immobilisation pH

Initially the effect of pH on the chemical immobilisation method for preparation of the enzyme electrodes was investigated. The performance of the electrodes was assessed by measurement of the dependence of the catalytic current density, normalised to the activity of each enzyme, on the substrate concentration in 50 mM sodium acetate buffer at pH 4.5. Enzyme electrodes using the Os(dmobpy)$_2$4AMP as mediator were prepared using EDC/NHS as coupling agent [13, 14-17]. Enzyme electrodes using the Os(dmobpy)$_2$PVI as mediator were prepared using PEGDGE as crosslinker [11, 12]. Testing for electrodes prepared using *Tv*CDH, FDH or GOx

was performed using lactose, fructose or glucose as substrates, respectively, in a flow through electrochemical cell at a flow rate of 0.5 mL min^{-1}. Lactose was chosen as substrate for *Tv*CDH, because all CDHs exhibit high activity for this substrate, and in contrast to the cellodextrins as substrates, there is no substrate inhibition [33, 34]. The modified electrodes were placed in a flow through electrochemical cell and examined for their response to injected samples in the flow injection mode at a constant applied potential of 200 mV and 150 mV vs. Ag/AgCl (3 M KCl) for $Os(dmobpy)_2$4AMP ($E^{\circ\prime}$ = 40 mV) and $Os(dmobpy)_2$PVI ($E^{\circ\prime}$ = -10 mV) respectively (see Chapter 2). The mediated electrochemistry response of the enzyme electrodes to their corresponding injected substrate when immobilised at human physiological condition is shown in Figures 3, 4 and 5. The electrodes were compared with respect to their ability to oxidise substrate at different concentrations. For example, in the case of FDH, upon the addition of high concentrations (30 mM) of fructose, sigmoidal-shaped cyclic voltammograms, characteristic of catalytic oxidation of fructose by the enzyme were obtained for all enzyme electrodes prepared by co-immobilisation of MWCNT, FDH and one of either $Os(dmobpy)_2$PVI or $Os(dmobpy)_2$4AMP redox mediators on graphite disk electrode as shown in Figure 2.

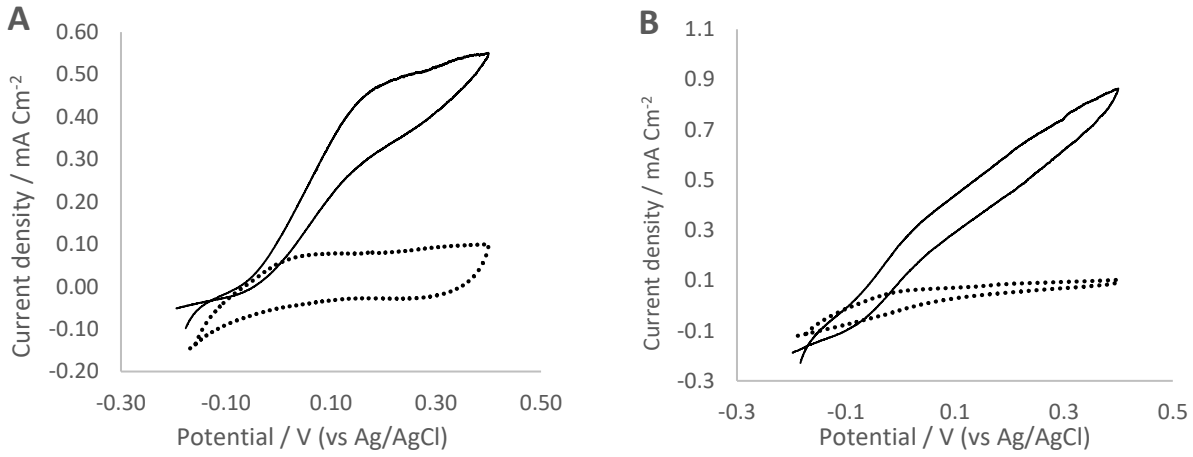

Figure 2: CVs recorded at 1 mV s^{-1} in the absence (dotted line) and presence (solid line) of fructose for FDH enzyme electrodes. Electrodes were prepared at human physiological conditions by co-immobilising FDH (2.72 μg), $Os(dmobpy)_2$4AMP (7.8 μg), MWCNT (100 μg), CMD (12.5 μg) and EDC/NHS as crosslinker (A), and FDH (2.12 μg), $Os(dmobpy)_2$PVI (20 μg), MWCNT (139 μg) and PEGDGE (7.5 μg) as crosslinker (B) at graphite disk electrodes. Experiments were performed in 50 mM sodium acetate buffer at pH 4.5 containing 30 mM fructose.

In comparison Pedro *et al.* [45] reported on a mediated amperometric biosensor for fructose based on D-fructose dehydrogenase. The enzyme was incorporated in a carbon paste matrix containing $Os(bpy)_2Cl_2$ as redox mediator that achieved electron transfer at 0.1 V (vs. Ag/AgCI) with maximum apparent current densities of 1.2 mA cm $^{-2}$. In this chapter using a low potential redox mediator, a maximum catalytic current of 5.7 mA U $^{-1}$ cm^{-2} is reported for FDH under the optimal pH conditions and at an applied potential of 0.15 V (vs. Ag/AgCI) as in figure 9.

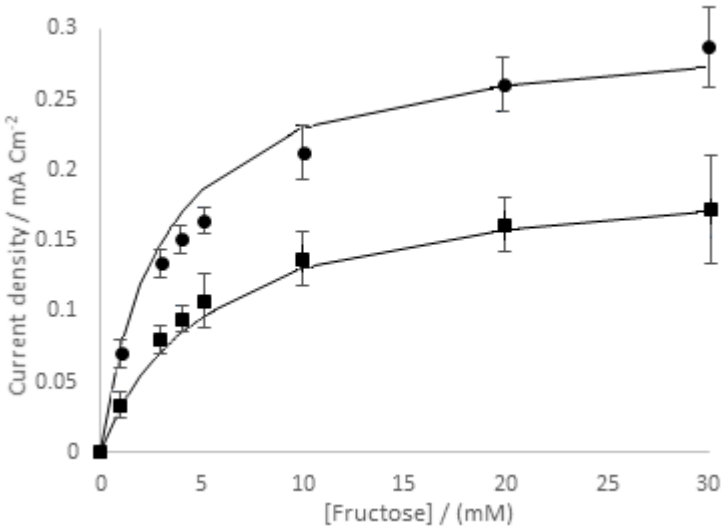

Figure 3: Dependence of average catalytic current density (n=3) on the fructose concentration. Electrodes were prepared at human physiological conditions by coimmobilising FDH, MWCNT and either $Os(dmobpy)_2$4AMP (●) or $Os(dmobpy)_2$PVI (▪) and Michaelis-Menten steady state approximation (solid line) for each enzyme electrode. Experiments were performed in 50 mM sodium acetate buffer at pH 4.5 with a flow rate of 0.5 mL min^{-1} (other conditions are as in Figure 2).

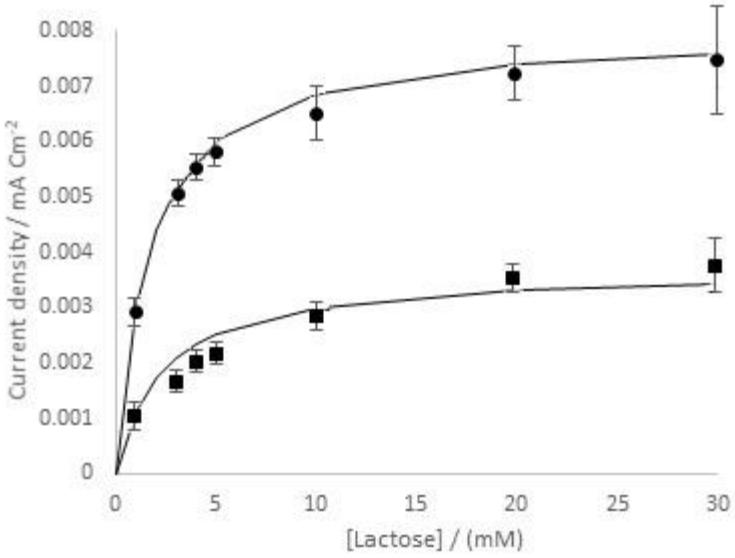

Figure 4: Dependence of average catalytic current density (n=3) on the lactose concentration. Electrodes were prepared at human physiological conditions by coimmobilising *Tv*CDH, MWCNT and either $Os(dmobpy)_2$4AMP (●) or $Os(dmobpy)_2$PVI (▪) and Michaelis-Menten steady state approximation (solid line) for each enzyme electrode. Experiments were performed in 50 mM sodium acetate buffer at pH 4.5 with a flow rate of 0.5 mL min^{-1}, (other conditions is as in Figure 2).

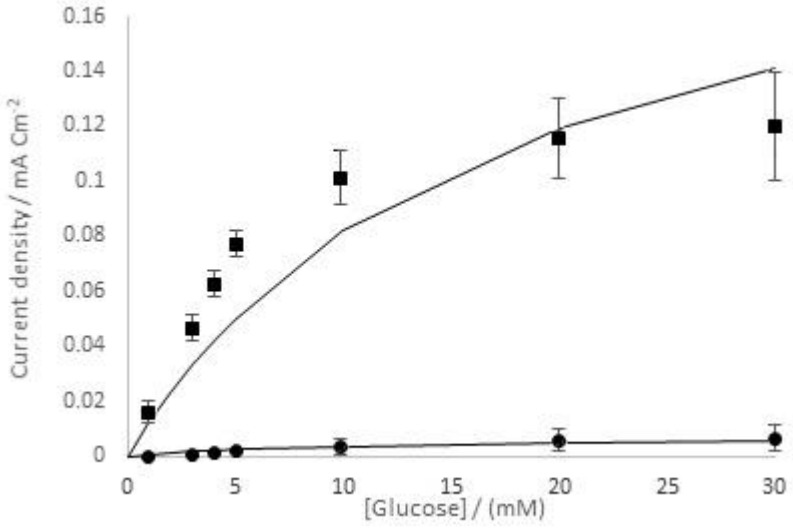

Figure 5: Dependence of average catalytic current density (n=3) on the glucose concentration. Electrodes were prepared at human physiological conditions by coimmobilising GOx, MWCNT and either $Os(dmobpy)_2$4AMP (●) or $Os(dmobpy)_2$PVI (▪) and Michaelis-Menten steady state approximation (solid line) for each enzyme electrode. Experiments were performed in 50 mM sodium acetate buffer at pH 4.5 with a flow rate of 0.5 mL min^{-1} (other conditions are as in Figure 2).

For all enzyme electrodes, the increase in catalytic current density as a function of substrate concentration is apparent (Figures 3, 4 and 5). Under physiological immobilisation conditions selected, films prepared using FDH and *Tv*CDH produce lower catalytic current density with Os(dmobpy)$_2$PVI redox polymer than the Os(dmobpy)$_2$4AMP redox complex while with GOx, the osmium polymer generates a higher current. For comparison, maximum saturated current density j_{max}^{app} for films of Os(dmobpy)$_2$PVI or Os(dmobpy)$_2$4AMP, each coimmobilised with FDH or *Tv*CDH on graphite electrodes, produced 200 and 300 or 4 and 8 µA cm^{-2}, respectively, under FIA conditions (Table 1). An estimate of the apparent Michaelis constant, K_M^{app}, and maximum saturated current densities j_{max}^{app} is obtained by non-linear least-squares fitting of the data to the Michaelis-Menten model and using the Lineweaver-Burke plots of the transformed data to verify the fit. The K_M^{app} values observed for films of Os(dmobpy)$_2$PVI or Os(dmobpy)$_2$4AMP, each coimmobilised with FDH or *Tv* CDH on graphite electrodes, were measured at 5.25 and 3.03 mM or 2.31 and 1.64 mM respectively and suggest that *Tv*CDH displays a higher affinity for lactose compared to FDH for fructose under these conditions. Films of Os(dmobpy)$_2$PVI or Os(dmobpy)$_2$4AMP, each co-immobilised with GOx on graphite electrodes, produced 220 or 8 µA cm^{-2}, and K_M^{app} values of 16.9 or 11.78 mM, respectively, under FIA conditions which agree well with reported values [29].

Enzyme electrodes	***j*$_{max}$, ^{app} (µA cm^{-2}) with Os(dmobpy)$_2$4AMP**	***j*$_{max}$, ^{app} (µA cm^{-2}) with Os(dmobpy)$_2$PVI**	**K_M^{app} (mM) with Os(dmobpy)$_2$4AMP**	**K_M^{app} (mM) with Os(dmobpy)$_2$PVI**
FDH	300 ± 10	200 ± 40	3.03 ± 0.01	5.25 ± 0.1
*Tv*CDH	8.0 ± 0.1	4.0 ± 0.2	1.64 ± 0.01	2.31 ± 0.03
GOx	8.0 ± 0.1	220 ± 30	11.78 ± 0.02	16.9 ± 0.2

Table 1: Enzyme electrode performance for electrodes prepared at human physiological conditions by coimmobilising Os(dmobpy)$_2$4AMP or Os(dmobpy)$_2$PVI and MWCNT with either *Tv*CDH , FDH or GOx at graphite electrodes. Experiments were performed in 50 mM sodium acetate buffer at pH 4.5 containing lactose, fructose and glucose, respectivlely. The flow rate was 0.5 mL min^{-1} (n=3).

To investigate the effect of pH of immobilisation on the response, the dependence of the catalytic current density, normalised to the activity of each enzyme (U), on the pH of immobilisation was studied at 5 different pH values (pH 4.5 and 5.5 in sodium acetate buffer or pH 6.5, 7.0 and 7.5 in phosphate buffer (Figures 6, 7 and 8). Enzyme electrode response was performed in 50 mM sodium acetate buffer at pH 4.5 containing 30 mM lactose, fructose or glucose at the flow rate of 0.5 mL min^{-1}. While the application of sodium acetate as buffer may interfere with EDC/NHS coupling, reports show that it doesn't have any effect [35].

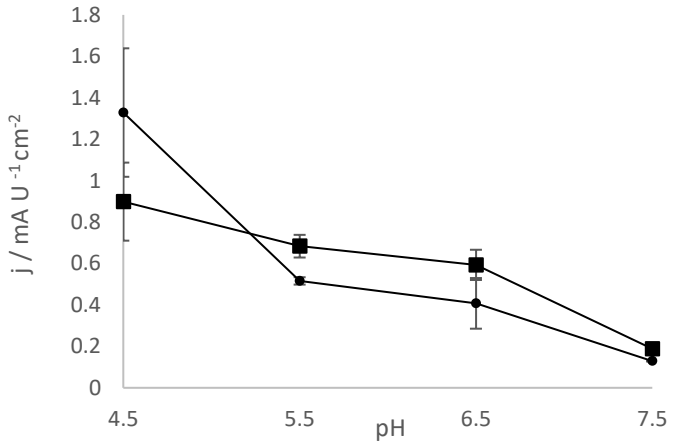

Figure 6: Dependence of catalytic current density (n=3), normalised to the activity of enzyme (U), on the pH of immobilisation. Electrodes were prepared by co-immobilising FDH, MWCNT and either $Os(dmobpy)_2$4AMP (●) or $Os(dmobpy)_2$PVI (▪). Experiments were performed in 50 mM sodium acetate buffer at pH 4.5 containing 30 mM fructose. The flow rate was 0.5 mL min^{-1}.

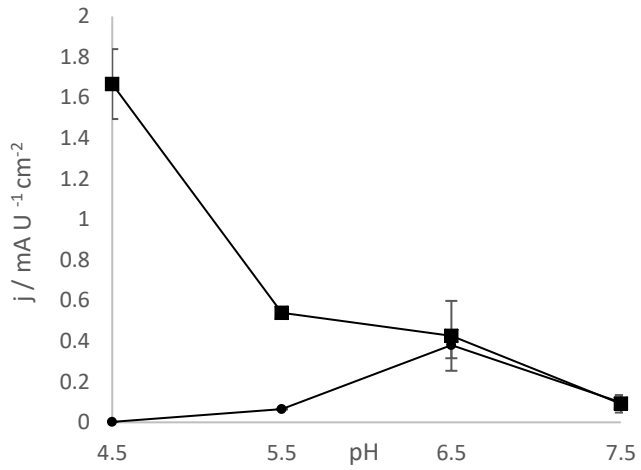

Figure 7: Dependence of catalytic current density (n=3), normalised to the activity of enzyme (U), on the pH of immobilisation. Electrodes were prepared by coimmobilising *Tv*CDH, MWCNT and either $Os(dmobpy)_2$4AMP (●) or $Os(dmobpy)_2$PVI (▪). Experiments were performed in 50 mM sodium acetate buffer at pH 4.5 containing 30 mM lactose. The flow rate was 0.5 mL min^{-1}.

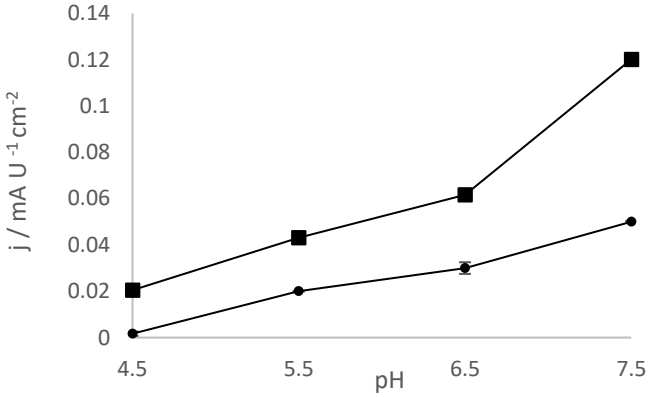

Figure 8: Dependence of catalytic current density (n=3), normalised to the activity of enzyme (U), on the pH of immobilisation. Electrodes were prepared by coimmobilising GOx, MWCNT and either $Os(dmobpy)_2$4AMP (●)or $Os(dmobpy)_2$ PVI (▪). Experiments were performed in 50 mM sodium acetate buffer at pH 4.5 containing 30 mM glucose. The flow rate was 0.5 mL min^{-1}.

With GOx, despite the acid labile nature of EDC and PEGDGE crosslinking, as the immobilization pH is increased the enzyme electrode response also increases to reach the highest levels measured at pH 7.5 for both crosslinking methodologies. It can be observed that for FDH, the maximum relative response with both cross-linking methodologies was achieved

in pH 4.5. These results coincide with the activity profile of the enzyme in solution [39]. Thus pH 4.5 and 7.5 were chosen for cross-linking of enzyme electrodesfor FDH and GOx, respectively. In case of TvCDH, an optimum bioelectrocatalytic current is achieved for an immobilisation pH 6.5 for the $Os(dmobpy)_2$4AMP enzyme electrodes coupled using EDC/NHS and pH 4.5 for the $Os(dmobpy)_2$PVI enzyme electrodes cross-linked using PEGDGE, and those values were selected for further experiments.

5.3.2 Effect of pH on response

To investigate the effect of pH further, the dependence of the catalytic current density, normalised to the added enzyme activity of corresponding enzyme, on the pH of the carrying buffer at the selected immobilisation pH was studied with the results presented in Figures 9, 10 and 11. Enzyme electrodes were prepared at the selected pH of immobilisation for each enzyme by co-immobilising $Os(dmobpy)_2$4AMP, MWCNTs, CMD and EDC/NHS as crosslinker, or $Os(dmobpy)_2$PVI, MWCNTs and PEGDGE as crosslinker for *Tv*CDH, FDH and GOx. Experiments were performed in either pH 4.5 or pH 5.5 in 50 mM sodium acetate buffer or at pH 6.5 or 7.5 in 50 mM phosphate buffer saline (0.1 M KCl).

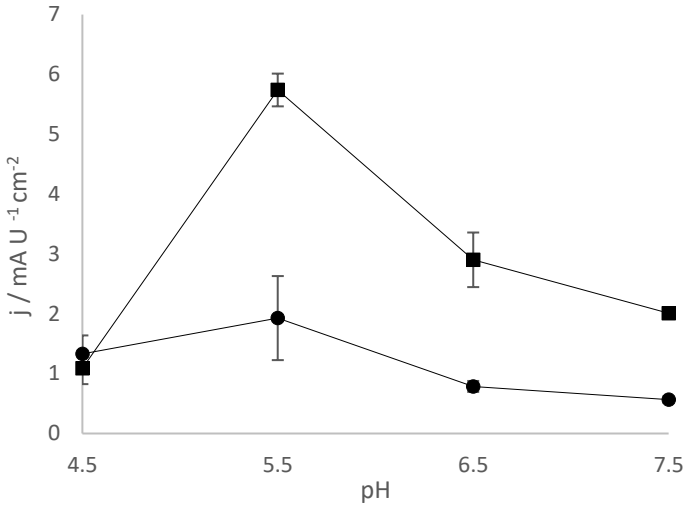

Figure 9: Dependence of catalytic current density (n=3), normalised to the activity of enzyme (U), on the pH of the carrying buffer at the optimum immobilisation pH. Electrodes were prepared by coimmobilising FDH, MWCNTs and either Os(dmobpy)$_2$4AMP (●) or Os(dmobpy)$_2$PVI (▪) at graphite electrodes. Experiments were performed in either pH 4.5 or 5.5 in 50 mM sodium acetate buffer or at pH 6.5 or 7.5 in 50 mM phosphate buffer saline. The peak current measured at 30 mM concentration of fructose. The flow rate was 0.5 mL min^{-1}.

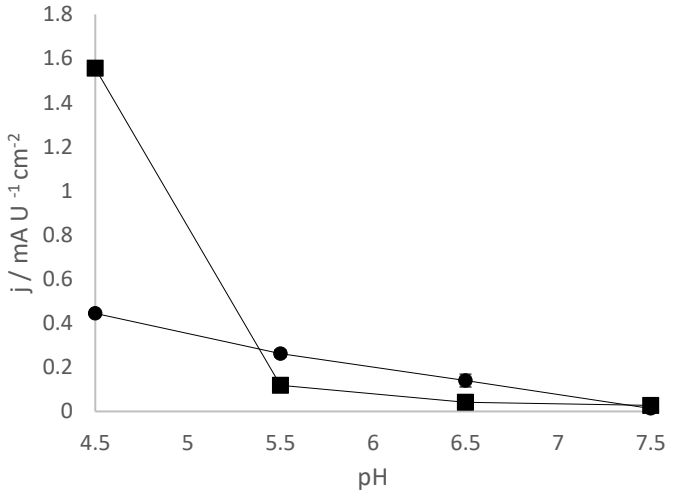

Figure 10: Dependence of catalytic current density (n=3), normalised to the activity of enzyme (U), on the pH of the carrying buffer at the optimum immobilisation pH. Electrodes were prepared by coimmobilising *Tv*CDH, MWCNTs and either Os(dmobpy)$_2$4AMP (●) or Os(dmobpy)$_2$PVI (▪) at graphite electrodes. Experiments were performed in either pH 4.5 or 5.5 in 50 mM sodium acetate buffer or at pH 6.5 or 7.5 in 50 mM phosphate buffer saline. The peak current measured at 30 mM concentration of lactose. The flow rate was 0.5 mL min^{-1}.

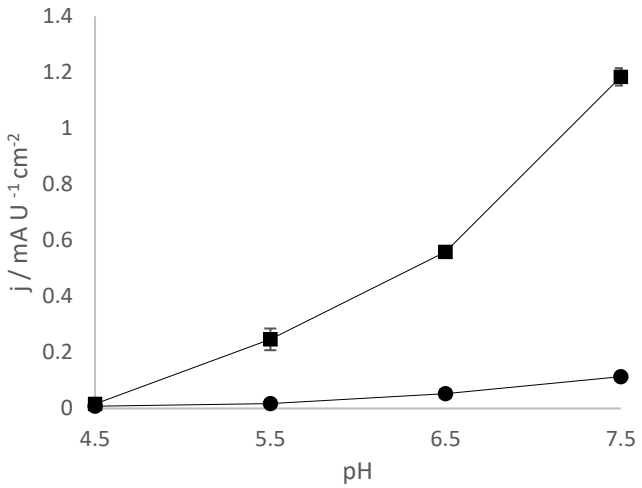

Figure 11: Dependence of catalytic current density (n=3), normalised to the activity of enzyme (U), on the pH of the carrying buffer at the optimum immobilisation pH. Electrodes were prepared by coimmobilising GOx, MWCNTs and either $Os(dmobpy)_2$4AMP (●) or $Os(dmobpy)_2$PVI (▪) at graphite electrodes. Experiments were performed in either pH 4.5 or 5.5 in 50 mM sodium acetate buffer or at pH 6.5 or 7.5 in 50 mM phosphate buffer saline. The peak current measured at 30 mM concentration of glucose. The flow rate was 0.5 mL min^{-1}.

For FDH enzyme electrodes prepared by co-immobilization of components at the selected pH, the maximum relative response was achieved in the pH range of 5.0-5.5 for both redox polymer and redox complex-based enzyme electrodes. These results coincide with the activity profile of the enzyme in solution [39]. In case of *Tv*CDH, there highest bioelectrocatalytic current is seen at around pH 4.5, whereas the catalytic current then decreases with increasing pH, and almost complete and irreversible loss of response is observed at pH 7.0. The *Tv*CDH and FDH enzymes have isoelectric points of 4.4 [48] and 5 [46, 47] respectively. In low pH conditions the enzymes are positively charged thus increasing the IET possibly by screening negative, repulsing charges present at the interface of the CYT and DH domains, decreasing the distance the electrons need to pass from the DH domain to the CYT domain, leading to an increased rate of the IET and higher current densities. With GOx enzyme electrodes the current increases as pH is altered from pH 4.5 to pH 7.5 with the highest current at pH 7.5. Higher pHs can result in the denaturation of the enzyme, as reported previously [40].

5.4 Conclusion

The catalytic current outputs for Os(dmobpy)$_2$PVI is higher compared to Os(dmobpy)$_2$4AMP when enzyme electrodes are prepared by co-immobilization of components at selected pH for enzyme electrodes based on FDH, *Tv*CDH and GOx using FIA. This can be due to the fact that osmium polymers such as Os(dmobpy)$_2$PVI are less likely to drift away into the bulk of the solution than monomeric electron acceptors such as Os(dmobpy)$_2$4AMP. Optimum immobilisation pH with Os(dmobpy)$_2$PVI is pH 4.5 for *Tv*CDH and FDH and pH 7.5 for GOx. However, with Os(dmobpy)$_2$4AMP, the selected immobilisation pH is 4.5, 6.5 and 7.5 for FDH, *Tv*CDH and GOx, respectively. Maximum catalytic current for FDH, *Tv*CDH and GOx when immobilised using the selected pH is achieved with the carrying buffer of pH 4.5, 5.5 and 7.5, respectively, and is the same regardless of selected redox mediator. The catalytic current normalised to enzyme activity for FDH and *Tv*CDH using the two redox mediators is higher compared to that of GOx, revealing the contribution of CYT domain to ET through the redox mediators. Furthermore, the findings shed further light for construction of biosensors and biofuel cell anodes, since lower potentials prevent the oxidation of interfering compounds and increase the overall obtained cell voltage on application to biofuel cells.

5.5 References

[1] M.J. Cooney, V. Svoboda, C. Lau, G. Martin, S.D. Minteer, Energy and Environmental Science, 1 (2008) 320-337.

[2] A. Heller, B. Feldman, Accounts of Chemical Research 43 (2010) 963-973.

[3] N. Mano, F. Mao, and A. Heller, Journal of the American Chemical Society, 124 (2002) 12962-12963.

[4] C. Danilowicz, E. Cort´on, F. Battaglini, and E. J. Calvo, Electrochimica Acta, 43 (1998) 3525-3531.

[5] E. J. Calvo, C. Danilowicz, and L. Diaz, Journal of the Chemical Society, Faraday Transactions, 89 (1993) 377-384.

[6] D. Leech, P. Kavanagh, and W. Schuhmann, Electrochimica Acta, 84 (2012) 223-234.

[7] R. J. Forster and J. G. Vos, Macromolecules, 23 (1990) 4372-4377.

[8] MacAodha D., Ferrer M. L., Ó Conghaile P., Kavanagh P. and Leech D. Physical Chemistry Chemical Physics 14 (2012) 14667-14672.

[9] T. O. Tran, E. G. Lammert, J. Chen, S. A. Merchant, D. B. Brunski, J. C. Keay, M. B. Johnson, D. T. Glatzhofer and D.W. Schmidtke, American Chemical Society, 27 (2011) 6201-6210.

[10] I. Osadebe and D. Leech, ChemElectroChem, 1 (2014) 1988-1993.

[11] B.A. Gregg, A. Heller, The Journal of Physical Chemistry, 95 (1991) 5970-5975.

[12] T.J. Ohara, R. Rajagopalan, A. Heller, Polymer Materials Science and Engineering, 70 (1993) 182-183.

[13] S. Lofas, B. Johnsson, Journal of the Chemical Society, Chemical Communications, 9 (1990) 1526-1528.

[14] M.E. Fischer, N.J. Mol, M.J.E. Fischer (Eds.), Humana Press, 627 (2010) 55-73.

[15] T. Lai, Q. Hou, H. Yang, X. Luo, M. Xi, Acta Biochimica et Biophysica Sinica, 42 (2010) 787-792.

[16] S. Nandini, S. Nalini, J. Sanetuntikul, S. Shanmugam, P. Niranjana, J.S. Melo, G.S. Suresh, Analyst, 139 (2014) 5800-5812.

[17] M. Moyo, J.O. Okonkwo and N.M. Agyei, Sensors, 12 (2012) 923-953.

[18] F. Daigle, D. Leech, Analytical Chemistry, 69 (1997) 4108-4112.

[19] R. Ludwig, W. Harreither, F. Tasca, L. Gorton, ChemPhysChem, 11 (2010) 2674-2697.

[20] F.F. Morpeth, Biochemical Journal, 228 (1985) 557.

[21] G. Henriksson, G. Johansson, G. Pettersson, Biochimica et Biophysica Acta 1144 (1993) 184-190.

[22] G. Henriksson, G. Pettersson, G. Johansson, A. Ruiz, E. Uzcategui, European Journal of Biochemistry 196 (1991) 101-6.

[23] R. J. Forster and J. G. Vos, Macromolecules, 23 (1990) 4372-4377.

[24] E. M. Kober, J. V. Caspar, B. P. Sullivan, and T. J. Meyer, Inorganic Chemistry, 27 (1988).

[25] A. B. P. Lever, Inorganic Chemistry, 29 (1990) 1271-1285.

[26] E. M. Kober, J. V. Caspar, B. P. Sullivan, T. J. Meyer, Inorganic Chemistry, 27 (1988) 4587-4598

[27] R. J. Forster, J. G. Vos, Macromolecules, 23 (1990) 4372-4377

[28] R. Appelqvist, G. Marko-Varga, L.Gorton, A. Torstensson, G. Johansson, Analytica Chimica Acta, 169 (1985) 237-247.

[29] R. Kumar, D. Leech, Bioelectrochemistry 106 (2015) 41-46

[30] I. Osadebe, D. Leech, ChemElectroChem, 1 (2014) 1988-1993.

[31] S. Chaikin, W. J. Brown, American Chemical Society, 71 (1949) 122-125.

[32] P. Gacesa, W. J. Whish, Biochemical Journal, 175 (1978) 349-352.

[33] W. Harreither, V. Coman, R. Ludwig, D. Haltrich, L. Gorton, Electroanalysis, 19 (2007) 172-180.

[34] L. Stoica, T. Ruzgas, R. Ludwig, D. Haltrich, L. Gorton, Langmuir, 22 (2006) 10801-6.

[35] N. Nakajima, Y. I. Bioconjugate, Chem journal, 6 (1995) 123-130

[36] Z. Grabarek, and J. Gergely, Analytical Biochemistry, 185 (1990) 131-5.

[37] M. B. Hallberg, G.Henriksson, G. Pettersson, C. Divne, Journal of Molecular Biology, 315 (2002) 421-434.

[38] B. M. Hallberg, G. Henriksson, G. Pettersson, A.Vasella, C. Divne, The Journal of Biological Chemistry, 278 (2003) 7160-7166.

[39] U.B. Trivedi, D. Lakshminarayana, I.L. Kothari, P.B. Patel, C.J. Panchal, Sensors and Actuators B 136 (2009) 45-51.

[40] M. A. Rahmana, M. Wonb, Y.B. Shim, Biosensors and Bioelectronics (2004).

[41] R. Ludwig, W. Harreither, F. Tasca, L. Gorton, ChemPhysChem, 11 (2010) 2674-2697.

[42] R. Ludwig, R. Ortiz, C. Schulz, W. Harreither, C. Sygmund, L. Gorton, Analytical and Bioanalytical Chemistry, 405(2013) 3637-3658.

[43] M. Zamocky, R. Ludwig, C. Peterbauer, B. M. Hallberg, C. Divne, P. Nicholls, D. Haltrich, Current Protein & Peptide Science, 7 (2006) 255-280.

[44] G. Henriksson, G. Johansson, G. J. Pettersson, Biotechnology Journal, 78 (2000) 93-113.

[45] P. A. Paredes, J. Parellada, V. M. Fernandez, I. Katakis & E. Dominguez, Biocensors and Bioelectronics, 12 (1997) 1233-1243.

[46] M.Ameyama, E.Shinagawa, K.Matsushita and O.Adachi, Journal of Bacteriologyn, 145 (1981).

[47] M.Ameyama; Methods in Enzymology, 89 (1982) 20.

[48] L. Stoica, T. Ruzgas, R. Ludwig, D. Haltrich, and L. Gorton, American Chemical Society, 22 (2006), 10801–10806.

Chapter 6

Development of an *in vitro* model for studying the effect of crosslinking on anti-calcification of bovine pericardium

6.1 Introduction

Despite the fact that mechanical heart valves offer lifelong durability they also commit patients to anti-coagulation treatment for the rest of their life [14]. On the other hand, bioprosthetic valves with glutaraldehyde (Glut) treatment have superior hemodynamic performance to mechanical heart valves. However, early onset calcification as the primary cause of biomaterial breakdown, limits the use of such valves to implantations in the elderly only. The life span of bioprosthetic valve implants could be significantly increased by inhibiting valve calcification. Thus, different approaches have been taken towards reducing the calcification of bioprosthetic heart valves. In an attempt to study the inhibition of this calcification, an *in vitro* method was used for the comparative testing of different anti-calcification treatments. Calcification is quantified by measurements of the calcium content in solution at discrete time periods. The scope of the present work is to study the process of calcific deposit formation in bovine precardium tissues using the constant supersaturation method and comparing the different anti-calcification treatments. Therefore the main objective of this study is allowing the differentiation of calcification rates where the samples were subjected to different tissue treatments. The present study compared control tissue response to that treated with Glut treatments and that treated with an epoxy functionalised polymers as crosslinking agents.

6.2 Experimental

6.2.1 Materials

The study was performed in co-operation between the National University of Ireland Galway and Boston Scientific company in Galway, Ireland. All chemicals were obtained from Sigma Aldrich unless otherwise stated. A double wall Quickfit Pyrex jacketed beaker with the capacity of 1 liter as reactor with frames to support tissue, stirring plate with magnet bar and a hot water bath and a pump to maintain the temperature was used (Figure 1). Thermofisher calcium ion-selective electrode (ISE) was used to measure the concentration of the calcium ion in solutions and a VWR pH meter, with accuracy ±0.001 to control pH. Fresh bovine pericardium were shipped from New Zealand and rinsed extensively in sterile saline solution on arrival and then treated with either Glut, Glut + T-Guard™ (Boston Scientific's anti-calcification treatment). In addition a commercial polyethylene glycol diglycidyl ether (PEGDGE) and a proprietary PEG epoxy polymer (PEP developed and kindly donated by W. Wang University College Dublin (UCD), Dublin, Ireland) were used as epoxy crosslinker for comparison. PEGDGE was used previously in chapters 4 and 5 as crosslinker for enzyme immobilisation to create a redox hydrogel to entrap enzyme and mediators in films.

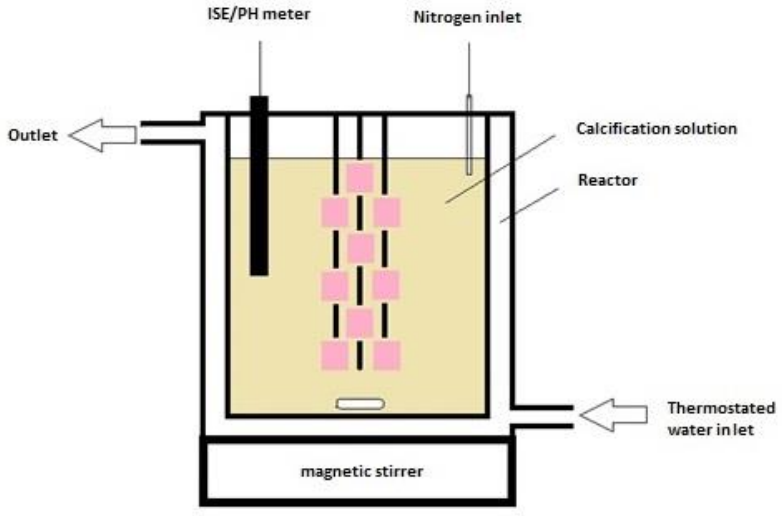

Figure 1. Schematic of the apparatus used for the development of calcific deposits *in vitro*. The vertical black lines represent frames and the pink squares the 1 cm^2 valve tissues attached to the frames.

6.2.2 Bovine pericardium treatment

As reported on previously, cross-linking of dermal sheep collagen tissue using 1,4-butanediol diglycidyl ether (BDDGE) [16] at two different pH ranges of 4-6 and 8-10 has been evaluated. During the cross-linking process under basic conditions (pH 8-10), the epoxide groups of BDDGE react with amine groups while in the acidic conditions (pH 4-6) cross-linking will mainly involve carboxylic acid groups. Cross-linking at pH 9.0 resulted in a material with a high shrinkage (denaturation) temperature (T_s) of 69°C and a high resistance towards enzyme degradation however reaction of the tissue with BDDGE at pH 4.5 yielded a material with T_s of 64°C and a lower stability towards enzymatic degradation. Thus, Cross-linking of tissue at pH 9.0 resulted in materials with a high degree of cross linking and excellent enzymatic resistance, in addition higher pH values removes cellular contents and has the potential of killing prions (viruses) [16-18]. Consequently, in this study PEGDGE-treated tissues were prepared by cross-linking the tissues with PEGDGE at pH 9.0 with the concentration of 2% at room temperature for 14 d. The PEP-treated tissues were prepared in higher and lower pH conditions than 9.0 for comparison: treatment at pH 10.5, concentration 2% (PEP 2%) or treatment at pH 7.0, concentration 14% (PEP 14%) for 28 d. The higher concentrations of PEP may damage the collagen to some extent that was not observed in this study. The Glut-treated tissues were prepared with 0.625% V/V Glut in 0.15 M PBS buffer at pH 7.4 for 1 h at room temperature according to the literature [16]. The Glut + T-Guard™-treated tissues were prepared by exposure of Glut-treated tissues with T-Guard™ anti-calcification solution. As illustrated in Figure 1, the samples were cut in 1 cm^2 dimensions and sewn to the frames. In an attempt to assure reproducibility, all the samples were taken from the same bovine pericardium and 6 of each were tested to ensure repeatability.

Cross-linker	Conc. (m/v)	Temperature	Solvent	Functional groups
Glutaraldehyde (Glut)	0.625%	22°C	pH 7.4 buffer	Aldehyde in excess
PEG diglycidyl ether	2%	22°C	pH 9 buffer	Epoxy
PEG epoxy polymer (PEP 2%)	2%	40°C	pH 10.5 buffer	Epoxy
PEG epoxy polymer (PEP 14%)	14%	40°C	pH 7 buffer	Epoxy

Table 1. The crosslinking groups and conditions of the chemicals for treatment of the bovine precardium tissues.

6.2.3 Shrinkage Temperature

Shrinkage temperature was assessed using a differential scanning calorimeter (DSC, Q20, TA Instruments). To estimate this 3 mm tissue discs were rinsed in saline, weighed and sealed in Tzero hermetic aluminium pans and scanned from 30 to 100°C at 5°C per minute in the DSC. Decomposition temperature was determined as the shrinkage temperature value. Analyses were performed in replicates of three.

6.2.4 Enzymatic degradation

To estimate enzymatic degradation, 4 mm tissue discs were cut, rinsed in saline and placed in Protein LoBind eppendorf tubes with 500 Units collagenase type I in TES-CaCl2 (0.05 M TES, 5 mM CaCl2) buffer solution. Control samples for each crosslinking groups were prepared by placing the tissue in TES-CaCl2 buffer only. All samples were incubated at 37°C for 3 hours and then sealed in aluminium hermetic pans, loaded onto the DSC and scanned from 30 to 100°C at 5°C per minute. The energy required to denature the collagen (Total energy J/g) was recorded for each sample and the difference between test (exposed to collagenase) and control (TES-CaCl2 buffer only) samples was calculated.

6.2.5 Calcification studies

To set up the experiments for this study, a thermostated double-walled water-jacketed Pyrex glass reactor equipped with magnet bar and a frame as sample holder was filled with the Golomb and Wagner's calcification metastable solution [6]: 3.87 mM $CaCl_2$, 2.32 mM K_2HPO_4, 5.72 g of Trizma HCl and 1.66 g of Trizma base dissolved in one litre of de-ionised water. Blending Trizma Base and Trizma HCI produces any desired pH between 7 and 9, with a reasonable buffering capacity at the desired temperature. In general, as the solution increases in temperature from 25°C to 37°C, the pH decreases an average of 0.025 pH units per °C: by weighing the correct ratio of trizma base and acid the predicted pH was achieved in the desired temperature with an accuracy of ± 0.05. The temperature was maintained at 37°C using a water bath and a pump. The pericardium treated tissue samples were mounted on glass frames and submerged into the calcification solution for a period of 2 weeks and the solution was changed every 48 hrs during the period of the experiment to maintain the electrolyte concentrations at a pH value of 7.4 and physiological temperature of 37 °C. Half of the samples were removed after the 1st week for analysis. Upon completion of the test, samples were rinsed with de-ionised water to remove excess solution and loosely attached deposits and the level of calcification deposits on the surface of the tissue evaluated. The calcified samples were analysed morphologically and chemically by the identification of the calcium phosphate salts deposited. Light microscopy with staining and Scanning Electron Microscopy coupled with Energy Dispersive X-ray (SEM/EDX) was used to analyse the crystals.

6.2.6 Calcium staining

Calcium forms a red chelation complex with alizarin red stain as (figure 6) and the staining sensitivity depends on both the concentration of the dye and the pH of the solution. As was reported by Shoji [15], the best results were obtained with an alizarin red S concentration of 1.5–3.0% and optimal pH of the solution of 4.0–6.0 for HA. The tissues with calcific deposits were embedded in parafin blocks for routine histological techniques. Sections of the tissues were cut with microtome (longitudinal sectioning) and were subjected to 95% alcohol and slides were then thoroughly air dried for the next part. Sections were placed in a Coplin jar filled with

a solution of 1.5 % aqueous alizarin red S at pH 4.2 with 10% ammonium hydroxide for staining for 5 minutes and rinsed quickly in distilled water. A 0.05% fast green in 0.2% acetic acid solution was added to the sections as counterstain for 1 minute before samples were rinsed in three changes of distilled water. Sections were finally dehydrated, cleared, and mounted in synthetic resin and examined under an optical microscope. Staining and optical microscopy was conducted with assistance from Dr. Mark Canney and Dr. Kerry Thompson at the National University of Ireland Galway.

6.2.7 Scanning Electron microscopy & Energy-Dispersive X-Ray spectroscopy

Scanning electron microscopy (SEM) generates images by scanning a focused electron beam across the surface of a sample. In conjunction with other methods, SEM has been frequently used to characterise the morphology and distribution of crystal deposits as shown in Figure 7. Tissue samples were treated with 2.5% glutaraldehyde followed by PBS washes and a series of ethanol dilutions washes (50%, 75%, 80%, 90% and 100%) for 5 minutes each at 4°C. Finally, the tissue were treated with hexamethyldisilizane for 30 minutes and then allowed to air dry overnight. Samples were then gold coated and examined using a Hitachi S-4700 scanning electron microscope with amplification ranging from 30X to 500,000X.

6.2.8 Energy-dispersive X-ray spectroscopy

Energy Dispersive X-ray Spectroscopy (EDX) is an analytical capability that can be coupled with several applications including SEM, Transmission Electron Microscopy (TEM) and Scanning Transmission Electron Microscopy (STEM). EDX, when combined with these imaging tools, can provide elemental analysis or chemical characterisation on areas as small as nanometres in diameter.

6.3 Results and discussion

6.3.1 Crosslinking degree - shrinkage temperature and resistance to enzymatic degradation

Thermal shrinkage temperatures were obtained using differential scanning calorimetry and can be used as an index of crosslinking. This study compares PEP crosslinking of bovine pericardium with tissue treated with either Glut or PEGDGE crosslinking, and a comparison to untreated (raw) tissue as a control. Figure 2 shows the typical thermal shrinkage temperature curve obtained for PEP14%. The PEP and PEGDGE treated tissue showed significantly higher shrinkage temperature than raw bovine pericardium and reached approximately 74-75°C (Figure 3), although each of these treatments resulted in a lower shrinkage temperature than the Glut-treated tissue. In addition to the shrinkage temperature data, the resistance to enzymatic degradation results confirms the crosslinking effect of PEP and PEGDGE. To confirm cross-linking, tissue treated with the different cross-linking agents was incubated with collagenase (test samples) or with buffer only (control samples). The objective of this test is to verify if there is a significant difference in the total energy required to denature 1g of collagen between test and control samples. If the material is crosslinked, there should be no significant difference between exposing it and not exposing it to collagenase. As seen in Figure 4, all treated tissues showed no significant difference between test and control, whereas the raw untreated tissue showed significant difference. Note that the *in vitro* anti calcification model, tissue cross-linking and characterisation were conducted in collaboration with Lígia Bré and Dr. Ray McCarthy at Boston Scientific Galway.

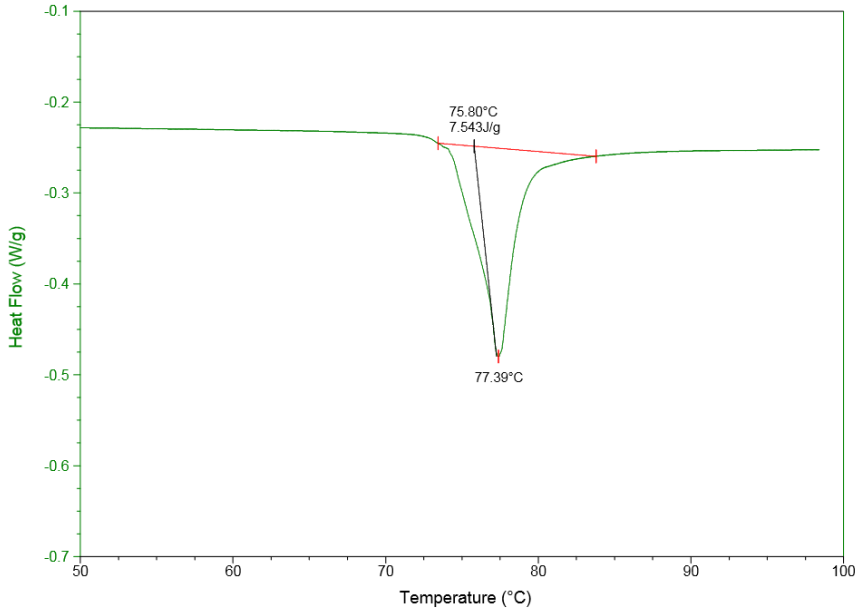

Figure 2: Thermal shrinkage temperature curve obtained for PEP14% treated tissues using differential scanning calorimetry.

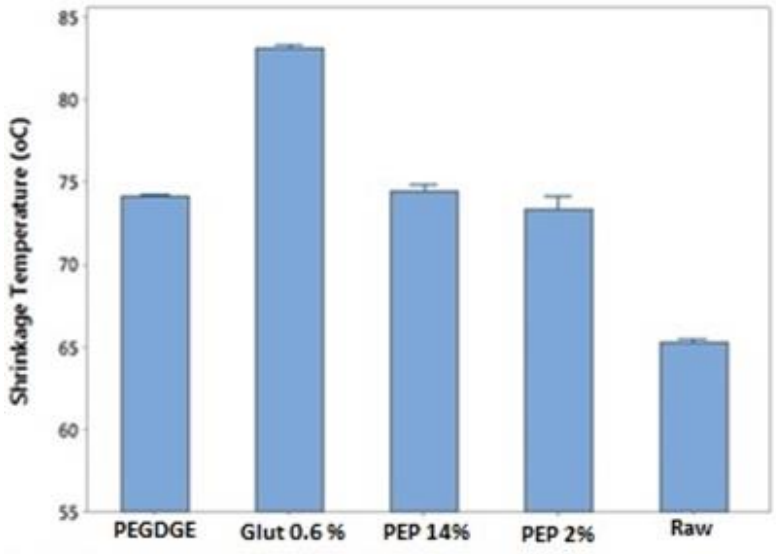

Figure 3: Thermal shrinkage temperatures obtained using differential scanning calorimetry for treated tissues.

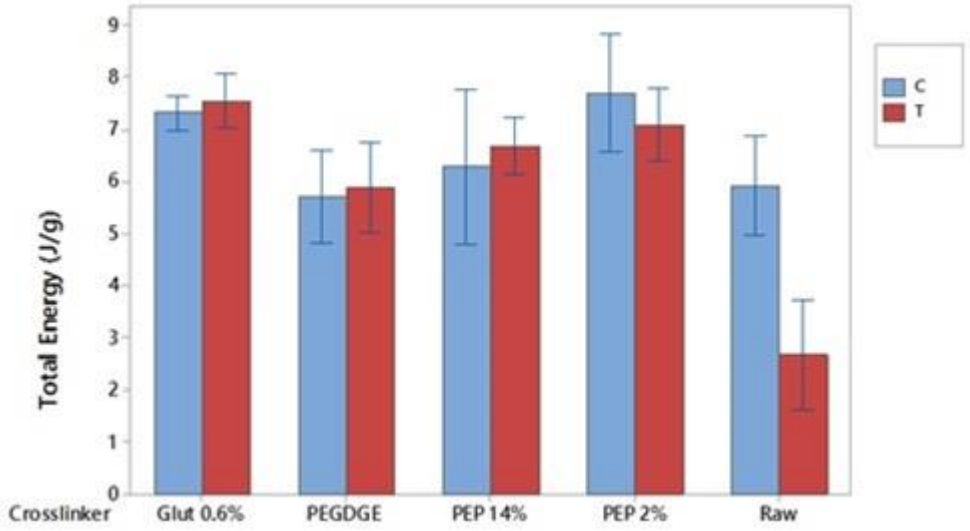

Figure 4: Total energy required to denature the collagen of tissue treated with different cross-linking agents incubated with collagenase (test samples or T) or with buffer only (control samples or C).

6.3.2 *In vitro* calcification

In this study Golomb and Wagner's calcification solution compound was used, while Starcher and Urry's compound was previously used by Deiwick *et al.* [6] for their in-vitro calcification studies of bioprostheses. The Golomb and Wagner's calcification metastable solution yields a ratio of calcium to phosphate (Ca/PO_4) of 1.67 while the Starcher and Urry's solution consists of 20 mM barbital buffer, pH 7.41, containing 55 mM KCl, 1.25 mM KH_2PO_4 and 1.5 mM $CaCl_2$ yielding a Ca/PO_4 ratio of 1.2 [7]. Comparison of the Ca/PO_4 content for these two compounds shows that Golomb and Wagner's compound is more physiologically representative of hydroxyapatite and is more aggressive than its counterpart (Ca/PO_4 molar ratio of 1.5 indicates the presence of hydroxyapatite). Hydroxyapatite (HA) is a naturally occurring mineral form of calcium apatite with the formula $Ca5\ (PO4)_3(OH)$.

$$CaCl_2 + K_2HPO_4 \rightarrow CaHPO_4 + KCl$$

$$5CaHPO_4 + H_2O \rightarrow Ca_5(PO_4)_3OH + 2H_3PO_4$$

According to the equation above calcium monohydrogen phosphate hydrolyses slowly to the thermodynamically more stable HA. Phosphoric acid is formed as a by-product: Tris buffer maintains the pH of the buffer at physiological condition (pH 7.4). In the study the temperature is maintained at 37 °C using a water bath and a pump. The solubility of hydroxyapatite has a negative temperature coefficient and precipitates more at higher temperatures ie. at 37°C [13]. The pericardium treated tissues were mounted on glass frames and submerged into calcification solution for a period of 2 weeks and the solution was changed every 48 hrs during the period of the experiment to maintain the supersaturation at a pH value of 7.4 and physiological temperature of 37 °C. After the first week, half of the samples of all treatment groups were taken out of the calcification solution to undergo analysis of the calcified deposits while the rest of the samples were subjected to an additional 1 week of calcification. A calcium ion selective electrode (ISE) was used to measure the calcium content of calcification solution in order to estimate the calcium consumption rate. The measurements of the calcium concentration analysis were performed from fresh and used solutions every 48 hrs. The consumption rate of the calcium decreased slightly with the time showing higher level of calcium consumption on the first days indicative of the mineral deposits formation on the samples. In addition when half of the samples were removed for analysis, the calcium consumption dropped noticeably (Figure 5).

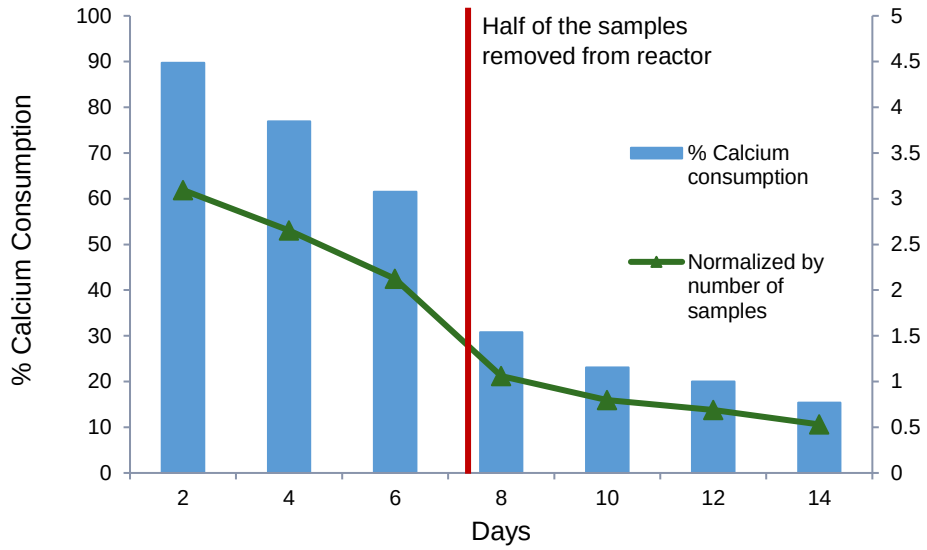

Figure 5: Calcium concentration analysis performed by calcium ISE from fresh and used calcification solutions every 48 h.

6.3.3 Statistical evaluation

For the statistical analysis of the calcification results of the treated valves, Fisher's test was used. Statistical significance defined as a p value was less than 0.001 for the calcium deposits.

6.3.4 Histological results

As described in section 6.2.6, tissues with calcific deposits form a red chelation complex with alizarin red stain for microscopic examination. The optical microscopy of samples revealed extensive crystalline calcific deposits occurred on the tissues after the first week which was far denser after two weeks of the experiment visualised as dark red with alizarin red stain. From the results in Figure 6 the PEP-treated tissues show the least calcification. As expected, calcium deposition initiated on the surface of the tissue and with increased time (2 weeks) nodules can be observed in the center of the tissue sample suggesting that the calcium and phosphate ions are penetrating the tissue layers over time. In the specific case of PEP 14%, it is possible to observe that, after two weeks of exposure to calcification solution, there is no evidence of calcium penetrating the tissue. Moreover, when compared to the other treated tissue at 2 weeks,

there are virtually no red complexes formed on the tissue surface either. For each sample, the predominance of red stain on one side of the tissue in comparison with the other is relative to the rough and smooth side of the bovine pericardium tissue. Bovine pericardium, also known as pericardial sac, is formed by two layers: the outermost fibrous pericardium and the inner serous pericardium which correspond to the rough and smooth side, respectively. As the name indicates, the rough side has a high content of fibrous material that can also be partially loose after the treatment and regular handling, and this is the preferred site for calcium and phosphate deposition. However, as staining is only a qualitative method, further analysis was performed using SEM/EDX.

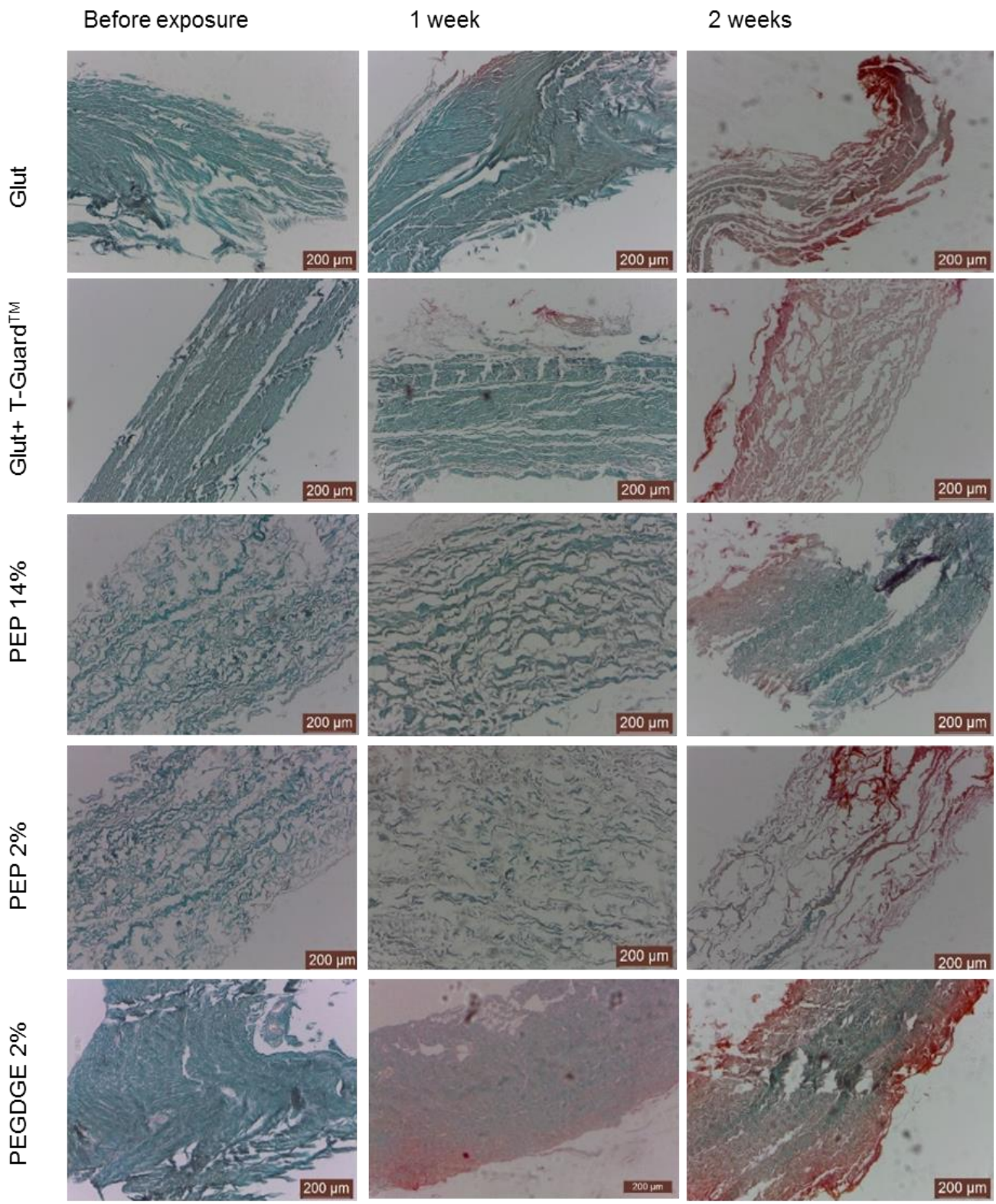

Figure 6: The microscopic examination of calcific deposits on treated tissues visualised as dark red with alizarin red stain obtained for two different time points.

6.3.5 SEM/EDX

Parallel sections from the same block of the tissue samples were examined by SEM. In SEM, the accelerated electrons with significant amounts of kinetic energy interact with the solid samples and the energy is dissipated as a variety of signals. These signals include secondary electrons (that produce SEM images), backscattered electrons (BSE), diffracted backscattered electrons (EBSD that are used to determine crystal structures and orientations of minerals), photons (characteristic X-rays that are used for elemental analysis), visible light and heat. The most common SEM mode is detection of secondary electrons. By scanning the sample and collecting the secondary electrons with a biased detector, an image displaying the topography of the surface is created. The tissues were placed on aluminium sample holders for SEM. The samples were dehydrated in graded aqueous ethanol solutions, sputtered with gold and examined with scanning electron microscope. Examination of the deposits revealed that the extension of calcific deposits increased with time during the study (Figure 7). At week one, calcium agglomerates that cover the complete surface area can be observed for both Glut and PEGDGE 2%-treated tissue. The PEP 2%-treated tissue shows areas with agglomerates of defined calcium nodules covering portions of the smooth surface. The PEP 14% and Glut + T-Guard™-treated tissues revealed a mixture of calcific nodules and non-calcified fibrous material, with mineralisation covering a smaller area of PEP 14%-treated tissue. After two weeks of exposure to the calcification solution tissue samples from all groups were fully covered in a dense layer of calcium deposits that appears similar to scaling. Experiments in this part were conducted with assistance from Dr. Eadaoin Timmins at the National University of Ireland Galway.

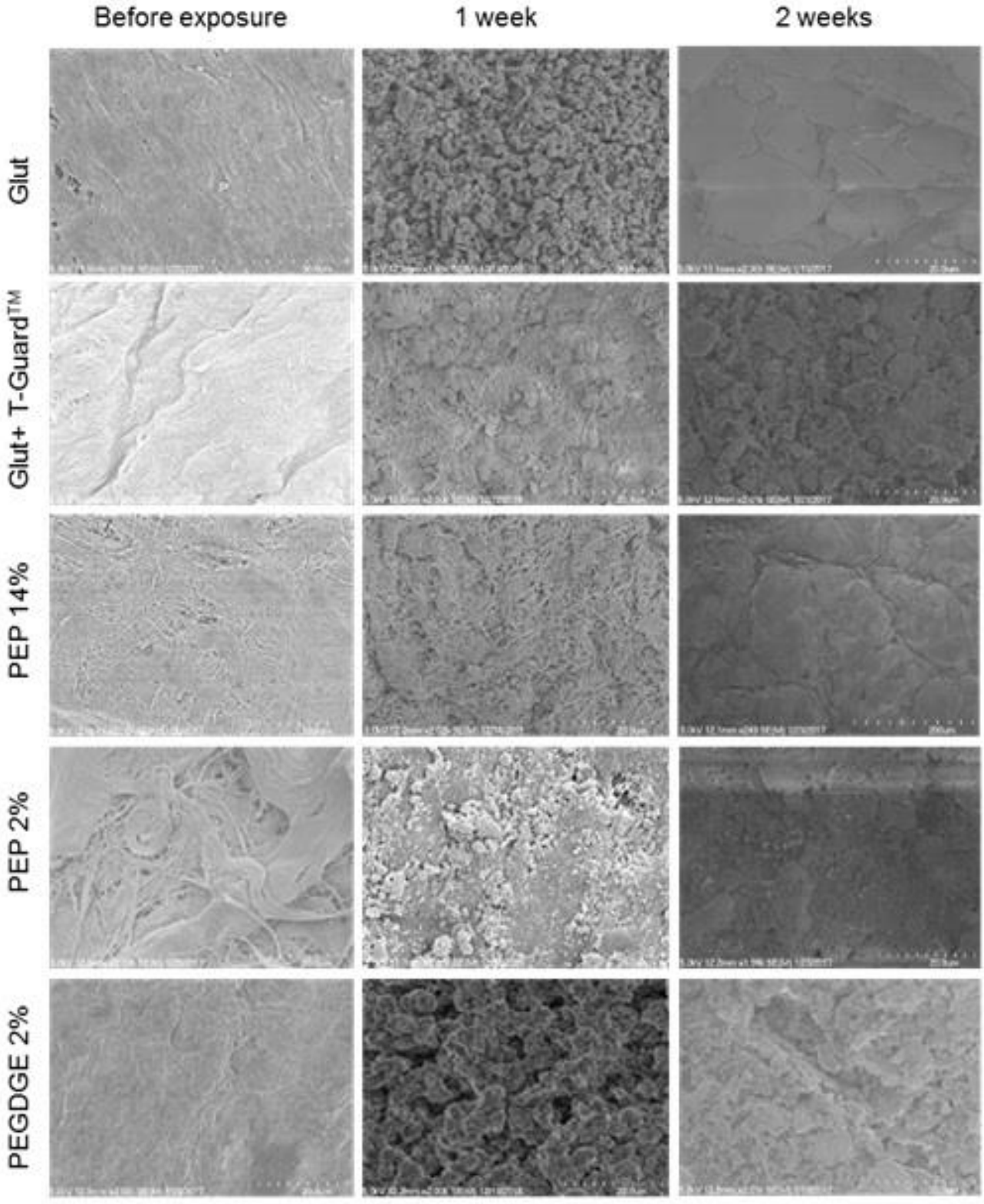

Figure 7: SEM images (1000x magnification) of treated tissues demonstrate the extension of calcific deposits obtained for two different time points.

The SEM-EDX analysis identified the deposits as calcium phosphate salts. The impact of the electron beam on the sample produces x-rays that are characteristic of the elements present on the sample. Its characterisation capabilities are due to the fundamental principle that each element has a unique atomic structure allowing unique set of peaks on its X-ray emission spectrum [9]. At rest, an atom within the sample contains unexcited electrons. When the beam interacts with the sample, it excites an electron in an inner shell, ejecting it from the shell while creating an electron hole where the electron was. Then an electron from an outer shell with higher energy fills the hole, and the difference in energy is released in the form of an X-ray. As the energies of the X-rays are characteristic of the difference in energy between the two shells and of the atomic structure of the emitting element, EDX allows the elemental composition of the specimen to be measured [10]. Analysis of the samples showed that calcium phosphate deposits were present at various, random locations of the tissues examined. In addition the SEM/EDX provided a more clear evidence of calcification extension for different treatments as compared to staining analysis. Figures 8 and 9 show the calcification deposit values obtained for two different time points, each bar representative of 20 data points indicate clearly an increase in the mineral quantity (weight %) with time. While all three agents namely Glut + T-Guard™, PEP 14% and PEP 2% inhibited calcification, PEP 14% exhibited the least amount of calcium crystallisation. Statistical analysis with one-way ANOVA and Fisher's test of calcium at one week showed that apart from glut treated and raw samples, all groups were significantly different at 1 week. From lowest to highest – PEP 14%, PEP 2%, Glut + T-Guard, Raw and Glut, and finally PEGDGE. Phosphorous showed the same group order but fewer significant differences with both glut and raw, and glut and PEGDGE not being significantly different.

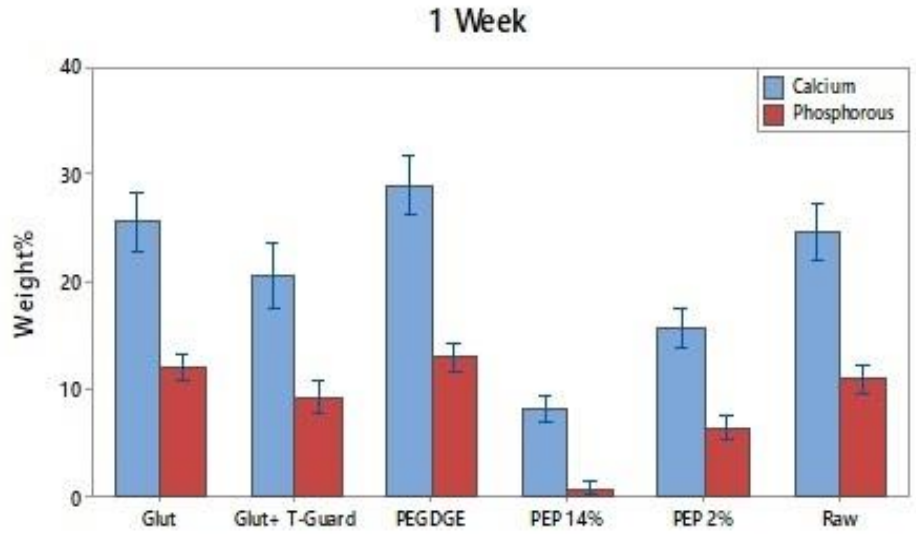

Figure 8: Measurement of the elemental composition values of the calcific deposits obtained After 1 week by SEM/EDX, each bar representative of 20 data points.

In comparison to week 1, smaller differences were observed for the statistical analysis of calcium deposits at two weeks. However the trend remained the same as after 1 week with lowest to highest – PEP 14%, PEP 2%, Glut + T-Guard, Raw and Glut, and finally PEGDGE. Statistical analysis of phosphorous reveals that only PEP 14% is significantly lower from all other treatments. For both time points, the calcium content was respectively 70% and 40% lower for PEP 14% in comparison with Glut. The abundance of calcium deposits in the Glut-treated samples and the lower amounts of deposits with PEP-treated tissues validates the results observed by light microscopy. In the present study, the commercial crosslinker (PEGDGE)-treated tissues had similar levels of calcification to those of glutaraldehyde. This can be associated to its low solubility as compared to PEP and thus low tissue penetration. While the three agents, namely Glut + T-Guard™, PEP 2% and PEP 14% revealed a lower calcification rate compared to the glut control, none was able to totally prevent the process from occurring.

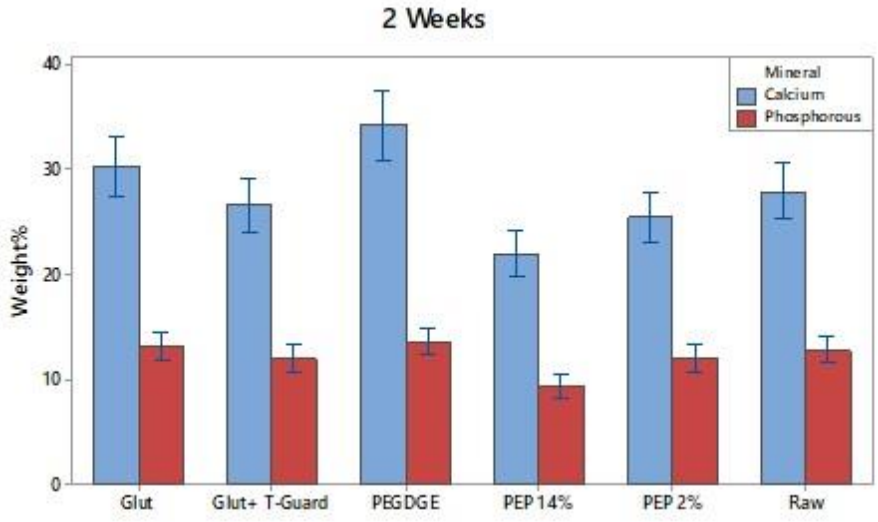

Figure 9: Measurement of the elemental composition values of the calcific deposits obtained After 2 weeks by SEM/EDX, each bar representative of 20 data points.

Focusing on the mineralisation progression between one week and two weeks', it is possible to observe that the calcium deposition increased for all groups by the end of 2nd week and that a higher amount of calcium phosphate was deposited on the tissue from the groups with lower calcium content at week 1. While the PEP 14%, PEP 2% and Glut+ T-Guard™ - treated pericardium tissues showed a calcium content increase of 63%, 38% and 23 %, PEGDGE, Glut and raw tissues suffered an increase of 16%, 15% and 11% respectively (Figure 10). In addition the data shows that the phosphorous deposition increased for all groups and it appears to reach a plateau by the end of 2nd week, with all groups having similar levels of phosphorous except for PEG epoxy 14% (PEP 14%). While the PEP 14%, PEP 2% and Glut+ T-Guard™- treated pericardium tissues showed a phosphorous content increase of 47%, 91% and 23 %, it was 4%, 9% and 14% for PEGDGE, Glut and raw tissues respectively (Figure 11). These trends, for both calcium and phosphorous, suggest that at the end of the second week, there is a saturation of the tissue samples.

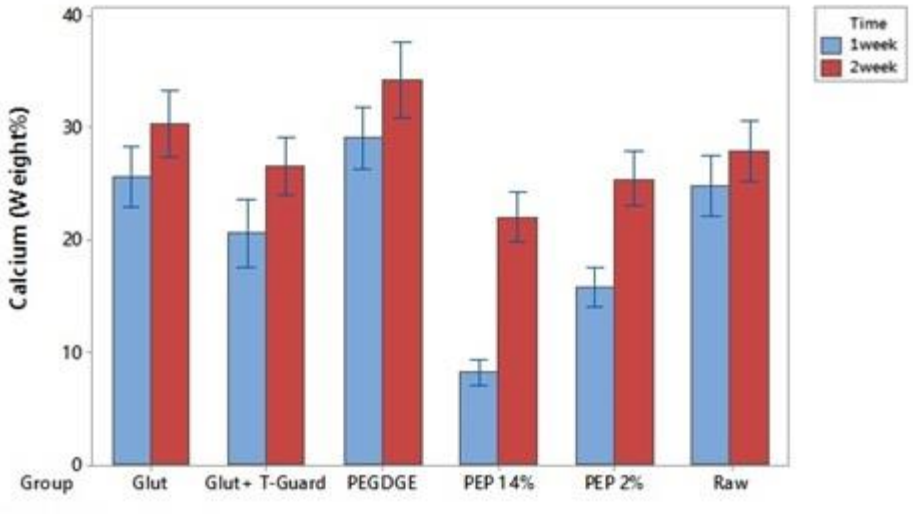

Figure 10: Comparison of the calcific deposits obtained after 1 and 2 weeks by SEM/EDX, each bar representative of 20 data points.

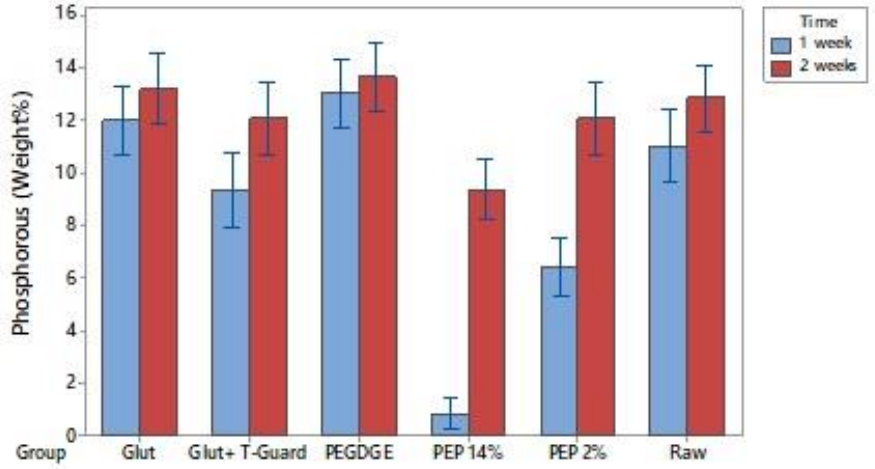

Figure 11: Comparison of the phosphorous deposits obtained after 1 and 2 weeks by SEM/EDX, each bar representative of 20 data points.

These studies demonstrate that the application of a novel polyepoxy crosslinker, PEG epoxy polymer (PEP) has promising advantages compared to Glut crosslinking for bioprosthetic heart valves. The broader reactivity of epoxides such as PEP than Glut for preparing bioprosthetic

leaflet materials in terms of amino acid reactions has been reported previously that results in significantly greater collagenase resistance. Glut is the predominant chemical agent for the treatment of collagenous tissues, rendering a higher crosslinking degree than alternative treatments. The main reaction of collagen crosslinking is the one occurring between the aldehydes in GA and the amines in the hydroxylysine residues of the collagen molecules. Crosslinking by Glut shows adequate structural properties with good hemodynamic performance and low antigenicity however calcification is a major obstacle that prevents its use in the patients younger than 65 year old. For comparison, Glut + T-Guard™ anticalcification-treated tissues were prepared by exposure of Glut-treated tissues with T-Guard™ anticalcification solution. Treatment with T-Guard™ removes cellular debris that would otherwise act as nucleation sites for calcium to deposit. Polyepoxide crosslinking as an alternative to Glut treatment has been hypothesised to inhibit mineralisation, perhaps because of novel molecular rearrangements [1-5] and coating effect on the tissue surface. Epoxy-amine reaction forms an irreversible bond however with Glut crosslinking, aldehyde-amine can form both reversible and irreversible bonds in aqueous conditions, depending on pH, concentration and complexes formed. Reversible bonds are not only problematic on the possibility of aldehyde leaching but also because carbon can coordinate with calcium ions and form nucleation sites. Epoxy crosslinking compared to Glut can involve reactions with not only amino groups, such as the hydroxylysine amino side chains in collagen, but also with the sulfur-containing amino acids such as cysteine and methionine [11]. Thus, the crosslinked connective tissue matrix resulting from PEP-amino acid reactions will have a far more complex structure involving collagen-collagen and collagen protein bonds that would also hypothetically reduce collagenase digestibility. In addition, polymer technology can contribute to the bio prosthetic heart valve durability. Polymeric cross linkers can not only replace Glut and mask antigens but also provide higher tissue flexibility which reduces mechanical stress. As reported in this study, PEP crosslinking promotes resistance to intrinsic bioprosthetic calcification, which is the most common clinical failure mode of bioprosthetic heart valves. Furthermore, the next step is to test for *in-vivo* efficacy for those treatements that show promise over the currently accepted treatment.

6.4 Conclusion

Calcification of bioprosthetic implants is a clinically important pathologic process limiting the anticipated durability and, hence, use of tissue-derived valves. A key common feature is the involvement of devitalised cells and cellular debris. As a method to investigate calcification process, *in vitro* calcification provides valuable information on the calcification potential of different materials in the presence of established controls. However, it has its own limitations including the fact that the process of valve calcification might be different in the individual patient. Glut treatment does not adequately protect vascular tissues from calcification.

6.5 References

[1] H.W. Sung, S.H. Shen, R. Tu, American Society for Artificial Internal Organs, 39 (1993) M532-M536.

[2] Y. Noishiki, K. Takahashi, K. Yamamoto, A. Matsumoto, Y. Yamane, T. Miyata, American Society for Artificial Internal Organs 32 (1994) M751–M756.

[3] Z. Tang, Y. Yue, American Society for Artificial Internal Organs, 41(1995)72-78.

[4] DJ. Myers, G. Nakaya, MN. Girardot, GW. Christie, The Journal of Heart Valve Disease, 4 (1995) S98-S101.

[5] JM. Lee, CA. Pereira, LW. Kan, Journal of Biomedical Materials Research, 28(1994) 981-992.

[6] P. Boloori Zadeh, SC. Corbett, H. Nayeb-Hashemi, Materials Science and Engineering, 35 (2014) 335-340.

[7] B. Starcher, D. Urry, Biochemical and Biophysical Research Communications, 53 (1973) 210-216.

[8] H. McDowell, T. M. Gregory, and W. E. Brown, Journal of Research of the National Bureau of Standards, 81(1977).

[9] J. I. Goldstein, (2003), Springer Publishing. (2012).

[10] A. Schuessler, Shape Memory and Superelastic Technologies, (2001) 25-32.

[11] IS Alferiev, JT Hinson, M Ogle, E Breuer, RJ. Levy, Biomaterials, 22 (2001) 2501-2506.

[12] KG Brockbank, YC Song, Transplantation, 75 (2003) 1133-5.

[13] C. Giachelli, American Journal of Pathology, 154(1999) 671-5.

[14] L. Bre, R. McCarthy, W. Wang, Current Medicinal Chemistry, 21(2014) 2553-64.

[15] K. Shoji, N. Seikeigeka Gakkai Zasshi, 67 (1993) 201-10.

[16] R. Zeeman, P. Dijkstra, P. van Wachem et al., Journal of Biomedical Materials Research, 46 (1999) 424-33.

[17] L. Shechter, J. Wynstra, Journal of Industrial and Engineering Chemistry, 48(1956)86-93.

[18] L. Shechter, J. Wynstra, R. Kurkjy, Journal of Industrial and Engineering Chemistry, 48(1956) 94-7.

Chapter 7

Conclusions and future directions

7.1 Conclusions

The main aim of this thesis is to investigate different strategies for the optimisation of biocatalytic anodes and cathodes for application to biosensing and energy generation under *in vivo* conditions. Chapter two described the synthesis, characterisation and purification of a range of osmium polypyridyl complexes. The complexes were characterised electrochemically and using a range of analytical techniques including CHN, microanalysis and mass spectrometry. The resulting osmium polypyridyl complexes are further used for the synthesis of redox polymers and tetherable polypyridyl complexes. The resulting complexes and polymers are characterised and purified where needed. Chapter three reports on a comparison of glucose oxidation by enzyme electrodes based on coupling of GOx and a low potential osmium-based amine-functionalised redox mediator previously synthesised $Os(dmobpy)_2$4AMP to carboxymethyl dextran (CMD) and a range of conductive and non-conductive nanoparticles as alternate supports to probe whether the size and property of the supports can improve current density and/or stability for these electrodes. The study showed that the anodes decorated with MWCNTs and Au nanoparticles produced current densities more than 100% higher than plain graphite anodes while those of silica-decorated anodes with similar morphologies produced 3.5 % higher than the control. Interestingly for all enzyme electrodes with the nanoparticles support, redox site surface coverage and enzyme activity are similar indicating that the higher saturated current densities for MWCNTs and AuNPs are due to contribution to conductivity. Furthermore, using a previously reported DoE-optimised anode,

the performances of glucose oxidising enzyme electrodes based on coupling of GOx or FADGDH and an amine-functionalised osmium complex Os(dmobpy)$_2$4AMP to CMD and acid treated MWCNTs was investigated. A considerable decrease in current is observed for GOx-based electrodes when operated in the presence of oxygen, in comparison to the FADGDH-based electrodes. In addition, oxygen reduction by the mediator is apparent for all enzyme electrodes, including FADGDH-based electrodes, in oxygen saturated conditions. EFCs assembled from anodes based on Os(dmobpy)$_2$4AMP with FADGDH or GOx and a cathode containing *Mv*BOd co-immobilised with Os(dcbpy)$_2$PVI and MWCNTs were tested for power generation under pseudo-physiological conditions. A maximum power output of 80 μW cm^{-2} in air saturated, 5 mM glucose solutions was generated. Chapter four focuses on the optimisation of amounts of individual components such as MWCNTs, *Mv*BOd and Os(dclbpy)PVI using a response surface methodology in order to maximise current capture from oxygen on enzyme electrode surfaces. The components were co-immobilised using PEGDGE on graphite electrodes. DoE optimised enzyme electrodes result in oxygen reduction current density of 0.32 ± 0.03 mA cm^{-2} in pseudo-physiological conditions and 0.8 ± 0.05 mA cm^{-2} in saturated oxygen solutions, at an applied potential of 0.1 V vs. Ag/AgCl. EFCs are assembled and tested for power generation in pseudo-physiological buffer conditions using the optimised biocathode and an anode containing Os(dmobpy)$_2$PVI redox polymer co-immobilised with FADGDH and MWCNTs. EFCs produce power densities of 76 ± 10 μW cm^{-2} under conditions mimicking those of a physiological environment and a maximum power output of 92 ± 9 μW cm^{-2} in oxygen saturated conditions. Chapter five reports on a comparison of the catalytic current output of *Tv*CDH, FDH and GOx utilising two different low potential mediators of either Os(dmobpy)$_2$PVI or Os(dmobpy)$_2$4AMP in a flow injection analysis system. Carboxymethyl dextran (CMD), bearing carboxylic functional groups, as chemical support is applied for immobilisation of amine-containing osmium redox complexes, and PEGDGE is applied as crosslinker for immobilisation of redox polymer, at electrode surfaces to provide "wired" enzyme electrodes. Catalytic current outputs for Os(dmobpy)$_2$PVI was determined to be higher compared to Os(dmobpy)$_2$4AMP when immobilised at the selected pH with FDH, *tv* CDH and GOx using FIA. This can be due to the fact that osmium polymers such as Os(dmobpy)$_2$PVI are less likely to drift away in to the bulk of the solution than monomeric electron acceptors such as Os(dmobpy)$_2$4AMP. Optimum immobilisation pH with

Os(dmobpy)$_2$PVI is 4.5 for *Tv*CDH and FDH and 7.5 for GOx. However with Os(dmobpy)$_2$4AMP, the optimum immobilisation pH is 4.5, 6.5 and 7.5 for FDH, *Tv*CDH and GOx respectively. Maximum catalytic current for FDH, *Tv*CDH and GOx when immobilised in the optimum pH was achieved with the carrying buffer in the pH of 4.5, 5.5 and 7.5 respectively for both mediators. The catalytic current normalised to enzyme activity for FDH using the different redox mediators was higher compared to GOx, revealing the contribution of CYT domain to ET through the redox mediators. The findings shed further light on construction of biosensors and biofuel cell anodes, since lower potentials prevent the oxidation of interfering compounds and increase the overall obtained cell voltage for application to biofuel cells. Finally in chapter six an *in vitro* calcification test method is established to evaluate the calcification rate of treated bovine pericardium in the presence of a calcium rich solution. Calcification of bioprosthetic implants is a clinically important pathologic process limiting the anticipated durability and, hence, use of tissue-derived valves. The main objective of this model is allowing the differentiation of calcification rates where the samples were subjected to different tissue treatments. Tissue valve calcification is initiated primarily within residual cells that have been devitalised, usually by Glut pretreatment. The mechanism involves reaction of calcium-containing extracellular fluid with membrane associated phosphorus to yield calcium phosphate mineral deposits. A novel polyepoxide crosslinker PEP that was hypothesised to confer both material stabilisation and calcification resistance when used to prepare bioprosthetic heart valves is studied. The PEP was used to crosslink bovine pericardium and control materials were crosslinked with Glut. In addition PEGDGE, a commercial epoxide crosslinker was used for comparison. It is shown that the application of PEG epoxy polymer (PEP) for the fixation process increases the biostability of aortic wall without hindering collagen crosslinking. The application of cross-linking chemicals to inhibit the calcification rates is a link to enzyme electrode modification for biosensor and biofuel cell application.

7.2 Future directions

7.2.1 Fuel cells

Future work could focus on the optimisation of combinations of redox complexes or polymers, nanostructured materials and sugar oxidising and oxygen reducing enzymes with the aim of enhancing power outputs, ideally sufficient to power implantable devices (chapters 3, 4 and 5). For the fuel cell application as the power is dependent on differences of potentials and the current generated, there has to be a compromise between the need to have a high cell voltage and a high current, hence the application of osmium based complexes with tunable redox potentials. This thesis demonstrated the wide range of possible redox complexes (detailed in chapters 2), encompassing a large range of redox potentials, that could be synthesised for use as redox mediators for enzyme based electrodes. Chapters four and five demonstrated that osmium redox polymers proved to be highly effective mediators for sugar oxidation and oxygen reduction. Future studies could investigate the use of other ligands to produce a larger library of possible mediators. In order to improve cell voltages, current density and/or current stability of EFCs, the combination of synthesised novel mediators with the wide variety of different anodic and cathodic enzymes available could then be screened, using a range of crosslinking methodologies. Moreover, as in chapter 4, the approach of incorporating a MWCNT scaffold, *Mv*BOd, redox polymer and crosslinker to enhance the performance of an oxygen reducing cathode could be used to screen a wide range of oxygen reducing and glucose oxidising enzymes and osmium based mediators. In addition, future work could focus on the use of enzyme cascades by co-immobilisation of multiple sugar oxidising enzymes in an effort to extract more than two electrons from the fuel for the improvement of the power output of EFCs [1-3]. For example, in an enzyme cascade while one enzyme would oxidise glucose, a second enzyme could oxidise the resulting metabolite of the first enzyme. Application of multiple enzyme cascades for full or partial oxidation of fuels has been demonstrated to improve power output in biofuel cell assemblies [4]. Palmore *et al.* [5] initially reported on enzyme cascades by demonstrating complete oxidation of methanol to carbon dioxide using alcohol, aldehyde and formate dehydrogenase. Enzyme electrodes prepared using such a combination to mimic

metabolic pathways and optimised using DoE approach may provide a promising route to increased power density of EFC.

As another promising approach, protein engineering can be applied to develop useful or valuable proteins by altering the properties of biocatalysts and tuning for the ideal properties [6]. There are two general strategies for protein engineering: rational protein design and directed evolution. Rational protein design approach make protein-sequence predictions that will fold to specific structures where the proteins can be designed from scratch or by making calculated variants of a known protein structure and its sequence. As another useful strategy, directed evolution is a method that mimics the process of natural selection (survival of the fittest against different environmental factors) to evolve proteins or nucleic acids toward a user-defined goal. It consists of subjecting a gene to iterative rounds of mutagenesis inorder to modify the properties of the protein [7]. Many nanostructured materials, such as mesoporous media, nanoparticles, nanofibers, and nanotubes, have been demonstrated as efficient hosts of enzyme immobilisation. When conductive nanostructure materials are used, the large surface area of these nanomaterials can increase the enzyme loading, and thus improving the power density of biofuel cells [8]. It appears to be reasonable to expect that progress in nanostuctured biocatalysts will play a critical role in overcoming the major obstacles in the development of powerful biofuel cells. Another future direction is the development of a compact paper-based microfluidic EFC for use as *in vivo* applications. As the eventual application of EFCs would be utilisation as power supply for implantable and semi-implantable devices, miniaturisation of EFC at microscale would be required due to medical devices becoming more sophisticated. To enhance efficiency and mobility as well as reducing sample and reagent volumes, processes are often miniaturised on a single chip. A lab-on-a-chip (LOC) is a device that integrates one or several laboratory functions on a single chip of only millimeters to a few square centimeters in size. LOCs deal with the handling of extremely small fluid volumes down to less than pico liters. LOC is closely related to, and overlaps with microfluidics that has practical applications to the design of systems in which small volumes of fluids will be handled [9]. To control the flow within a micro fluidic device, many techniques have been introduced such as capillary forces. In some applications, the working fluid is manipulated by active (micro) components as micro valves or micro pumps. Micro valves determine the flow direction or the mode of movement of pumped liquids while micro pumps supply fluids in a continuous manner or are

used for dosing. Another novel technique is rotary drives applying centrifugal forces for the fluid transport on the passive chips. This force is enough to remove a pump and could be varied by rotating at known frequencies, reducing the operation, maintenance and device simplicity. Although micro fluidic fuel cells are a young technology, important progress has been made in the area. These cells yield significant amounts of energy with a very simple architecture. However, reports have shown that glass or plastic based microfluidic fuel cell utilising external pressure sources such as pumps to maintain the reactants in motion could limit their miniaturisation and portability [10]. Paper based enzymatic microfluidic fuel cells benefit from the laminar flow where the fluids are driven by capillary action and no external pressure sources, e.g. pumps, are needed. The paper-based microfluidic enzymatic fuel cell is based on fluid delivery and removal, reaction sites and electrode structures all confined to a microfluidic channel (Figure 1). At the end of the paper strip, the membrane is covered by an absorbent pad consisting of two additional layers of the same porous material. The anode is placed under the paper strip, while the cathode is attached on top to facilitate oxygen access from the atmosphere. Whereas glucose is oxidised in the anode side and oxygen reduced in the catholyte comes from air through the porous cathode. The substrate continues to flow until it is completely absorbed by the absorbent pad.

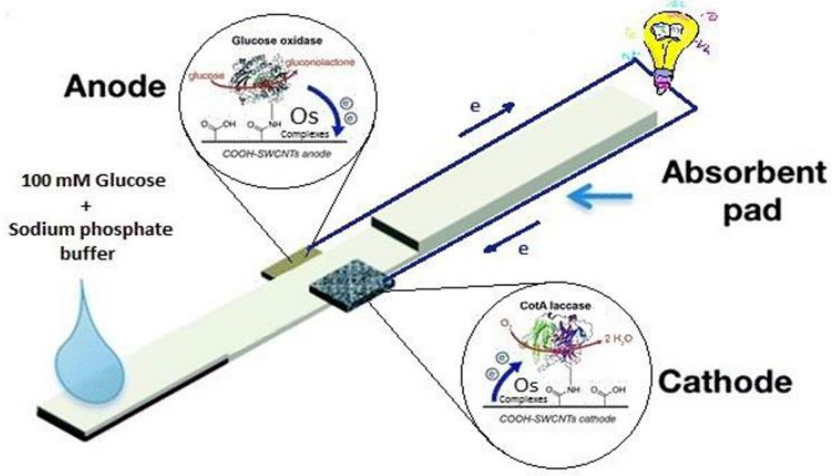

Figure 1: Carbon nanotube electrodes patterned on carbon paper used to create membraneless glucose/O_2 microfluidic biofuel cells. EFC composed of Laccase and osmium redox mediator in the cathodic compartment and glucose oxidase and osmium redox mediator in the anodic compartment.

A recent report on a compact paper-based enzymatic microfluidic glucose/O_2 fuel cell based on FAD-GDH enzyme and the redox polymer $Os(dmobpy)_2PVI$ for the anode and bilirubin oxidase enzyme and the mediator $Os(bpy)_2PVI$ as the cathode generated a maximum power density of 20 to 90 μW cm^{-2} at 0.45V [11]. Moreover, another report on paper-based microfluidic fuel cell shows a maximum power density of 1.65 μW cm^2 at 0.24 V for 4.2 minutes when fed with glucose as fuel. This approach shows the potential of implementing a microfluidic fuel cell in a paper platform. It is also worth noticing that the pumping systems required for non-paper-based microfluidic fuel cells might represent a significant power consumption, which can sometimes exceed the amount of power delivered by the fuel cell itself [12]. In addition, these paper-based biodevices are relatively inexpensive in comparison to glass or plastic and are fast and simple to operate [13, 14] and can prove advantageous for use in EFCs.

7.2.2 The effect of crosslinking on anti-calcification of bovine pericardium

The application of PEG epoxy polymer (PEP) for the treatment process in chapter 6 increases the biostability of aortic wall without hindering collagen crosslinking. However, certain draw backs still remain. High superficial calcification is not desired and is not physiological, yet it is present in the valves tested using the new method. Future work must orient toward optimisation of this method either by alternation of the PEP concentration or crosslinking time.

7.3 References

[1] F. Tasca, L. Gorton, M. Kujawa, I. Patel, W. Harreither, C.K. Peterbauer, R. Ludwig, G. Nöll, Biosensors and Bioelectronics, 25 (2010) 1710-1716.

[2] M. Shao, M. Nadeem Zafar, C. Sygmund, D.A. Guschin, R. Ludwig, C.K. Peterbauer, W. Schuhmann, L. Gorton, Biosensors and Bioelectronics, 40 (2013) 308-314.

[3] P. Kavanagh, D. Leech, Physical Chemistry Chemical Physics, 15 (2013) 4859-4869.

[4] Z. Zhu, T. Kin Tam, F. Sun, C. You, Y.H. Percival Zhang, Nature Communications, 5 (2014).

[5] G.T.R. Palmore, H. Bertschy, S.H. Bergens, G.M. Whitesides, Journal of Electroanalytical Chemistry, 443 (1998) 155-161.

[6] Liszewski, Kathy (15 February 2015). Genetic Engineering & Biotechnology News (paper), 35 (2015) 1.

[7] Lutz S., Current Opinion in Biotechnology, 21(2010) 734-43.

[8] X. Dominguez-Benetto, S. Srikanth, Y. Satyawali, K. Vanbroekhoven and D. Pant, Journal of Microbial and Biochemical Technology, (2013) S6

[9] V. Chokkalingam, B. Weidenhof, M.Krämer, WF. Maier, S. Herminghaus, R. Seemann, Lab on a Chip, 10 (2010) 1700-5.

[10] J.P. Esquivel, F.J. Del Campo, J.L. Gomez de la Fuente, S. Rojas, N. Sabate, Energy & Environmental Science, 7 (2014) 1744-1749.

[11] M. José, G. Guerrero, F. Javier, JP. Esquivel, D. Leech and N.Sabaté, Biosensors and Bioelectronics, 98 (2017) 421-427

[12] M. José, J. Pablo, D. Sánchez, P. Godignon, F. Xavier, F. Javier, F. Giroud, S. Minteer, N.Sabaté, Lab on a Chip, 13 (2013) 2972-2979.

[13] N.K. Thom, K. Yeung, M.B. Pillion, S.T. Phillips, Lab on a Chip, 12 (2012) 1768-1770.

[14] N.K. Thom, G.G. Lewis, M.J. DiTucci, S.T. Phillips, RSC Advances, 3 (2013) 6888-6895.

Appendix

Selected Presentations

- **A. Ekhtiari**, P. Ó Conghaile, I. Osadebe, R. Kumar, P. Kavanagh and D. Leech, Poster presentation at XXIII International Symposium on Bio electrochemistry and Bioenergetics from 14th to 17th June 2015 in Malmo, Sweden. Title: Glucose-Oxidizing Enzymatic Fuel Cell Anodes: Nanomaterials as Support for Redox Components on Electrodes.
- **A. Ekhtiari**, P. Ó Conghaile, I. Osadebe, R. Kumar, P. Kavanagh and D. Leech, Poster presentation at 67th Irish Universities Chemistry Research Colloquium in Maynooth University on June 25th & 26th. Title: Glucose-Oxidizing Enzymatic Fuel Cell Anodes: Nanomaterials as Support for Redox Components on Electrodes.
- **A. Ekhtiari** and D. Leech, Poster presentation at Analytical Research Forum 2016 (ARF16) 8 July 2016, London, United Kingdom. Title: Mediated enzyme electrodes for application to enzymatic fuel cells.
- **A. Ekhtiari**, P. Ó Conghaile and D. Leech, Poster presentation at International Symposium on Bio electrochemistry and Bioenergetics from 2nd to 7th July 2017 in Lyon, France. Title: Mediated enzyme electrodes for application to enzymatic fuel cells.

Courses/Workshops attended during the doctoral program

- Process Development and Scale-Up in the Pharmaceutical Industry course
- Graduate Workshop on Key Enabling Technologies course
- Teaching and learning course
- Core Skills in Chemistry module; Basic molecular modelling (Spartan), High performance liquid chromatography, An introduction to literature searching using Scifinder and Reaxys, Gas chromatography, Characterisation and purity assessment of organic compounds, Molecular

modeling using molecular dynamics, Mass Spectroscopy, Scanning Electron Microscopy, Electrochemical methods, Health and safety and fire training at NUIG

- Work based placement at Boston scientific company
- Academic secondment at Lund university
- The online course of the European Patent Office passed which included courses: Introduction to the European patent system, Patentability requirements at the EPO, Using CPC in classification, searching prior art based on patent applications
- Laboratory demonstration for Undergraduates at NUIG
- First BIOENERGY summer school from 28th September to 4th October 2014 at Saint Pierre d'Oléron, France which included courses in teambuilding, presentation skills as well as lectures related to bio electrochemistry.
- A key to a successful interview ‘’how not to be afraid’’ Biological and Chemical Research Centre - University of Warsaw.
- BIOENERGY Workshop from 18th to 20th February 2015 at BOKU - University of Natural Resources and Life Sciences, Vienna, Austria which included courses in Molecular biology, Protein structure, Homology modelling, and structure visualisation, Protein engineering and evolution, Enzyme screening, Enzyme kinetics and How to write a scientific paper.
- BIOENERGY meeting in Southampton from 29th to 1st March 2015 with the workshop on project planning and progress report presentation.
- BIOENERGY - joint measurement campaign and midterm review meeting in Ruhr-Universität Bochum from 7th to 18th September- A work shop on enzymatic biofuel cells involving exchange of material and knowledge with other students from the consortium.
- BIOENERGY Limerick meeting which included fabrication of gold nanoporous electrodes in laboratory and characterisation of the electrodes by scanning electron microscopy.
- Participated as a representative of Chemistry at the University open day on Saturday, April 25th 2015
- As a representative of Chemistry at the NUIG attended the open day on Saturday, April 25th 2015
- As a representative of Chemistry at the NUIG attended the Galway Science and Technology Forum hosting of "TeenTech" event at NUI Galway on April 17th 2015 and on 7th March 2016. Teen Tech is a high-profile event that was developed in the UK with the goal of encouraging children to develop their interests in Science and Technology.